Durham E-Theses

Adsorption of Dendritic Fluorocarbon End-Capped Poly(Ethylene Oxide) at an Air-Water Interface – A Synthetic, Analytical and Computational Study

BARTRAM, SIMON

How to cite:

BARTRAM, SIMON (2009) *Adsorption of Dendritic Fluorocarbon End-Capped Poly(Ethylene Oxide) at an Air-Water Interface – A Synthetic, Analytical and Computational Study*, Durham theses, Durham University. Available at Durham E-Theses Online: http://etheses.dur.ac.uk/39/

Use policy

Adsorption of Dendritic Fluorocarbon End-Capped Poly(Ethylene Oxide) at an Air-Water Interface – A Synthetic, Analytical and Computational Study

Simon A. Bartram

Ph.D. Thesis

**Durham University**

Chemistry Department

May 2009

Submitted in partial fulfilment of the requirements for the degree of

Doctor of Philosophy

Abstract

Adsorption of Dendritic Fluorocarbon End-Capped Poly(Ethylene Oxide) at an Air-Water Interface – A Synthetic, Analytical and Computational Study

Adsorption of amphiphilic polymer molecules to an interface can induce interesting properties on both the bulk of the material as well as the interface itself. Previous experiments carried out by other groups at Durham University have shown that functionalizing PEO with fluorocarbon groups can lead to a remarkably large increase in adsorption and evidence has been provided for the formation of brush-like structures at an air/water interface[1]. However the maximum size of the fluorocarbon unit is limited by its solubility in organic solvents.
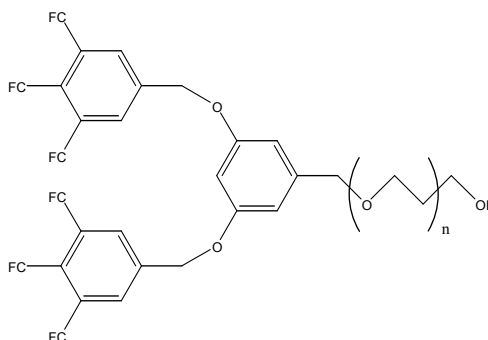
In order to try and overcome this problem a new synthetic strategy has been employed wherein the PEO chain is functionalized using a dendrimer, enabling multiple functional groups to be attached to a single polymer chain. Conformational and concentration dependence information can be found using *neutron reflectometry*[1, 2].

A key component of this project is to utilize molecular dynamics (MD) to simulate the behaviour of these polymers at liquid surfaces. For relatively short polymer chains, it is possible to quantitatively model the distribution function for chains at a water-air interface by employing atomistic simulation techniques, allowing for direct predictions of the neutron reflectivity data[3]. For long chains atomistic representations of the polymer and water are no longer feasible but we model the poly(ethylene oxide) using coarse-

grained models. The advantage of coarse-graining (CG) is that it allows us to simulate much longer chains and much higher surface concentrations allowing direct predictions for the neutron reflectivity based on the calculated distribution functions for the CG-polymer at each surface concentration[4].

By direct comparison of experimental and computational data we will substantially increase our understanding of the behaviour of amphiphilic polymer molecules at interfaces. This study will also enable us to synthesize materials with very high surface adsorption.

References

[1] R. W. Richards and J. Sarica, *Langmuir* **2003**, *19*, 7768-7777.

[2] B.-K. Cho, A. Jain, S. M. Gruner and U. Wiesner, *Science* **2004**, *305*, 1598-1601.

[3] P. M. Anderson and M. R. Wilson, *J. Chem. Phys* **2004**, *121*, 8503-8510.

[4] G. Srinivas and M. L. Klein, *Molecular Physics* **2004**, *102*, 883-889.

Declaration

The material contained within this thesis has not been previously submitted for a degree at Durham University or any other university. The research within this thesis was conducted by the author unless stated otherwise.

The copyright of this thesis lies with the author and no quotation should be published from it without his prior consent and any information used from it should be correctly acknowledged.

<div align="center">

Simon Andrew Bartram

May 2009

</div>

Acknowledgments

There are so many people that I wish to thank for helping me during my time at Durham University, I only hope that I am able to remember them all here in these acknowledgments. The first of these is the Engineering and Physical Sciences Research Council for the funding of the studentship that made this Ph.D. work possible.

I am hugely grateful to Dr. Mark Wilson for giving me the opportunity to be a part of his excellent research team and for letting me share in his vast array of scientific and computational knowledge and expertise. The members of Mark's research team made every effort to help and support me through my computational simulation work and I am particularly indebted to Zack and Jorge for their help with this part of my project.

I am also extremely grateful to Dr. Nigel Clarke whose knowledge of polymer science is second to none and made me feel very welcome as part of his team from day one. The others members of Nigel's research team not only made me feel very comfortable and welcome as a member of the group but also contributed greatly in helping me to understand the science of polymers necessary to make this work possible. I would particularly like to thank Stephen and Kim who helped me massively during the early days when I was learning the ropes of this project and Jude; who has been a very good friend of mine for many years and has been an absolute joy to work with for the last 3 years.

For their generous and expert assistance with the synthetic part of my project I would like to thank Dr. Lian Hutchins and his team. The knowledge and help that I was able to call upon from Lian, Amil, Solomon, Helen and the rest of the guys in and around the synthesis lab made my time working there both productive and enjoyable.

I would also like to thank all of my colleagues in the materials chemistry building who not only helped me with any questions I had in each of their areas of expertise; but whom I also came to regard as personal friends who made my days much more enjoyable than they might otherwise have been. In particular here I must give a special mention to Dr. Richard Thompson. The expert scientific and machinery assistance, encouragement and friendship that Richard has given to me throughout both my masters degree year and the duration of my Ph.D. project has been invaluable.

vi

Finally I would like to thank my wonderful friends, family and girlfriend Sally for keeping me sane during the difficult times, for the interesting questions and suggestions that helped me with my own understanding of my work and for all of their support and encouragement in general. I love you all!

"There are two possible outcomes: if the result confirms the hypothesis, then you've made a measurement. If the result is contrary to the hypothesis, then you've made a discovery."

- Enrico Fermi

"There is a theory which states that if ever anybody discovers exactly what the Universe is for and why it is here, it will instantly disappear and be replaced by something even more bizarre and inexplicable. There is another theory which states that this has already happened."

- Douglas Adams

"Chemists are, on the whole, like physicists, only 'less so'. They don't make quite the same wonderful mistakes, and much what they do is an art, related to cooking, instead of a true science. They have their moments, and their sources of legitimate pride. They don't split atoms, as the physicists do. They join them together, and a very praiseworthy activity that is."

- *Anthony Standen*

Contents

Chapter One – Introduction and Overview

Chapter Two – Theory

Chapter Three – Synthesis

Chapter Four – Analysis and Results

Chapter Five – Computer Simulations

Chapter Six – Conclusions and Outlook

Index of Tables and Figures

Appendix:

Chapter One: Introduction and Overview

1.1 Polymers and Amphiphilicity

Polymer molecules are long chain molecules made up from repeat units of smaller molecules, which are known as *monomers*[1]. Many important materials contain polymer molecules, including naturally occurring materials such as silk, wool and linen, which are based on biopolymers and are used with little or no modification[2]. Synthetic polymers were discovered during the 19th century but were not manufactured in significant amounts until the 1930's[3]. Originally, synthetic polymers were used as substitutes for their biopolymer equivalents but in more modern times they have far outgrown this initial purpose and now synthetic polymers are an important class of materials themselves. Modern synthetic polymers can be made very specifically for use in a wide range of applications from semi-conducting devices to modern medical applications such as replacement hip joints[4-8]. Polymers are used to produce materials of this type as they are more easily formed and altered than many other materials. Therefore it is very important to study and understand the properties and interactions of polymers to be able to put them to as many uses as possible[9-12].

Polymers synthesized from *hydrophobic* monomers will also exhibit hydrophobic properties themselves. The term hydrophobic usually refers to materials that do not mix well with water (or other polar solvents) and polymers that display this behaviour are generally composed of carbon and hydrogen, naturally occurring hydrophobic polymers include alkanes or similar molecules from crude oil. Hydrophobic polymers placed in a polar solvent will tend to curl up and pack together in order to minimize the energetically unfavourable polymer-solvent interactions. Polymer-polymer and solvent-solvent interactions are maximized as they are much more energetically favourable in this kind of system.

The exact opposite behaviour can be seen with *hydrophilic* polymers. Typical naturally occurring hydrophilic polymers include proteins and sugars. These polymers are made up from monomers containing electronegative elements (most commonly oxygen),

which interact favourably with polar solvents and will therefore become dissolved in order to maximize the polymer-solvent interactions. If these interactions are significantly more favourable than polymer-polymer and solvent-solvent interactions then the polymer will tend to extend itself to allow full solvation and maximize these interactions. One of the most common and well-known synthetic polymers to exhibit such hydrophilic behaviour is poly(ethylene oxide)[4, 13-15] or PEO (or sometimes referred to as PEG), shown in figure 1.1.1.
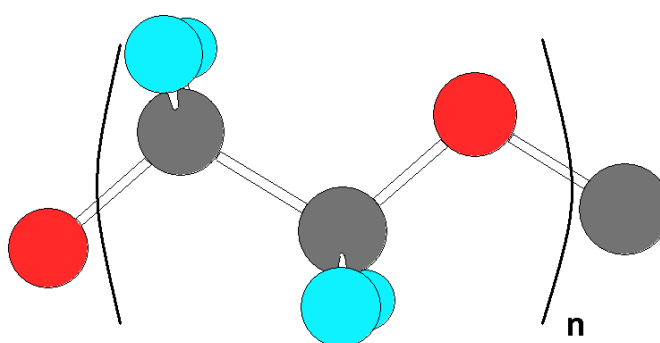
Figure 1.1.1: Schematic showing the structure of poly(ethylene oxide)

Often it is desirable to combine the properties of two or more polymers and this can sometimes be achieved by simple blending. Unfortunately this is not the case for the vast majority of potential polymer combinations as many polymers are immiscible with one another and phase separation of the different polymers occurs. However, in these cases, it is still possible to covalently bond the two blocks together to form a block copolymer (see figure 1.1.2) and whilst microscale segregation of the polymers can occur, macroscale segregation is prevented by the covalent linkages[16]. These block copolymers typically have small domain sizes together with excellent interphase adhesion, leading to the possibility of materials with high degrees of transparency and useful mechanical properties.
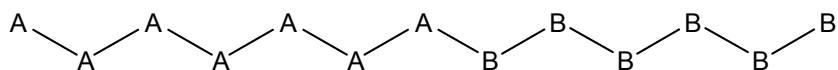
Figure 1.1.2.1: an AB diblock copolymer
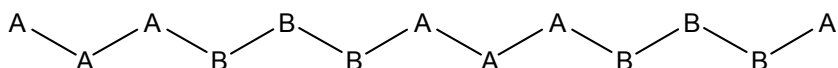
Figure 1.1.2.2: an AB block copolymer
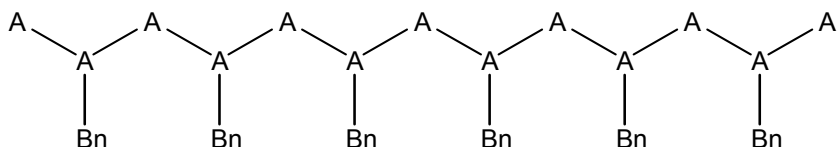
Figure 1.1.2.3: an AB graft copolymer
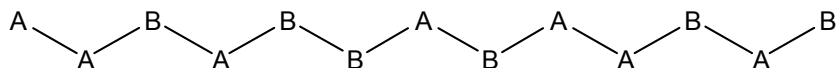
Figure 1.1.2.4: an AB random copolymer

Figure 1.1.2: Schematic showing typical types of AB copolymer (this is the simplest type of block copolymer with only 2 monomer types)

Block copolymers can also be synthesized to combine the properties of two different polymers in a single macromolecule for an application which requires its use in solution. A prime example of this type of block copolymer is an amphiphilic surfactant molecule, which is made up from both hydrophobic and hydrophilic components (the

case where monomer types A and B in figure 1.1.2.1. have opposing hydrophobic/hydrophilic properties)[17-22].

The most commonly employed method for the synthesis of block copolymers is the sequential addition of two or more monomers to a single living polymerization reaction. Anionic polymerization in particular has been the most important technique for preparing block copolymers and is still employed in many industrial processes today. There are more modern techniques emerging, such as living radical polymerization which has provided a useful alternative for block copolymer synthesis where other living polymerization techniques are simply not viable for chemical reasons. In some cases where the target block copolymer structure cannot be synthesized by one polymerization technique it is possible to combine more than one of these mechanisms to achieve the desired result. The synthesis of block copolymers can therefore be used to generate macromolecules tailored to a specific application, by adjusting the composition of the copolymers.

1.2 Interfacial Behaviour of Polymers

1.2.1 Adsorption at Interfaces

The adsorption of amphiphilic polymer molecules to an interface is of extreme importance and is currently a case for intense study throughout the scientific community[23-28]. The adsorption process induces a concentration differential at or near the interface influencing both the bulk and interfacial properties of the system. It is these properties that are already utilized today in products such as lubricants and adhesives[28, 29]. Studies are also underway to use this type of molecule for specific targeting in drugs using a biodegradable polymer shell to deliver and release the drug at a specific place in the body and over a set amount of time[24, 25, and 27].

An interface is defined as a boundary between two different types of matter or space and can be simplified down to boundaries between solid, liquid, and gas(vacuum) so we can have the following types of interface: gas (vacuum)-liquid, gas (vacuum)-solid, liquid-liquid, liquid-solid and solid-solid.

The majority of work done with amphiphilic polymers is studied at a gas (vacuum)-liquid interface and the simplest interface of this type is an air-water interface as this can be easily created experimentally and is an ideal model for more complex biological systems. Placing a block copolymer of the type discussed above, with both hydrophobic and hydrophilic components, into such a system will result in the polymer arranging itself at the air-water interface in such a way that the hydrophilic sections of the copolymer will sit inside the water surface and the hydrophobic parts will sit outside of the water[26, 30].

Due to the recent progress in chemistry, chemical engineering and more specifically in polymer science and technology, new polymeric materials can be made that allow us to attach small hydrophobic groups on to a water soluble polymer at either one or both terminal ends of the polymer[31]. Studies have been carried on diblock copolymers with a large hydrophilic tail component and a smaller hydrophobic component grafted to one end. The *aggregation* of the hydrophilic tail group into the bulk of the water and the *segregation* of the hydrophobic head group away from the bulk of the water will result in the molecule becoming tethered at the interface[32-34]. The terms aggregation and segregation are used to describe the direct mutual and repulsion (respectively) between the molecules via van der Waals forces and/or chemical interactions.

The interest in these types of molecule was sparked when it was discovered that by end-grafting polymer molecules on to colloidal particles it was possible to effectively prevent flocculation[35]. This led to the conclusion that tethered polymer layers can be used to modify the properties of surfaces and interfaces, therefore leading to a great deal of interest in the arrangement, or self assembly, of these molecules and the subsequent effect of this on the surface properties of a solution. It is well known that a polymer chain in solution is free to adopt a wide variety of conformations simply by rotation about the single bonds in the backbone of the molecule and these chain conformations can be described as following a random walk[4] (shown schematically in figure 1.2.2.1). A chain that is adsorbed to a surface does not have so much freedom to follow a random walk due to the restriction of the interface to which it is tethered. In this case half of the space into which the polymer chain in solution is free to diffuse is not available to a tethered chain, leading to some very interesting and novel conformations.

1.2.2 Surface Tethering and Conformations

When a polymer is tethered at an air-water interface it can form one of a number of conformations depending on the packing density of such molecules at the surface.

In order to understand the significance of packing density it is necessary to consider the dimensions of an unperturbed chain in free space. A critical value at this point is the radius of gyration[36] for the polymer; to define this term we must first define the end-to-end distance of the polymer:

$$r^2 = nl^2$$

Equation 1.2.2.1

where r is the end-to-end distance of polymer, n is the number of monomer repeat units and l is the vector between adjacent monomers.
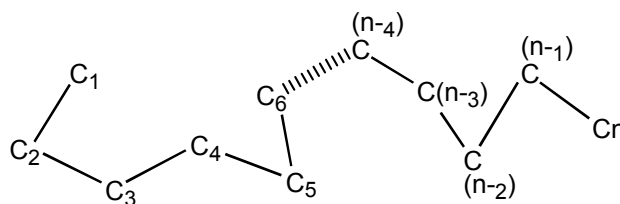
Figure 1.2.2.1: Schematic representation of a polymer backbone

This end-to-end distance is simply a measure of the distance between one terminal end of the polymer and the other and is found by summation of the vectors between each monomer site.

The radius of gyration for a polymer can be defined either in terms of monomer masses or total number of monomers in a given polymer:

$$R_g^2 = \frac{\sum_i ms_i^2}{\sum m} = \frac{\langle \sum_{i=1}^{n} S_i^2 \rangle}{n}$$

Equation 1.2.2.2

therefore:

$$R_g = \sqrt{\sum_{i=1}^{n} \frac{S_i^{\,2}}{n}}$$

Equation 1.2.2.3

where R_g is the radius of gyration, m is the mass of the monomer unit and S_i is the distance of a given monomer unit from center of gravity.

This value for radius of gyration[37] is of extreme importance when considering the conformational behaviour of a tethered polymer at the interface. The conformations adopted by these polymers are directly related to the radius of gyration for the polymer and the density of polymers at the interface; figures 1.2.2.2 to 1.2.2.5 show schematic representations of some of the more common conformations.

The first conformation shown in the schematic (figure 1.2.2.2) arises when the space between tethered ends (or graft points) is much greater than the radius of gyration for the polymer[38, 39]. The chain minimizes its energy by lying at the surface and has very little or no interaction with surrounding chains. This is known as the 'pancake' conformation and is typically adopted by polymers at low grafting density in a poor solvent (polymer - solvent interactions are unfavourable, such as a hydrophobic polymer in water).
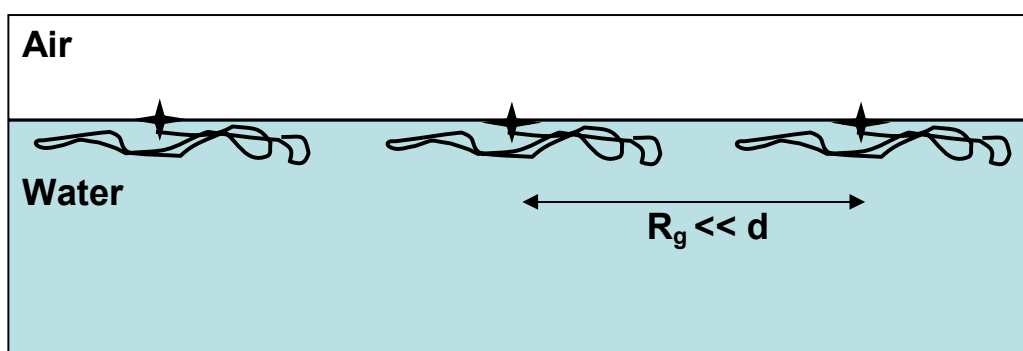
Figure 1.2.2.2: Schematic of a tethered polymer in the 'pancake' conformation

The second conformation shown in the schematic (figure 1.2.2.3) is also observed when the space between tethered ends (or graft points) is much greater than the radius of gyration for the polymer. However, in this case the polymer-solvent interactions are more favourable than the polymer - surface interactions and as a result the chains extend down into the solvent to minimize their energy. This is known as the 'mushroom' conformation and is typical of a tethered hydrophilic polymer (such as PEO) in water.
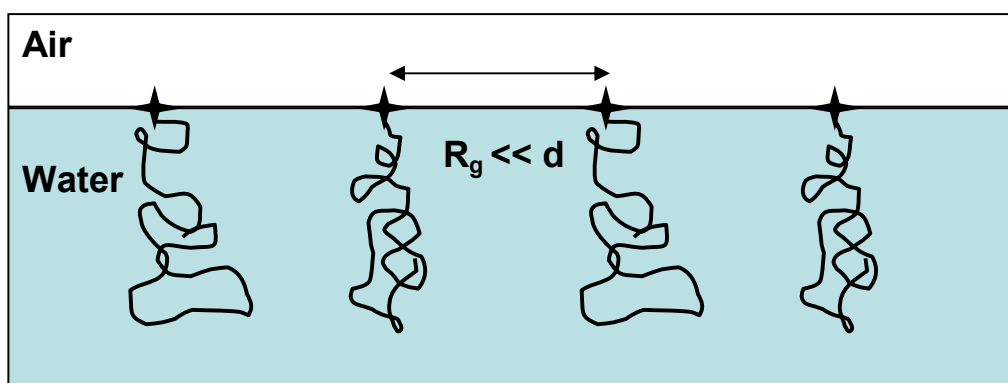
Figure 1.2.2.3: Schematic of tethered polymer in the 'mushroom' conformation

The third conformation shown in the schematic (figure 1.2.2.4) occurs when the radius of gyration for the polymer is greater than the mean distance between graft points and therefore typically occurs for polymer systems with a reasonably high graft density.
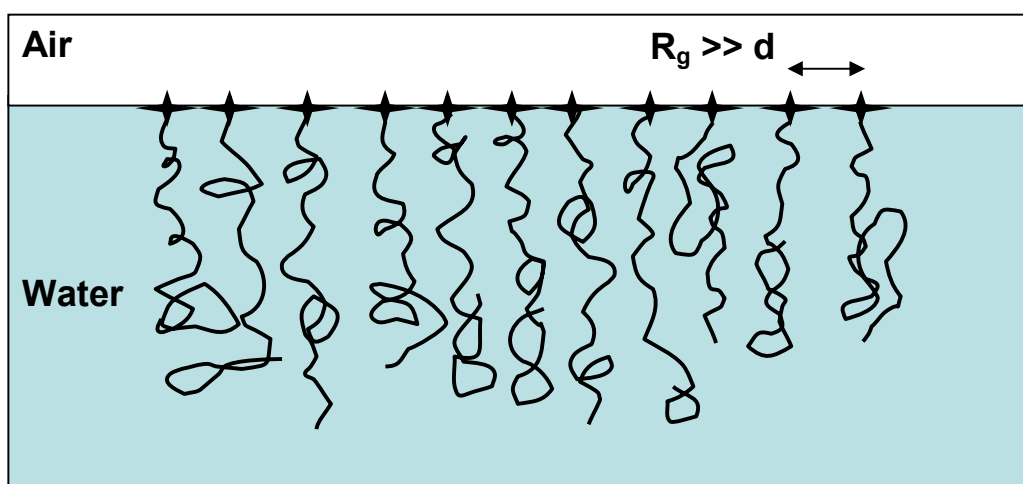
Figure 1.2.2.4: Schematic of a tethered polymer in the 'brush' conformation

The interactions are similar to that of a mushroom conformation except that the tethering is sufficiently dense that the polymer chains are crowded and forced to stretch away from the surface or interface due to repulsive excluded volume interactions between chain segments. These stretched configurations are found under thermodynamic equilibrium conditions when the energy loss resulting from the reduction of the excluded volume interactions compensates the entropy penalty from the stretching of the chains from their initial random walk configurations. The height of the resulting solvated brush layer is commonly found to be several times the unperturbed radius of gyration of the free chains in solution. This is known as a polymer brush conformation, and has been previously described by de Gennes[40].

There are several scaling law predictions that can be applied to polymer mushroom and brush conformations[41]. Considering a surface-grafted polymer with a statistical step length, a, and degree of polymerization, N, the tails of which are surrounded by a polymeric matrix with degree of polymerization, P. The behaviour of such a polymer can be defined in term of the grafting surface density, σ. Low surface densities where the grafted polymers have enough space to prevent overlap of the molecules the grafted chains exhibit *ideal* statistics and adopt a *mushroom* conformation. For these low grafting densities the radius of the mushroom can be expressed as $N^{1/2}a$ and this is also the layer thickness, h. When the grafting density of is greater than the inverse of degree of polymerisation ($N^{1} \le \sigma$) the grafted polymers begin to overlap with one another but the ideal value for the mushroom radius remains the same. Increasing the grafting density above this value (up to a value of $P^{-1/2}$) the molecules begin to stretch because of the need to satisfy space filling requirements. Increasing the grafting density further excludes more and more of the matrix molecules and as σ approaches 1 the grafted polymer adopts what is known as a 'dry brush' regime, here the brush layer thickness is $\sim Na\sigma$. The brush layer thickness of these regimes can be described using the following equations:

for $0 < \sigma \le N^{-6/5}$

Swollen mushroom ($P < N^{1/2}$)

$$h \sim N^{3/5}aP^{-1/5}$$

Equation 1.2.2.4

Ideal mushroom ($P > N^{1/2}$)

$$h \sim N^{1/2}a$$
Equation 1.2.2.5

for $N^{-6/5} < \sigma < 1$

Stretched wet brush ($P < N^{1/2}$)

$$h \sim NaP^{-1/3}\sigma^{1/3}$$
Equation 1.2.2.6

for $N^{-1} \leq \sigma \leq N^{-1/2}$

Unstretched brush layer ($P > N^{1/2}$)

$$h \sim N^{1/2}a$$
Equation 1.2.2.7

for $N^{-1/2} \leq \sigma \leq 1$

Stretched dry brush ($P > N^{1/2}$)

$$h \sim Na\sigma$$
Equation 1.2.2.8

These regimes can also be applied to a polymer that is tethered at an air-water interface. In this case however the water solvent has no value for *P* and only the *swollen mushroom* and *stretched wet brush* regimes are possible.

Upon increasing the graft density above the conditions required for brush formation we reach a point where there is physically no room available to add more chains to the interface. This is known as the *Critical Micellization Concentration* and above this point we see the formation of micelles, shown in the schematic (figure 1.2.2.5).

Note - micelles can also be formed by some molecules without the necessity of a surface excess layer.

In this case the tethered head groups (e.g. highly hydrophobic head groups in a water solvent) will attempt to lower the highly unfavourable head group - solvent interactions by migrating together to form a pocket where there is very little solvent

present. As a result the polymer chains will extend out from the core of the micelle and spread into the solvent to minimize their energy.
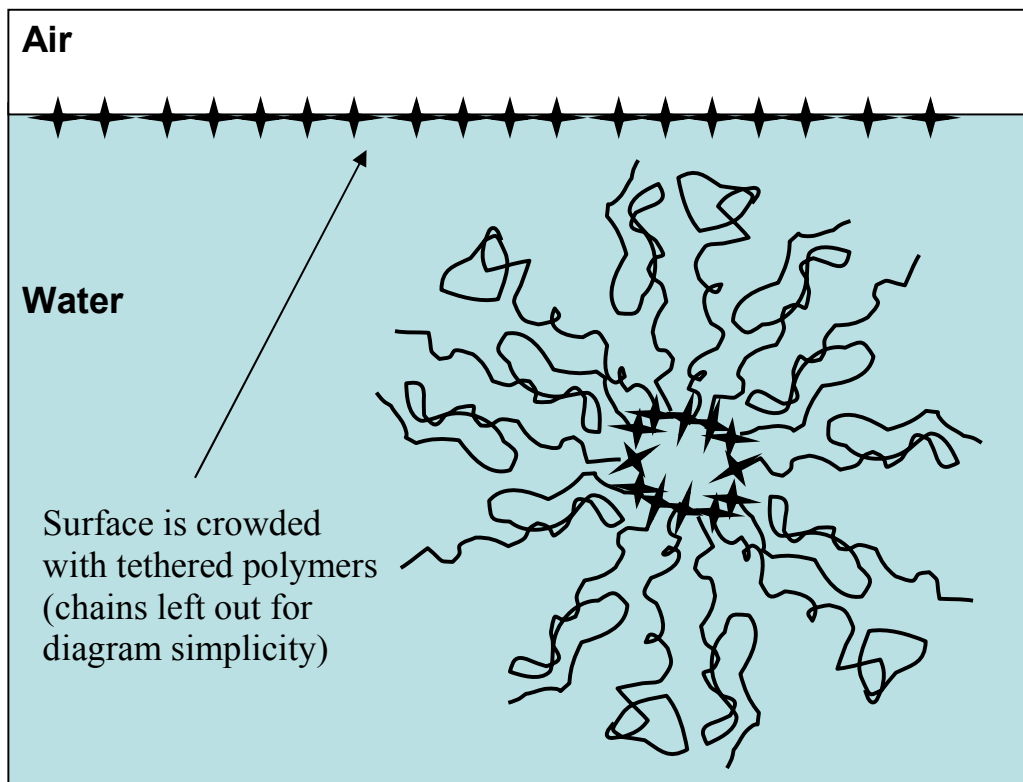
Figure 1.2.2.5: Schematic representation of micelle formation of polymer chains

There are two methods employed experimentally to populate an air-water interface with polymeric materials. The first method is to spread an insoluble polymer onto a liquid surface, in which case the formation of micelles is avoided. This is achieved by first dissolving the polymer in an appropriate volatile solvent that is a good solvent for the polymer but insoluble in the liquid substrate. This insoluble polymer solution can then be spread onto the liquid substrate surface and the volatile solvent will evaporate leaving the polymer film behind. The second method is carried out by dissolving a surfactant polymer in the liquid substrate. Diffusion of the polymer will lead to self assembly of a surface excess layer due to the amphiphilic nature of the polymer.

1.2.3 Poly(Ethylene Oxide) – Selected Previous Studies

Poly(ethylene oxide), or PEO, is a unique member of the polyepoxides, with the general formula $[(CH_2)_nO]_x$, in that it is soluble in both organic and aqueous solvents[14, 17]. PEO has a surface tension of 31 mN/m, much lower than that of pure water, which is 72.8 mN/m. As a result, although PEO is water soluble, it has also been shown that PEO can form stable spread films at the air-water interface under certain circumstances [33, 42, and 43].

Adsorbed solutions and spread films of PEO have been the centre of many investigations due to the intriguing properties of PEO. Surface properties of linear PEO and copolymers containing PEO (examining the effects of molecular weight, concentration, temperature and various other factors) on the coverage of PEO at the air-water interface have been extensively studied in recent times[11, 43-47].. Studies carried using neutron reflectometry have confirmed the existence of a stable spread film of linear PEO monolayer at an air-water interface[48] at a surface concentration of $0.5mg/cm^2$. At this concentration it has been shown that the linear PEO chains penetrate the liquid substrate due to a looping of the molecules (illustrated in figure 1.2.3.1). Neutron reflectometry experiments have also been employed to determine the surface organization of adsorbed solutions of linear PEO at an air-water interface. Results from these experiments show distinct differences between the surface structures of the linear PEO formed from spread monolayer and those formed from the adsorbed solutions[49, 50].
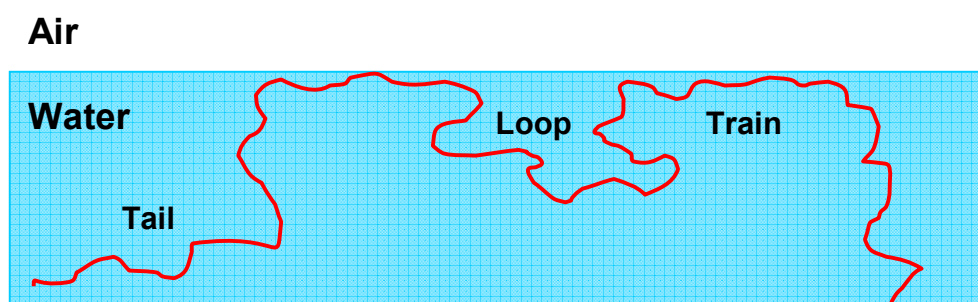
Figure 1.2.3.1: Illustration of the tail, loop, train conformation of an absorbed polymer

Recently, polymer brushes formed at the air-water interface by end capped PEO with hydrophobic groups have been investigated[32-34]. Modified PEO chains have been shown to be some of the most efficient non-ionic surfactants available. Several variations of PEO synthesized with hydrophobic end groups such as residues of alcohols, alkylphenols, esters, alkylamines and many other functional groups have been synthesized and proven to be highly surface active. However, the highest surface activity at the critical micelle concentration (CMC) at 293 K reported for PEO was obtained by incorporating either a fluorinated[34] or siloxane[32] terminal group. For example, the introduction of low molecular weight non-ionic fluorocarbon surfactants has been shown to reduce the surface tension of aqueous solutions to around 15 mN/m.

Surface layers of fluorinated alcohol groups as well as polymers of PEO functionalized with perfluoroalkyl end-caps have previously been investigated at an air-water interface[51]. Surface structure and organization was investigated using infrared reflectance spectroscopy by measuring the reflectance intensities of the C-F bond stretching motions in the end-cap attached to the PEO. These intensities could be used directly to give a direct comparison of the surface concentration with respect to the bulk concentration and therefore give a concentration versus depth profile. Results obtained in this experiment confirmed the theoretical assumption that the functionalized end-capped polymers were adsorbed more strongly to the interface and also therefore much more highly organized at the surface than the unfunctionalized equivalent PEO. Furthermore it was shown that PEO functionalized with perfluoroalkyl end groups are able to form a brush-like structure at the air-water interface (as described previously), particularly at high surface concentrations.

The surface behaviour of PEO functionalized with a perfluorodecanoyl end cap has also been investigated at both an air-water interface and a polymer-air interface. The PEO was functionalized at either one or both ends and studied as a spread film. In the case of the polymer-air interface the materials were analyzed by X-ray photoelectron spectroscopy (XPS). The surface energy of the fluorinated end group is considerably lower than that of the PEO polymer tail and as a result the end groups are adsorbed preferentially to the polymer-air interface. Analysis of the XPS results showed that the perfluorodecanoyl chain ends that adsorb to the polymer surface are relatively close-

packed leaving a zone just beneath the surface that is depleted of fluorine. Further investigations showed that the PEO samples with both ends capped were found to have a slightly higher surface affinity than PEO capped at one end and a slight effect of molecular weight on surface fluorine content was also observed. This led to the conclusion that the conformations of the adsorbed chains were brush-like in architecture with the amount of brush extension (chain stretching) scaling almost linearly with respect to the molecular weight of PEO. In the case of the air-water interface the materials were studied using polarized infrared reflectance spectroscopy. Analysis of the results showed that these functionalized PEO surfactants were highly surface active with good surface tethering strength and at concentrations above 2 mg ml^{-1} the surface tension of the interface was found to be as low as 13.6 mN/m at 293 K. Further analysis revealed that the molecular area per chain was only slightly lower for the PEO capped only at one end compared to that for the PEO with both ends capped. These results for the molecular area per chain led to the conclusion that for singly end capped PEO the chains form a brush configuration. The fact that there was only a slight increase in molecular area per chain for the doubly end capped PEO led to the conclusion that the PEO chains with both ends capped also form a brush conformation. Therefore only a small percentage form looped chains with both ends adsorbed to the surface.

More recently a study was carried out to investigate spread films of PEO end capped with alkane groups[52]. Using a Langmuir trough to compare the isotherms of pure PEO with those of the modified alkane capped PEO it was seen that the hydrophobic end groups have a dramatic effect on increasing the tethering strength of the polymeric material to the air-water interface under compression. Under increasing compression however it was found that, despite their hydrophobic ends, the polymer detached from the surface and was expelled back into the bulk solution. When trying to quantify the results from these experiments using polymer brush theory (scaling theory) an agreement between the theory and the experimental results could not be found. This was due to the inability of the theoretical model to account for adsorbed chain configurations (loops and trains from the loop-train-tail model of Jenkel and Rumbach[53]). Follow up investigations employed computer simulations of adsorbed polymer solutions of hydrophobically end capped PEO using scaling and mean field theory[54]. Using this computer simulation

technique they found that, at low grafting density, the adsorbed polymer could best be described as a two-dimensional semi-dilute solution rather than as a continuous layer as modeled by the polymer brush theory. As the grafting density is increased the monolayers become unstable due to the free end of the adsorbed polymers leading to the dissolution of the polymer into the bulk solvent. Grafting the chains to the interface and increasing the surface concentration leads to the formation of a stable polymer brush conformation.

1.3 Introduction to Dendrimers

1.3.1 Background

Traditional polymer chemistry has focused on linear polymers and these have been extensively studied and are now widely in use in everyday life. More recently it has been found that the properties of highly branched (hyperbranched) polymers can vary dramatically from the properties of the equivalent conventional linear polymers. Therefore the structure of these materials also has a great impact on the applications for which these polymers can be used. These dendrimers are a relatively new class of materials and are generally recognized as the fourth major class of macromolecular architecture. Many synthetic strategies have been reported in recent years (as well as older methods of copolymer synthesis), leading to a broad range of dendrimer types[55]:

1.3.2 Dendrimer Classifications

1. Random hyperbranched polymers – As the name suggests these polymers are randomly branched with no specific architecture[56, 57]. Generally synthesized from an AB_x monomer type where x is at least 2 and A will only react with B, some monomers will only undergo single A-B reactions leading to a linear section of polymer, other will undergo 2 or more A-B reactions to form branches and occasional intramolecular A-B reactions will lead to termination. As a result of these random terminations and the uncontrolled nature of the reactions these hyperbranched

polymers tend to have a relatively low molecular weight and high polydispersity. A typical example of this kind of structure is shown schematically in figure 1.3.2.1.
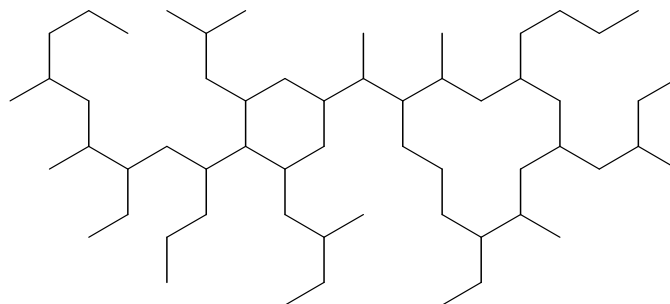
Figure 1.3.2.1: Schematic representation of a randomly hyperbranched polymer
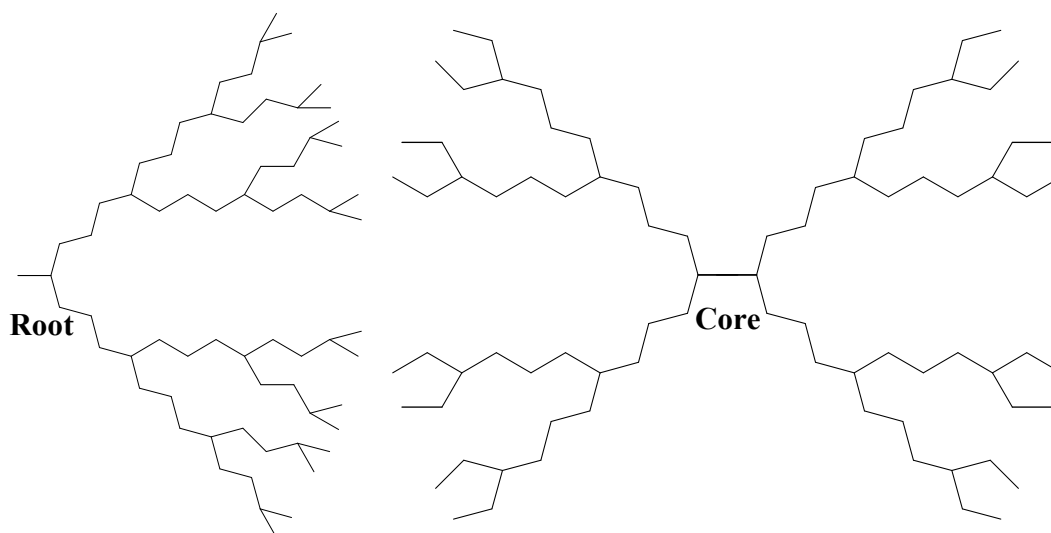
Figure 1.3.2.2: Schematic representation of a 4th generation dendron and a 3rd generation dendrimer

2. Dendrons – The word 'dendron' is derived from the Greek word meaning 'tree-like' and the phrase was first used to describe these molecules by Tomalia et al[58] in 1984 with reference to their work on poly(amidoamide) or (PAMAM) dendrimers. Dendrons are highly organized branched tree-like structures attached to a root molecule. The branching of these dendrons is controlled during synthesis and this leads to highly organized structures with a polydispersity generally between 1 and

1.05. A typical example of this kind of structure is shown schematically in the rooted molecule in figure 1.3.2.2.

3. Dendrimers – Identical to dendrons in almost every aspect. Dendrimers are highly organized structures branching from a central core molecule. Unlike dendrons however, these dendrimers have a spherical structure rather than a tree-like one. Dendrons and dendrimers are given generation numbers corresponding to the number of branching points in the structure. A typical example of this kind of structure is shown schematically in the cored molecule in figure 1.3.2.2.

4. Dendrigraft polymers – The most recently discovered (in 1991 by two independent groups[59, 60]) and least extensively studied form of hyperbranched polymers. These dendrigraft polymers exhibit properties between the two extremes of the disordered randomly hyperbranched polymers and the highly ordered dendrons and dendrimers. The basic structure of dendrigraft polymers is a polymer backbone containing reactive groups upon which a dendron-like side chain can be grafted. Analogous to dendrons and dendrimers; each grafting step is referred to as a generation. A typical example of this kind of structure is shown schematically in figure 1.3.2.3.
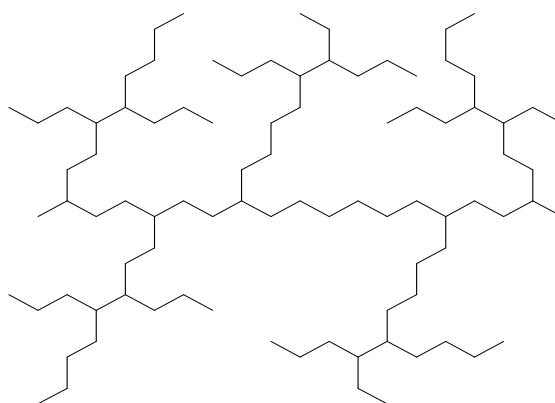
Figure 1.3.2.3: Schematic representation of a 3rd generation dendrigraft polymer

The addition of a dendritic head group molecule to a linear polymer can drastically alter the properties of the original polymer.

1.4 Project Aims

1.4.1 Theory

A diblock copolymer of the type shown in figure 1.4.1.1 will have some adsorption towards an air-water surface due to the hydrophobic nature of the fluorocarbon species. Previous experiments carried out by other groups at Durham University[11] have shown that functionalizing PEO with fluorocarbon groups can lead to a remarkably large increase in adsorption compared to that of PEO alone and evidence has been provided for the formation of brush-like structures at an air/water interface.
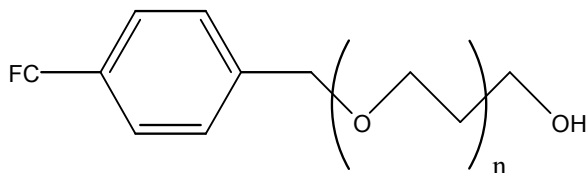
Figure 1.4.1.1: A diblock copolymer of Poly(ethylene oxide) with a hydrophobic
linear head group
NB: FC = a fluorocarbon chain such as CF$_3$ or C$_2$F$_5$ etc

However the maximum size of the fluorocarbon unit is limited by its solubility in organic solvents. In order to try and overcome this problem a new synthetic strategy has been employed wherein the PEO chain is functionalized using a dendrimer, enabling multiple functional groups to be attached to a single polymer chain. See Figure 1.4.1.2

The attachment of many hydrophobic fluorocarbon chains[61] to a single poly (ethylene oxide) chain should result in enhancement of the extent of adsorption beyond the levels that have previously been possible for this class of materials, and could lead to polymer brush formation at the air - water surface.
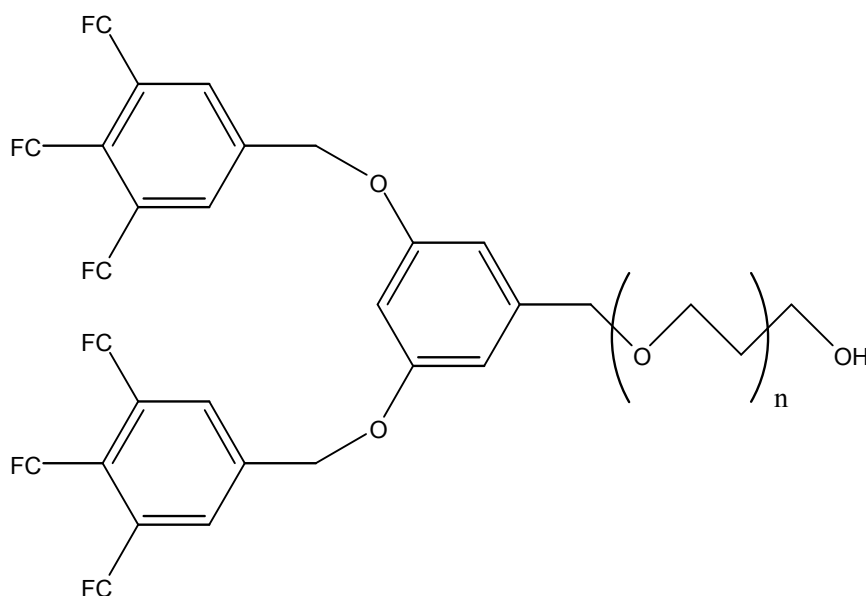
Figure 1.4.1.2: Poly(ethylene oxide) chain with a hydrophobic dendritic head group

1.4.2 Project Design

The aim of this project is to investigate surface organization and dynamics of a dendritic fluorocarbon end capped poly(ethylene oxide) at an air - water interface and to employ molecular dynamics techniques to simulate and predict the results obtained from experimental methods. This project gains inspiration from previous work done on similar linear fluorocarbon materials at the University of Durham[11]. As mentioned previously it has been shown that functionalizing PEO with fluorocarbon groups can lead to a remarkably large increase in adsorption, but this effect is greatly diminished with increasing PEO molecular weight. The question remains that if we are able to add further fluorocarbon units to a single PEO chain[62-64], are we able to tether a chain of much higher molecular weight to an air – water interface?

In an attempt to answer this question PEO chains in excess of 10,000 g mol^{-1} will be synthesized with dendritic fluorocarbon head groups. The generation of dendrimer will be varied along with the number of fluorocarbon groups attached to each generation and the size of the fluorocarbon groups (CF_3 and C_8F_{17} groups). With this variation we can

investigate what numbers of fluorocarbon species are necessary to tether PEO chains of higher molecular weights to an air – water interface. Using neutron reflectivity measurements we can study the organization of these polymers at the air – water interface and by varying the concentration of the dendritic PEO in the system we can follow the change in structure from 'mushroom' conformation at lower concentrations, through to 'brush' formation at high concentrations, which is of huge interest in this project. Using surface tensiometry isotherms can give an understanding of the density and packing at the surface and neutron reflectivity can resolve the precise location of the dendritic head group and the polymer chain backbone and an exact structural organization can be inferred.

Computer simulation techniques will be employed to simulate the experimental conditions as accurately as possible. Molecular dynamic simulations[65, 66] will be used to calculate and observe changes in structure and motion of the polymer molecules in a simulated water solvent, eventually leading to the simulation of a layer of amphiphilic polymer molecules at a model air – water interface. The current model fitting procedures employed for interpreting neutron reflectivity spectra are highly time consuming and have a fundamental flaw in so far as there are many different results that can match any given spectrum, making it very difficult to be completely confident in derived results. Using the data produced by computer simulations it is possible to predict spectra for neutron reflectivity data for any simulated system. Therefore it is possible to construct a simulation system directly comparable to that used in neutron reflectivity experiments and achieve a direct comparison between simulation and experimental data, giving more reliability to the results obtained. Similarly it is always questionable whether a computer simulated system is a true representation of a real chemical system. Neutron reflectivity presents a unique opportunity to test the validity of these simulations and each experimental method can contribute to the validation of the other.

1.4.3 Project Outline

There are several disciplines and techniques that will be studied and employed throughout the work carried out in this thesis. These will be discussed in detail in the chapters to follow.

Chapter 2 will describe details of the theoretical background for the synthetic methods used to produce dendritic functionalized PEO molecules, as well as describing the physical properties of these kinds of molecule, the theory and usage of computer simulation methods and the theoretical background and practical application on neutron reflectometry.

Chapter 3 will describe, in detail, all of the methods employed during the synthesis of the materials used in this project. These methods include anionic polymerization, convergent dendrimer synthesis, various types of Williamson coupling reactions, catalyzed trans-esterification and a detailed description of the work-up and purification methods employed. There is also a discussion of the analytical methods used to characterize the products of these syntheses.

Chapter 4 will show the results of various experimental techniques carried out on the materials synthesized in this project, including surface tension measurements and neutron reflectometry and will discuss conclusions drawn from these results.

Chapter 5 will describe in detail the computer simulation methods employed in this project and how the computer models were constructed to be able to draw direct comparison with experimental results.

1.5 References

[1] E. S. Efrem, *Polymers: A Bibilography with Indexes*, Nova Science Publishers Inc (United States), **2002**.

[2] C. Vasile and G. E. E. Zaikov, *Focus on Natural And Synthetic Polymer Science*, Nova Science Pub Inc, **2006.**

[3] W. Arguelles-Monal, *Natural and Synthetic Polymers: Challenges and Perspectives*, John Wiley & Sons Inc, **2001**.

[4] N. Bikales, *Water-soluble Synthetic Polymers*, Plenum: New York, **1973**.

[5] C. A. Finch, *Chemistry and Technology of Water-soluble Polymers*, Plenum: New York, **1973**.

[6] Y. L. Meltzer, *Water-soluble Polymers: Recent developments*, Noyes Data Corp.: Park Ridge, **1979**.

[7] G. A. Stahl and D. N. Schulz, *Water-soluble Polymers for petroleum recovery*, Plenum: New York, **1988**.

[8] W. M. Kulicke, R. Kniewske and J. Klein, *Prog. Poly. Sci.* **1982**, *8*, 373-468.

[9] B.-K. Cho, A. Jain, S. M. Gruner and U. Wiesner, *Science* **2004**, *305*, 1598-1601.

[10] B. Lin, P. T. Boinske and J. W. Halley, *J. Chem. Phys* **1996**, *105*, 1668-1681.

[11] R. W. Richards and J. Sarica, *Langmuir* **2003**, *19*, 7768-7777.

[12] J. Scheirs, *Modern Fluoropolymers: High Performance Polymers for Diverse Applications*, John Wiley & Sons, **1997**.

[13] K. Devanand and J. C. Selser, *Macromolecules* **1991**, *24*, 5943-5947.

[14] P. Molyneux, *Water-soluble Synthetic Polymers; Properties and uses*, CRC Press: Boca Raton, FL, **1983**.

[15] A. Matsuyama and F. Tanaka, *Phys. Rev. Lett.* **1990**, *65*, 341-344.

[16] F. B. C. Z. Roslaniec, *Block Copolymers*, CRC, **2000**.

[17] D. Chao, S. Itsuno and K. Ito, *Polymer Journal* **1991**, *23*, 1045-1052.

[18] J. K. Cox, K. Yu, B. Constantine, A. Eisenberg and R. B. Lennox, *Langmuir* **1999**, *15*, 7714-7718.

[19] E. P. K. Currie, F. A. M. Leermakers, M. A. C. Stuart and G. J. Fleer, *Macromolecules* **1999**, *32*, 487-498.

[20] M. S. Kent, *Macromol. Rapid Commun* **2000**, *21*, 243-270.

[21] K. Senshu, M. Kobayashi, N. Ikawa, S. Yamashita, A. Hirao and S. Nakahama, *Langmuir* **1999**, *15*, 1763-1769.

[22] P. Alexandridis, *Amphiphilic Block Copolymers: Self-Assembly And Applications*, Elsevier Science & Technology (Netherlands), **2000**.

[23] H. Kong, C. Gao and D. Yan, *J. Mater. Chem.* **2004**, *14*, 1401-1405.

[24] A. Breitenbach, K. F. Pistel and T. Kissel, *Polymer* **2000**, *41*, 4781-4792.

[25] S. H. Chui, S. J. Rowan, S. J. Cantrill, P. T. Glink, R. L. Garrall and J. F. Stoddart, *Tetrahedron* **2000**, *58*, 807-811.

[26] H. Hand and M. C. Williams, *Chem. Eng. Sci* **1973**, *23*, 63-69.

[27] A. Malzert, F. Boury, P. Sauliner, J. P. Beniot and J. E. Proust, *Langmuir* **2000**, *16*, 1861-1867.

[28] R. Tadmor, J. Janik, J. Klein and L. J. Fetters, *Phys. Rev. Lett.* **2003**, *91*, 115503-115507.

[29] J. Klein, *Journal of Physics: Condensed Matter* **2000**, *12*, A19-A27.

[30] V. N. Kalashnikov and A. M. Kudin, *Nature* **1973**, *242*, 92-99.

[31] I. Gitsov, K. L. Wooley and J. M. J. Frechet, *Angew. Chem. Int. Ed. Eng* **1992**, *31*, 1200-1202.

[32] M. J. Owen, *Siloxane Polymer*, Prentice Hall, Englewood Cliffs, NJ, **1993**.

[33] M. J. Schick, *Non-ionic Surfactants*, Marcel Dekker, New York, **1967**.

[34] C. Selve, J. C. Ravey, M. J. Stebe, C. E. Moudjahid, E. L. Moumni and J. J. Delpuech, *Tetrahedron* **1991**, *47*, 411-413.

[35] E. J. Clayfield and E. C. Lumb, *J. Colloid Interface Sci* **1966**, *22*, 269-284.

[36] G. Xu, S. S. Rane, C. A. Helfer, W. L. Mattice and C. Pugh, *Modelling Simul. Mater. Sci. Eng* **2004**, *12*, S59-S71.

[37] G. D. Smith, D. Bedrov and O. Borodin, *Communication to JACS editor* **2000**.

[38] A. Halperin, M. Tirrell and T. P. Lodge, *Adv. Polym. Sci* **1992**, *100*, 31-38.

[39] I. Szeilfer and M. A. Carignano, *Adv. in Chem. Phys.* **1996**, *44*, 165-170.

[40] P. G. de Gennes, *Macromolecules* **1980**, *13*, 1069-1075.

[41] F. T. Kiff, R. W. RIchards, H. L. Thompson, D. G. Bucknall and J. R. P. Webster, *J. Phys. II France* **1997**, *7*, 1871-1891.

[42] I. Pirma, *Polymeric Surfactants*, New York, **1992**.

[43] J. A. Henderson, R. W. Richards and J. Penfold, *Macromolecules* **1993**, *26*, 4591-4600.

[44] Q. R. Huang and C. H. Wang, *Langmuir* **1996**, *12*, 2679-2683.

[45] A. F. Miller, R. W. Richards and J. r. P. Webster, *Macromolecules* **2001**, *34*, 8361-8369.

[46] S. K. Peace, R. W. Richards and N. Williams, *Langmuir* **1998**, *14*, 667-668.

[47] B. B. Sauer and H. Yu, *Macromolecules* **1989**, *22*, 786-791.

[48] M. Kawaguchi, S. Komatsu, M. Matsuzumi and A. J. Takahashi, *Colloid Interface Sci.* **1984**, *102*, 356-363.

[49] J. R. Lu, J. Penfold, R. W. Richards, T. J. Su and R. K. Thomas, *Polymer* **1996**, *37*, 109-114.

[50] A. R. Rennie, R. J. Crawford, E. M. Lee, R. K. Thomas, T. L. Crowley, S. Roberts, M. S. Qureshi and R. W. Richards, *Macromolecules* **1989**, *22*, 3475.

[51] Y. Ren, M. S. Shoichet, T. J. McCarthy, H. D. Stidham and S. L. Hsu, *Macromolecules* **1995**, *28*, 358-365.

[52] C. Barentin, P. Muller and J. F. Joanny, *Macromolecules* **1998**, *31*, 2198-2211.

[53] E. Jenkel and B. Rumbach, *Elektrochem.* **1951**, *55*, 612-618.

[54] C. Barentin and J. F. Joanny, *Langmuir* **1999**, *15*, 1802-1811.

[55] D. A. Tomalia, *Prog. Poly. Sci.* **2005**, *30*, 294-324.

[56] P. A. Gunatillake, G. Odian and D. A. Tomalia, *Macromolecules* **1988**, *21*, 1556-1562.

[57] Y. H. Kim and O. W. Webster, *Polym. Prepr.* **1988**, *29*, 310-311.

[58] D. A. Tomalia, J. R. Dewald, M. J. Hall, S. J. Martin and P. B. Smith in *Vol.* Society of polymer science, Kyoto, Japan, **1984**, 65-69.

[59] M. Gauthier and M. Moller, *Macromolecules* **1991**, *24*, 4548-4553.

[60] D. A. Tomalia, D. M. Hedstrand and M. S. Ferrito, *Macromolecules* **1991**, *24*, 1435-1438.

[61] A. Hirao, G. Koide and K. Sugiyama, *Macromolecules* **2002**, *35*, 7642-7651.

[62] E. W. Buhleier, W. Wehner and F. Vogtl, *Synthesis* **1978**, 155-162.

[63] C. J. Hawker and J. M. J. Frechet, *J. Am. Chem. Soc* **1990**, *113*, 4252-4261.

[64] D. A. Tomalia, *Polym. J.* **1985**, *17*, 117-132.

[65] P. M. Anderson and M. R. Wilson, *J. Chem. Phys* **2004**, *121*, 8503-8510.

[66] E. Khurana, S. O. Nielsen and M. L. Klein, *J. Phys. Chem. B.* **2006**, *110*, 22136-22142.

Chapter Two: Theory

2.1 Synthesis

Polymeric materials are of huge industrial importance and are used in many everyday objects such as clothing fibres, plastic furniture, housing for electronic equipment and countless other manufactured goods. Polymers are also being developed for other advanced technologies in medicine such as artificial joints and targeted drug delivery as well as other technologies like optical devices etc[1-4]. The commercial demand for new polymeric materials with unique topologies and improved properties is constant and therefore the need to design and manipulate synthesis routes for well defined polymers is of great importance to both industrial and academic institutes. Water Soluble Polymers in particular have provided a wide range of functionalities and benefits to a variety of applications. Water Soluble Polymers are easy to work with, and are often used as thickeners, stabilizers, film formers, rheology modifiers, emulsifiers, lubricity aids and conditioners, which make them essential ingredients in many products including detergents and household products, food, paints and coatings, personal care, pharmaceuticals, and other speciality applications[5, 6].

Polymeric materials are separated into two classes and named according to their method of preparation. The synthesis of the first class involves the loss of a small molecule, usually water or a similar fragment, with each addition of a monomer unit. Polymers built up in this way are known as 'condensation polymers'. This method is generally not preferred due to the presence of the by-product that would subsequently need to be separated from the final product. The second (and more widely produced) class is prepared using an initiating species, which can either be an ionic or radical species. Monomers can then react sequentially with the initiating species, reforming the active site at the terminal end each time. Polymers built up in this way are known as 'addition polymers'. This method has the obvious advantage of forming no bi-products during the reaction and in most cases where the rate of initiation is faster than the rate of propagation: the polymers will grow at an equal rate and lead to all chain lengths being almost the same (low polydispersity). One of the most useful forms of addition

polymerization involves a propagating species that is stable and is regenerated with the addition of each monomer. Provided that there are no impurities present in the system it is not necessary for the rate of initiation to be greater than the rate of propagation and the reaction will continue until all available monomer units are converted into polymeric material. This 'living' polymerization will only come to an end by exhaustion of all monomer molecules or by the addition of a terminating species. As a result, simply controlling the monomer to initiator ratio allows precise engineering of the molecular weight of the final polymer product.

2.1.1 Addition Polymerization Techniques

There are 3 different mechanisms by which a living addition polymerization can be achieved. The first method is known as 'free radical' polymerization[7-12] and is still widely used in industry to make polymers such as poly(ethylene).
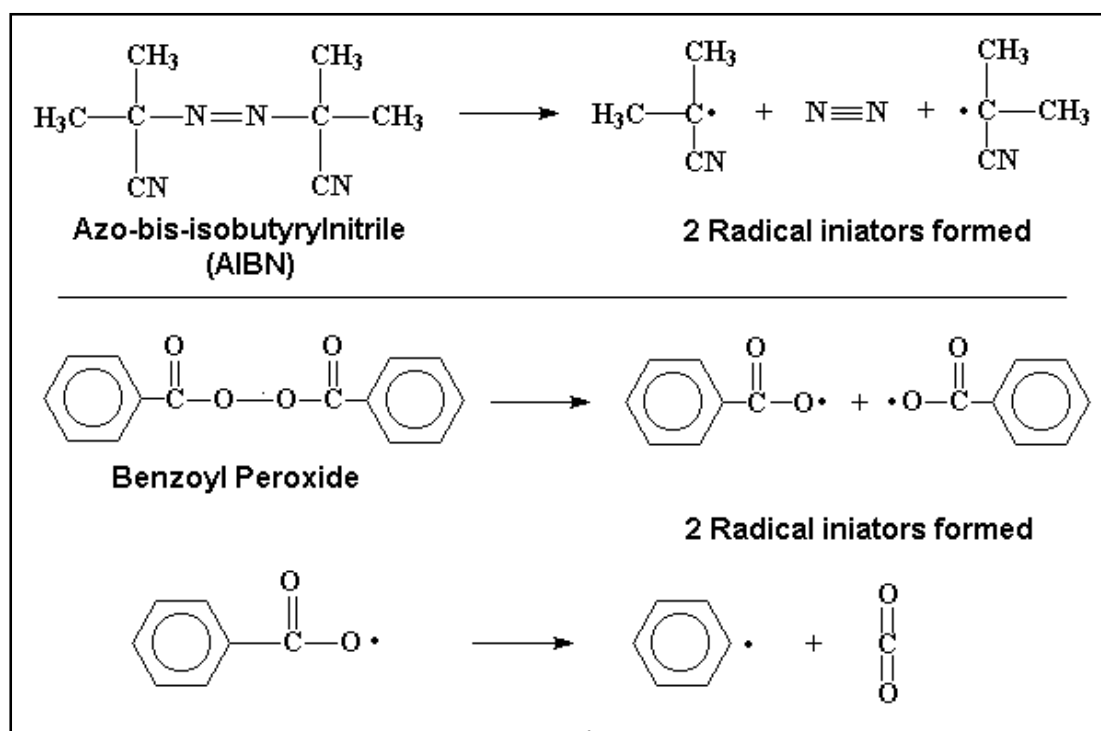
Figure 2.1.1.1: Examples of free radical initiators

The most common types of radical initiator are peroxides and azo compounds. These groups decompose to form two radical initiator species.

Propagation of free radical polymerization is very fast for linear monomeric species due to the instability of the radical group, making this method ideal for commercial production of polymers on a large scale[10, 13].
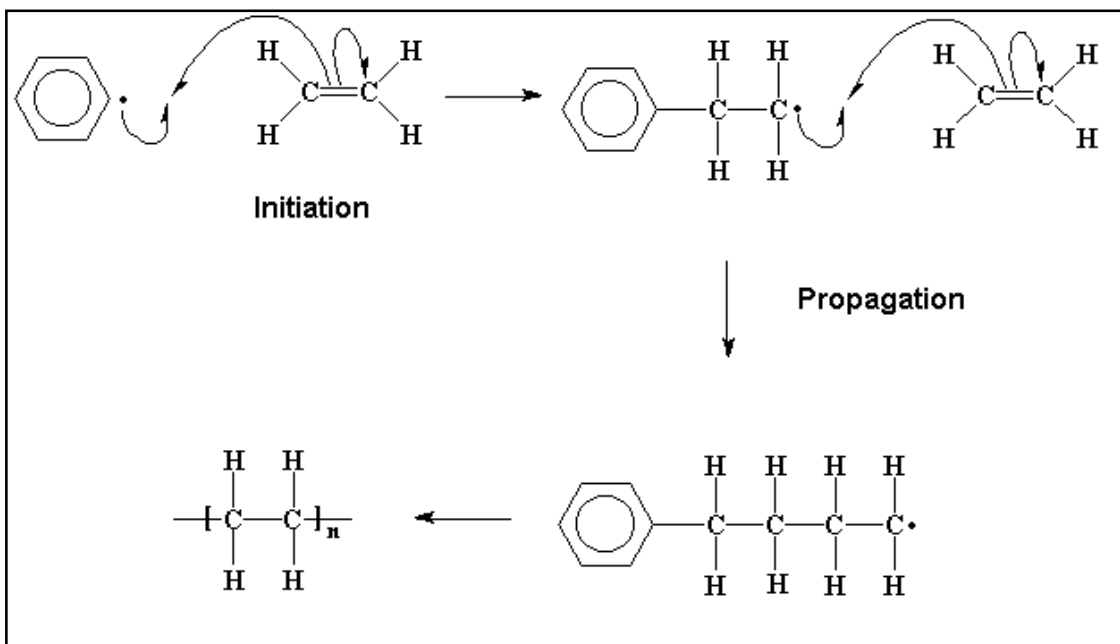
Figure 2.1.1.2: Initiation and propagation of a free radical polymerization

However, the presence of any substituents on the monomer can lead to resonance-stabilization of the chain end radical and will therefore inhibit the propagation rate, making this method for polymerization unsuitable for the production of many important polymers.

The second method is known as "cationic" polymerization[14] and is primarily used in industry to make vinyl polymers and the largest commercial use of this method is to make poly(isobutylene). The initiating species of this cationic vinyl polymerization is a cation (typically aluminum trichloride, or $AlCl_3$) that will react with (and break) the double bond of the isobutylene monomer to form a bond between the initiator and the monomer. This will also regenerate a new, larger, carbocation and the process can then repeat until all monomer units are exhausted. The number of substituents on the monomer

has little significant effect on the propagation rate for cationic vinyl polymerization. However, the presence of electron withdrawing groups will inhibit the initiation and propagation processes.
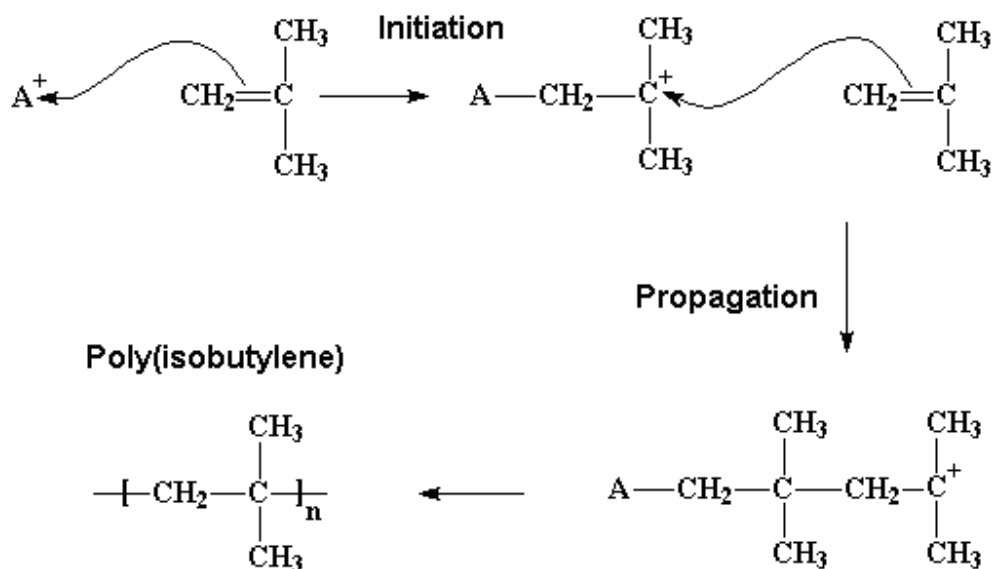
Figure 2.1.1.3: Cationic vinyl polymerization

The third and final method is known as "anionic" polymerization[15, 16] and can be used to make many industrial important polymers such as poly(styrene), poly(ethylene oxide), poly(methyl methacrylate) etc. The initiating species in this case is a carbanion, which is an organo-metallic molecule with a negative charge induced on a carbon atom by a positive metal ion (a typical example is butyl lithium, which is used in industry to make synthetic natural rubber).

Monomers containing electron-withdrawing species adjacent to the **C=C** double bond with the metal ion attached are ideally suited to this method of polymerization. A general example of this is shown in figure 2.1.1.4, where X is an electron-withdrawing group. Monomers used in industry are typically dienes, methacrylates, styrenes or cyclic molecules like ethylene oxide.

The initiation step involves nucleophilic attack by the negatively charged carbon from the organo-metallic initiator on the carbon adjacent to the electron-withdrawing

group of the monomer. A single bond is formed between the two carbons and the double bond is opened to form a new negative charge on the terminal chain carbon. This process can then repeat until no more monomer units are present to form a polymer of a specific molecular weight (controlled simply by the initiator to monomer ratio) and low polydispersity.

Figure 2.1.1.4: Initiation and Propagation of an anionic polymerization

However, in order to achieve a polymer of a specific molecular weight and precise polydispersity it is essential that the initiation step is a faster process than the propagation step. This can be achieved be altering various factors in the synthesis, including the solvent used and the type of initiator employed. Polar solvents are ideal for this type of reaction as they help to solvate the metal ion and keep it from aggregating back to the initiating species, therefore maximizing the efficiency of the nucleophilic initiator. Other solvating species can be employed in the reaction to ensure dissociation of the metal ion from the initiator. Typical examples are crown ethers e.g. 15-Crown-5 is ideal for solvating sodium ions and 18-Crown-6 for potassium ions.

As with all living polymerizations the propagating species is regenerated after the addition of each monomer until either an impurity in the system or a specific termination molecule is added. The most common impurity in a system of this type is a polar solvent (water being the most obvious example) and this can cause premature termination and lead to poor polydispersity and lower molecular weight than required. Therefore it is important to keep all such systems dry and preferably under vacuum to minimize the presence of impurities. Once the polymerization has been allowed to run to exhaustion a termination species with specific functional groups can be added to produce polymers with desired properties at the terminal end[17, 18]. This process is often referred to as 'end-capping' and is often used to introduce specific properties such as hydrophobicity etc.

2.1.2 End Functionalization of Polymers

As stated in the previous section it is possible to grow a polymer in a living polymerization and introduce a terminating species with the desired properties and therefore synthesize a polymer with one property dominant along the chain and a contrasting property associated with the terminal end[19, 20]. However, it is difficult to ensure that 100% of all propagating chains are terminated by the desired end group. An excess of the terminal group is required to ensure an acceptable yield of functionalized polymers and some of the chains will still remain unfunctionalized.

A more efficient method for introducing functionalization to the end of a polymer chain of this type is to begin with an initiator that exhibits the desired properties of the

terminal end of the product. Using this method 100% (so long as impurities are minimized) of the chains will have the desired end terminal, the propagation can then simply be stopped by addition of a simple termination molecule such as water or hydrochloric acid etc. The disadvantage to the method is that introducing functionalization to the initiating species may alter the capability of the molecule to act as an initiator for the polymerization.

2.1.3 Dendrimer Synthesis

There are two general methods of synthesizing dendrimers; divergent and convergent[17, 21-23]. The divergent method begins with a core molecule and is constructed one layer, or generation, at a time. In contrast, for the convergent method the dendrimer is synthesized by beginning with the outer arms of the molecule and attaching them together and terminating at the core. Both methods follow stepwise processes and must be worked up, purified and the functional groups changed or replaced between every single step.
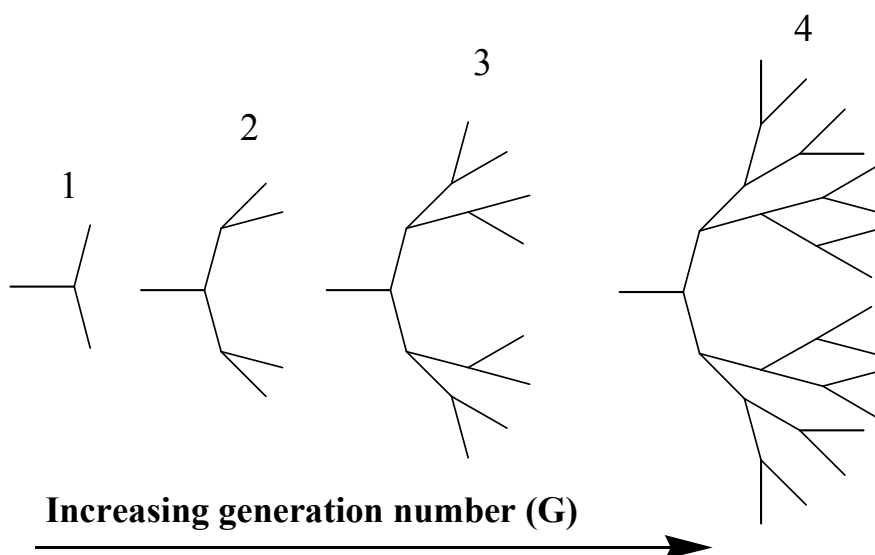
Figure 2.1.3.1: Schematic diagram showing divergent dendrimer synthesis
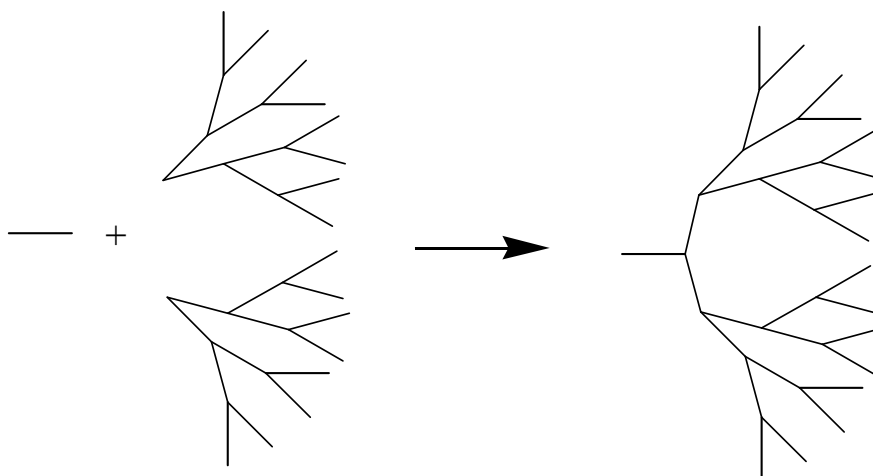
Figure 2.1.3.2: Schematic showing convergent dendrimer synthesis

The transformation of the functional groups between each step is especially important for the divergent method of dendrimer synthesis. It is necessary to ensure that the surface groups are initially unreactive or protected and only converted to a reactive group once the next stage of the reaction is underway. If the surface groups were simply left to react with any monomer in the system then the product would be a polydisperse hyperbranched polymer. It is also necessary to keep strict control of the reaction conditions during dendrimer synthesis; simply allowing the dendrimer to grow until no more monomer can reach the reactive sites due to steric hindrance will also result in a polydisperse product. As demonstrated in the cartoons in the figures above steric hindrance soon becomes an issue when synthesizing dendrimers. The maximum generation number can be increased significantly by increasing the size of the core molecule or the spacing between monomers but there is still an upper limit to how many generations can be added to a dendrimer before there is simply not enough room to add any more.

2.1.4 Dendrimer properties

The method by which dendrimer molecules are synthesized leads to a precise and monodisperse spherical structure, which gives dendrimer molecules interesting and unique properties. The structure of a dendrimer can lead to two separate chemical

environments within the same molecule; the interior of the molecule is largely unaffected by the exterior environment due to the tightly packed exterior shell and the surface of the dendrimer can be functionalized with almost any chemical group during the termination step of the synthesis. This duel chemical environment and the existence of voids in the dendrimer interior has led to many actual and potential applications of dendrimer molecules as hosts for transportation of small molecules in biological systems, as catalysts (due to the large surface area and ease of recovery), DNA transfecting agents and as quantum dots etc.

2.2 Introduction to Computational Simulations

2.2.1 Background

Rapid advances in the field of computer technology have been matched by the speed of development in computer simulation methods over recent years[24]. In the last few years increases in the speed, memory size and the flexibility of computers has been exponential and this has opened-up a vast number of new possibilities for studying scientific and engineering problems[25]. This has enabled the study of many new ideas and theories on a scale never seen before[26]. However, the complexity of problems studied and the accuracy of the results required is still so demanding that computing resources available are hardly able to keep up with the demand.

Computer simulations play an increasingly important role in modern scientific research and have many advantages over experimental laboratory research[27]. The computer simulation of an experimental system is essentially a numerical experiment that differs from laboratory work in a number of crucial ways[28]. In a computer simulation the system can be designed with the freedom to choose both the type of model we wish to study and the environmental conditions (temperature, pressure etc.) under which we wish to study it, including conditions that are extremely difficult to produce in a laboratory experiment. This allows us to investigate an enormous range of phenomena and gives a tremendous amount of flexibility in investigating the understanding of such systems. However, it must be recognized that there are also severe limitations to these computer

simulations. These limitations arise from factors such as finite simulation time, finite system size and so forth, and are reflected in the accuracy of the results obtained from such an experiment.

2.2.2 Simulation Methodology

For any atomistic computer simulation study a basic methodology is followed to build up the system:

- Construction of a single molecule, containing all atoms ('atomistic' model).

- Construction of a bulk system, this can either be a replication of the single molecule to form a bulk phase or the construction of solvent molecules in which to place the molecule.

- Simplifying the model so that a larger system can be investigated while avoiding the need for huge amounts of computer time.

- Using the output from the simulation to calculate data for real experimental values and to predict properties displayed by the real system.

2.2.3 Simulation Models

Chemical systems are generally modeled by analyzing the inter-particle interactions between nearby atoms in the system. For smaller systems containing relatively few atoms, such as a single polymer molecule or many smaller molecules, say a solvent like water, it is possible to simulate the system atomistically; whereby a single atom in the simulation represents each atom in the real molecule. For this type of simulation it is possible to explore a few thousand atoms over a timescale of several nanoseconds and therefore it is possible to observe phenomena such as phase transitions and molecular motion[29-31].

Larger chemical systems that contain multiple large molecules or larger molecules within a simulated solvent will require a lot more computer time and require a system that can simplify the model to cut down simulation time. A simple way of reducing the number of atoms in the system is to fuse any hydrogen atoms into the heavier atoms to which they are attached. This 'united atom' approximation can reduce the computational time dramatically in organic systems where the hydrogen atom is very common and in the case of a molecule like methane (CH_4) there are 5 atoms represented by a single particle[32-34]. However, realistically the number of atoms in the system is reduced less significantly to around one third of the original number as the most common sites to be modeled are things like CH_2 etc.

In polymeric systems it is often essential to reduce the number of individual particles in the simulation down even further in order to achieve a system that can be modeled on a realistic time-scale. The 'coarse graining' method of molecular representation is used and can represent sections of a polymer, small molecules and groups of solvent molecules as single particle sites. A typical example would be to represent a single repeat unit of PEO (-CH_2-CH_2-O-) as a single site and therefore represent the whole polymer as a chain of beads or hard spheres with potentials and interactions representative of the sum of the constituent parts. Another example would be to take a number of water molecules and represent them as a single particle, coarse graining 3 water molecules down to a single site would reduce the number of atoms in the system 12-fold by representing 12 atoms as a single particle.

Further approximations made in the simulation of large bulk systems include 'periodic boundary conditions' and 'non-bonded cutoffs' which are explained later. Using all of these methods to lower the number of simulation sites it is possible to simulate a system of hundreds of thousands of atoms over a timescale equivalent to hundreds of nanoseconds[33-35].

2.2.4 Force Fields

In order to model a molecule we must have a data set that describes how the different parts of the model will interact with one another. A force field is one way of

doing this and is a function that describes the energy potential of interacting particles. There have been many different force fields developed for a vast range of systems but since all the work to be carried out in this project involves polymers in a liquid phase then the *Optimized Potentials for Liquid Simulation – All Atom*, or OPLS-AA[35, 36], force field is the ideal energy potential for our systems. The parameters contained within these force fields are constantly tested and updated. New parameters for specific interactions are developed by various research groups and there are newer versions of the same force field now available such as the OPLS-2001 force field, among many others[37-45].

2.2.4.1 OPLS-AA Force Field

The OPLS-AA force field[35, 39, 45-48] contains the five fundamental interaction types that exist between particles in the real world. The energies of these five interactions make up partial contributions towards the total energy of the system and are given in the following equation 2.2.4.1.1:

$$E_{Total} = E_{Str} + E_{bend} + E_{Tor} + E_{Elec} + E_{Van} \qquad \text{Equation 2.2.4.1.1}$$

Where E_{Total} is the sum of all interaction energies, E_{Str} is the sum of all the bond-stretching energies, E_{Bend} is the sum of all the bond angle-bending energies, E_{Tor} is the sum of all the torsional energies, E_{Elec} is the sum of all the electrostatic energies and E_{Van} is the sum of all the Van Der Waals interaction energies.

2.2.4.2 Definition OPLS-AA Components

The bond-stretching term is defined in terms of a harmonic oscillator with the bond between any two atoms modeled as an ideal spring[49]. Although this simple spring model is rather crude the results obtained give reasonable agreement with experimental values and a more complicated model is not necessary for the purposes of this project.
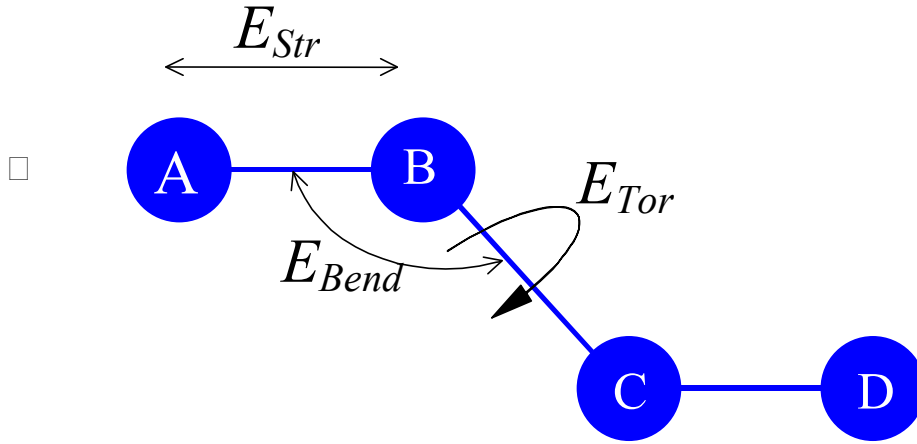
Figure 2.2.4.2.1: Diagram to show mechanism of interaction terms

The energy contribution from the bond stretching in a harmonic oscillator model is given by equation 2.2.4.2.2:

$$E_{Str} = \sum_{bonds} k_s (R_{ab} - R_0)^2$$

Equation 2.2.4.2.2

Where k_s is the spring force constant, R_{ab} is the vector along the bond between atoms a and b at any given time and R_0 is the unperturbed bond length between atoms a and b

The bond angle-bending term is defined in an analogous way to the bond-stretching term, where the energy variation with the bending of an A-B-C angle (as shown in figure 2.2.4.2.1) is found by using a harmonic potential[46]. The energy function is given by equation 2.2.4.2.3:

$$E_{Bend} = \sum_{angles} k_b (\theta_{ab} - \theta_0)^2$$

Equation 2.2.4.2.3

Where k_b is the spring force constant, θ_{ab} is the A-B-C bond angle at any given time and θ_0 is the unperturbed A-B-C bond angle.

The torsional energy function gives the variation in energy as the dihedral angle of an A-B-C-D bond is altered (see figure 2.2.4.2.1). The energy function for such a dihedral rotation is given by equation 2.2.4.2.4:

$$E_{Tor} = \sum_{dihedrals} \frac{V_1}{2}(1+\cos\phi) + \frac{V_2}{2}(1+\cos(2\phi)) + \frac{V_3}{2}(1+\cos(3\phi)) + \frac{V_4}{2}(1+\cos(4\phi))$$

Equation 2.2.4.2.4

Where V_1, V_2, V_3 and V_4 are force constants that are specific to a particular A-B-C-D arrangement of atoms and ϕ is the A-B-C-D dihedral angle at any given time.

The electrostatic term is primarily necessary for modeling systems with charged particles (i.e. ionic components). However, it remains an extremely important component for modeling systems consisting of atoms with varying electronegativities and contributes a large amount to the total energy of the system. These electrostatic contributions are given in terms of a Coulomb potential shown in equation 2.2.4.2.5.

$$E_{Elec} = \sum_{a=1} \sum_{b=a+1} \frac{q_a q_b}{4\pi\varepsilon_0 R_{ab}}$$

Equation 2.2.4.2.5

Where q_a is the electrostatic charge associated with atom a, q_b is the electrostatic charge associated with atom b, ε_0 is the coulombic charge and R_{ab} is the distance between atoms a and b at any given time.

The Van der Waals interactions are represented using a Lennard-Jones potential[50], which has many forms depending on the system to be modeled (an example is given in figure 2.2.4.2.2). One of the most common forms is given in equation 2.2.4.2.6:

$$E_{Van} = \sum_{a=1} \sum_{b=a+1} 4\varepsilon_{ab} \left(\frac{\sigma_{ab}^{12}}{R_{ab}^{12}} - \frac{\sigma_{ab}^{6}}{R_{ab}^{6}} \right)$$

Equation 2.2.4.2.6

Where ε_{ab} is the energy well depth, σ_{ab} is the cross-over point (minimum A-B distance where the potential equals zero) and R_{ab} is the distance between atoms a and b at any given time
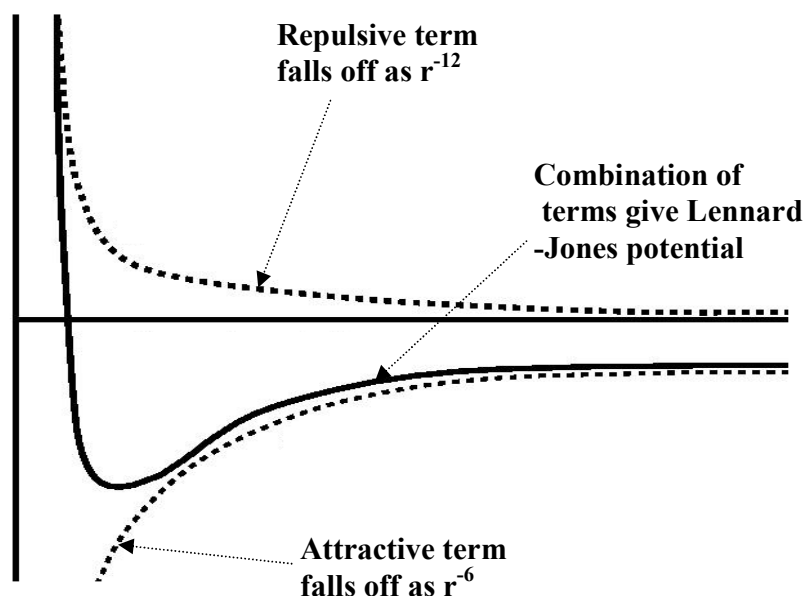
Figure 2.2.4.2.2: Diagram showing the general form of a Lennard-Jones potential

2.2.5 Molecular Dynamics

The starting configuration of a system to be modeled is generally determined by a Boltzmann distribution of energies consistent with the temperature of the system. The molecular dynamics[51-53] (MD) method of simulation calculates the trajectories of all the particles in the system and evaluates the forces exerted on each atom from interactions with all surrounding atoms[53-55]. This information is then transferred to the atom in question as an adjustment in motion (velocity and acceleration) according to Newton's laws of motion. This results in a time-dependent simulation of the system as each atom experiences changes in position, velocity and acceleration from interactions with all surrounding atoms.

Such a system is incredibly complex to model with a large number of particles and requires a large amount of computational power. As previously mentioned there are ways in which to reduce the amount of computer time necessary.

The first of these methods is to break down the time over which the system is modeled into a series of time-steps. The particles in the system are allowed to interact and move for a certain amount of time (typically of the order of pico-seconds) and then the energies of the system are analyzed while the particles are stationary. The process is repeated over a specified time range and the information obtained can be used to follow the trajectories and energies of the system as a series of 'jumps' through time.
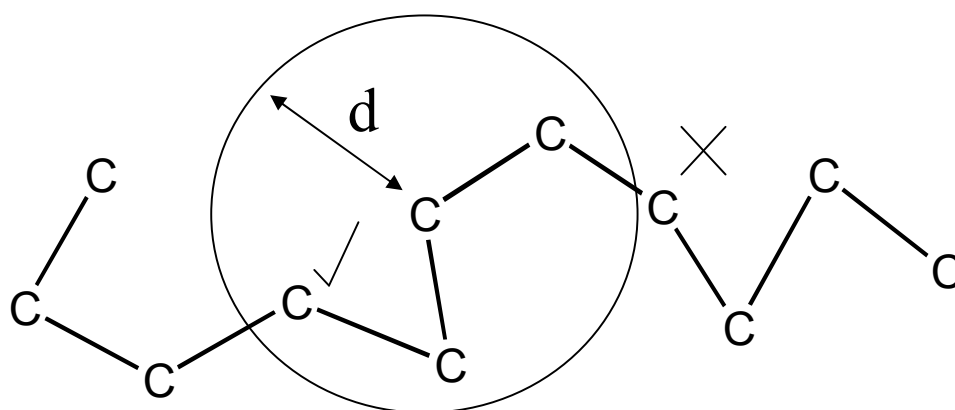
Figure 2.2.5.1: Diagram Illustrating NBC condition, non-bonded interactions inside the circle are calculated, the ones outside are not

The second method is known as 'non-bonded cutoffs' and the basic idea is that interactions between non-bonded atoms that are far apart from one another are negligible. Without this simplification the MD simulation would attempt to calculate the interaction of every particle in the system with every other particle regardless of inter-atomic distance. This would greatly increase the amount of computer time necessary for the calculation and so a 'cutoff' value for the distance at which particles cease to interact with any great contribution to the system is introduced. Interactions between particles separated by a distance greater than this value are not calculated thus greatly reducing computer simulation time, an example is shown in figure 2.2.5.1.
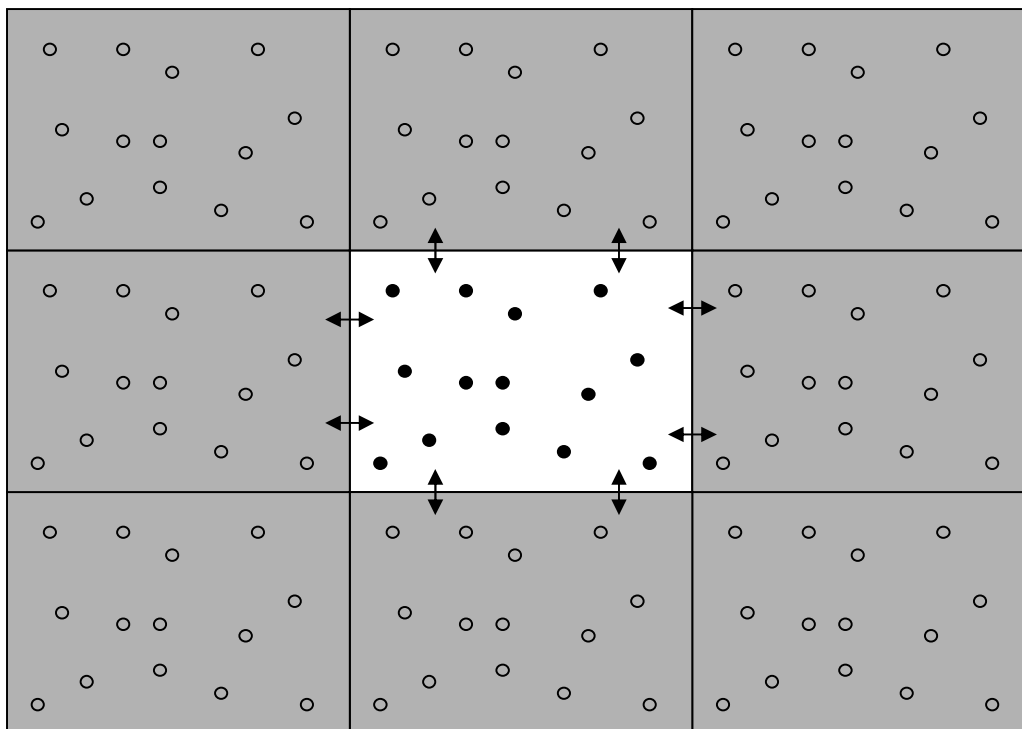
Figure 2.2.5.2: Diagram Illustrating PBC condition. Original simulation is the central box; boundary copies are shaded in grey

When a bulk system, such as the one used in this project, is modeled it is possible to employ a technique known as 'period boundary conditions' or (PBC). All the particles in the simulation are placed inside a 'simulation box' and this box is replicated on all sides on an infinite lattice and the result is that the original simulation is surrounded on all sides by an image of itself (see figure 2.2.5.2). The circle shown in figure 2.2.5.1 still applies to this system so we must be careful to limit the size of the cutoff distance so that the circle does not overlap itself when PBC conditions are applied (setting PBC box size to a minimum of twice the cutoff distance). The main reason for applying PBC conditions is to remove the effect of particles in the system coming into contact with the non-interacting walls of the simulation box. Instead the particles near the edge of the box experience the interactions of the periodic image particles in the neighbouring box and a more realistic simulation environment is created.

2.3 Neutron Reflectometry

2.3.1 Overview and Brief History

Chadwick at Cavendish laboratory (Cambridge University) first discovered the existence of the neutron in 1932 and demonstration experiments were carried out 4 years later. The first neutron scattering experiments were not carried out until the years of the Second World War, utilizing the reactors constructed during the Manhattan project. In 1943 Ernest Wollan constructed the first instrument dedicated to neutron scattering. Wollan alongside Clifford Shull developed the simple 2-axis instrument over the next ten years and various classic experiments were carried out to improve the instrument and the technique[56]. The work carried out during this time provided the first ever direct evidence for the existence of antiferromagnetic materials[57] and various techniques were developed including polarized neutron scattering, utilizing the fact that neutrons have a spin of ½, which was then used to separate nuclear and magnetic scattering from interactions with ferromagnetic materials[58]. In 1994 a Nobel Prize was awarded to Clifford Shull for his work on this technique and Ernest Wollan would have also received the prize if not for his death in 1984.

2.3.2 The Power of Neutrons

Neutrons passing through a material experience interactions with the nuclei of the atoms (rather than the electron cloud, which is the case in X-ray scattering techniques). As a result the scattering cross section[63] of an atom is not directly proportional to its atomic number (unlike in X-ray scattering where the cross section is directly related to the number of electrons in the atom).

This gives neutron scattering several advantages[60, 61] over its X-ray counterpart:

- The scattering is dependant on variations in the nucleus and so allows isotopes of the same element to be distinguished, therefore isotopic substitution can be used to label parts of a molecule.

- Lighter atoms such as Hydrogen and Deuterium can be detected even in the presence of larger atoms.

- It is possible to distinguish between elements that have very similar atomic numbers.

- The interaction of neutrons with the nuclei of atoms is weak enough that they are inherently a highly penetrating and non-destructive probe, but still strong enough to be measured, allowing the probing of delicate biological systems and complexes.

- Neutrons can have wavelengths of similar size to atomic spacing (0.05 to 20 angstroms) allowing diffraction experiments to be performed.

- Neutrons are spin ½ particles and as such have a magnetic moment that can be used to probe variations in the magnetic properties of materials.

2.3.3 Overview of Neutron Techniques

There are several techniques that use the unique properties of neutrons[59-63] to probe materials; however the primary technique for studying surfaces of materials as used in this project is neutron reflectivity[64].

2.3.3.1 Neutron Reflectivity

Many techniques can be used to probe surfaces and interfaces of materials, however they often require experimental conditions that are not ideal such as high vacuum and may require a strong interaction between the probe and the material (leading to some destruction of the sample). Neutrons are weakly scattered by matter and therefore allow the study of 'buried' interfaces[65].
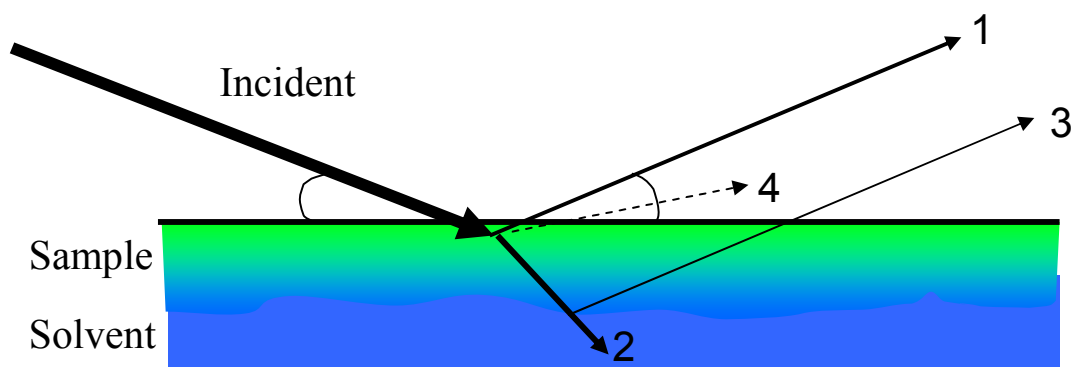
Figure 2.3.3.1.1: Schematic of processes that occur when an incident beam of neutrons hits an interface/surface (the incident and reflected angles shown are equal and typically ~ 0.5° to 2°)

A beam of neutrons incident on a surface will undergo 4 different processes as shown schematically figure 2.3.3.1.1. These processes are described below:

1. Specular neutron reflection[66, 67]. This is used to study structure of samples perpendicular to the surface and can probe thicknesses of a few angstroms up to a few microns. Order within the plane is not necessary and therefore this technique can be used to study disordered interfaces such as polymers at air –water.

2. Transmission. The beam is slightly (the diagram is exaggerated) diffracted upon hitting a sample with a different refractive index and transmitted into the sub-phase.

3. Reflection. If multi-layers are present then we will see an interference pattern[68] between the reflected beams similar to ellipsometry techniques.

4. Non-specular reflection. This is caused by roughness of the sample interface or thermal/physical vibrations of the system as well as from structures within the plane. This effect is minimised by experimental conditions such as the use of a vibration-dampening table.

Since the reflective properties of neutrons are analogous to that of light waves we can apply the same basic rules of optics to reflectometry with only a slight alteration necessary[68, 69]. The scattering length density and reflection of neutrons can be expressed in much the same way as refractive index and scattering angle of light. We can use the following equation for refractive index,

$$n = 1 - \delta$$
<div align="right">Equation 2.3.3.1.1</div>

where,

$$\delta = \frac{\lambda^2}{2\pi} Nb$$
<div align="right">Equation 2.3.3.1.2</div>

Where n is the refractive index, λ is the neutron wavelength (typically 0.05 to 20 angstroms), N is Atomic number density (is directly related to atomic mass and density of the material and b is the scattering length of the atom.

It is worth noting that for X-rays the equation is very similar,

$$\delta = \frac{\lambda^2}{2\pi} r_0 \rho_e$$
<div align="right">Equation 2.3.3.1.3</div>

As previously stated the reflection of neutrons occurs through interaction with the nucleus, and the values for scattering length vary almost randomly with atomic number[70]. The scattering lengths of hydrogen and deuterium are given below as a prime example:

For Hydrogen atoms, b = -0.374×10^{-12} cm

For Deuterium atoms, b = 0.667×10^{-12} cm

Simply by changing from one isotope of an element to another the scattering length has changed dramatically, by magnitude and by sign and this has a direct influence on the amplitude of the reflected neutron wave. This property of neutrons is extremely useful and affords us a powerful method of distinguishing between polymers and the

surrounding solvent or even separate segments of the same polymer simply by the substitution of hydrogen and deuterium.

This comparison becomes even more apparent when we calculate scattering length densities (SLD) for molecules,

$$SLD = \sum_i b_i n_i = \sum_i b_i \frac{\rho_i N_A}{A_i}$$
Equation 2.3.3.1.4

Where A_i is the atomic mass, ρ_i is the physical density of the component i, N_A is Avogadro's number and b_i is the scattering length of the atomic component.

By combination of these equations we can see that the refractive index of a surface is related directly to the SLD[63] of a material and therefore inherently related to the atomic composition of the material at the surface. Some typical values for scattering length density are given in table 2.3.3.1.2:

Material	Scattering Length Density (SLD)/ 10^{-6} Å^{-2}
Air	0
Water (H_2O)	-0.55
Heavy water (D_2O)	6.35
Silicon (Si)	2.07
Poly(Ethylene Oxide)	0.56
Deuterated Poly(Ethylene Oxide)	6.33
Poly(Ethylene)	-0.33
Deuterated Poly(Ethylene)	8.24

Table 2.3.3.1.2: Typical Scattering Length Densities of common and relevant molecules

Reflectivity is measured as a function of the scattering vector, or momentum transfer, Q. This is shown schematically in figure 2.3.3.1.3.
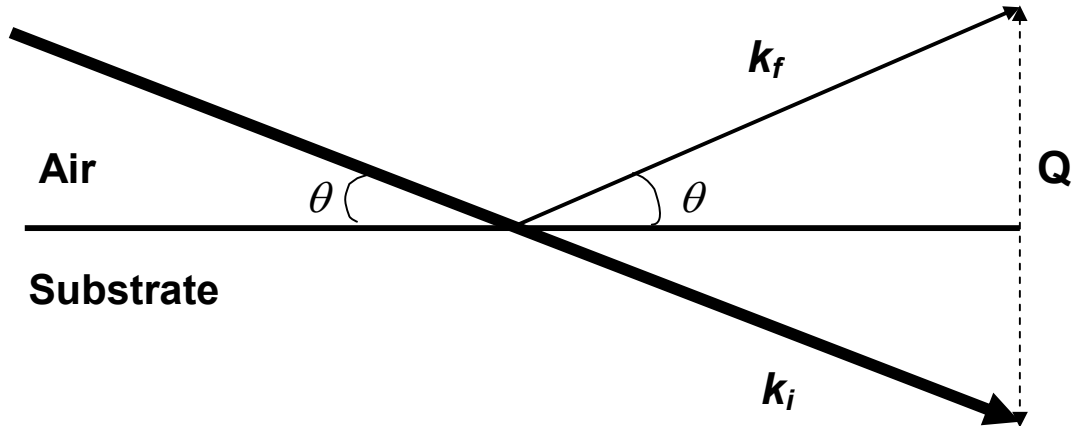
Figure 2.3.3.1.3: Schematic showing Q in terms of wave-vectors

Where k_i is the wave-vector of incident beam, k_f is the wave-vector of reflected beam, Q is the scattering vector (momentum transfer) and θ is the angle of incidence.

Q is related to wavelength, λ, and grazing angle, θ, by the following equation:

$$Q = k_0 - k_1 = \frac{4\pi}{\lambda} \sin \theta \qquad \text{Equation 2.3.3.1.5}$$

Using this equation the organization of layered interfaces can be probed at various depths by altering either λ or θ and monitoring the reflectivity over a range of Q values afforded by these changes. Variation of θ is a simple process involving the insertion of a 'super mirror' into the neutron beam at a specific angle, this alters the angle of incidence on the sample. The alteration of λ however is much less trivial and for pulsed neutron sources involves a 'time of flight' measurement. The basic principle is that neutrons with a shorter wavelength will travel at a greater velocity than those of longer wavelength. Therefore with a 'pulsed' neutron source it is possible to measure the velocity of a neutron by a simple calculation of known distance over known traveling time and it is then simple to calculate, to a reasonable degree of accuracy, the wavelength of the neutron. The general procedure is to carry out an experiment at a fixed angle and collected data (Q values) using time sensitive detectors, resulting in a plot of I vs Q then

change to another fixed angle and carry out the experiment again. A plot of I against Q can be used to give us information about layer organization parallel to the sample surface.

2.3.3.2 Neutron Reflectivity Optics
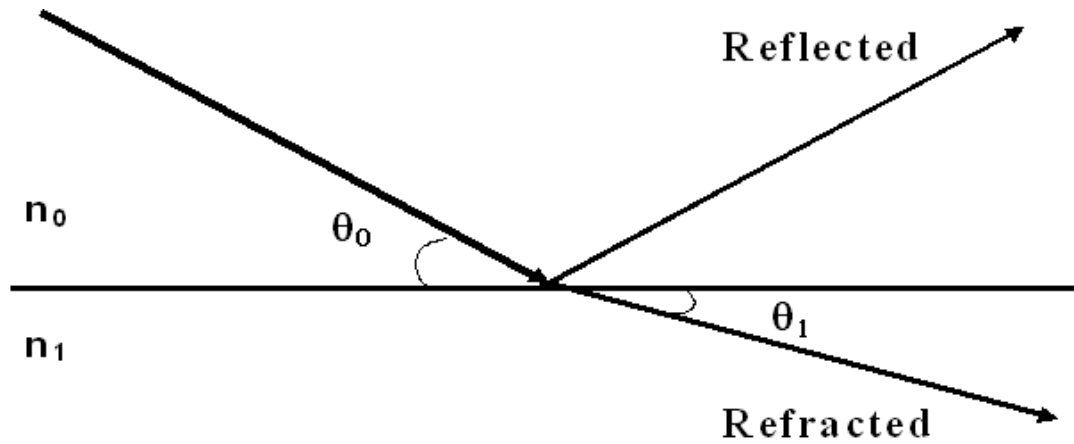
Figure 2.3.3.2.1: Schematic showing some basic optics for a neutron beam

When a neutron beam hits an interface at a critical angle, θ_c, then total reflection of the beam is observed. From Snell's law the following conditions must be satisfied:

$$n = \frac{n_1}{n_0} = \frac{\cos\theta_0}{\cos\theta_1}$$

Equation 2.3.3.2.1

At total reflection:

$$\theta_0 = \theta_c \quad \theta_1 = 0.0 \quad \cos\theta_1 = 1.0$$

Equation 2.3.3.2.2

where n_0 and n_1 are the refractive indices of respective layers.

Combination of previous equations leads to the following equation for the critical angle:

$$\cos\theta_c = 1 - Nb\frac{\lambda^2}{2\pi} \quad \theta_c = \sqrt{\frac{Nb}{\pi}}$$

Equation 2.3.3.2.3

2.3.3.3 Neutron Reflectivity Applications

This project is based around the organization of a monolayer between two 'infinite' media, in this case a polymer monolayer between an air – water substrate interface. An air – deuterated water interface has a critical angle that corresponds to a critical momentum transfer value, Q_c, of 0.018 Å^{-1}, which is lower than any value that will be obtained experimentally and so the critical angle is never encountered. Therefore the reflectivity, R(Q), of the system to be analyzed can be expressed using Fresnel's law:

For $\theta > \theta_c$:

$$r_{01} = \left| \frac{n_0 \sin \theta_0 - n_1 \sin \theta_1}{n_0 \sin \theta_0 + n_1 \sin \theta_1} \right|^2 \qquad \text{Equation 2.3.3.3.1}$$

For a thin film at an interface:

$$R(Q) = \left| \frac{r_{01} + r_{12} e^{-2i\beta}}{1 + r_{01} r_{12} e^{-2i\beta}} \right|^2 \qquad \text{Equation 2.3.3.3.2}$$

where:

$$\beta_1 = \left(\frac{2\pi}{\lambda} \right) d_1 \sin \theta_1 \qquad \text{Equation 2.3.3.3.3}$$

Where r_{01} and r_{12} are the Fresnel coefficients for the respective interface and d is the monolayer thickness

Combination of the previous three equations allows us to determine an expression for the overall reflectivity[68, 71] of the polymer monolayer at the interface:

$$R(Q) = \left| \frac{r_{01}^2 + r_{12}^2 + 2r_{01}r_{12} \cos 2\beta}{1 + r_{01}^2 r_{12}^2 + 2r_{01}r_{12} \cos 2\beta} \right| \qquad \text{Equation 2.3.3.3.4}$$

It can be seen from this expression that the data produced from a neutron reflectivity experiment can be related directly to both the thickness of the monolayer in the system as well as the composition of the material in the monolayer. Since the maxima in the reflectivity spectrum occur when $\cos 2\beta = +1$ and the minima when $\cos 2\beta = -$ the monolayer thickness, d, is inversely related to the separation of the maxima/minima in the data. Since Q is dependent on scattering angle and therefore scattering length density (SLD) it is possible to extract monolayer composition data from the profile. However this is not a trivial exercise as in practice it is not possible to use a Fourier transform to directly convert the data into composition information since all phase information is lost from the data. Therefore interpretation of neutron reflectivity data is generally achieved through comparison with simulation data from a model system.

2.4 References

[1] N. Bikales, *Water-soluble Synthetic Polymers*, Plenum: New York, **1973**.

[2] B.-K. Cho, A. Jain, S. M. Gruner and U. Wiesner, *Science* **2004**, *305*, 1598-1601.

[3] C. A. Finch, *Chemistry and Technology of Water-soluble Polymers*, Plenum: New York, **1973**.

[4] W. M. Kulicke, R. Kniewske and J. Klein, *Prog. Poly. Sci.* **1982**, *8*, 373-468.

[5] P. Williams, *Handbook of Industrial Water Soluble Polymers*, **2007**.

[6] A. Nussinovitch, *Water-Soluble Polymer Applications in Foods*, Wiley-Blackwell, **2003**.

[7] D. Batt-Coutrot, D. M. haddleton, A. P. Jarvis and R. L. Kelly, *European Polymer Journal* **2003**, *39*, 2243-2252.

[8] M. Kamigaito, T. Ando and M. Sawamoto, *Chem. Rev.* **2001**, *101*, 3689-3746.

[9] K. T. Lim and M. Y. Lee, *Polymer* **2002**, *43*, 7043-7049.

[10] K. Matyjaszewski, *Chem. Eur. J.* **1999**, *5*, 3095-3102.

[11] K. Matyjaszewski, *J. Chem. Rev* **2001**, *101*, 2921-2990.

[12] F. Lecolley, C. Waterson, A. J. Carmichael, G. Mantovani, S. Harrison, H. Chappell, A. Limer, P. Williams, K. Ohno and D. M. Haddleton, *J. Mater. Chem.* **2003**, *13*, 2689-2695.

[13] T. E. Patten, J. Xia, T. Abernathy and K. Matyjaszewski, *Science* **1996**, *272*, 866-868.

[14] V. Percec and M. Lee, *Macromol. Sci. Pure Apply. Chem* **1992**, *A29*, 723-740.

[15] D. R. Iyengar, S. M. Perutz, C. A. Dai, C. K. Ober and E. J. Kramer, *Macromolecules* **1996**, *29*, 1229-1234.

[16] K. Patel, T. Desai and B. Suthar, *Makromol. Chem.* **1985**, *186*, 1157-1166.

[17] C. J. Hawker and J. M. J. Frechet, *J. Am. Chem. Soc* **1990**, *112*, 7638-7647.

[18] K. L. Wooley, C. J. Hawker and J. M. J. Frechet, *J. Am. Chem. Soc* **1991**, *113*, 4252-4261.

[19] I. Gitsov, K. L. Wooley and J. M. J. Frechet, *Angew. Chem. Int. Ed. Eng* **1992**, *31*, 1200-1202

[20] I. Gitsov, L. Wooley, C. J. Hawker, P. T. Ivanowa and J. M. J. Frechet, *Macromolecules* **1993**, *26*, 5621-5627.

[21] R. Esfand and D. A. Tomalia, *Dendrimers and other dendritic polymers*, Wiley, Chichester, **2001**.

[22] M. Jayaraman and J. M. J. Frechet, *J. Am. Chem. Soc* **1998**, *120*, 12996-12997.

[23] T. M. Miller, T. X. neenan, R. Zayas and H. E. Blair, *J. Am. Chem. Soc.* **1992**, *114*, 1018-1025.

[24] J. W. Halley, Y. Duan and B. Nielsen, *J. Phys. Chem. B.* **2001**, *115*, 3957-3966.

[25] O. Borodin, G. D. Smith and R. Douglas, *J. Phys. Chem. B.* **2003**, *107*, 6824-6837.

[26] O. Borodin and G. D. Smith, *J. Phys. Chem. B.* **2003**, *107*, 6801-6812.

[27] T. Koga, H. Jinnai and T. Hashimoto, *Physica A.* **1999**, *263*, 369-377.

[28] O. Borodin, R. Douglas, G. D. Smith, F. Trouw and S. Petrucci, *J. Phys. Chem. B.* **2003**, *107*, 6813-6823.

[29] M. J. Field, *A Practical Introduction to the Simulation of Molecular Systems*, Cambridge University Press, **2007**.

[30] P. Klaver, *Atomistic Simulation of Cu/ta Thin Film Deposition & Other Phenomena*, **2004**, 61-74.

[31] H. Donnerberg, *Atomistic Simulation of Electro- and Magnetooptic Oxide Materials (Springer Tracts in Modern Physics)*, Springer-Verlag Berlin and Heidelberg GmbH & Co. K, **1998**, 1-5

[32] P. R. Sundararajan and T. A. Kavassalis, *J. Chem. Soc., Faraday Trans.* **1995**, *91*, 2541-2549.

[33] K. Muralidharan, P. A. Deymier and J. H. Simmon, *Modelling Simul. Mater. Sci. Eng.* **2003**, *11*, 487-501.

[34] H. Rafii-Tabar and A. Chirazi, *Phys. Rep.* **2002**, *365*, 145-249.

[35] P. M. Anderson and M. R. Wilson, *J. Chem. Phys* **2004**, *121*, 8503-8510.

[36] W. L. Jorgensen, D. S. Maxwell and J. Tirado-Rives, *J. Am. Chem. Soc* **1996**, *118*, 11225-11236.

[37] B. Albinsson and J. Michl, *J. Am. Chem. Soc* **1995**, *117*, 6378-6379.

[38] B. Albinsson and J. Michl, *J. Phys. Chem.* **1996**, *100*, 3418-3429.

[39] O. Borodin, G. D. Smith and D. Bedrov, *J. Phys. Chem. B.* **2002**, *106*, 9912-9922.

[40] S. T. Cui, J. I. Siepmann, H. D. Cochran and P. T. Cummings, *Fluid Phase Equib.* **1998**, *146*, 51-61.

[41] O. Okada, K. Oka, S. Kuwajima and K. Tanabe, *Mol. Simul.* **1999**, *21*, 325-342.

[42] G. D. Smith, R. L. Jaffe and D. Y. Yoon, *Macromolecules* **1994**, *27*, 3166.

[43] M. Sprik, U. Rothlisberger and M. L. Klein, *J. Phys. Chem. B.* **1997**, *101*, 2745-2749.

[44] M. Sprik, U. Rothlisberger and M. L. Klein, *Mol. Phys.* **1999**, *97*, 355-373.

[45] E. K. Watkins and W. L. Jorgensen, *J. Phys. Chem. A.* **2001**, *105*, 4118-4125.

[46] R. Faller, H. Schmitz, O. Biermann and F. Muller-Plathe, *J. Comput. Chem.* **1999**, *30*, 1009-1017.

[47] H. Meyer, O. Biermann, R. Faller, D. Reith and F. Muller-Plathe, *J. Chem. Phys* **2000**, *113*, 6265-6275.

[48] G. Srinivas, M. L. Klein, J. C. Shelly, S. O. Nielsen and D. E. Dishcer, *J. Phys. Chem.* **2004**, *108*, 8153-8160.

[49] G. Srinivas and M. L. Klein, *Molecular Physics* **2004**, *102*, 883-889.

[50] J. C. Shelly, M. Y. Shelly, R. C. Reeder, S. Bandyopadhyay, P. B. Moore and M. L. Klein, *J. Phys. Chem. B.* **2001**, *105*, 9785-9792.

[51] S. Neyertz and D. Brown, *J. Chem. Phys.* **1995**, *102*, 9725-9735.

[52] D. Rigby and R.-J. Roe, *J. Chem. Phys.* **1987**, *87*, 7285-7292.

[53] E. Khurana, S. O. Nielsen and M. L. Klein, *J. Phys. Chem. B.* **2006**, *110*, 22136-22142.

[54] D. Brown, J. H. R. Clarke, M. Okuda and T. Yamazaki, *J. Chem. Phys.* **1994**, *100*, 6011-6018.

[55] J. I. Mckechnie, D. Brown and J. H. R. Clarke, *Macromolecules* **1992**, *25*, 1562-1567.

[56] E. O. Wollan and C. G. Shull, *Phys. Rev.* **1948**, *73*, 830-841.

[57] C. G. Shull and J. S. Smart, *Phys. Rev.* **1949**, *76*, 1256-1257.

[58] C. G. Shull, E. O. Wollan and W. A. Strauser, *Phys. Rev.* **1951**, *81*, 483-484.

[59] S. King, P. Griffiths, J. Hone and T. Cosgrove, *Macromol. Symp.* **2002**, *190*, 33-42.

[60] P. G. Cummins, J. Penfold and E. Staples, *Langmuir* **1992**, *8*, 31-35.

[61] M. T. F. Telling and K. H. Anderson, *Phys. Chem. Chem. Phys.* **2005**, *7*, 11255-11261.

[62] R. P. May, *Neutrons, X-Rays and Light*, Elsevier Sceince B. V., **2002**, 445-448.

[63] V. F. Sears, *Neutron News* **1992**, *3*, 26-37.

[64] D. G. Bucknall, *Modern Techniques for Polymer Characterisation*, John Wiley & Sons Ltd., **1999**.

[65] E. Fermi and W. Zinn, *Phys. Rev.* **1946**, *70*, 103-104.

[66] J. Lekner, *Theory of Reflection*, Martinus Nijhoff, Dordrecht, **1987**.

[67] J. Penfold, *Neutron, Xray and Light Scattering*, Elsevier, Amsterdam, **1991**.

[68] M. Born and E. Wolf, *Principles of optics*, Pergamon Press, Oxford, **1980**.

[69] J. S. Higgins and H. C. Benoit, *Polymers and Neutron Scattering*, Clarendon Press, Oxford, **1994**.

[70] L. Koester, U. i. Bonse and H. Raunch, *Neutron Interferometry*, Oxford Science Publications, **1979**.

[71] L. G. Parratt, *Phys. Rev.* **1954**, *95*, 359-369.

[72] R. P. May, *Neutrons X-Rays and Light* **2002**, 463-480.

Chapter Three: Synthesis

3.1 Introduction

Poly (ethylene oxide), or PEO, is a water soluble polymer that spontaneously adsorbs to the surface to form a surface excess layer when dissolved in water[1-3]. Previous studies have shown that modification of PEO by functionalizing either one end or both ends of the polymer chain with a hydrophobic end cap will enhance the surface activity of the polymer molecule[4-7]. Previous work[5, 6, and 8] has shown that modified PEO incorporating fluorocarbon end groups have proven to be among the most highly surface active[9]. PEO chains have been functionalized by fluorinated end caps at one or both ends to tether them to an air/water interface at sufficiently high grafting density that excluded volume interactions between the PEO chains cause them to stretch, forming a brush-like layer[10]. However, when the molecular weight of the PEO chains is increased, the tethering strength of these linear fluorinated head groups is insufficient to anchor them at the air/water surface and the grafting density decreases. In order to try and overcome this problem a new synthetic strategy will be employed wherein the PEO will be functionalized using a dendritic end cap molecule, enabling multiple fluorinated functional groups to be attached to a single PEO chain[11-13]. This should dramatically increase the tethering strength of the molecule to an air/water interface and result in the self assembly of a brush-like layer with increased structural order due to the increase in molecular weight.

The target materials for this work consist of a series of PEO chains of varying molecular weight, functionalized with dendrons of varying generation and fluorocarbon content. The most efficient method for introducing functionalization to the end of a polymer chain of this type is to begin with an initiator that exhibits the desired properties of the terminal end of the product. Using this method 100% of the chains will have the desired end terminal and the propagation can simply be stopped by addition of a simple termination molecule (such as water or hydrochloric acid for example). The disadvantage of this method is that introducing functionalization to the initiating species may alter the capability of the molecule to act as an initiator for the polymerization.

A control material analogous to the target materials but with no fluorocarbon functionality present was first synthesized to ensure that the synthetic method chosen was successful in principle. The properties of this control material could then be compared directly to those of the target material to fully investigate the specific effect of the fluorocarbon groups.

A suitable synthetic strategy is required to assemble the desired polymer products, including the synthesis of the head groups themselves. The first part of this chapter will describe in detail the synthetic routes to all of the PEO polymers (including variations in molecular weight and isotopic composition), head groups and methods of attaching the two parts together as well as any problems encountered during the syntheses and how they were overcome. Details of the reagents and solvents used during synthesis can be found at the end of the synthetic section and the final part of the chapter describes the analytical methods employed to characterize the product materials.

3.2 Results and Discussion

3.2.1 Synthesis of Dibenzyloxybenzyl End Capped Poly(Ethylene Oxide) by Anionic Polymerization

The first step in the synthesis of the dibenzyloxybenzyl end capped poly(ethylene oxide) is to weigh out and purify the ethylene oxide monomer. The ethylene oxide gas was distilled under vacuum into a round bottomed flask containing around 1g of calcium hydride (used as a drying agent), fitted with a Young's tap and a magnetic stirrer. As ethylene oxide is a gas, and must be handled very carefully and extracted from the gas cylinder under vacuum distillation, it is very difficult to distill over a precise amount into the flask. For this reason the round bottomed flask and contents must be weighed prior to distillation so the amount of ethylene oxide in the flask can then be calculated from the weight of the flask after distillation. During the distillation the flask is kept under liquid nitrogen to freeze the ethylene oxide gas to the solid that can simply be weighed on a balance. Once 10g of ethylene oxide was distilled into the flask it was then transferred to

a high vacuum line to be purified further. The purification process is simple and involves repeated freezing of the ethylene oxide with liquid nitrogen and removal of any gases using the high vacuum line, allowing the ethylene oxide to thaw and stir for a while under ice water (the ethylene oxide must be kept chilled at all time to prevent boiling in the sealed system). This whole process is repeated several times over 2 or 3 days until the ethylene oxide is as dry and pure as possible (NMR was used to confirm purity and absence of water).

The solvent to be used for the polymerization, Tetrahydrofuran (THF), is also placed on the high vacuum line in a round-bottomed flask along with a wire of sodium metal and a small amount (around 1g) of benzophenone as an indicator for the presence of air or water (benzophenone forms a purple coloured complex with sodium and in the presence of air or water this complex is unable to form). The freeze – vacuum – thaw process carried out on the ethylene oxide is also employed here to remove water, air and other impurities.
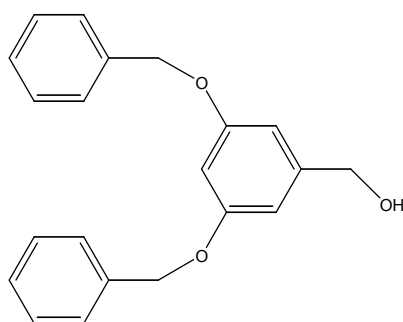
Figure 3.2.1.1: 3,5-dibenzyloxybenzyl-alcohol

The reaction vessel for the polymerization is referred to as a 'Christmas tree' flask due to its unique shape (see figure 3.2.1.2). This flask is specifically designed for anionic polymerization and consists of a large main reaction chamber (labeled 1 in figure 3.2.1.2) where the polymerization is carried out and a number of smaller side chambers (labeled 2 in figure 3.2.1.2) through which samples can be extracted for analysis at various stages during the polymerization to follow the reaction as it proceeds. There is also a small side chamber containing polystyryllithium (polystyrene that is in the propagation step of

synthesis and has not been terminated, also called living polystyrene) in benzene (labeled 3 in figure 3.2.1.2). This polystyryllithium is used to wash out the reaction vessel prior to carrying out a polymerization, this works by sacrificially reacting with any impurities in the vessel and therefore removing the possibility of those impurities interfering with the polymerization reaction to be carried out.
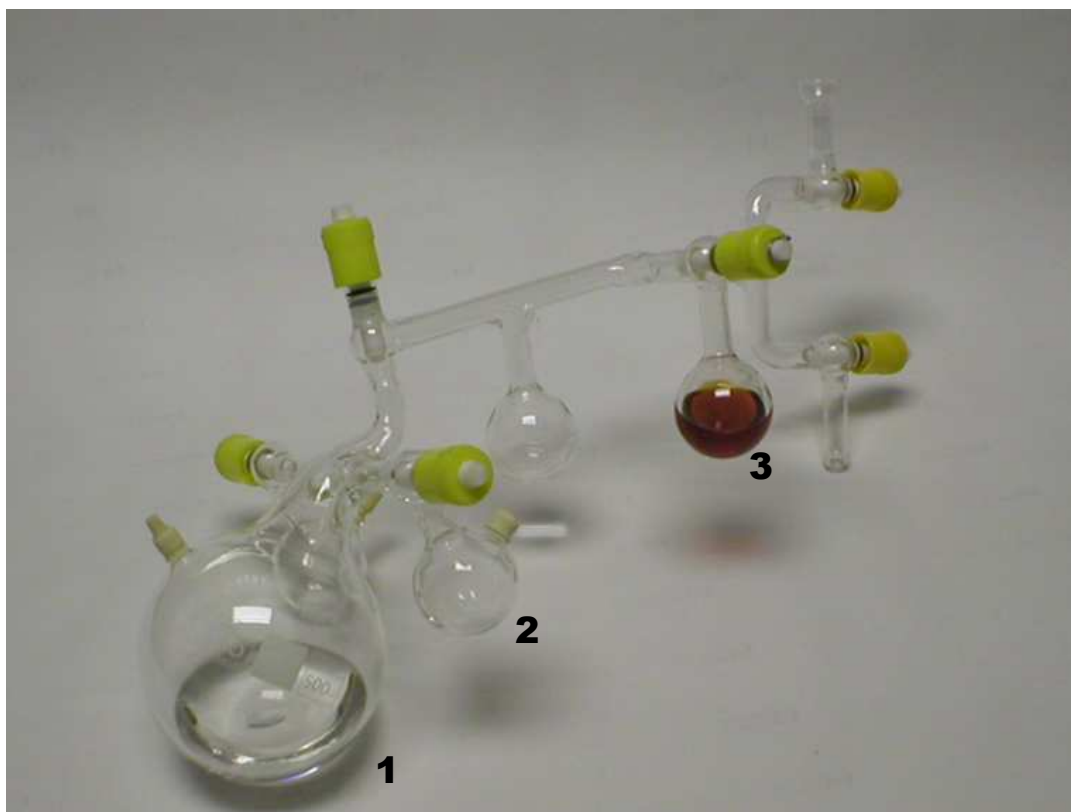
Figure 3.2.1.2: Christmas tree reaction vessel used for polymerization

The 3,5-dibenzyloxybenzyl-alcohol initiator was purchased from Aldrich and characterized using NMR, showing no obvious peaks that could be a result of impurities. Calculations showed that 0.33g of the initiator were needed to synthesize functionalized poly(ethylene oxide) chains with a molecular weight of 10,000 gmol^{-1}. This amount of the initiator was placed into the main reaction vessel of the christmas tree flask and this was also placed on the high vacuum line to dry. The initiator was left under high vacuum overnight to ensure as much moisture is driven off as possible then around 50 mL of

benzene was distilled into the reaction vessel to dissolve the dendrimer initiator. The benzene/initiator mixture was then frozen by immersing the flask in liquid nitrogen and the system was evacuated under high vacuum. Once the vessel was degassed the mixture is immersed in warm water and allowed to melt. The benzene was then distilled under vacuum into an empty flask, along with any water and impurities picked up by the benzene during this asiotropic drying process, leaving behind the purified and dry initiator, which is left under vacuum overnight again to drive off any remaining benzene.

The next step is to transfer the dried and purified THF by distillation into the main reaction vessel of the christmas tree flask in order to dissolve the dendritic initiator. The distillation of the THF is stopped once the reaction vessel is filled to around 1/3 of its volume to prevent any risk of expansion and explosion of the reaction vessel. Gentle heating with tepid water and stirring is applied to ensure the initiator is fully dissolved in the THF solvent.

The term 'initiator' has been used to describe the dendron used in this reaction. However, in order to begin the polymerization process it is necessary to add a compound to the dendron in order to convert it into an initiating species. In this case the addition of a diphenylmethyl potassium (in a 0.9:1 molar ratio with respect to the initiator concentration) deprotonates the alcohol group of the dendron and replaces it with a potassium ion, an excess of diphenylmethyl potassium would result in the initiation of the polymerization of unfunctionalized poly(ethylene oxide), this reaction is shown in figure 3.2.1.3. The diphenylmethyl potassium is added to the mixture using a gas-tight syringe flushed with nitrogen gas so as to ensure no air is able to enter the system. At the same time 10 mL of dibutyl magnesium is added in the same way to the ethylene oxide as a final purification step and both mixtures are stirred for an hour to ensure good mixing.

The final step is to distill over the ethylene oxide into the same reaction vessel as the initiating dendron. Once all of the ethylene oxide has been distilled across, and the dibutyl magnesium residue is all that remains, the reaction is left to proceed over a weekend (or 4 days) at room temperature under vacuum.
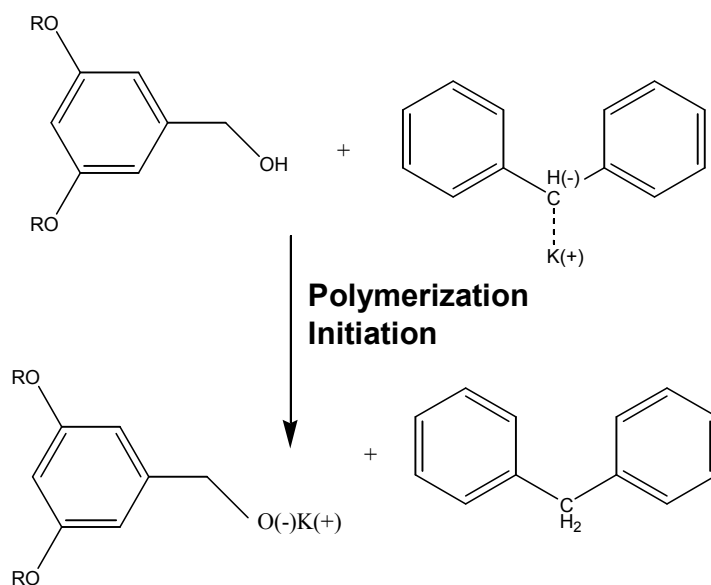
Figure 3.2.1.3: General reaction scheme for initiator formation

When the polymerization has reached a stage where all monomer units are consumed and the reaction is finished it is necessary to introduce a terminating species to the mixture. In this case 2 mL of glacial acetic acid is introduced by gas-tight syringe in molar excess to the initiator species to replace the K^+ ion of the propagating species and generate the alcohol-terminal polymer. The propagation and termination steps for this type of polymerization are shown in figure 3.2.1.4.

After several attempts using small amounts of the reaction mixture to test various methods of working up and purifying the product it was found that the following simple method was most effective. Once the product is terminated the majority of the THF solvent was removed using a rotary evaporator, leaving just enough solvent to keep the product in solution. The solution was then transferred to a beaker containing around 500mL of hexane (this causes the polymer to precipitate out of solution as hexane is a non-solvent for poly(ethylene oxide)). The white crystalline solid polymer is then recovered from the hexane using a Buchner funnel and dried in a vacuum oven (at room temperature) overnight. The polymer is then re-dissolved in a small amount of THF and filtered to remove solid impurities. Then precipitation in hexane is carried out again and

the whole process repeated until purity is achieved.For this control material, where no fluorocarbon groups are present, a yield of >90% was achieved.
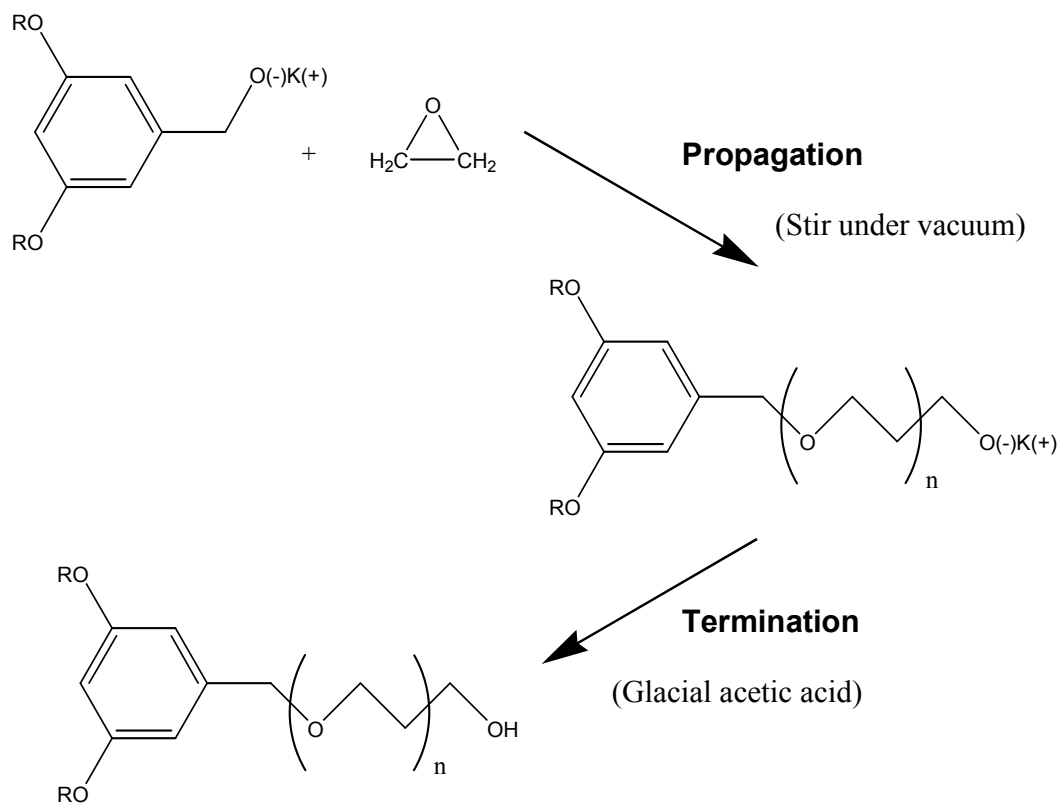
Figure 3.2.1.4: General reaction scheme for polymerization method

3.2.2 Synthesis of First Generation Fluorinated Dendrimers

Much of the synthesis of the dendrons used in this project was carried out in house by Dr Amilcar Pillay Narrainen[12, 13]. However, due to shortage of materials or the need for variations on the dendrimers already made it was necessary to synthesize the majority of the dendritic materials as and when they were necessary. The synthetic route employed was essentially the same as that outlined in the paper by Pillay Narrainen et al[13] with necessary moderations made for each specific dendrimer type.

As only a single generation dendron is required during this synthesis the method can be described as either convergent or divergent[11, 14, 15]. Methyl 3,5-dihydroxybenzyl alcohol is purchased from Aldrich with >99.99% purity to be used as the core or root of the dendron. The methyl 3,5-dihydroxybenzyl alcohol is dissolved in dry acetone along with a 1.1 molar excess of potassium carbonate with a small amount of 18-crown-6 and stirred under an inert nitrogen atmosphere for 2 hours to ensure the reactant has dissolved fully and allow good mixing. A 2.2 molar excess (with respect to concentration of methyl 3,5-dihydroxybenzyl alcohol) of 3,5-ditrifluoromethylbenzyl bromide is then dissolved and stirred thoroughly in dry acetone in a separate flask. The 3,5-ditrifluoromethylbenzyl bromide solution is then introduced to the reaction mixture via syringe to maintain the inert atmosphere of the system.
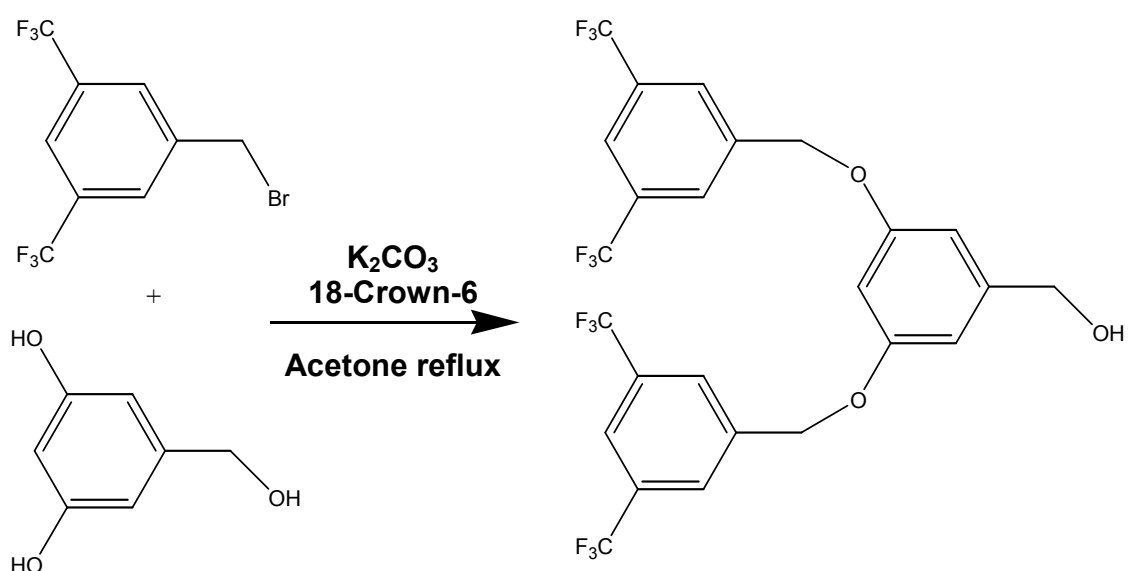
Figure 3.2.2.1: Williamson coupling dendrimer synthesis

Finally the reaction mixture is then warmed to 60°C causing the acetone to reflux and is left stirring overnight. After 18 hours the reaction has gone to completion and the solvent is removed using a rotary evaporator. The crude product is then redissolved in dichloromethane and washed with water to remove the 18-crown-6 from the system. The combined dichloromethane washes are then dried over magnesium sulphate, which is

then removed by filtration. The dichloromethane is removed in a rotary evaporator and the residue is precipitated into hexane, where it can then be extracted using a Buchner funnel. Purification of the product is achieved simply by repetition of the method used to extract the crude product. The pure product is then placed in a vacuum oven overnight to remove any remaining solvent or water and give a yield of around 90%. The whole synthetic process is then repeated using 4-trifluoromethylbenzyl bromide in place of the 3,5-ditrifluoromethylbenzyl bromide to give us the two products shown in figure 3.2.2.2.
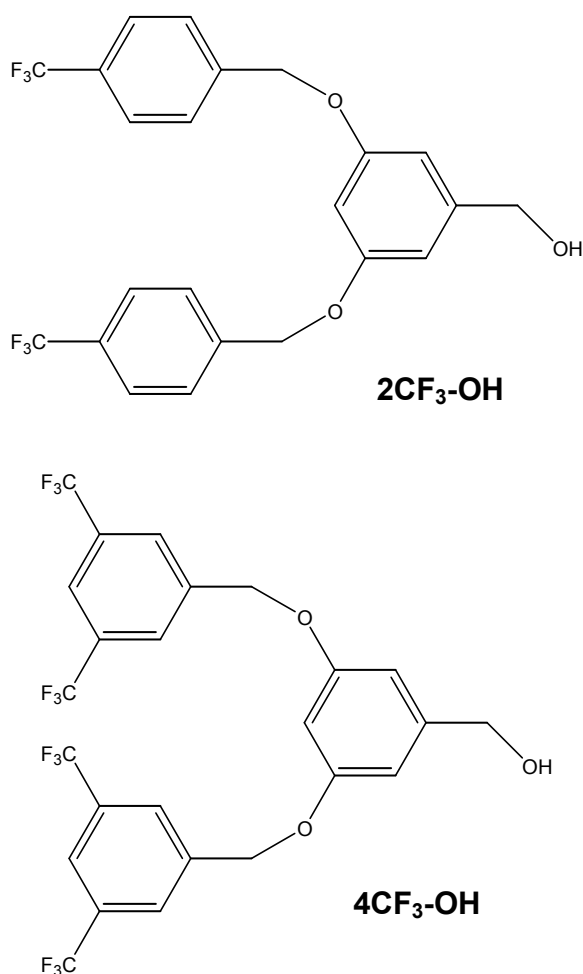
Figure 3.2.2.2: Chemical structure of 2CF$_3$-OH and 4CF$_3$-OH

The first generation dendritic head group product synthesized from 4-trifluoromethylbenzyl bromide has two CF$_3$ functional groups attached to a phenyl ring

and has an alcohol functionalization. Therefore this molecule will be referred to as 2CF$_3$-OH and also the product synthesized from 3,5-ditrifluoromethylbenzyl bromide will be referred to as 4CF$_3$-OH for the same reasoning.

3.2.3 First Generation Fluorinated Dendrimers as Initiators for Anionic Polymerization

The first attempt to synthesize the functionalized polymers was carried out using the 2CF$_3$-OH dendron shown in figure 3.2.2.2. The experimental setup, reactant purification steps, termination process and purification of the product were followed exactly as described above for the synthesis of the dibenzyloxybenzyl end capped poly(ethylene oxide) in section 3.2.1.

However, at the end of this trial experiment there was no presence of any white precipitate upon introduction of the reaction mixture to hexane. The only course of action was to use a rotary evaporator to strip off all solvent in the mixture and to characterize the remaining residue. A ^{1}H-NMR spectrum of the residue revealed that no obvious ethylene oxide peak (the dominant feature of the control sample) was present; suggesting that initiation of the polymerization had not been achieved. The mass of residue remaining coincides with the mass of initiator used in the synthesis plus some impurities or side reaction products.

There are three possible explanations for the inhibition of polymerization initiation. The first is that the potassium initiator could be reacting with the fluorocarbon groups of the dendrimer in preference to the alcohol initiation site. A second explanation is that the introduction of CF$_3$ fluorocarbon units directly bonded to the phenyl ring of the dendron could alter the chemistry at the alcohol initiation site. The third possibility is that human or mechanical error may have led to impurities being allowed into the reaction. However, if this was the case it is much more likely that initiation of polymerization would still have occurred and would have resulted in an unfunctionalized product with high polydispersity.

To test that human or mechanical error was not responsible for the failure of the synthesis a second attempt was carried out using the $2CF_3$-OH dendron shown in figure 3.2.2.2. The experimental setup, reactant purification steps, termination process and purification of the product were followed exactly as described previously and great care was taken to ensure no impurities were allowed into the system. As the second-generation dendron with 4 CF_3 groups was used any chemical effects bestowed upon the initiator by CF_3 groups that prevent initiation would be enhanced.

As with the previous trial run there was no presence of any white precipitate upon introduction of the reaction mixture to hexane; leading to the conclusion that the introduction of CF_3 fluorocarbon units has a direct effect on the chemistry of the reaction.

A further trial experiment was carried out to determine whether direct bonding of the fluorocarbon groups to the phenyl ring was responsible for the prevention of initiation of the polymerization reaction. The head group used for this trial synthesis is shown in figure 3.2.3.1 and has two C_8F_{17} fluorocarbon groups separated from the phenyl ring by an ether linkage and a propyl spacer, this molecule is referred to as $2C_8F_{17}$-OH.
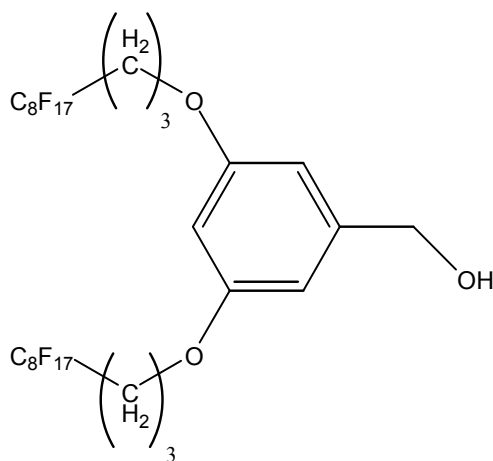
Figure 3.2.3.1: Chemical structure $2C_8F_{17}$-OH dendron

The attempted polymerization was carried out in exactly the same way as in the successful control experiment, followed by the same work up and purification techniques. As with all of the previous attempts using fluorocarbon functionalized initiators there was

no presence of any white precipitate upon introduction of the reaction mixture to hexane. This leads to the conclusion that the potassium based initiator is reacting with the fluorocarbon groups in preference to initiation of the alcohol group, resulting in no initialization of polymerization. Evidence for this explanation can be seen when a Teflon (which is a fluorocarbon material chemical very similar to our CF_3 and C_8F_{17} components) stirrer is used for this type of reaction; the stirrer develops a black coating on the surface of the stirrer suggesting a reaction between the Teflon and the potassium initiator.

3.2.4 Synthesis of Benzyl End Capped Poly(Ethylene Oxide) by Williamson Coupling Reaction

The poly(ethylene oxide) used in this reaction was purchased with a specific structure that has an alcohol terminal group at one end and an $O\text{-}CH_3$ group at the other (shown in figure 3.2.4.1), the reason for this being that we only want to end-cap one terminal of the poly(ethylene oxide); the end with the reactive alcohol group[16-19].

1g of poly(ethylene oxide) was weighed out accurately and placed in a vacuum oven overnight to dry. Once dried the poly(ethylene oxide) was placed into a round bottomed flask under a nitrogen atmosphere and enough THF (from the in-house solvent purification system) added to dissolve the polymer. A 10% molar excess of sodium hydride (NaH) and 15-crown-5 (a crown ether) was then introduced to the flask. The 15-crown-5 has a cavity in the structure that is the perfect size to solvate Na^+ ions, which in turn activate the alcohol site of the poly(ethylene oxide) chain.

In a separate flask (also under nitrogen atmosphere) a 10% molar excess of benzyl bromide, with respect to poly(ethylene oxide) concentration, was dissolved in dry THF. Both flasks were stirred for 4 hours to allow the sodium hydride to react with the PEO and ensure good mixing, then both flasks were chilled in ice water and the dendron solution was carefully introduced into the reaction vessel containing the poly(ethylene oxide). The mixture was allowed to slowly warm to room temperature and left to react for

24 hours overnight. The next day a small amount of distilled water was added to the system to neutralize the excess sodium hydride.
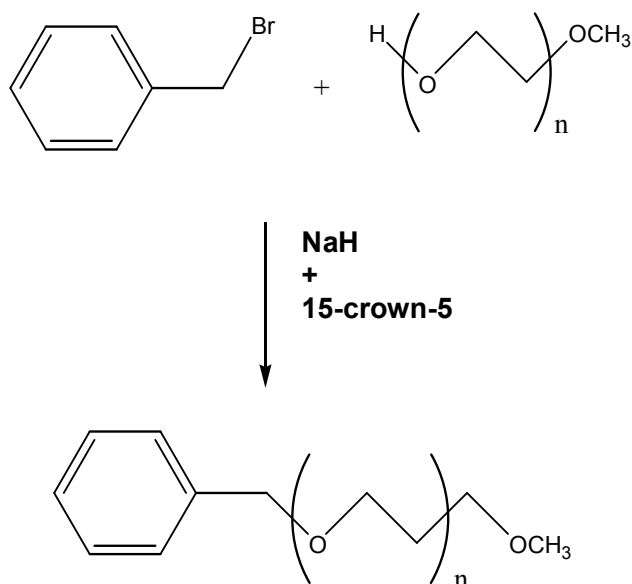
Figure 3.2.4.1: Reaction scheme for Williamson coupling of benzyl bromide and poly(ethylene oxide)

The first step in the extraction and purification process is to remove the majority of the THF solvent using a rotary evaporator, leaving just enough solvent to keep the product in solution. The mixture is then transferred to a beaker containing an excess amount of hexane (this causes the product to precipitate out of solution as hexane is a non solvent for PEO). The white crystalline solid is then recovered from the hexane using a Buchner funnel and placed in a vacuum oven overnight to remove any remaining solvent or water. The polymer is then re-dissolved in a small amount of THF and filtered to remove solid impurities. Then the process of precipitation is carried out again and the whole cycle is repeated until purity is achieved.

Characterization of the sample obtained in this control experiment show that there is a peak present representative of poly(ethylene oxide) and also some aromatic signals present due to the phenyl group from the benzyl bromide. However integration of these

peaks reveals that the reaction seems to have only been partially successful, i.e. not all of the PEO chains contain the end functionalization. GPC measurements confirm that the PEO has not degraded and remains at 11,000 gmol^{-1} as was purchased. This leads to the conclusion that although this synthetic approach is plausible, we must drive the reaction further by adjusting the conditions of the experiment.

To confirm that this synthetic route is successful the experiment was repeated with the following exceptions:

- The sodium hydride and poly(ethylene oxide) were allowed to react overnight to ensure that all of the poly(ethylene oxide) chains become activated
- All reactants including the sodium hydride and the dendritic end-cap were pre-dried in a vacuum oven to prevent any water from contaminating the system
- Hydrochloric acid was added at the end of the reaction instead of water to ensure the sodium hydride is fully neutralized.

Characterization of the product again shows that there is a peak present representative of poly(ethylene oxide) and aromatic signals present due to the phenyl group from the benzyl bromide. However, on this occasion integration of these peaks reveals that the reaction seems to have gone to completion with a conversion rate of around 92%.

3.2.5 Synthesis of First Generation Fluorinated Dendritic End Capped Poly(Ethylene Oxide) by Williamson Coupling Reaction

The first attempt to synthesize the functionalized polymers was carried out using the 4CF$_3$-Br dendron shown in figure 3.2.5.1. The experimental setup, reactant purification steps, termination process and purification of the product were followed exactly as described above for the synthesis of the benzyl end capped poly(ethylene oxide) in section 3.2.4 with the 4CF$_3$-Br dendron used in place of the benzyl bromide end cap.
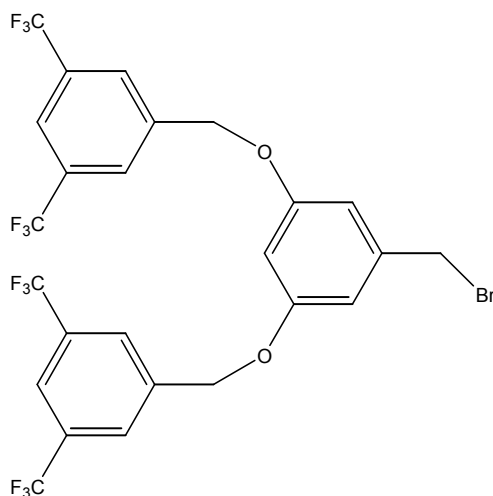
Figure 3.2.5.1: Chemical structure of 4CF$_3$-Br dendrimer

Characterization of the polymer obtained from this synthesis experiment shows that there is a peak present representative of poly(ethylene oxide). There are no peaks in the NMR spectrum that would correspond to the presence of an aromatic group in the sample, again this suggests that the polymer recovered from the reaction is simply the poly(ethylene oxide) starting material. GPC measurements confirm that the poly(ethylene oxide) has not degraded and remains at 11,000 gmol^{-1} as was purchased. This leads to the conclusion that this synthetic route is also hampered by the presence of fluorocarbon groups attached to the dendrimer.

A further trial experiment was carried out (analogous to the trial carried out in section 3.2.3) to determine whether direct bonding of the fluorocarbon groups to the phenyl ring was responsible for hindering this reaction. The head group used for this trial synthesis is also analogous to the one shown in figure 3.2.3.1 and has two C$_8$F$_{17}$ fluorocarbon groups separated from the phenyl ring by an ester linkage and a propyl spacer, this molecule is referred to as 2C$_8$F$_{17}$-Br. Again the synthesis was found to be unsuccessful and the recovered polymer was simply the poly(ethylene oxide) starting material.

3.2.6 General Problems with Fluorinated Materials

Both the Williamson coupling end-capping and anionic polymerization synthetic methods are effective in producing control materials with no fluorocarbon groups present but appear to be fundamentally flawed when fluorocarbon groups are introduced to the dendron. Attempts have been made using both synthesis techniques to produce target materials containing dendrons with small CF_3 groups and with larger fluorocarbon groups separated from the phenyl ring of the dendron by an ethylene oxide link. However, all of these materials are prone to same limitations and all attempts at synthesis have failed.

Several studies have been carried out by various research groups to investigate the specific properties of fluorinated materials and the effects induced on molecules by the presence of fluorinated groups[20-24]. Similar issues have been found with various fluorinated materials, where the properties of a reaction site on a molecule have been drastically altered by the presence of a fluorinated group in the starting materials.

3.2.7 Synthesis of First Generation Fluorinated Dendritic End Capped Poly(Ethylene Oxide) by Catalyzed Trans-Esterification

Having established that the anionic polymerization and Williamson coupling methods of synthesis are ultimately incapable of producing the materials of interest to this project, due to the influence of the fluorinated components of the dendrons, a new approach was needed.

The catalyzed trans-esterification coupling method can be used to form a bond between a molecule containing an alcohol group and another containing an ester group. These ester linkages are strong and robust and should be ideal for coupling fluorinated dendrons to a poly(ethylene oxide) chain to achieve the target materials outlined previously in this project. One major advantage of this catalyzed trans-esterification coupling method is that no solvent is required and as a result it should be relatively easy to prevent impurities (water in particular that can be very difficult to remove from most solvents) from getting into the system. Another major advantage to this method is the

variety of catalysts that can be used to carry out this reaction; therefore it should be possible to find a catalyst that is not affected by fluorinated groups.
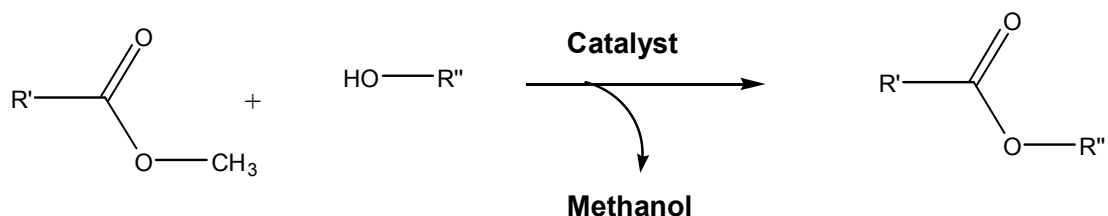
Figure 3.2.7.1: General reaction scheme for catalyzed trans-esterification

3.2.7.1 Synthesis of Starting Materials

In previous syntheses, the fluorinated dendrons have had either an alcohol or bromine as the functional group. In order to proceed with this reaction it is first necessary to synthesize the fluorinated dendritic ester. The fluorinated components of the dendrons are purchased from Sigma-Aldrich in the form of an alcohol (perflourooctyl propanol) with the formula $C_8F_{17}(CH_2)_3OH$. The first step is to brominate this molecule following the route outlined in figure 3.2.7.2.1.

3.2.7.2 Synthesis of 1-Bromo Perfluorooctyl Propane

The solvent required for this reaction is a 2:1 volume ratio of dichloromethane and Tetrahydrofuran (DCM and THF). 100 mL of this solvent mixture was placed in a 250 mL round-bottomed flask with a side-arm and then chilled in an ice bath under an inert nitrogen atmosphere. A flow of nitrogen was passed over the solution while 10g of perfluorooctyl propanol was introduced to the solvent, the system was then sealed and the mixture stirred for an hour using a magnetic stirrer to ensure the perfluorooctyl propanol is fully dissolved in the DCM/THF solvent. A 10% molar excess (with respect to perfluorooctyl propanol concentration) of carbon tetrabromide (or tetrabromomethane,

CBr$_4$) was then introduced to the reaction vessel via the side arm of the flask, a constant flow of nitrogen was passed through the reaction vessel to maintain the inert atmosphere, and the mixture was again stirred for an hour to ensure good mixing. A 10% molar excess of triphenylphosphine (PPh$_3$) was then introduced drop-wise to the chilled mixture as the reaction is highly exothermic. After leaving the reaction to proceed overnight a small amount of the reaction mixture was taken for NMR. At this point only around 25-30% of the alcohol starting material had been successfully brominated. To drive the reaction to completion another 0.5 M of PPh$_3$ was added drop-wise and the ice bath removed, after 4 hours another small sample was extracted for NMR revealing that the reaction had gone to completion. A small amount of water was then added to quench any unreacted substrates and the solvent removed using a rotary evaporator.
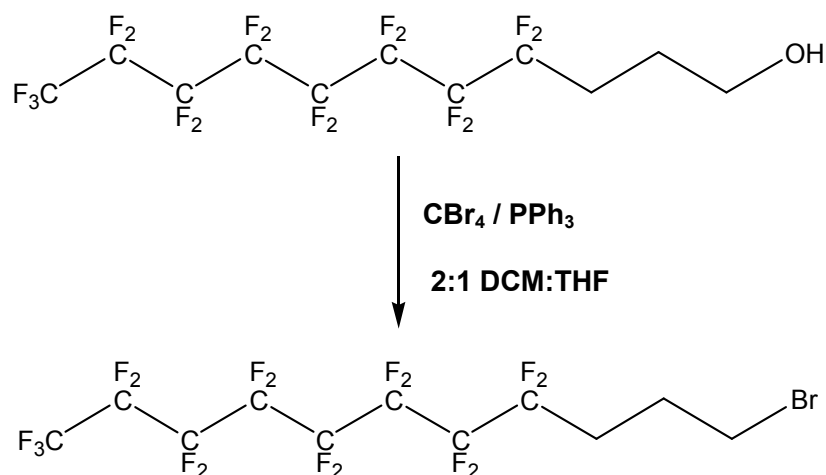
Figure 3.2.7.2.1: Reaction for the bromination of the alcohol group

The crude product was then redissolved in dichloromethane and washed with water to remove any unreacted CBr$_4$, PPh$_3$ and any other water soluble impurities. The combined dichloromethane washes were then dried over magnesium sulphate, which was then removed by filtration using a Buchner funnel. The dichloromethane was removed using a rotary evaporator and the residue redissolved in hexane and any insoluble impurities were removed by filtration. The hexane was then removed using a rotary

evaporator and the product was then extracted by fractional distillation under reduced pressure to give a final yield of around 80%.

3.2.7.3 Synthesis of Fluorinated Dendritic Ester End-Capping Agent

Purified 1-bromo perfluorooctyl propane was then attached to the methyl 3,5-dihydroxybenzoate via a Williamson coupling reaction to form the fluorinated dendritic ester end capping agent to be used in the catalyzed trans-esterification reaction. The synthetic route is outlined as follows and shown in figure 3.2.7.3.1.
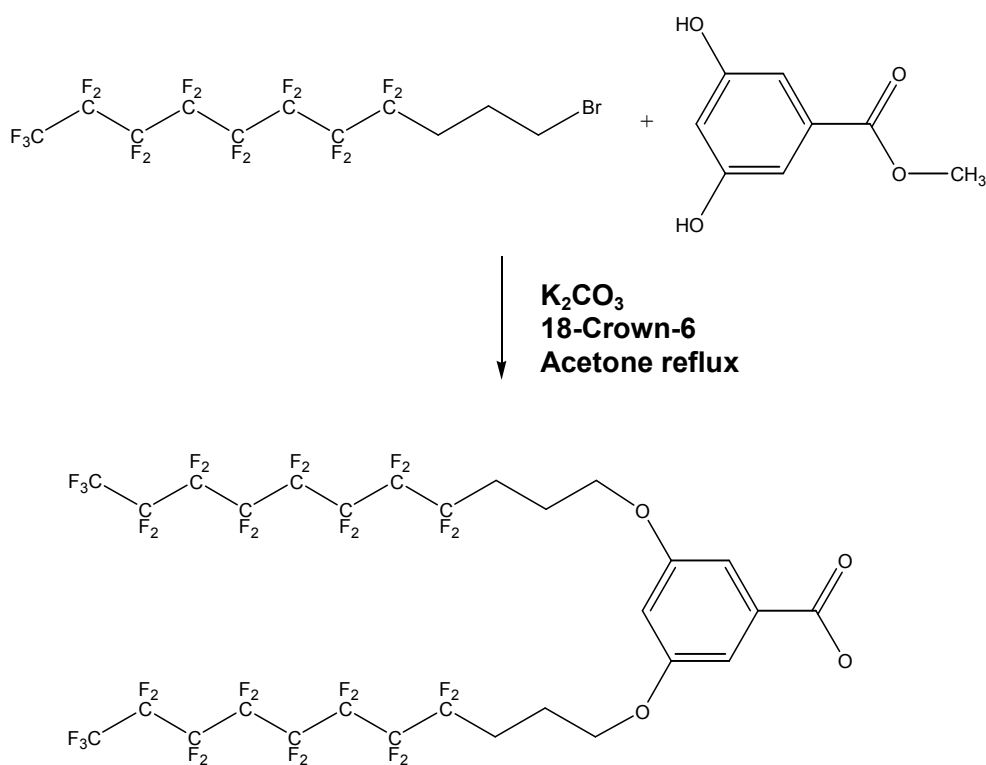
Figure 3.2.7.3.1: Williamson coupling reaction to form fluorinated dendritic ester

0.5g of methyl 3,5-dihydroxybenzoate was dissolved in 100 mL of dry acetone along with a 10% molar excess of potassium carbonate (K_2CO_3). A 0.9:1 molar ratio of

18-crown-6 with respect to 3,5-dihydroxybenzoate concentration was then introduced to the reaction mixture, which was then stirred under an inert nitrogen atmosphere for 2 hours to ensure good mixing. A 1.1 molar excess (with respect to concentration of methyl 3,5-dihydroxybenzoate, in this case 3.25g) of 1-bromo perflourooctyl propane is then dissolved in dry acetone (50 mL or as much as is necessary to fully dissolve the 1-bromo perflourooctyl propane) and introduced to the reaction mixture via syringe to maintain the inert atmosphere of the system. The system was then warmed to 60°C causing the acetone to reflux and was left stirring overnight.

After 18 hours the reaction had gone to completion and the solvent was removed using a rotary evaporator. The crude product was then redissolved in dichloromethane and washed with water to remove the 18-crown-6 from the system. The combined dichloromethane washes were then dried over magnesium sulphate, which was then removed by filtration. The dichloromethane was removed in a rotary evaporator and the product was precipitated into hexane and recovered by filtration using a Buchner funnel. Purification of the product is achieved simply by repetition of the method used to extract the crude product. The pure product is then placed in a vacuum oven overnight to remove any remaining solvent or water to give a yield of around 85%. The dendritic product has two C_8F_{17} fluorocarbon groups separated from the phenyl ring by an ester linkage and a propyl spacer, this molecule is referred to as $2C_8F_{17}$-COOH.

3.2.7.4 Synthesis of Deuterated Poly(Ethylene Oxide)

In order to achieve a good contrast for neutron reflectometry experiments it is necessary to use deuterated materials (in this case deuterated poly(ethylene oxide) to be attached to the dendrimer shown above). However, purchasing deuterated polymers can be extremely expensive and for this reason it is necessary to synthesize deuterated poly(ethylene oxide) in house[3,4]. It is also essential to synthesize the deuterated poly(ethylene oxide) with the reactive alcohol group on one end and an unreactive group on the other, as the dendrimer group is only required at one end of the polymer.

The anionic polymerization reaction is very sensitive to water and therefore it is essential that all reagents are purified and kept dry before use.
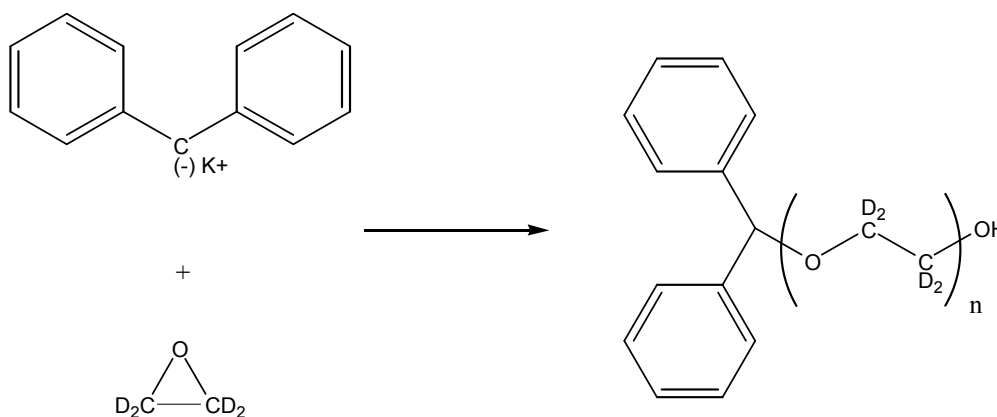
Figure 3.2.7.4.1: Polymerization of deuterated poly(ethylene oxide)

The synthetic route was followed exactly as described in section 3.2.1 with the following exceptions:

- No dendritic initiator was utilized; the initiating species was simply the diphenylmethyl potassium.
- 5 g of deuterated ethylene oxide was used with enough diphenylmethyl potassium to make deuterated poly(ethylene oxide) with a molecular weight of 5000 g mol^{-1}.

Once the polymerization was complete and the termination step carried out by addition of glacial acetic acid, the solvent was removed on a rotary evaporator and the polymer was recovered by addition to hexane and filtered off using a Buchner funnel. The polymer was dried overnight in a vacuum oven to give a final yield in excess of 90%. Characterization by NMR and GPC shows the product to have a molecular weight of around 3,600 g mol^{-1} with a polydispersity (Mw/Mn) of 1.04.

This lower molecular weight is most likely due to an inaccuracy in the concentration of the anionic polymerization initiator; some of the solvent in the stock solution of diphenylmethyl potassium may have evaporated over time therefore

increasing the concentration of the initiating species and reducing the molecular weight of the synthesized polymer.

After some considerations it was decided that this low molecular weight of 3,600 g mol^{-1} was not sufficient and that it would be prudent to synthesize the materials with a molecular weight of around 10,000 g mol^{-1} to compare directly with the similar previously synthesized polymers. Therefore the synthetic process was repeated using 5 g of deuterated ethylene oxide great care was taken care to add the correct amount of the diphenylmethyl potassium initiator to produce a deuterated poly(ethylene oxide) chain of around 10,000 g mol^{-1}.

Characterization by NMR and GPC showed this product to have a molecular weight of around 8,800 g mol^{-1} with a polydispersity (Mw/Mn) of 1.07.

3.2.7.5 Synthesis of End Capped Poly(Ethylene Oxide) by Catalyzed Trans-Esterification
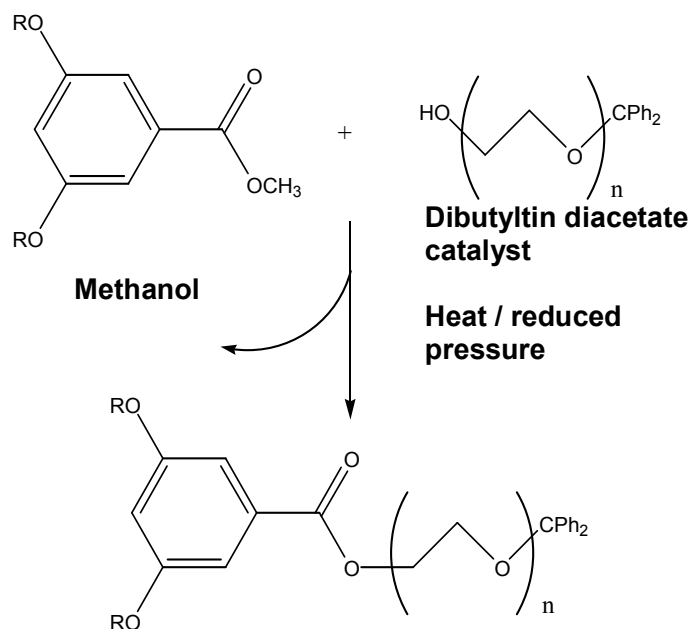
Figure 3.2.7.5.1: Catalyzed trans-esterification reaction

2g of the previously synthesized deuterated poly(ethylene oxide) was placed into a round bottomed flask under a nitrogen atmosphere along with a 10% molar excess of the fluorinated ester dendrimer ($2C_8F_{17}$-COOH). The system was fitted with a reflux condenser and heated to 160°C with stirring. To this was added a catalytic amount (1 mL) of dibutyltin diacetate introduced via a gas tight syringe in order to keep the system free from moisture and air, then the mixture was stirred for 4 hours to allow the reaction to begin to proceed. After 4 hours the system was reduced in pressure to 10 mmHg to help remove the methanol side product and drive the reaction to completion, another 1 mL of dibutyltin diacetate was also added to the reaction at this stage as the catalyst is quite volatile and will boil away during the reaction. After 4 more hours at reduced pressure the system was cooled to room temperature and raised to atmospheric pressure and the crude reaction mixture was dissolved in a small amount of dry THF. The polymer product is then precipitated into a mixture of hexane and methanol and recovered by filtration using a Buchner funnel. This process is repeated to improve purity and after drying in a vacuum oven gives a yield of around 70%.

The purification process was repeated until the obvious impurity peaks of the NMR spectra were removed, the polymer was then submitted for elemental analysis and the results are shown in table 3.2.7.5.2. By comparing the predicted and actual compositions of the $2C_8F_{17}$ dendritic end capped poly(ethylene oxide) product it was shown that around 22% of the poly(ethylene oxide) was successfully end capped during the synthesis.

Element	Theoretical Composition - 100% Conversion	Actual Composition of Product
C	46.14%	52.71%
H	0.32%	1.27%
F	13.96%	3.07%

Table 3.2.7.5.2: Elemental analysis of difluorinated end capped poly(ethylene oxide) product

A second attempt was made to try to improve the conversion of the reaction. Most conditions were repeated exactly as before with the following modifications:

- 0.5mL of the dibutyltin diacetate catalyst was added every half hour throughout the reaction to replace the catalyst lost through boiling.
- The reaction was allowed to proceed under reduced pressure for 8 hours instead of 4 hours and catalyst was added throughout this entire period.
- A 0.2 molar excess of fluorinated dendritic ester was used.
- A reaction temperature of $180^{\circ}C$ was used and the pressure monitored very carefully throughout.

Element	Theoretical Composition - 100% Conversion	Actual Composition of Product
C	46.14%	49.26%
H	0.32%	1.48%
F	13.96%	7.54%

Table 3.2.7.5.3: Elemental analysis of second synthesis of difluorinated end capped poly(ethylene oxide) product

Elemental analysis results (shown in table 3.2.7.5.3) showed that the conversion rate for this reaction was around 54%. Given the limited amount of time left for synthesis of materials in time for the scheduled beam time at the neutron source at ISIS it was decided that this conversion rate would suffice and it was necessary to move on with the synthesis of the analogous trifluoroalkyl material.

The same synthetic route was modified to synthesize the analogous trifluoroalkyl material with very similar results. The only necessary alteration to the synthetic method was during the Williamson Coupling stage (described in section 3.2.7.3), during which the methyl 3,5-dihydroxybenzoate is replaced with methyl 3,4,5-dtrihydroxybenzoate and a 3.3:1 molar ratio of 1-bromo perfluorooctyl propane with respect to concentration of

methyl 3,4,5-dtrihydroxybenzoate is also applied. The altered structures are shown in figure 3.2.7.5.4.

Elemental analysis results (shown in table 3.2.7.5.5) showed that the conversion rate for this reaction was around 51%.
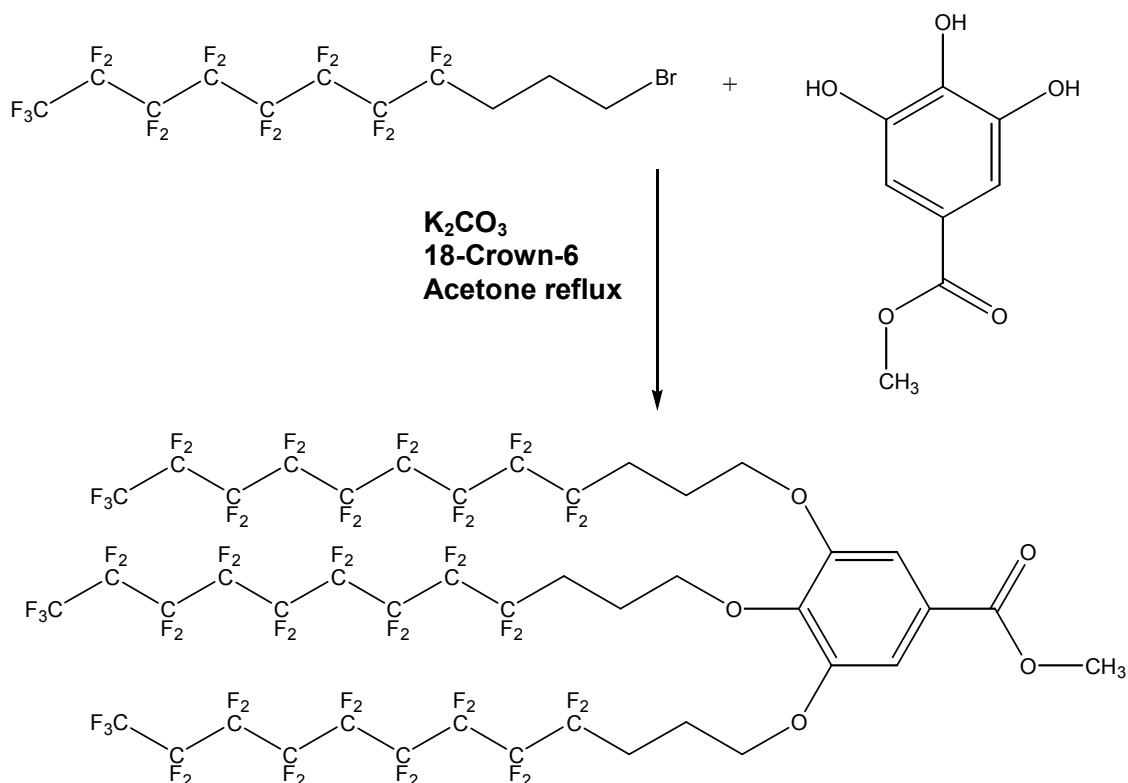
Figure 3.2.7.5.4: Williamson coupling dendrimer synthesis

Element	Theoretical Composition - 100% Conversion	Actual Composition of Product
C	44.02%	46.81%
H	0.41%	1.71%
F	19.11%	9.74%

Table 3.2.7.5.5: Elemental analysis of second synthesis of trifluorinated end capped poly(ethylene oxide) product

3.2.8 Synthesis of First Generation Dodecyl Functionalized Dendritic End Capped Poly(Ethylene Oxide)

In order to fully understand the hydrophobic effect of functionalizing poly(ethylene oxide) with fluorinated head groups it is necessary to synthesize a control molecule. By replacing the fluorinated head groups with the equivalent simple alkyl chains it is possible to compare the hydrophobic properties and the tethering strength of the two materials to an air-water interface and therefore determine the specific effects of the fluorine on the molecule.

As mentioned previously, the ideal synthetic route for these molecules is to synthesize the head group first and then to grow the poly(ethylene oxide) chain from an alcohol group at the centre of the dendrimer. For the fluorinated head groups this method was not possible as the fluorine interfered with the initiation of the polymerization. For these alkyl equivalent materials however this technique should be clean and pure with a 100% conversion rate.

3.2.8.1 Synthesis of Starting Materials

Methyl 3,5-dihydroxybenzyl alcohol is dissolved in dry acetone along with a slight molar excess of caesium carbonate. In this synthesis caesium carbonate is preferred to potassium carbonate as it removes the need for the 18-crown-6, which in the previous synthesis proved to be time consuming and troublesome to remove from the product.

A 1.2 molar excess of 1-bromododecane was then dissolved in dry acetone in a separate flask and introduced to the reaction mixture via syringe to maintain the inert atmosphere of the system. The system was then warmed to 60°C causing the acetone to reflux and was left stirring overnight. The reaction was followed by NMR and at this stage it was found that the reaction had only reached approximately 40% conversion. This was due to the fact that the caesium carbonate had become stuck to the sides of the reaction flask overnight and had to be agitated with a metal wire to return it to the solution.
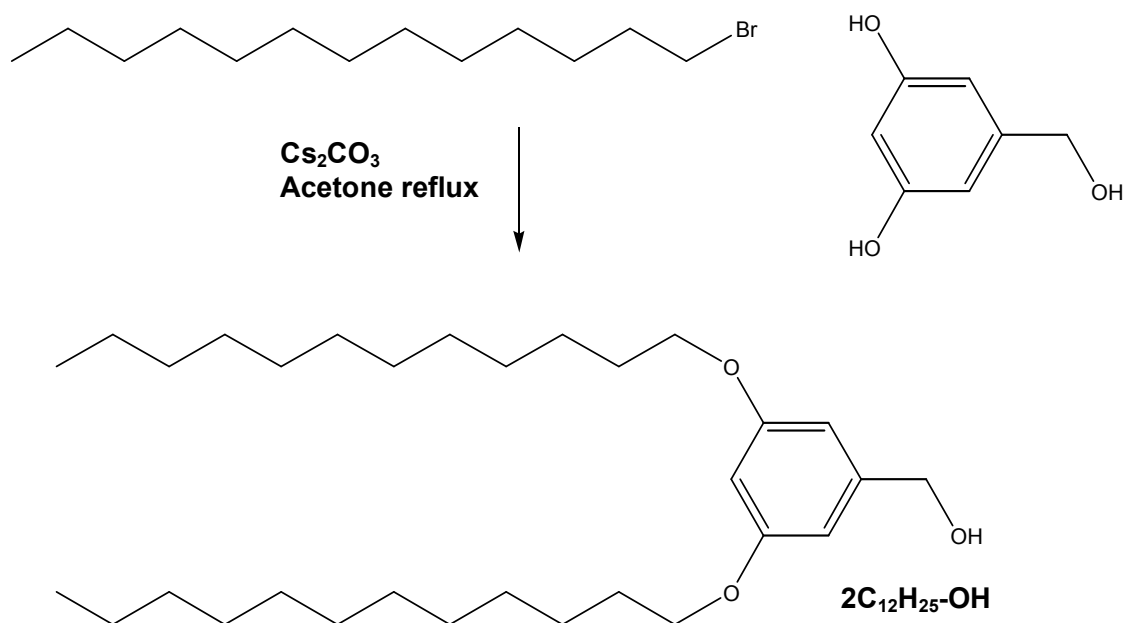
Figure 3.2.8.1.1: Dodecyl head group synthesis via Williamson coupling reaction

The reaction was allowed to proceed for another night and after 40 hours the reaction had gone to completion. The solvent was then removed using a rotary evaporator and the crude product was then redissolved in dichloromethane and washed with water to remove the caesium carbonate from the system. The combined dichloromethane washes were then dried over magnesium sulphate, which was then removed by filtration. The dichloromethane was removed in a rotary evaporator and the product was precipitated into hexane, where it was then extracted by simple filtration using a Buchner funnel. The pure product was then placed in a vacuum oven overnight to remove any remaining solvent and water to give a final yield of around 93%.

The product is the didodecyl dendritic end cap with an alcohol functional group shown in figure 3.2.8.1.1 and is given the name $2C_{12}H_{25}$-OH.

3.2.8.2 Synthesis of Dodecyl Functionalized Dendritic End Capped Poly(Ethylene Oxide) by Anionic Polymerization

As with all the previous materials it is necessary to synthesize deuterated poly(ethylene oxide) in order to achieve a good contrast in later neutron reflectivity experiments. However, in this case it is possible to use deuterated ethylene oxide and grow the polymer from the alcohol functional group of the dendrimer.
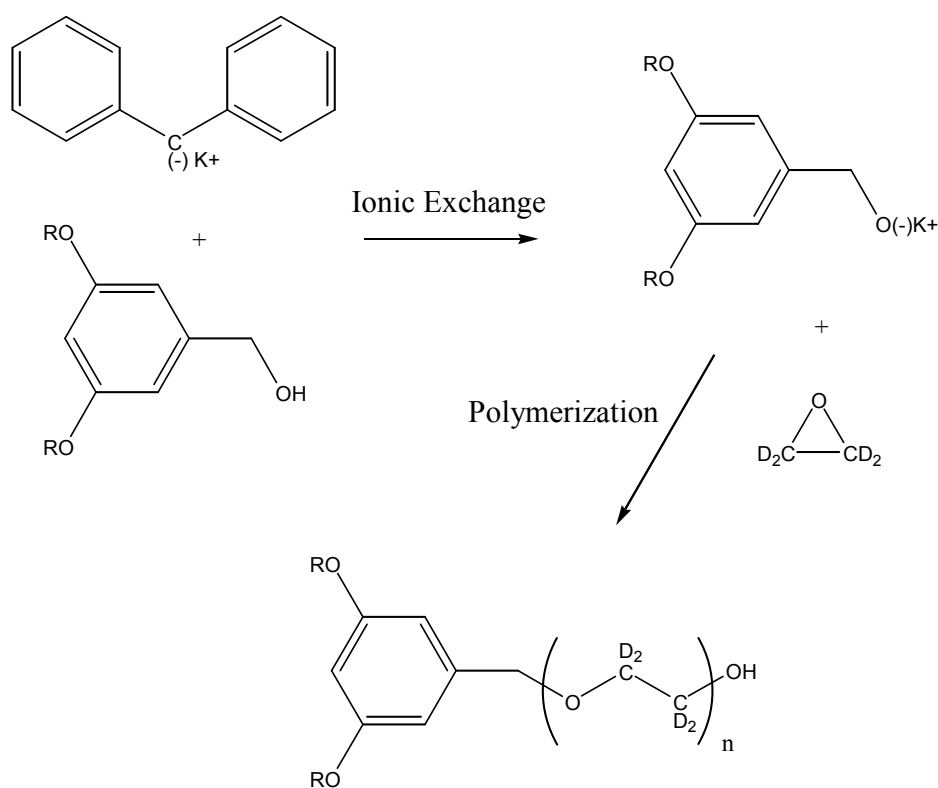
Figure 3.2.8.2.1: Polymerization of deuterated poly(ethylene oxide)

The purification of starting materials, synthetic route and work up of final product was carried out in the same way as the synthesis of dibenzyloxybenzyl end capped poly(ethylene oxide), described in section 3.2.1, with the following exceptions:

- 2C$_{12}$H$_{25}$-OH functionalized dendritic end cap is used in place of dibenzyloxybenzyl alcohol as the initiator for the polymerization.

- 5g of deuterated ethylene oxide is used in order to synthesize deuterated polymer for use in neutron reflectometry experiments.

Upon completion of the synthesis and purification steps the polymer product was found to have been successfully synthesized with a final yield of 89%.

3.2.9 Summary of Synthesized Materials

Product Name	End Cap Functionality	Poly(Ethylene Oxide) Molecular Weight
Anionic Polymerization		
2C$_{12}$H$_{25}$10k	2 * C$_{12}$H$_{25}$ groups (100% conversion)	9500±650 gmol^{-1}
2C$_{12}$H$_{25}$5k	2 * C$_{12}$H$_{25}$ groups (100% conversion)	4500±200 gmol^{-1}
2C$_{12}$D$_{25}$10k	2 * C$_{12}$D$_{25}$ groups (100% conversion)	9500±900 gmol^{-1}
2C$_{12}$D$_{25}$5k	2 * C$_{12}$D$_{25}$ groups (100% conversion)	4500±250 gmol^{-1}
Catalyzed Trans Esterification		
2C$_8$F$_{17}$10k22	2 * C$_8$F$_{17}$(CH$_2$)$_3$ groups (22% conversion)	10000±700 gmol^{-1}
2C$_8$F$_{17}$10k54	2 * C$_8$F$_{17}$(CH$_2$)$_3$ groups (54% conversion)	10000±700 gmol^{-1}
3C$_8$F$_{17}$10k51	3 * C$_8$F$_{17}$(CH$_2$)$_3$ groups (51% conversion)	10000±700 gmol^{-1}

Table 3.2.9.1: Table showing various successfully synthesized polymer products

A series of polymers were prepared by the methodologies detailed in this section. Variations in molecular weights, slight variations in the structure of the end cap and deuteration of some of the dodecyl functionalities were carried out; the various polymers successfully synthesized are detailed in table 3.2.9.1.

It is important to emphasize here that all materials made by catalyzed trans esterification contain deuterated PEO tail groups with a Mw of 8800 to 8900±700 gmol^{-1}.

3.3 Experimental

3.3.1 Materials

3.3.1.1 Anionic Polymerization

All of the chemicals used in anionic polymerization were degassed repeatedly by freeze-evacuate-thaw cycles until a pressure of below 1×10^{-5} mmHg was sustained. Ethylene oxide (EO, Aldrich, 99.5+%) and ethylene-d_4 oxide (dEO, Aldrich, 98%) were subjected to further purification steps; distillation from Calcium Hydride (CaH_2) to remove any water present, then immediately before use; distillation from dibutylmagnesium ($Mg(Bu)_2$, Aldrich, 1.0 M solution in heptane). The tetrahydrofuran (THF) solvent was purified by the in-house solvent purification system, which passes the solvent through a system of columns designed to remove both protic impurities and oxygen, and also subjected to the same degassing technique (a sodium/benzophenone complex was used as an indicator to the presence of water and air). 3,5-dibenzyloxybenzyl-alcohol (Aldrich, 97%) was pre-dried in a vacuum oven and then degassed and purified by aziotropic drying using benzene (Aldrich, 99.9+%, purified by degassing and drying over CaH_2). Diphenylmethylpotassium (1M solution in THF) was previously synthesized in house by the reaction of potassium naphthalene with a slight molar excess of diphenylmethane[25]. Hexane (Aldrich, 95+%, anhydrous) used in the precipitation of the product was used as received.

3.3.1.2 End-Capping and Dendrimer Synthesis via Williamson Coupling Reaction

Methyl 3,5-dihydroxybenzyl alcohol (Aldrich, 99%), potassium carbonate (K_2CO_3, Sigma-Aldrich, 99+%), 18-crown-6 (Aldrich, 99%), 15-crown-5 (Aldrich, 98%) and Poly (ethylene oxide) (methyl terminated, 10,000g/mol), were all dried in a vacuum oven

overnight prior to use. 3,5-ditrifluoromethylbenzyl bromide (Aldrich, 97%), 4-(trifluoromethyl)benzyl bromide (Aldrich, 98%), benzyl bromide (Aldrich, 98%) and dry sodium hydride (NaH, Aldrich, 95%) were used as received. The acetone, THF and dichloromethane (DCM) solvents were all purified by the in-house solvent purification system as described in section 3.3.1.1.

Cesium carbonate (Cs_2CO_3, Aldrich, 99%) used in the synthesis of dendritic head groups was pre-dried in a vacuum oven prior to use.

3.3.1.3 Synthesis of Dendritic Esters and Catalyzed Trans-Esterification

Perflourooctyl propanol (check data sheet), potassium carbonate (K_2CO_3, Sigma-Aldrich, 99+%), 18-crown-6 (Aldrich, 99%), methyl 3,5-dihydroxybenzoate (Aldrich, 97%) and methyl 3,4,5-dtrihydroxybenzoate (Aldrich, 97%) were dried in a vacuum oven overnight prior to use. Carbon tetrabromide (CBr_4, Aldrich, 99%) and triphenylphosphine (PPh_3, Sigma-Aldrich, 99%) were used as received. The acetone, THF and DCM solvents were all purified by the in-house solvent purification system as described in section 3.3.1.1.

All starting materials previously synthesized to be used in the catalyzed trans-esterification synthesis were pre-dried in a vacuum oven. The dibutyltin diacetate catalyst (Aldrich, technical grade) was used as received.

3.3.2 Analysis

All of the end-capped polymers prepared were characterized using ^{1}H, ^{13}C and ^{19}F nuclear magnetic resonance (NMR) spectroscopy, gel permeation chromatography (GPC) and elemental analysis. A brief outline of each of these techniques is given below, as well as examples of results obtained.

3.3.2.1 Nuclear Magnetic Resonance Spectroscopy (NMR)

Deuterated solvents are required for use in NMR in order to prevent swamping of the spectrum from the hydrogen contained in the solvent. Deuterated chloroform ($CDCl_3$, Aldrich, 99.9% D, 0.03% v/v TMS), deuterated DCM (CD_2Cl_2, Goss/Cambridge Isotope Laboratories Inc., 99.9% D, 0.03% v/v TMS) and deuterated benzene (C_6D_6, Aldrich, 99.6% D, 0.03% v/v TMS) were used as received for general analytic purposes. 10mL of $CDCl_3$ was purified by distillation from CaH_2 to be used for samples that are highly sensitive to the presence of water. Samples were prepared as a 5% solution by weight in deuterated solvent.

NMR spectroscopy was carried out using either a high resolution Varian Inova 500 MHz spectrometer for detailed analysis of final products or a lower resolution Mercury 400 MHz spectrometer for fast analysis while following a reaction as it proceeds. All ^1H, ^{13}C and ^{19}F NMR resonances are quoted relative to the control tetramethylsilane (TMS) resonance.

3.3.2.2 Gel Permeation Chromatography (GPC)

All GPC experiments were carried out using a system comprising of a Viscotek TDA 302 refractive index detector with 3 x 30mL PLgel 7.5mm columns. Analyses of all polymer products were carried out using dimethylformamide (DMF) as the eluent with a flow rate of 1.0mL/min at a constant temperature of 60°C. Molecular weights were calculated using a calibration curve generated from poly(ethylene oxide) standards with known molecular weights and very low polydispersity.

3.3.2.3 Elemental analysis

Elemental analysis was carried out to determine the percentage of carbon, hydrogen and fluorine present in the end capped polymer products. Theoretical mass

percentages of each atom type are first calculated for an ideal product with 100% conversion. Then the samples are analyzed to give the actual mass percentages of the product; comparing these 2 results gives us the extent to which the product has been successfully converted. Repeating the elemental analysis measurements on identical samples makes it possible to calculate an error for each sample.

3.4 References

[1] I. Pirma, *Polymeric Surfactants*, New York, **1992**.

[2] M. J. Schick, *Non-ionic Surfactants*, Marcel Dekker, New York, **1967**.

[3] M. J. Owen, *Siloxane Polymer*, Prentice Hall, Englewood Cliffs, NJ, **1993**.

[4] Q. R. Huang and C. H. Wang, *Langmuir* **1996**, *12*, 2679-2683.

[5] A. F. Miller, R. W. Richards and J. R. P. Webster, *Macromolecules* **2001**, *34*, 8361.

[6] S. K. Peace, R. W. Richards and N. Williams, *Langmuir* **1998**, *14*, 667-668.

[7] B. B. Sauer and H. Yu, *Macromolecules* **1989**, *22*, 786-791.

[8] R. W. Richards and J. Sarica, *Langmuir* **2003**, *19*, 7768-7777.

[9] C. Selve, J. C. Ravey, M. J. Stebe, C. E. Moudjahid, E. L. Moumni and J. J. Delpuech, *Tetrahedron* **1991**, *47*, 411-428.

[10] P. G. de Gennes, *Macromolecules* **1980**, *13*, 1069-1075.

[11] I. A. Ansari, N. Clarke, L. R. Hutchings, A. P. Narrainen, A. E. Terry, R. L. Thompson and J. R. P. Webster, *Langmuir* **2007**, *23*, 4405-4413.

[12] A. P. Narrainen, L. R. Hutchings, I. Ansari, N. Clarke and R. L. Thompson, *Macromolecules* **2007**, *40*, 1969-1980.

[13] A. P. Narrainen, L. R. Hutchings, I. A. Ansari, N. Clarke and R. L. Thompson, *Soft Matter* **2005**, *2*, 126-128.

[14] C. J. Hawker and J. M. J. Frechet, *J. Am. Chem. Soc* **1990**, *113*, 4252-4261.

[15] C. J. Hawker and J. M. J. Frechet, *J. Chem. Soc. Chem. Commun.* **1990**, *15*, 1010-1013.

[16] I. Gitsov, L. Wooley, C. J. Hawker, P. T. Ivanowa and J. M. J. Frechet, *Macromolecules* **1993**, *26*, 5621-5627.

[17] A. Dworak, A. Kowalczuk-Bleja, B. Trzebicka and W. Walach, *Polymer Bulletin* **2002**, *49*, 9-16.

[18] B. Forier and E. Dehaen, *Tetrahedron* **1999**, *55*, 9829-9846.

[19] I. Gitsov, K. L. Wooley and J. M. J. Frechet, *Angew. Chem. Int. Ed. Eng* **1992**, *31*, 1200-1202.

[20] M. Aschi, b. Chiavarino, M. E. Crestoi and S. Fornarini, *J. Phys. Chem.* **1996**, *100*, 19859-19863.

[21] J. Hrusak, D. Schroder, T. Weiske and H. Schwarz, *J. Am. Chem. Soc.* **1995**, *115*, 2015-2020.

[22] Y. K. Lau and P. Kebarle, *J. Am. Chem. Soc.* **1976**, *90*, 7452-7453.

[23] M. Tkaczik and A. G. Harrison, *J. Mass Spectrom. Ion Processes* **1994**, *132*, 73-76.

[24] R. Yamdagni and P. Kebarle, *J. Am. Chem. Soc.* **1976**, *98*, 1320-1324.

[25] F. Candau, F. Afchar-Taromi and P. Rempp, *Polymer* **1977**, *18*, 1253-1257.

Chapter Four: Analysis and Results

4.1 Introduction

The solution air surface has been widely studied for both polymers and small molecule surfactants. Whilst the surface-activity of end functional polymers in blends has been widely reported[1-6] the solution air surface of end functional polymers has received comparatively little attention. Until now, there has been no systematic study of the solution air properties of *multiply*-end functionalized polymers. Many polymer films and coatings are prepared from solutions, either by solution casting, or spin-coating and the self-organization of polymers within films is clearly linked to their self-organization in solution. Indeed it is quite possible the judicious use of surface active polymers in solution could be exploited to direct the self-assembly of polymers in films as the solution evaporates. Therefore the underlying science that is explored in this chapter has the potential to be exploited in the preparation of coatings, adhesives, repellant surfaces and conducting polymer devices.

The previous chapter was devoted to the preparation of a family of novel materials, which were expected to be highly surface active in aqueous solutions. This chapter describes the experimentally determined physical properties of these solutions. In particular the relationship between surface activity and adsorbed layer structure is discussed in relation to the chemical structure and functionalization of the polymers. Surface tensiometry was used to quantify surface activity of the functionalized polymers and neutron reflectometry enabled the first direct determination of the adsorbed layer structure of multi-end functional polymer at a solution-air surface.

4.2 Materials

The structure and calculated unperturbed solution dimensions of the multiply end-functionalized PEOs are summarized below in table 4.2.1 along with the values for the previously studied linear functionalized PEO[7].

Notation	Functionalization	Approx. Fluoro Group Surface Area (nm^2)	Radius of Gyration (nm)	Fluorine Content (%)
TDFO-PEO (F1)	tridecafluorooctanoyl isophorone monoisocyanate	0.55	4.18	2.47%
2C$_8$F$_{17}$10k54 (F2)	2 * C$_8$F$_{17}$(CH$_2$)$_3$ groups (54% conversion)	1.10	3.92 ± 0.21	3.31%
3C$_8$F$_{17}$10k51 (F3)	3 * C$_8$F$_{17}$(CH$_2$)$_3$ groups (51% conversion)	1.65	3.92 ± 0.21	5.05%

Table 4.2.1: Summary of calculated values for fluorinated materials

Here the approximate surface area for the fluorination components of each molecule is calculated from an estimate of 0.28 nm^2 for the cross-sectional area of a perfluorocarbon chain[8] using the following formula:

$$a_{FG} = \left(n_{PF} l_{PF} \right) \sqrt{a_{PF}}$$

Equation 4.2.1

where a_{FG} is the total surface area for the fluorinated group of each molecule, n_{PF} is the number of perflourocarbon (CF$_2$) groups in each molecule, l_{PF} is the average distance between perflourocarbon groups in the chain (0.13 nm) and a_{PF} is the surface area of a perflourocarbon group.

The z-average square radii of gyration, $\left\langle S^2 \right\rangle_z$ (in cm^2), for the PEO chains relevant to this study is a measure of the end to end distance of a free polymer chain in solution and can be calculated using the relationship determined by Kawaguchi et al[9]:

$$\left\langle S^2 \right\rangle_z = 4.08 \times 10^{-18} \times M_w^{1.16}$$

Equation 4.2.2

where Mw is the molecular weight of the polymer in g mol^{-1}.

As all the materials analysed by neutron reflectivity in this study contain a PEO segment with a molecular weight (M_n) of around 8800 to 8900 g mol^{-1} (with a maximum M_w/M_n of 1.07 giving range of around 8100 to 9600 g mol^{-1}), it is predicted using equation 4.2.2, that the z-average square radii of gyration for all of these materials will be around $1.39*10^{-13}$ to $1.70*10^{-13}$ cm^2. These values can then be converted to radius of gyration values, R_g, to give a range of between around 37.2 to 41.3 Å.

The fluorine content (%) for each molecule is calculated using the following simple formula:

$$\%F = \frac{M_F F_{con}}{M_{tot}}$$

<div align="right">Equation 4.2.3</div>

Where *%F* is the fluorine content (%) for each molecule, M_F is the molecular mass of fluorine calculated from the molecular formula and M_{tot} is the total molecular mass of the molecule.

4.3 Experimental Methodology

4.3.1 Surface tensiometry

Surface tension values for aqueous solutions of the polymers were collected using a Krüss K10 digital tensiometer. The temperature of the subphase was regulated at 298 K by using a Haake thermostat water circulator. This is very important as the main source of uncertainty in surface tensiometry comes from the fact that for almost all liquids the surface tension drops linearly with increasing temperature[3, 4]. The surface tension was measured by using the Du Noüy Ring method[10, 11], whereby a metal ring is immersed into the sample solution and then drawn out. This forms a liquid lamella that is stretched to its maximum and the surface tension is calculated from the resulting force needed to pull the ring away from the surface. Calibration is carried out on the equipment and zeroed with the ring apparatus hanging free. Glassware was previously cleaned by soaking in permanganic acid (mixture of sulphuric acid and few crystals of potassium

permanganate) overnight and the vessels were then rinsed several times with ultra high quality (UHQ) water and finally dried at room temperature. The polymer was dissolved in UHQ water in a volumetric flask and left overnight to ensure complete dissolution of the material. The dissolved polymer was poured into a 25 ml dish and diluted *in situ*. A range of concentrations from 0.000001% weight of material added per volume of solvent (referred to as $^w/_v$ from now on) up to around 1% $^w/_v$ of modified and unmodified PEO were investigated.

In order to fully investigate the influence of the fluorocarbon groups on the properties of the materials investigated here (in particular the strength of surface tethering) it is also necessary to investigate the properties of an unfunctionalized control material. In this case the control material is a deuterated poly(ethylene oxide) chain with a similar molecular weight to that of the final polymer synthesized during the end capping experiment described in section 3.2.7.4 containing the same diphenylmethyl group. This control sample makes it possible to isolate the contribution of the fluorocarbon groups to surface activity precisely. To investigate any hydrophobic effects of this diphenylmethyl group it is also necessary to carry out measurements on a completely unfunctionalized poly(ethylene oxide) chain. This was purchased from Sigma-Aldrich with a molecular weight (M_w) of 10000 g mol^{-1} and a reported polydispersity of 1.02.

4.3.2 Neutron Reflectometry

4.3.2.1 Scattering Length Density

The scattering length density (SLD) of a material is the sum of the neutron scattering lengths from the nuclei per unit volume and essentially gives a measurement of the influence that a material has upon a neutron beam that is incident upon it (SLD and neutron techniques in general are explained in more detail in section 2.3). The scattering length densities for any material can be calculated using the following formula:

$$SLD = \sum_i b_i n_i = \sum_i b_i \frac{\rho_i N_A}{A_i}$$

.

Equation 4.3.2.1.1

Where A_i = Isotopic mass,

ρ_i = Physical density of the component,

N_A = Avogadro's number,

b_i = Scattering length of the isotope.

Fortunately the SLD for normal water (H_2O) has a negative value and heavy water (D_2O) has a positive value (values shown in table 4.3.2.1.1) and it is therefore possible to mix these together in the correct proportions (91% H_2O to 9% D_2O) to make water with a SLD of zero; null reflecting water (NRW). The theory and explanation for these values can be found in section 2.3.3.

Material	Scattering Length Density (SLD)/ 10^{-6}Å^{-2}
Air/NRW	0
Water (H_2O)	-0.55
Heavy water (D_2O)	6.35
Poly(ethylene oxide)	0.56
Deuterated poly(ethylene oxide)	5.74
Fluorinated end-cap [$(C_8F_{17})_2C_6H_6$]	1.95

Table 4.3.2.1.1: Scattering length densities of main components in polymer solutions

The SLD values for materials relevant to this study are also shown in table 4.3.2.1.1 and the need for deuterated poly(ethylene oxide) can be seen when looking at the SLD values. The scattering length density of normal hydrogenous poly(ethylene oxide) is very small and would show very little contrast with NRW and the signal would mostly be lost in background noise, which is dominated by the incoherent scattering from H in the NRW. Deuterated poly(ethylene oxide) has a much larger scattering length density and

will therefore give much better contrast with NRW, which makes neutron reflectivity extremely sensitive to surface adsorption.
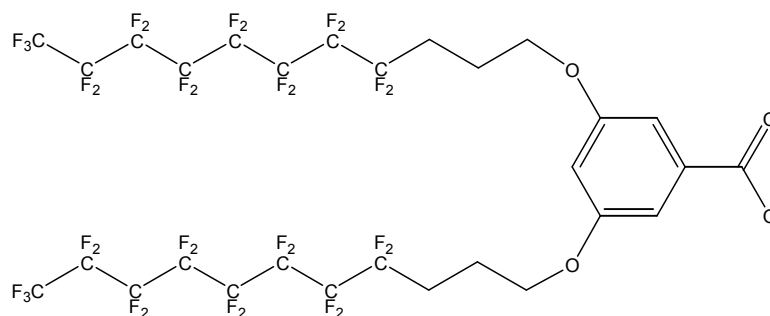
Figure 4.3.2.1.2: Illustration of end-cap (F2) attached to poly(ethylene oxide) used in neutron reflectometry

The calculated scattering length density for the fluorinated end cap as based on the structure shown in figure 4.3.2.1.2 (the exact structure of the end cap used in the synthesized materials). The calculated value falls between the value for deuterated poly(ethylene oxide) and NRW so it should therefore be possible to distinguish the separate components from the neutron reflectometry data.

4.3.2.2 Experimental Setup

Neutron reflectometry data on aqueous solutions of the fluorocarbon end-capped and alkyl equivalent end-capped polymers were collected using the SURF reflectometer at the ISIS pulsed neutron source, Rutherford Appleton Laboratory, Didcot, UK.

An aqueous stock solution of 1% $^w/_v$ of the difluorinated end capped deuterated (F2d) PEO (54% conversion) in NRW was prepared using volumetric pipettes and flasks. This stock solution was then diluted down using the same equipment by taking 10mL of the solution and adding 90mL of NRW to give solutions of 0.1111% $^w/_v$, 0.0123% $^w/_v$, $1.37 \times 10^{-3}\%$ $^w/_v$, $1.52 \times 10^{-4}\%$ $^w/_v$ and $1.69 \times 10^{-5}\%$ $^w/_v$. Solutions of the equivalent alkyl end-capped PEO and the unfunctionalized deuterated poly(ethylene oxide) were also prepared

in exactly the same way to be used as a control experiment to isolate the influences of the functional groups and their components. Due to restrictions applied by the quantity of the trifluorinated end capped deuterated (F3d) PEO (51% conversion) that could be synthesized in time for use in the neutron reflectometry experiments; a stock solution of 0.066% $^w/_v$ in NRW was prepared using the technique described above. This stock solution was then diluted down using the same equipment to give solutions of 0.0332% $^w/_v$, 0.0123% $^w/_v$, $4.24*10^{-3}$% $^w/_v$, $1.37*10^{-3}$% $^w/_v$, $1.52*10^{-4}$% $^w/_v$ and $1.69*10^{-5}$% $^w/_v$.

While this null reflecting solution is ideal for allowing us to observe the structure of each polymer as if it were floating in space, it is also very useful to observe the polymer in deuterated (heavy) water as profiles measured on only one phase contrast have no phase information. For example in a neutron reflectivity experiment carried out in NRW it is possible to invert the scattering length density profile and the calculated reflectivity would remain unchanged. There is very little contrast in SLD between deuterated water and the deuterated PEO chain segment of the materials, but a very large contrast between either of these materials and air. Therefore, this experiment will be very sensitive to any perturbation in the solution surface due to the presence of fluorocarbon or hydrogenous head groups. For this reason the materials were also diluted into deuterated (heavy) water in exactly the same way as described previously for NRW.

Once the solutions had been prepared and thoroughly mixed they were taken to the platform in the neutron beam end station. The sample holder consists of five 25mL Teflon troughs inside sealed containers with quartz inlet and outlet windows for the incident and reflected neutron beams. The solutions were added carefully to each trough via pipette to reduce the occurrence of any bubbles that may have an adverse affect (such as increased incoherent background scattering) on the results obtained. The resulting reflectivity is defined as the ratio of the intensity of the incident beam (measured by monitor) to the reflected beam (measured by a time of flight (TOF) detector). The raw data were converted to absolute reflectivity using calibration factors obtained from fitting to the reflectivity of deuterated water. By using two different incident angles (0.8° and 1.5°) of the neutron beam, the range of scattering vector explored was $0.039 \leq Q / \text{Å}^{-1} \leq 0.6$. A command file was used to control the data collection instruments. This included commands to collect data until a pre-determined flux of neutrons had been reached and

then automatically alter the incidence angle or to move to a different sample once this value was reached. Data collection times were heavily dependent on the beam current reaching the neutron source and on the chosen desired total neutron flux (affected greatly by the available beam current), polymer type and the subphase in which it is dissolved. . In general data collection times ranged from 30-60 minutes for low angle data to 2-4 hours for high angle data, with the data experiments in NRW taking an average of around 3 times longer to collect than those carried out in D_2O due to the weaker reflection from the NRW solvent.

4.3.2.3 Data Reduction

A problem that is associated with all neutron beam techniques, due to the relatively low flux levels available, as that of the background noise caused (primarily) by incoherent scattering of neutrons by interaction with protons in the bulk solvent (this is more significant for NRW as this is 90% H_2O). Therefore once each reading was taken it was necessary to determine the value for the background noise of the data, this is typically at Q values greater then ~0.3 Å^{-1} where the R(Q) values level of at a value between $8\text{-}9*10^{-6}$. Background signal values for each solvent type are then subtracted from the raw data. The data collected from both incident angles are then combined into a single ASCII file ready for analysis.

For neutron reflectivity experiments carried out on a solvent trough the simplest and most effective way of correcting for the signal generated by neutron interactions with the solvent is to take a measurement for the pure D_2O solvent under the same conditions and flux level as the samples to be studied. A scale factor is then derived from this R(Q) data on pure D_2O to yield a reflectivity in the critical region of 1 (i.e. $R(Q<Q_{crit})=1$. This scale factor can then be applied to all of the other solutions measured under the same conditions.

4.3.2.4 Data Fitting Methods

The analysis of raw data obtained from a neutron reflectometry experiment is not a trivial exercise as there is a major fundamental problem with relating neutron reflectivity

data directly to the composition of the material from which the data came. This is due to the fact that in practice it is not possible to use a Fourier transformation to directly convert the data into composition information since all of the phase information is lost from the data and there is therefore no unique solution to the composition for each data set. As a result, interpretation of neutron reflectivity data is generally achieved through comparison with simulation data from a model system.

A data fitting program has been developed by the instrument scientists at the Rutherford Appleton laboratory to analyze neutron reflectometry data. R(Q) vs. Q data (an example of 7 different sets of this data is shown in figure 4.3.2.4.1, these are for each concentration of the $3C_8F_{17}10k51$ material) is entered into the computer program.
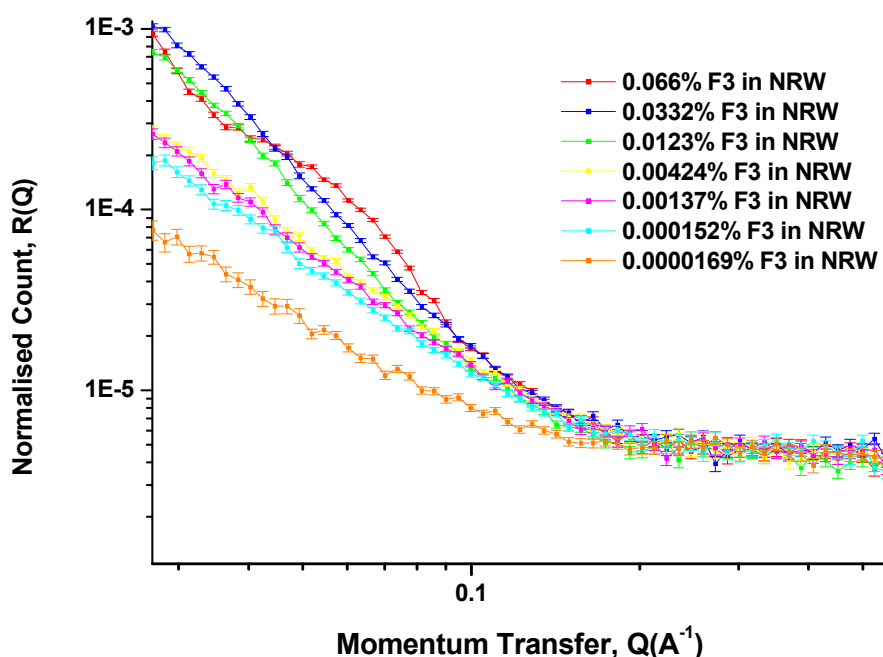
Figure 4.3.2.4.1: Example of neutron reflectometry data for all concentrations of $3C_8F_{17}10k51$ (F3d) material in NRW

Values for the background noise, number of layers expected in the system, scattering length densities and predicted roughness of each layer as well as information

on experimental setup such as incident beam angle etc are also entered into this computer program in order to achieve the best possible fit for each set of data.

Several trial estimates of each individual layer thickness and roughness are usually needed before a satisfactory fit is achieved and the accuracy of these fits is calculated by the fitting program as it carries out the iterations and tries to achieve a good fit and a χ^2 value is displayed in the output of the program to quantify the accuracy of a given fit. In this case a Pearson χ^2 test is used to measure the goodness of fit of the frequency distribution and therefore a value of 1 is optimal, however each case is judged individually as there may be background noise or scatter in the experimental data in which case a Pearson χ^2 value of 1 is virtually impossible to achieve.

Once satisfied that the calculated fits give an acceptable χ^2 value (generally as close to a value of 1 as possible, but each case is judged individually as there may be a lot of background noise or variations in the experimental data) the output from the program is examined to ensure that the profiles shown are realistic. The output from the fitting program consists of a value for the scattering length density, thickness and roughness of each layer and can be displayed as a scattering length density (SLD) vs. sample depth profile. These profiles are initially checked to for scattering length density values exceeding $6.35*10^{-6}$ Å^{-2} or significantly below zero could not arise from the components known to be present in solution. Density profiles with these features were rejected immediately as unphysical. Among the other things to check at this stage include the surface roughness as often the program would give a value for surface roughness that is far too large and in some cases could even be orders of magnitude greater than the thickness of the layer itself. The r.m.s. roughness of water is typically accepted as 3 Å[12] and even at the reduced surface tensions encountered here this should not exceed a value of 7 Å. Some apparent contribution to the surface roughness could be attributed to the fluorocarbon groups, which have an intermediate SLD with a value between that of dPEO and air. On this basis any fit to the data with an apparent surface roughness of > 10 Å was rejected immediately as unrealistic.

4.3.2.5 Simulations
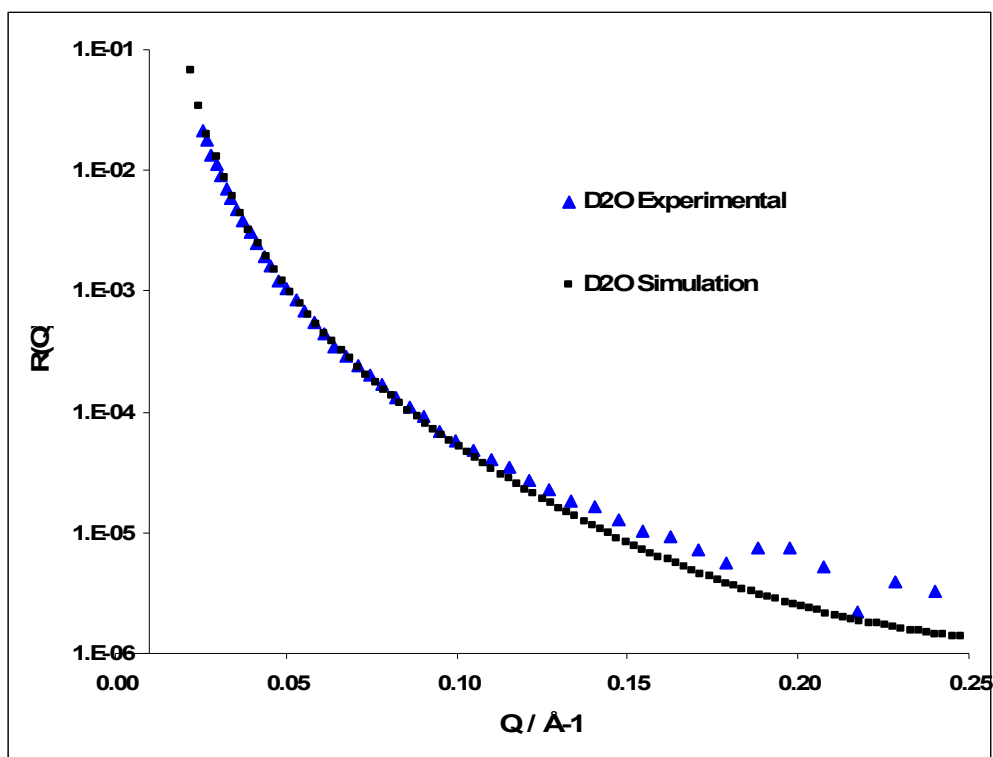
Figure 4.3.2.5.1: Comparison of experimental vs simulation R(Q) data for D$_2$O

The simplest possible case is one where we have a sample of pure deuterated water (D$_2$O) which has a calculated scattering length density of $6.35*10^{-6}$ Å^{-2} and a predicted surface roughness of around 3.5 Å. Plotting the R(Q) vs Q data for an experimental neutron reflectivity experiment on pure D$_2$O and the calculated R(Q) vs Q data for a simulation with these calculated parameters shows a very good match, this can be seen in figure 4.3.2.5.1.

It can be seen in figure 4.3.2.5.1 that the experimental and simulation R(Q) v Q data for D$_2$O show very good correlation up to a Q value of around 0.12 Å^{-1}. At this point the background noise begins to cause the experimental values of R(Q) to be higher than those predicted by the simulation and this highlights the necessity for the data reduction technique described earlier when carrying out neutron reflectivity experiments.

Several other simulations were also carried out and the R(Q) vs Q data calculated for these are shown in figure 4.3.2.5.2. The profiles shown were calculated using the parameters that represent pure D_2O with a 3 Å and 8 Å surface roughness (represented by the black and pink lines respectively), a monolayer of deuterated PEO (SLD value of $5.74*10^{-6}$ Å^{-2}, represented by the blue line) and for two different conformations of fluorocarbon $[(C_8F_{17})_2C_6H_6]$ end-cap (SLD value of $1.95*10^{-6}$ Å^{-2}) at the surface of a dPEO adsorbed layer (represented by the green and red lines). Figure 4.3.2.5.2 shows the SLD vs depth profiles used to calculate these R(Q) vs Q data.
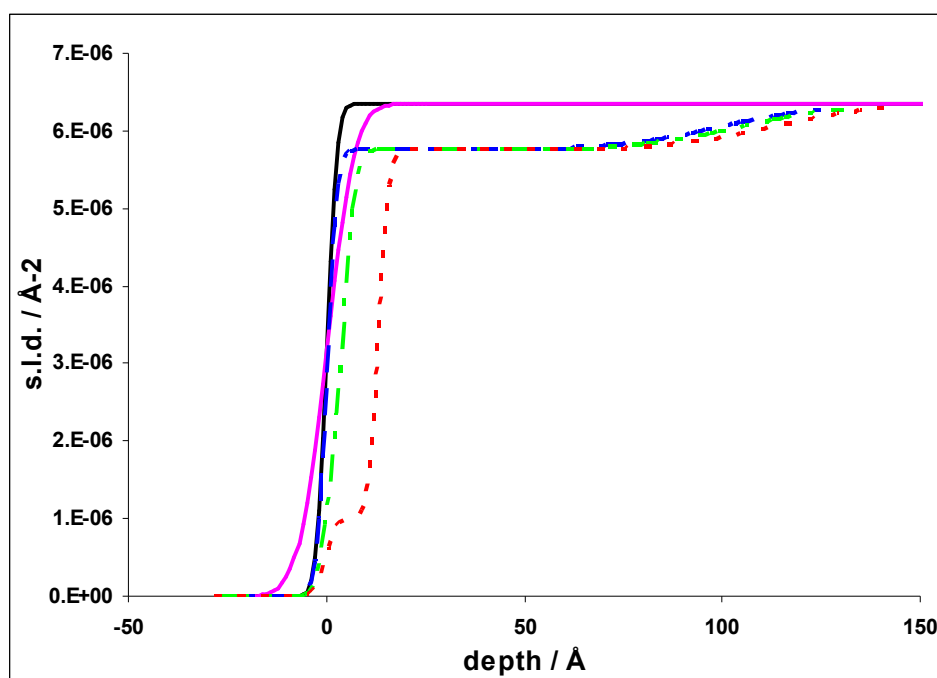
Figure 4.3.2.5.2: SLD vs depth profiles to calculate R(Q) vs Q data for simulations

Looking at the data shown in figure 4.3.2.5.3 instantly highlights the problem with studying these polymer materials in a D_2O solvent; the data sets look very similar systems and the small differences between them can be attributed to changes in surface roughness. However it may still be possible to draw some conclusions about the fine details of the exposed surface of the real systems that are to be studied by observing these changes in surface roughness, for example a system where the head groups are standing

out of the surface of the solvent should have a larger surface roughness than one where they are laid down and this should be observable in these D_2O solvent studies.
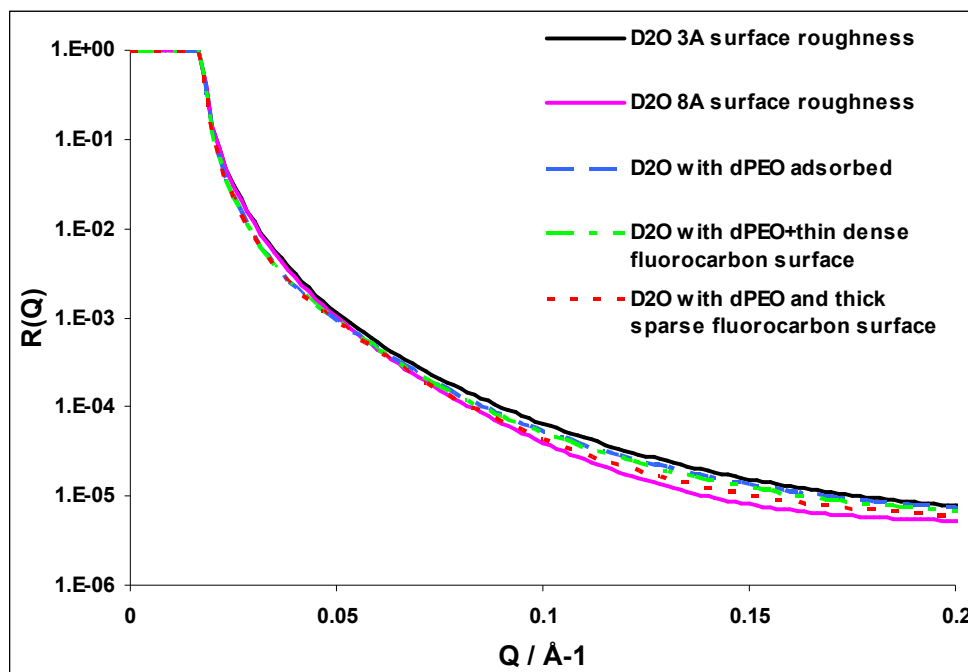
Figure 4.3.2.5.3: Comparison of simulation R(Q) data for deuterated PEO and fluorinated head groups

Looking back at figure 4.3.2.5.1 it is easy to see that there is much more information to be gained from the study of these materials in a NRW solvent than in D_2O. Therefore experiments were carried out on the range of solution concentrations of each material in NRW as a priority despite the fact that these NRW samples take up to three times longer to carry out.

4.4 Results

4.4.1 Surface Tension Isotherms
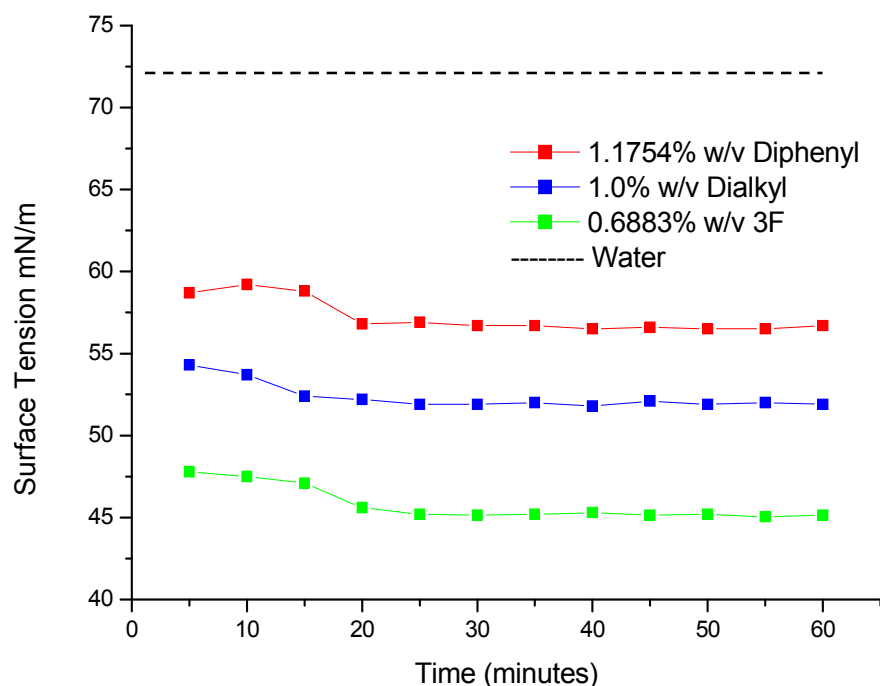
Figure 4.4.1.1: Surface tension vs time for sample equilibration

Preliminary surface tension experiments were carried out to investigate the amount of time it is necessary to allow for the surface tension of the sample to reach equilibrium. This is a measure of how quickly the surface active polymeric materials diffuse and self assemble at the air/water interface. The results shown in figure 4.4.1.1 indicate that the polymers very quickly arrange themselves at the air water interface as the initial measurements taken after 5 minutes show a dramatic decrease in surface tension from that of pure water. In all 3 cases studied it can be seen that immediately the surface tension is considerably lower than that of pure water (represented by the dashed black line), but there is still some fluctuation and steady decrease in surface tension over the

first 15-20 minutes of the experiment as the polymer equilibrates at the air/water interface.
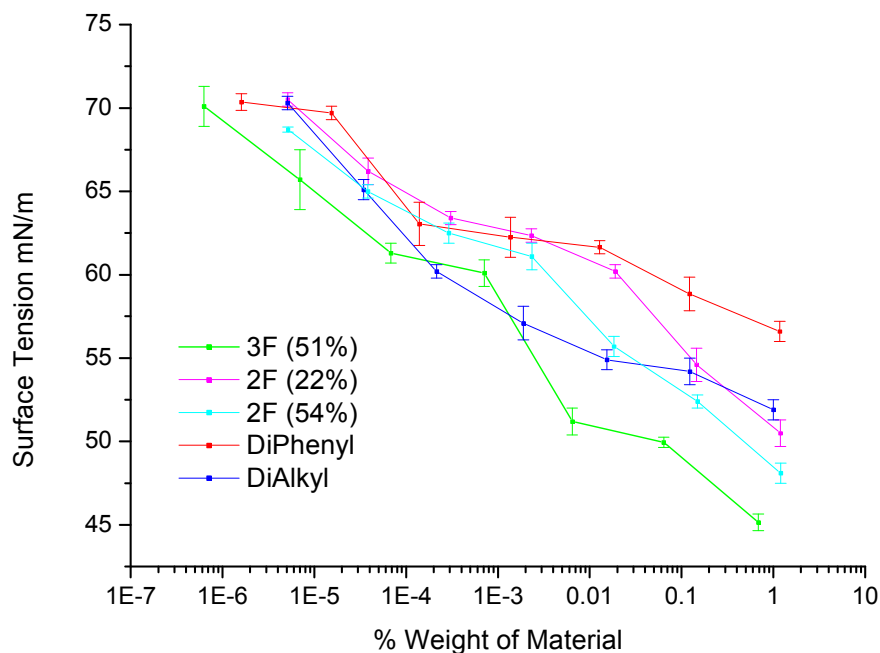
Figure 4.4.1.2: Surface tension results

A plot of surface tension against weight percentage of each of the functionalized PEO materials in distilled water is shown in figure 4.4.1.2 and the following observations can be made.

At very low concentrations ($<10^{-5}\%$ $^w/_v$) the surface tension of the system is very close to that of pure water, which shows that there is simply not enough of the material present to reduce the surface tension of a body of water with this surface tension to volume ratio. As the concentration of the poly(ethylene oxide) additives is increased (10^{-4}-$10^{-2}\%$ $^w/_v$) there is an obvious small decrease in the surface tension of the system to a value of around 62-63 mN/m and this small drop is expected even for a simple poly(ethylene oxide) chain additive. Above a concentration of around 0.01% $^w/_v$ there is an obvious difference in the surface tension depending on what functionalization is present on the poly(ethylene oxide) chain.

Previous studies by Lu *et al*[17] have shown that a simple unfunctionalized poly(ethylene oxide) material can reach surface tensions as low as 61mN/m. Therefore it is not surprising to see that the results for the poly(ethylene oxide) synthesized in-house containing a diphenylmethyl end group show a small but significant effect on the surface tension of the system. The diphenylmethyl end group is slightly hydrophobic and therefore causes a small increase in surface activity and a small reduction in the surface tension is observed as a result.

The results for the 20% difluorinated dendrimer capped poly(ethylene oxide), at a concentration of 1% $^{w}/_{v}$ in water, show a substantial reduction in the surface tension of water to a value around 50 mN/m. This is certainly a significant decrease in surface tension and it can be concluded that the fluorinated dendritic end caps are capable of tethering poly(ethylene oxide) to an air-water surface.

The results for the 100% dialkyl capped poly(ethylene oxide) show a surface tension at a concentration of 1% $^{w}/_{v}$ in water that is almost exactly the same as for the 20% difluorinated sample, however the dialkyl capped material reaches a lower surface tension measurement at lower concentrations than the 20% difluorinated equivalent. This is almost certainly due to the 100% functionality of the alkylated sample leading to surface saturation at a lower concentration, the very similar surface tension measurements for both samples at 1% $^{w}/_{v}$ is further evidence for this surface saturation.

The results for the 51% trifluorinated poly(ethylene oxide) sample show that the surface tension of this sample is lowest of any of this group of materials at any concentration. The surface tension is reduced to 50 mN/m at a concentration that is 2 orders of magnitude lower than any of the previous materials and reaches a value as low as 44 mN/m at its highest concentration (0.6883% $^{w}/_{v}$).

One method of quantifying these observations is to use a Gibbs adsorbtion isotherm to calculate the value for the surface excess, Γ, using the following equation:

$$\Gamma = \frac{1}{RT}\frac{\partial \gamma}{\partial \ln c}$$

Equation 4.4.1.1

where γ is surface tension in Jm^{-2} and c is concentration.
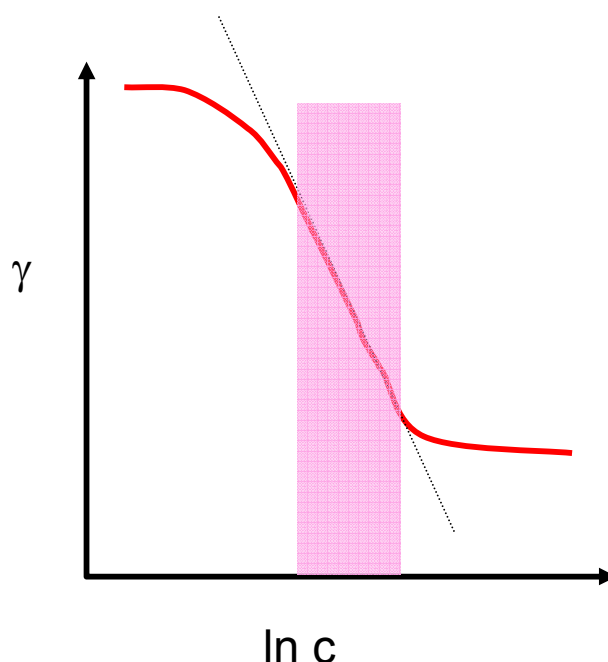
Figure 4.4.1.3: Example of gradient used to calculate surface excess

The gradient of a plot of surface tension vs natural log of concentration (as shown in figure 4.4.1.3) can be used to calculate surface excess in moles/m^2. This can then be converted to molecules/nm^2 using Avogadro's number and then further converted to give a value for the average surface area (nm^2) occupied per molecule, these values are given for each sample in table 4.4.1.4.

The density of PEO can be assumed to be 1.1 g cm^{-3} at a molecular weight of 10000 g mol^{-1} and below (density increases proportionally with molecular weight up to a value of 1.2 g cm^{-3} but at these lower molecular weights the effect is very small)[4]. Using Avogadro's constant, N_A, ($6.022*10^{23}$ mol^{-1}) the molecular mass of 10000 g mol^{-1} can be converted to $1.66*10^{-20}$ g per molecule, this is then divided by the density of 1.1 g cm^{-3} to give a value for the volume occupied per molecule of $1.51*10^{-20}$ cm^3 (15.1 nm^3). This value can be used to give an estimation of the depth that each molecule type reaches into the bulk of the sample (surface excess) by multiplying the value for the number of

molecules per surface area in nm² by this molecular volume; these results are also shown in table 4.4.1.4.

Sample	Limiting Gradient (mN/m)	Γ (Molecules/nm²)	nm² per molecule	Surface Excess (nm)
F3 (51%)	4.48	1.09	0.92	16.46
F2 (54%)	4.57	1.11	0.90	16.76
F2 (22%)	3.45	0.84	1.19	12.68
Dialkyl	5.00	1.22	0.82	18.42
Diphenyl	2.48	0.60	1.66	9.06

Table 4.4.1.4: Calculated values for surface area per molecule

4.4.2 Neutron Reflectometry

Neutron reflectometry experiments were carried out on the various concentrations of each material in deuterated water to investigate the structure of the adsorbed polymer layers. The R(Q) data for the 4 highest concentrations of the F2 material can be seen in figure 4.4.2.1 as well as R(Q) for a pure D₂O solvent sample and the previously simulated data for a system with the calculated SLD for D₂O of $6.35*10^{-6}$ Å⁻².

It can be seen in figure 4.4.2.1 that there is very little difference in the R(Q) data for these samples and that even the most concentrated material shows only subtle differences in R(Q) data but, as discussed previously, even though the difference is very small, there does seem to be a slight lowering in the R(Q) values for each increase in material concentration from pure solvent (purple stars) all the way up to the 1% $^w/_v$ F2 sample (red diamonds). Earlier simulations (figure 4.3.2.5.2) show that a slight lowering of R(Q) similar to this can be seen when the SLD of the material at the surface is lowered (from $6.35*10^{-6}$ Å⁻² for D₂O towards the value for the F2 head group at around $1.95*10^{-6}$ Å⁻²) or if the surface roughness is increased due to material at the surface. Clearly it is necessary

to investigate further by considering the NRW results, but these results do suggest that some material is present at the surface.
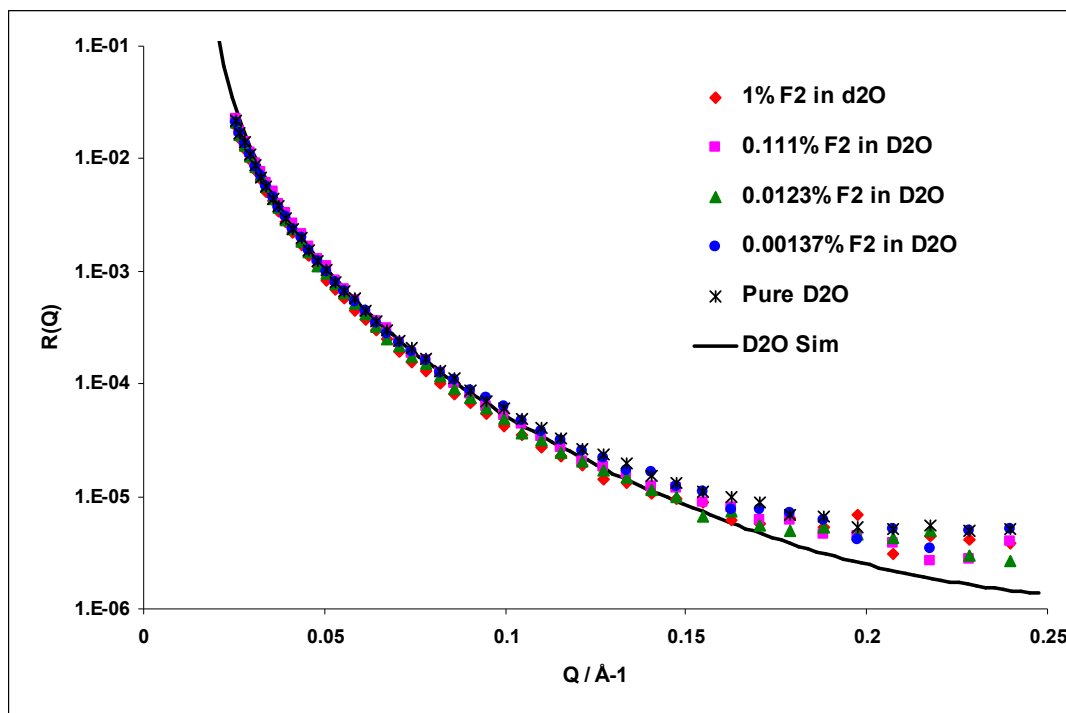
Figure 4.4.2.1: R(Q) data for decreasing concentration of F2 material in D$_2$O solvent

It has been shown already that there are much greater differences to be seen when comparing these materials in an NRW solvent, an example of this type of data is shown previously in figure 4.3.2.4.1. For each set of R(Q) data acquired an initial fit is attempted using a simple single layer model and for some of these data sets (typically lower concentration samples) a good fit can be achieved in this way. A good example of this is shown in figure 2.24.6 where an excellent fit (with a χ^2 value of 1.156) can be achieved for the lowest concentration of the F3 material using a single layer model in which the thickness, SLD and interface width between the surface layer and the subphase were the adjustable parameters.
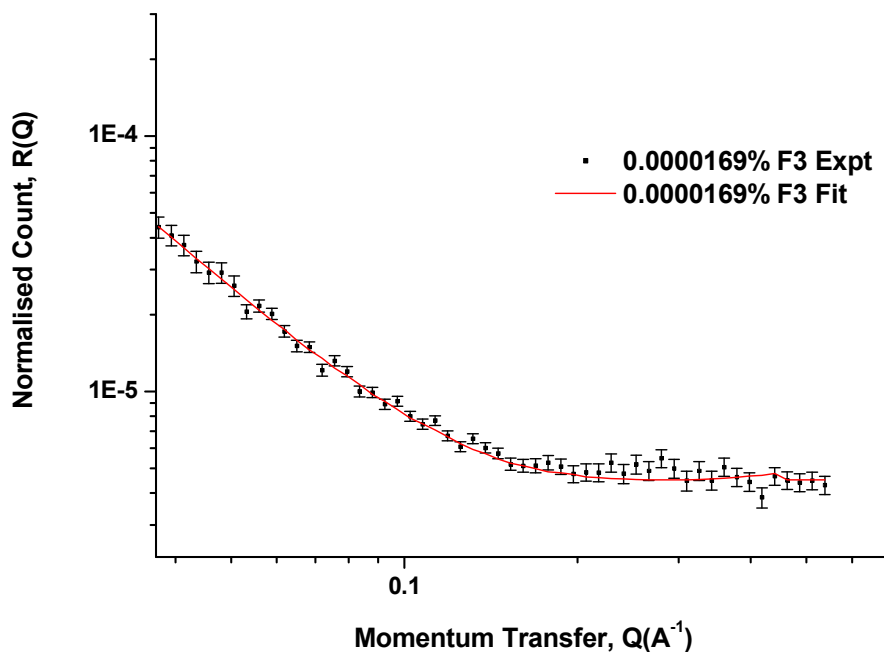
Figure 4.4.2.2: Neutron reflectometry data for lowest concentration of F3 material with single layer model fit

At higher concentrations the use of a simple single layer model is not sufficient to achieve a good fit and figure 4.4.2.3 shows the best fit that can be obtained when attempting to fit some high concentration data using the same simple single layer model as described previously. The total value for R(Q) across the whole Q range is around the correct number, which shows that the model is making a good attempt to fit the data correctly using only a single layer. However, it is obvious that this model fit does not capture the features of the data graph correctly and the associated χ^2 value of 26.8 serves to emphasize and quantify this point, therefore a more complicated model is clearly required.
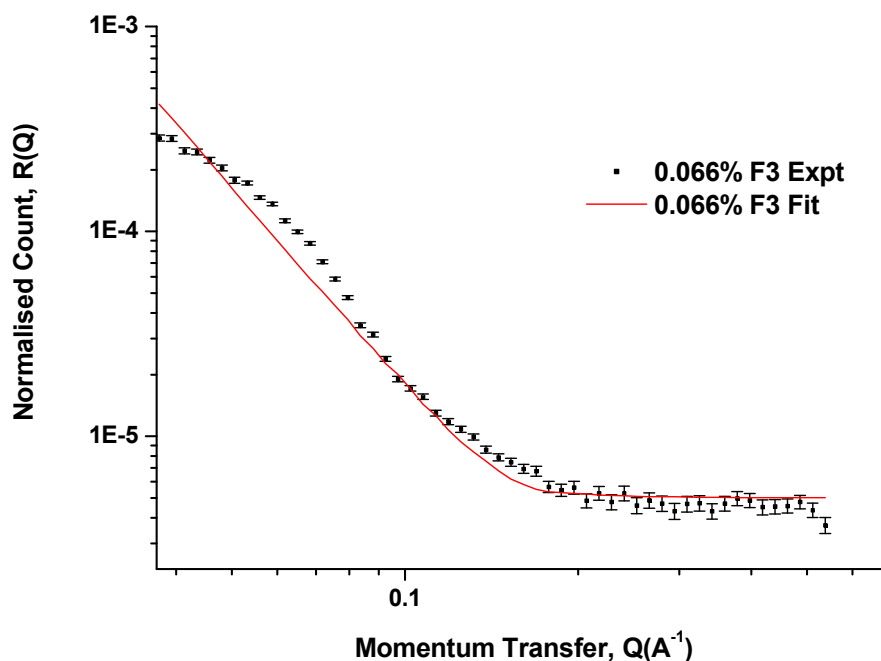
Figure 4.4.2.3: Neutron reflectometry data highest concentration of F3 material with single layer model fit

Using a double layer model it is possible to find a much better fit for the higher concentration samples that can capture the features of the data correctly and be used to produce more accurate SLD profiles for these samples. Figure 4.4.2.5 shows the data for the highest concentration of the $3C_8F_{17}10k51$ material with a double layer model giving a good fit with a χ^2 value of 3.1, which is much lower than that of the previous single layer model. The necessity for a more complex model is evidence for the fact that there is a more complicated self-assembled system occurring in the higher concentration samples.
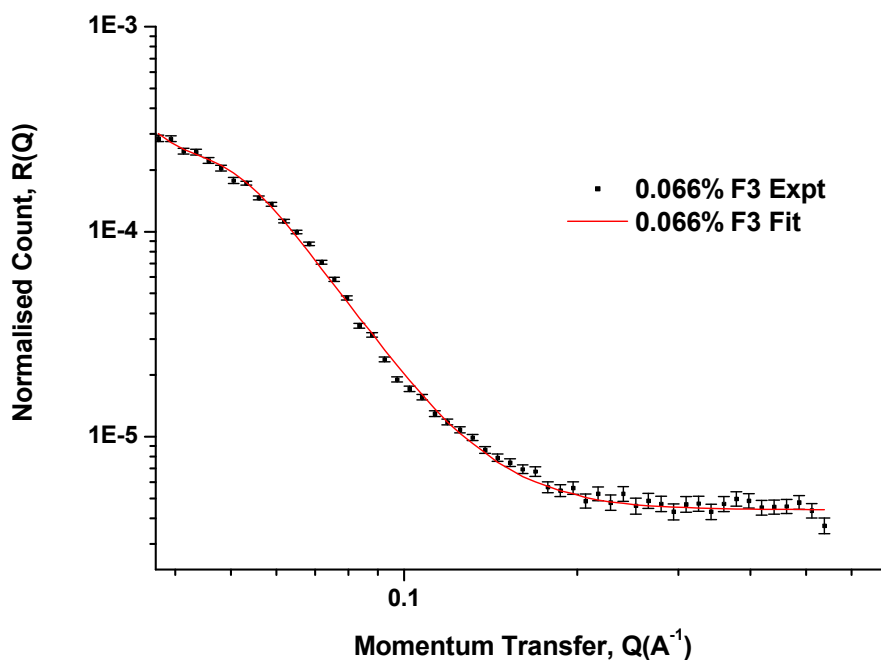
Figure 4.4.2.5: Neutron reflectometry data highest concentration of F3 material with double layer model fit

4.5 Discussion

4.5.1 Approach to Equilibrium

As previously discussed in section 4.4.1 the surface tension measurements for any sample containing one of the surface active materials takes an average of around 15-20 minutes to steady out and reach an equilibrium and thereafter the surface tension remains constant (within experimental fluctuation tolerances). In order to ensure that there are minimal fluctuations in surface tension during the subsequent experimental measurements (for surface tension and neutron reflectometry) it was decided that a minimum time of 30 minutes would be allowed to pass between the solutions being introduced to the experimental equipment and any measurements taking place.

After this equilibration time of 30 minutes we can assume that the material has completed adsorption to the interface and then experimental measurement procedures can begin. For the surface tension measurements this literally meant leaving the solution in the experimental glass container for 30 minutes to equilibrate while a constant temperature was maintained. For neutron reflectometry experiments (where it is very important to be efficient with the allocated experimental time) it was possible to carry out the necessary data collection on the pure solvent while the material-containing solutions were allowed to equilibrate in the adjacent troughs.

4.5.2 Surface Activity of Functionalized PEOs

As previously discussed in section 4.3.1; it is important to investigate an unfunctionalized control material in order to fully understand the properties of the functionalized materials investigated here and the control material purchased from Sigma Aldrich has a reported M_w of 10,000 g mol^{-1} and polydispersity of 1.02. It is worth reiterating here that the molecular weights of experimental material to be studied are slightly varied due to their respective head groups but all contain PEO chains of around 8800-8900 g mol^{-1}. More details of the exact composition of these materials can be found in the synthesis section (3.2).

Previous studies carried out by Lu *et al*[17] have shown that increasing the molecular weight of PEO from 17800 g mol^{-1} to 87000 g mol^{-1} causes only a small change in surface tension (around 2 mN/m) even at relatively high concentrations. Therefore the slight difference in molecular weight between the PEO materials used here should be insignificant for the purposes of this control experiment as this is a simple check to see if the diphenylmethyl group imparts any significant surface activity to the PEO[13, 14]. It is expected that a slight change in molecular weight would have very little effect on the surface tension measurements of the material in water as the polymers will behave in a very similar manner at these small molecular weights and the mass of material present in each experiment will be kept constant. Previous studies[15-17] speculate that, whatever the molecular weight, portions of the polymer are oriented out of the aqueous phase into the air

and molecular weight dependence of the surface tension was observed for highly concentrated solutions only.

Figure 4.5.2.1 shows a schematic representation of how the fluorinated dendritic end capped poly(ethylene oxide) might arrange itself at an air-water interface. The poly(ethylene oxide) chains are relatively hydrophilic and previous studies have shown that these usually extend into the bulk of the water solvent[18-21]. The dendritic head groups, and in particular the perfluorinated alkyl chains, are hydrophobic and will therefore segregate towards the air-water surface to minimize the interactions between them and the water. This surface tethering should have a significant effect on the surface tension of the water and this property can be measured with relative ease.
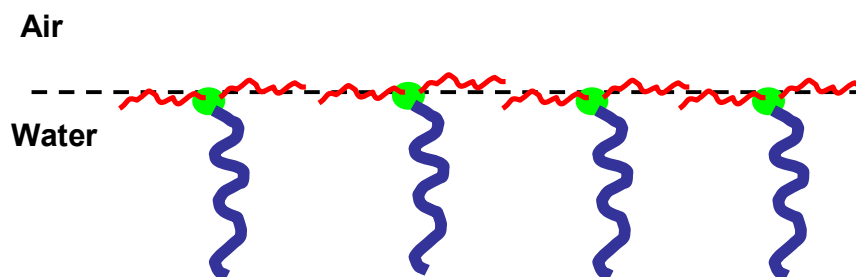
Figure 4.5.2.1: Cartoon showing possible surface structure

The surface tension measurements shown in section 4.4.1 are conclusive evidence that the materials are surface active and that increasing the amount of head group attached to the poly(ethylene oxide) increases the surface activity of the materials. Furthermore it can be seen that simple alkyl head groups can be used in place of the fluorinated head groups to achieve similar properties. Although fluorocarbons are known to have lower surface tensions than hydrocarbons[7], this benefit is only realized at the relatively high concentrations that are required to compensate for the partial functionalization.

Previous experiments[22] carried out on poly(ethylene oxide) functionalized with a linear tridecafluorooctanoyl component (TDFO-PEO, shown later in figure 4.5.2.4 and referred to as F1 from now on for convenience) have shown reduction in the surface tension of water to well below 50 mN/m. In these earlier experiments on linear polymers

the surface tension values were measured for materials containing PEO segments of 3 different molecular weights; these values are given in table 4.5.2.2.

.PEO molecular weight (g mol^{-1})	Fluorocarbon ends per polymer molecule ± 0.2	Maximum Concentration (g cm^{-3})	Surface Tension at Max Concentration (mN/m)
2000	1.1	~0.001	~22
5000	1.1	~0.05	~35
10000	0.9	~0.05	~42

Table 4.5.2.2: Surface tension results from previous work on TDFO-PEO

These previous results show that the linear diblock materials have a dramatic effect on the surface tension of water at low molecular weights. However, the tethering strength of these diblock copolymers appears to be rather low as the surface tension measurements increase significantly with respect to increasing molecular weight of the PEO component, reaching a similar surface tension value (around 40-45 mN/m) when a comparable molecular weight (around 10000 g mol^{-1}) to the materials used in this study is reached.

Further similarities can be seen when comparing materials of the same molecular weight in this study to those in the previous study on F1 materials. A value of 0.82 nm^2/molecule is calculated for the surface area occupied per molecule of the 10000 g mol^{-1} F1 sample and the same value is shown for the dialkyl sample studied here (results shown in table 4.4.1.4 in the results section).

This is perhaps not surprising when we consider the amount of fluorinated component present in each material as a percentage of the overall molecular weight and in order to make a direct comparison between the materials it is necessary to calculate the relative amount of fluorine present in each sample; this is shown in table 4.5.2.3.

Material	Mass of headgroup as a % of whole molecule	Mass of fluorine present as a % of whole molecule	Mass of fluorine as a % of headgroup
F1	7.51%	2.47%	32.89%
F2	5.90%	3.31%	56.10%
F3	8.13%	5.05%	62.12%

Table 4.5.2.3: Comparison of headgroup and fluorine amounts present in experimental materials

Note - The difluorinated and trifluorinated materials investigated here contain PEO that is functionalized to only slightly greater than 50%; whereas the comparable TDFO-PEO materials at 10000 g mol^{-1} are functionalized to almost 100% and this is reflected in the values shown in the first two columns of table 4.5.2.3.
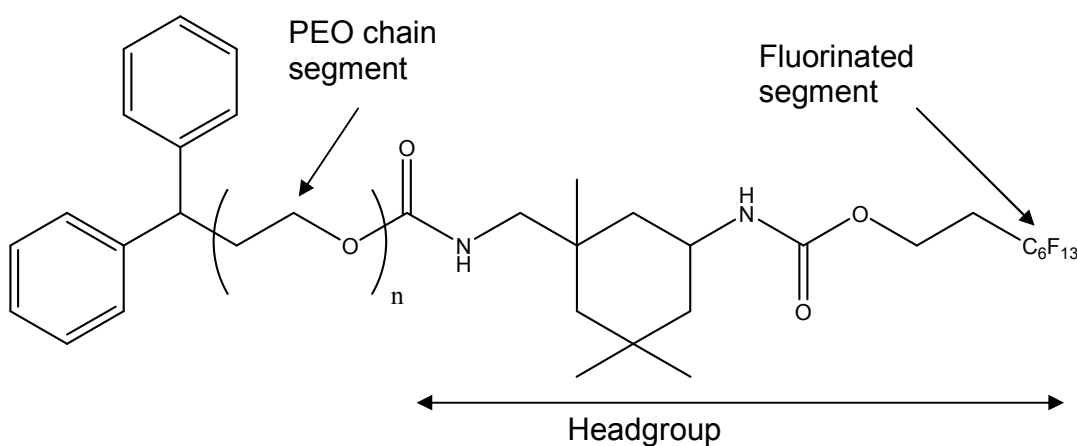
Figure 4.5.2.4: Structure of TDFO-PEO used in previous study

Comparing the head group masses of these molecules shows that the TDFO-PEO and trifluorinated materials have a similarly sized head group and the surface tension measurements for these molecules reflect this fact. However it can be seen that the trifluorinated material contains a much higher percentage of fluorine relative to the size

of the molecule despite the fact that it is only 51% functionalized. This would suggest that the fluorinated segment of the TDFO-PEO molecule is not the only contributing factor to the low surface tension measurements. Figure 4.5.2.4 shows the exact structure of this TDFO-PEO molecule type and it can be seen that there is a large alkyl component (a cyclohexane with multiple methane groups attached) that may be contributing significantly to the reduction in surface tension by these molecules. The results obtained for the surface tension of dialkyl materials investigated in this study (shown previously in figure 4.4.1.2) show that alkyl components do indeed cause a significant reduction in surface tension for these polymers.

Despite this observation of reduced surface tension achieved by simple alkyl components in these head groups it is important not to understate the importance of the fluorinated segments of these molecules. This point is emphasized by the fact that the difluorinated material (despite being only 54% functionalized) reaches a lower surface tension value that that of the dialkyl equivalent at higher concentrations.

Therefore it can be argued that poly(ethylene oxide) with 100% of the chains functionalized with the fluorinated dendritic head group would be able to tether poly(ethylene oxide) of a much higher molecular weight and show an even greater decrease in surface tension due to multiple fluorine groups being attached to each single poly(ethylene oxide) chain.

4.5.3 Structure of Adsorbed Layers

4.5.3.1 Surface Tension

Using the values for the surface area per molecule (A_m) for each sample at surface saturation that have been previously calculated in section 4.4.1 it is possible to calculate a value for the average distance between each molecule (D_m) simply by taking the square root of this value.

$$D_m = \sqrt{A_m}$$

Equation 4.5.3.1.1

For ease of reference the values for surface area per molecule (A_m, in Å^2) and average distance between each molecule (D_m, in Å) and radius of gyration (R_g, in Å) are shown here in table 4.5.3.1.1.

Sample	A_m (Å^2)	D_m (Å)	R_g (Å)
F3 (51%)	92	9.59	
F2 (54%)	90	9.49	
F2 (22%)	119	10.91	37.2 – 41.3
Dialkyl	82	9.05	
Diphenyl	166	12.88	

Table 4.5.3.1.1 Calculated values for A_m and D_m from surface tension results

As discussed in Chapter One, section 1.2, a brush conformation is expected when $D_m < R_g$ and this can clearly be seen to be the case here where D_m is a factor of 4 smaller in magnitude than R_g for all of the samples.

An alternative to this highly stretched polymer brush conformation that can be used to explain these results is that the polymer chains are strongly tethered to the surface but are not greatly perturbed from a random coil conformation. For this situation there must be a very strong overlap between the molecules and this is an acceptable proposal as there is a large amount of free space in between random coil of the polymer. The amount of free space available can be quantified by comparing the previously calculated volume of one polymer chain to the average volume occupied by one random coil, which can be calculated by the simple formula for the volume of a sphere (*$4/3\pi r^3$*) where *r* is the previously calculated value for the radius of gyration of the polymer (3.92 nm, see section 4.2). The value for the volume of one polymer chain is calculated as 15.1 nm^3 and the volume occupied by a random coil of this chain is calculated as 252.3 nm^3, leaving plenty of room for overlap between molecules.

These results show that while chain perturbation or stretching is possible and gives a good explanation of how to accommodate a high concentration of polymers at the surface, it is not essential and there is also room for the polymers to remain at the surface

in an unperturbed state. It is therefore necessary to study this surface organization in more detail in order to examine whether or not these chains are stretched into the bulk of the solvent, this can be successfully achieved using neutron reflectivity to probe the surface. While previous studies have been successfully carried out using a Gibbs adsorption isotherm on PEO of similar and higher molecular weights[17] the possibility of non ideal solution behaviour is one that brings these results into question and this is further justification for the use of neutron reflectivity to study the surface excess and organization of these materials.

4.5.3.2 Neutron Reflectivity in D_2O

It has been discussed previously in section 4.4.2 (and shown in figure 4.4.2.1) that the results obtained from experiments carried out in a D_2O solvent show only small differences in R(Q) data and the experimental data for the pure D_2O solvent is very well represented by a simulation using the calculated theoretical SLD of $6.35*10^{-6}$ $Å^{-2}$ and a surface roughness of 3.5 Å.

Although the differences in R(Q) data for the mostly strongly adsorbing material (1% $^w/_v$ F2) compared to that of pure D_2O are very subtle it is still possible to draw some conclusion from this small difference. Figure 4.5.3.2.1 shows the mid range of Q vs R(Q) data for these two experimental extremes in order to emphasize the differences between these two sets of data. It can be seen here that while the experimental data for the pure D_2O solvent is a very close match to that of the simulation using a surface roughness of 3.5 Å, the 1% $^w/_v$ F2 data is much better represented by a simulation using an SLD of $6.35*10^{-6}$ $Å^{-2}$ and a surface roughness of 7 Å.

This increase in surface roughness is consistent with the expectation that the roughness of the surface will increase with decreasing surface tension caused by the presence of the highly adsorbent material (shown in section 4.5.2). Since the mean squared roughness of an interface due to thermal energy (capillary waves) scales with inverse of surface tension, the surface roughness should scale with inverse square root of surface tension. The surface tension results show that a drop of around a factor of two is achieved with the most highly adsorbent materials and therefore the surface roughness

should be expected to increase by a factor of around 1.41 (square root of 2) at the most. The remaining contribution to the apparent increase in surface roughness is most likely due to the intermediate (between the values for D_2O and air) value for the SLD of the fluorocarbon groups that are present at the interface.
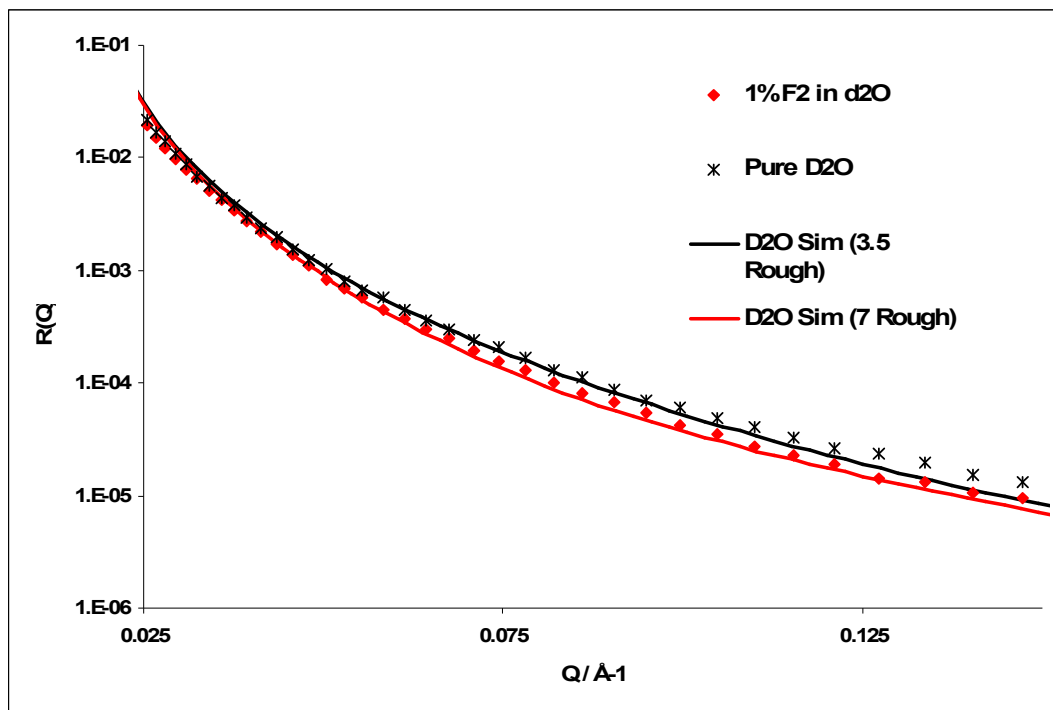
Figure 4.5.3.2.1: Comparison of simulated and experimental R(Q) data for pure D_2O solvent and highest polymer loading

4.5.3.3 Neutron Reflectivity in NRW

Using NRW in neutron reflectometry is an incredibly sensitive tool for probing surfaces and in particular surface ordering and layers[23-26]. It has already been shown that due to the surface active nature of the materials synthesized in this project a layered structure anchored at the surface is predicted. The easiest conformation to observe with neutron reflectivity would have all of the poly(ethylene oxide) chains strongly tethered to

the surface of the water by the hydrophobic head groups and all of the poly(ethylene oxide) chains lined up in a brush formation extending into the water solvent. This arrangement at the surface would lead to 3 sharp interfaces; between the air and the fluorinated groups, the fluorinated groups and the poly(ethylene oxide) and between the poly(ethylene oxide) and NRW. This formation is sketched in figure 4.5.3.3.1 (B). However this rigid and very structured conformation is unlikely to occur in most systems as the polymers are very flexible and adopt a random walk conformation in free solution. Although packing of the surface will force the polymers to stretch into the bulk solvent, the polymer is most likely to adopt a conformation that is stretched slightly further than the calculated theoretical value for the radius of gyration but much less than an all-trans conformation.

Another reason that this situation is unlikely to occur is due to the solubility of materials used here and therefore by definition there will be equilibrium between the surface and the bulk of the solution. The stretching of the PEO chains away from the surface will incur a free energy penalty, so the interplay between this increase in free energy and the tethering ability of the functional head groups is likely to result in a conformation that averages somewhere between the two extremes of a fully saturated surface and a completely empty one.

Despite these facts it is still expected that a similar ordered structure at the surface with the same interfaces present as in the ideal situation will be observed but with much less distinction between the layers. This formation is crudely represented by the cartoon drawing labeled A in figure 4.5.3.3.1.

The two sketched representations shown in figure 4.5.3.3.1 serve to illustrate the kind of behaviour that can be resolved with neutron reflectivity and careful use of (H/D) contrast variation. Many of these complications and possible effects on experimental results are discussed in the following section.

There is a slight affinity of PEO to adsorb to an air-water interface and this can be seen experimentally in section 4.4.1 by the lowering of water surface tension when unfunctionalized PEO is added. This tendency for PEO to adsorb to the surface would result in an enhanced surface density as PEO that is not forced into the bulk (by chain stacking or other steric hindrances) may also lie at the surface.
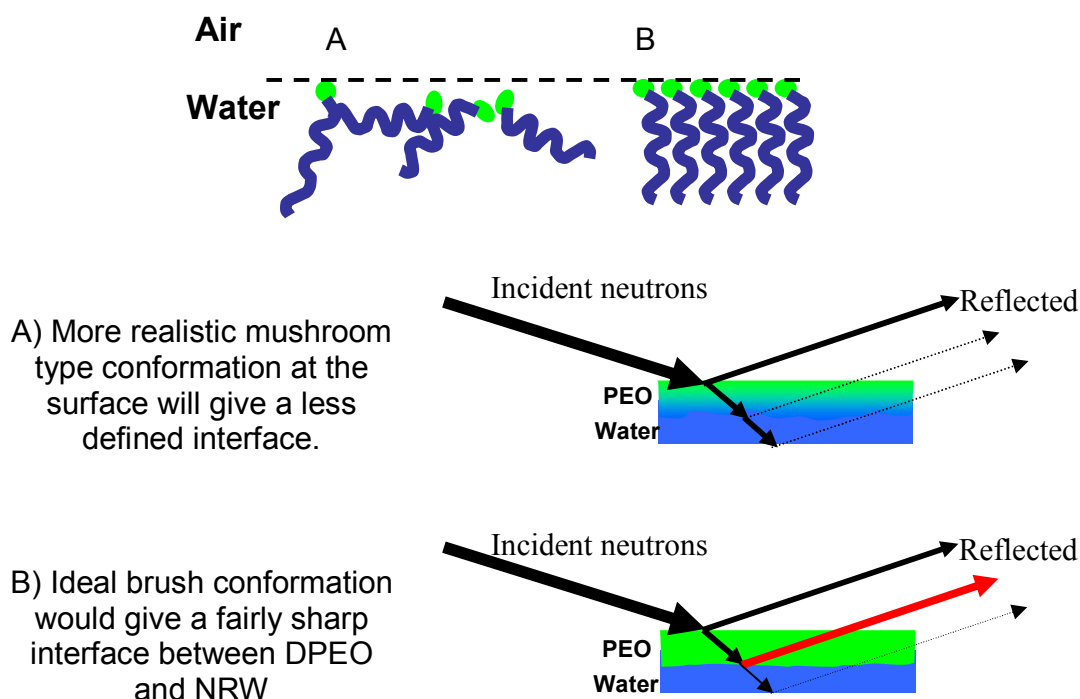
Figure 4.5.3.3.1: Possible surface organization and effect on incident neutron beam

At the higher concentrations explored in these experiments the surface density is too high for all of the molecules to adsorb towards the interface (the concentration at which this begins to occur is usually referred to as the critical micelle concentration (CMC) although it may not necessarily be the case that micelles are actually formed). At these high surface densities the molecules will need to overcome the problem of overcrowding either by forming micelles or additional layers below the surface (possibly in a random coil formation around the head group to minimize the interactions of the hydrophobic head groups with water).

Another consideration to make when analysing these materials is the fact that the polymer molecules synthesized in this project are not identical; and there is some molecular weight variation and the experimental materials typically contain around 50% PEO with a head group functionalization and the rest are unfunctionalized PEO molecules.

It is very important to take all of these factors (as well as general experimental errors and other possible sources of discrepancy between predicted and actual density profiles) into account when predicting, analysing and evaluating experimental data. These factors must also be taken into account when comparing experimental data with results obtained by computer simulations in chapter 5.

After all of the available data from the neutron reflectivity experiments carried out on each sample has been processed in the manner previously described it is possible to put together profiles of sample depth versus scattering length density for each sample type and observe how these profiles change as the concentration of the sample is varied. The profiles for the 54% difluorinated end capped, deuterated 10000 g mol^{-1} poly(ethylene oxide) (referred to as **F2** from now on for convenience) at varying weight percentage NRW are shown in figure 4.5.3.3.2.
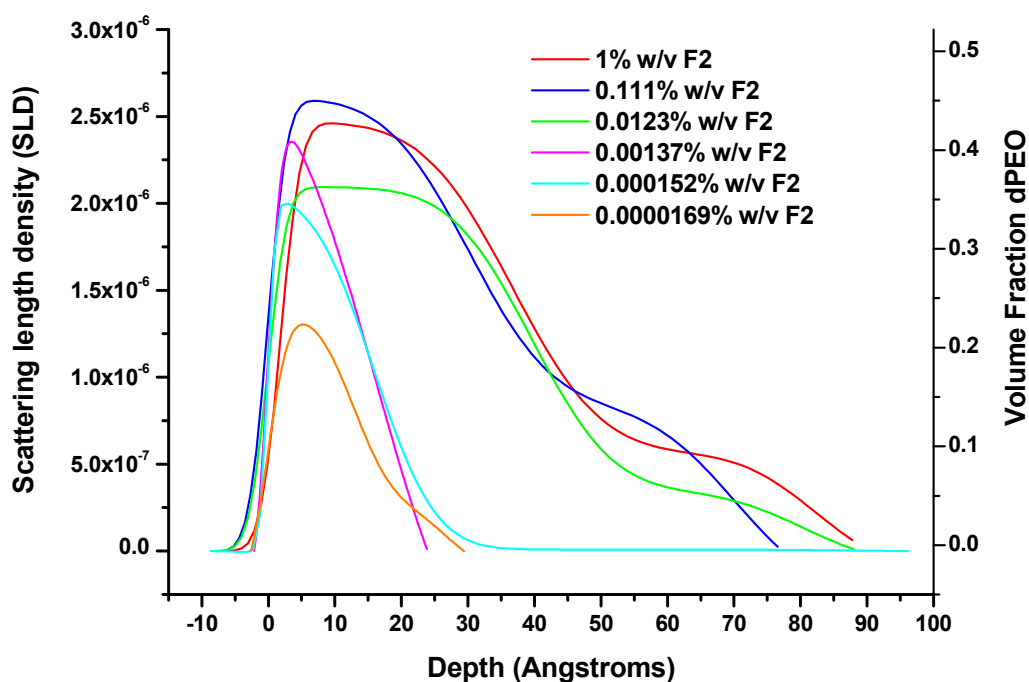
Figure 4.5.3.3.2: Scattering length density profiles and dPEO volume fraction for varying weight percentages of F2 in NRW

It is immediately apparent from the profiles shown in figure 4.5.3.3.2 that there is an excess of **F2** formed at the air-water interface. There is also a general trend in the profiles that shows a reduction of this excess at the interface as the concentration of **F2** in the sample is reduced. These general observations agree with earlier predictions that the fluorinated end capped material will adsorb to the air-water interface. The surface profiles for 1% $^{w}/_{v}$ and 0.111% $^{w}/_{v}$ show very little difference in surface excess and profile shape and this is probably due to surface saturation at these high concentrations, where there is simply no more room for more molecules to pack themselves at the surface.

Further evidence for this surface saturation comes from the depth into the sample that the **F2** material can be seen to reach. The calculated radius of gyration for these materials free in solution has a maximum value of 41.3 Å. We would expect that a tethered polymer would have an experimental value lower than this as one of the degrees of freedom for movement is removed and there is a considerable amount of material that can still be observed at depths of up to 75-85 Å. This is consistent with the prediction that a relatively tightly packed structure at the surface would force the polymer segments to stretch into the bulk of the NRW solvent and as a result the profiles for 1% $^{w}/_{v}$, 0.111% $^{w}/_{v}$ and even 0.0123% $^{w}/_{v}$ all display profiles that extend from the surface and into the bulk of the NRW solvent further than would be expected for a tethered chain that was free to adopt the normal radius of gyration. However it can be seen that the majority of the material in these high concentration samples appear to be stretched to almost exactly the value for the radius of gyration, leaving open the possibility that the material observable at depths beyond this value could be due to the presence of a second layer beneath the first or possibly the beginning of micelle formation.

It is important to note here that it is expected that there will be a significant amount of the **F2** material (as well as the unfunctionalized equivalent) present in the bulk NRW solvent, however this will not show up in these profiles as the low concentration of material has little effect on the observable SLD and this will be subtracted out in the background noise during the data processing stage. Neutron reflectometry is therefore primarily sensitive to gradients in SLD throughout the depth of a sample and these

observations of possible second layers or extended polymer brushes can not be considered to be an artifact of reflectivity from free polymer in the bulk of the solvent.

As previously discussed there is very little difference between the surface profiles of the 1% $^w/_v$ and 0.111% $^w/_v$ samples and it is assumed that the excess material remains confined in the bulk of the solvent and therefore does not have an effect on the surface probing of a neutron reflectivity experiment. When the concentration is reduced to 0.0123% $^w/_v$ the profile shape remains largely the same as the higher concentrations. However there is a significant reduction on the SLD of material and this can be seen in figure 4.5.3.3.2 where the higher concentration (1% $^w/_v$ and 0.111% $^w/_v$) samples show a maximum SLD of around $2.5*10^{-6}$ Å $^{-2}$ to $2.7*10^{-6}$ Å $^{-2}$ (represented by the red and blue lines) compared to a value of around $2.1*10^{-6}$ Å $^{-2}$ for the 0.0123% $^w/_v$ sample (represented by the green line). Despite this drop in SLD there is still evidence of surface saturation and polymer brush formation as the F**2** material can still be seen to reach a depth into the bulk solvent that is comparable to the higher concentrations. A possible explanation for this lower maximum SLD sample displaying similar extension into the bulk solvent comes from the arrangements of the head groups at the interface. At very high concentrations there will be a large surface excess of material and the molecules at the surface will be tightly packed and this results, as we have already seen, in the extension of the polymer segment into the bulk. However, there is also evidence from the D_2O neutron reflectivity results (section 4.4.2) and later in chapter five on the computer simulation of these molecules (in particular section 5.4.4) that suggest there is a more subtle structural rearrangement observable at the exposed solvent surface. This could be due to the fluorinated head group molecules extending out of the solvent and into the air either allowing for a more densely packed surface or due to the formation of small clusters of the fluorinated head groups. As the concentration decreases however there will be more space for the fluorinated arms to lie closer to the surface and push the molecules slightly further apart, but not enough room for the polymer chains to follow a similar relaxation deeper into the solvent surface due to their large size (figure 4.5.3.3.3 shows a cartoon representation of these possible types of surface head group arrangement and the computer simulated molecular representations shown later in section 5.4.4 also show

similar arrangements). This effect would go some way to explaining the SLD vs depth profiles seen for the 1% $^{w}/_{v}$, 0.111% $^{w}/_{v}$ and 0.0123% $^{w}/_{v}$ **F2** samples.
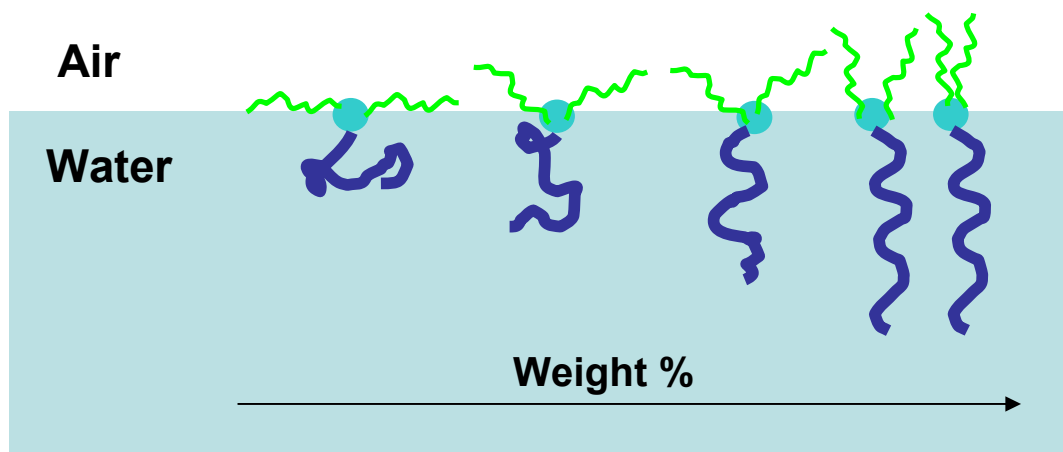
Figure 4.5.3.3.3: Cartoon representative of possible fluorinated head group arrangement

For the 0.00137% $^{w}/_{v}$ **F2** sample (represented by the pink line in figure 4.5.3.3.2) it can be seen that the maximum SLD of the material remains at a similar value to those of the much higher concentrations. This suggests that at around this concentration the surface is still fully saturated with material but that the polymer tail segment is no longer being forced into the bulk solvent by the presence of excess material. The material only appears to reach a depth of around 20 Å into the surface of the solvent and this is much less than the calculated value for the radius of gyration (37.2 to 41.3 Å). One possible explanation for this is that the tethered polymer is restricted in one dimension (i.e. it can not pass above the surface of the solvent into the air) and we may therefore expect a lower value for the radius of gyration. Another explanation is due to the slight affinity for PEO to adsorb to the interface (this has already been shown previously in the surface tension experimental results section and by previous studies[4,17]), as the materials are tethered strongly at the interface by the fluorinated head groups it is likely that the proximity of the PEO tails to the surface will enhance this effect. It is probably a combination of these two effects that leads to a flat mushroom-like conformation at the

interface where the material does not penetrate as far into the surface as the calculated radius of gyration values would predict.

The samples of 0.000152% $^W/_v$ and 0.0000169% $^W/_v$ **F2** show very similar profiles to that of the 0.00137% $^W/_v$ **F2** sample. As there is an equilibrium between the bulk solution and the surface it is expected that the surface excess will decrease with decreasing bulk concentration. It can be seen that this is indeed the case as the maximum SLD of each sample decreases as the concentration is lowered. These results (represented by the light blue and orange lines) show us that these **F2** molecules have a relatively high affinity for the air-water interface as even at very low concentrations the **F2** present in the sample will adsorb and self assemble at the surface of the solution.

Due to the restriction on the yield of **F3** material; a relatively dilute stock solution of 0.066% $^W/_v$ in NRW was prepared using the technique described previously and this stock solution was then diluted down to 0.0332% $^W/_v$, 0.0123% $^W/_v$, $4.24*10^{-3}$% $^W/_v$, $1.37*10^{-3}$% $^W/_v$, $1.52*10^{-4}$% $^W/_v$ and $1.69*10^{-5}$% $^W/_v$.

The data from the neutron reflectivity experiments carried out on each sample was processed in the same manner as previously described and then to put together to make profiles of sample depth versus scattering length density for each sample type. The profiles for the **F3** material at varying weight percentage in deionized NRW are shown in figure 4.5.3.3.4.

As was seen in the previous results for the **F2** material it is again immediately apparent from the profiles shown in figure 4.5.3.3.4 that there is an excess of **F3** formed at the air-water interface. There is again also a reduction of this excess of material at the interface as the weight percentage of **F3** in the solution is reduced and these observations are further evidence of the earlier predictions that the fluorinated end capped material will self assemble at an air-water interface. Despite the fact that the most concentrated solution of **F3** is much lower than that of the highest concentration of **F24** material (0.066% $^W/_v$ compared to 1% $^W/_v$) the surface excess of material in each case is very similar, with both of these solutions exhibiting maximum SLD values in excess of $2.5*10^{-6}$ Å $^{-2}$. Furthermore it can be seen that the highest (but still much lower than the highest **F2** sample) concentration **F3** sample shows material at greater depths below the

surface of the solution (a significant amount can still be seen at 120 Å depth before it begins to fall off towards the 140 Å region).
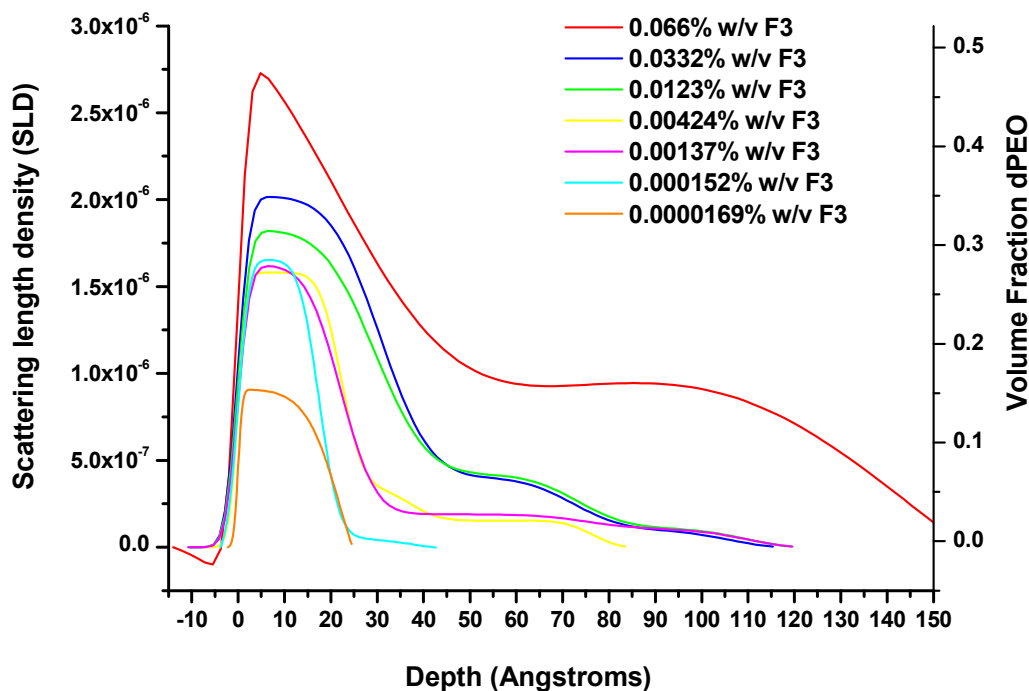
Figure 4.5.3.3.4: Scattering length density and dPEO volume fraction profiles for varying weight percentages of F3 in NRW

The likely explanation for these observations is that the presence of 3 hydrophobic fluorocarbon functional components on the head group of sample **F3** leads to a much higher affinity for the molecule to self-assemble at the air-water interface with a much higher surface tethering strength than is displayed by that of the **F2** material. This greater tethering strength induces the **F3** molecules to adsorb to the surface in greater concentrations than **F2** ones and are not as easily forced back into the bulk of solvent. Furthermore, this increased surface adsorption and therefore induced increase in surface concentration explains the increased depth into the sample at which the **F3** material can still be observed as the PEO tails are forced to stretch even further beyond the calculated value for radius of gyration than those in the **F2** system.

Previous surface excess values calculated from surface tension measurements (section 4.4.1) show that these materials, when tethered at the interface, are predicted to reach a depth into the bulk of around 165 Å at maximum surface concentration and perturbation. However, in order for this value to be a true measurement of surface excess for these materials there must be a maximum perturbation to force the PEO chains to stretch to this depth and this maximum perturbation assumes that there must be no overlap between the PEO chain molecules and that the system must be subject to an ideal solution. This is highly unrealistic as the PEO chains are able to form hydrogen bonding between one another via the surrounding water molecules and an entangled morphology between the chains is much more likely. This calculated maximum surface excess also relies on the molecular weight and chemical make up of each molecule in the system being identical. This is not the case in the experimental system due to the polydispersity of the polymer chains and the fact that these chains are not 100% functionalized with the fluorinated head group. These lower molecular weight impurities would contribute significantly to the surface tension measurements and give a larger value for the calculated surface excess. Therefore, while it is likely that the increase in surface excess with respect to increasing concentration shown in the results for neutron reflectivity is due to an increase in the stretching out of tethered chains up to a value of around 40-45 Å, for the observed depths of around 140 Å (seen here for the highest concentration material measured) it is much more likely that there are some multiple surface layers forming, where the surface is fully packed with **F3** molecules (and some other lower molecular weight molecules in the system) and the excess material is forced to form extra layered structures below the surface in order to minimize the contact between the hydrophobic head groups and the water solvent. These layered structures could either be in the form of extra polymeric layers or possibly micelles that have formed and aggregated towards the surface to allow favourable interactions between the PEO tails on the outside of the micelle and those in the tails of the surface polymer brushes.

From these results it does appear that there may be a critical concentration between 0.0332% $^w/_v$ and 0.066% $^w/_v$ where the **F3** molecules begin to form either micelles or a multi-layer structure; however there would need to be further testing carried out at intermediate concentrations to further investigate this claim. It would also be prudent to

suggest that further testing using other experimental techniques (such as light scattering experiments to investigate the presence of aggregation) should also be carried out to investigate these claims.

When the concentration of **F3** is reduced to 0.0332% $^w/_v$ and then to 0.0123% $^w/_v$ (for which there is a directly comparable result for the **F2** material), again, despite this drop in surface excess, there is still evidence of surface saturation and forced extension of the polymer material into the bulk of the solvent. The profile shapes are very similar to the equivalent **F2** sample where the SLD values are around $1.8*10^{-6}$ to $2.0*10^{-6}$ Å^{-2} and again the profiles can be seen to extend to a depth of around 40 Å with an observable amount of material at even greater depths. The same explanation as outlined above for the **F2** sample as to reason for the extension of the polymeric section of the molecule into the bulk solvent can be applied to this sample (see figure 4.5.3.3.3 and surrounding discussion). It is possible to draw similar conclusions for the two materials at the lower concentrations of 0.00137% $^w/_v$, 0.000152% $^w/_v$ and 0.0000169% $^w/_v$ as both materials show very similar profiles at equivalent concentrations.

Looking closely at these results there does also appear to be a common factor indicating a critical concentration at which the material becomes saturated at the surface and begins to extend into the bulk of the solvent. The profiles of both samples show extension of material into the bulk for sample concentrations of 0.0123% $^w/_v$ and above. Conversely there appears to be only a single surface layer for concentrations of 0.00137% $^w/_v$ and below. This critical concentration was observed during our second visit to the Rutherford Appleton Laboratory while briefly looking through the initial results for the **F3** material. Fortunately we were able to spot this early enough to allow an investigation of a sample of intermediate concentration while we were still on site with access to the neutron reflectivity instrument. Therefore a solution of concentration 0.00424% $^w/_v$ of the **F3** material was prepared immediately and added to the remaining solutions to be investigated. The profile obtained for this concentration is represented by the yellow line in figure 4.5.3.3.4 and it can immediately be seen that the material is still extending into the bulk of the solvent and the profile is almost identical to that of the 0.0123% $^w/_v$ sample. This result shows us that the critical concentration at which this **3F10d51**

material becomes surface saturated and begins to extend into the bulk of the solvent must lie within the region between 0.00424% $^w/_v$ and 0.00137% $^w/_v$.

4.5.3.4 Comparison of Single and Multiple Component Fluorinated Head Groups

Previous experiments[22] carried out on **F1** materials showed that a PEO chain with a molecular weight of around 10000 gmol^{-1} that had been functionalized with a linear fluorinated segment gave similar measurements for surface tension to the materials studied in this project (42 mN/m for **F1**, 47 mN/m for **F2** and 45 mN/m for **F3**). However, as it has been pointed out and discussed during this chapter, the values for surface tension and the subsequently calculated surface excess values are subject to many sources of error when dealing with these non ideal systems. Significant differences between the systems compared here arise from the fact that the **F2** and **F3** materials consist of around 45% unfunctionalized PEO chains and the **F1** materials were synthesized in such a way that all of the PEO chains contain the fluorinated functionality but an excess of the head group material remains within the sample. The presence of these other molecules, couples with the effects of polydispersity mean that there is the potential for huge error margins when calculating surface excess in this way. As a result of this uncertainty in the calculated values for surface excess from surface tension it is difficult to draw any conclusive comparisons between the **F1** and **F2/F3** materials from these results alone.

In contrast to the similar values for surface tension, the neutron reflectivity experiments carried out on the **F1** materials reveal a very different surface morphology than the ones shown here for the **F2** and **F3** ones. For the **F1** materials it was shown that there is a thin surface layer with a thickness of 20-25 Å and a second layer with an average thickness of 40-45 Å leading to a maximum depth of 60-65 Å at which the material can be seen and this is independent of bulk concentration. This value is comparable to 1.5 times the calculated value for the radius of gyration of a PEO chain at this molecular weight and at certain concentrations the **F2** and **F3** materials show very

similar results. The neutron reflectivity results for the **F2** materials show a surface excess of around 20 Å at very low concentrations and this quickly increased to around 40-45 Å once the surface becomes fully loaded with material. At concentrations above 0.0123% $^w/_v$ it can be seen that some of this material extends further into the bulk, with a significant contribution to the SLD profile still seen at depths of around 70-80 Å. This effect is even more pronounced for the **F3** materials, where similar trends are found at the lower concentrations but at only a relatively high concentration of 0.066% $^w/_v$ (much lower than the 1% $^w/_v$ highest concentration studied for the **F1** and **F2** materials) the material is shown to extend as far as 140 Å in to the bulk. This effect of chain stretching can be explained by the increased surface tethering strength imparted onto the PEO chains by the presence of a greater number of fluorinated groups in the end cap. For the **F1** material the results show that the observed surface excess remains at a constant value of around 60-65 Å and is independent of concentration. However, there is no information given with regards to the volume fraction (or SLD from the reflectivity experiments) of this 10000 gmol^{-1} **F1** material at the surface. It is likely that, although the spatial extent of the adsorbed layer is independent of the bulk concentration, the volume fraction of PEO at the surface will be increasing with bulk concentration as the PEO chains of the **F1** material aggregate to the surface and are held loosely at the interface. The independence of the surface excess value (which remains at a value that is 1.5 times that of the calculated radius of gyration) on bulk concentration can be explained by the fact that the energetic cost of stretching the chains to accommodate more material at the surface requires a more strongly tethering functional group. For the **F2** material it can be seen that a different explanation is required as the surface excess values are very much dependent on the bulk concentration of the material. The lower concentrations show a low surface excess of around 20-25 Å, which is a very similar value to that shown for the top layer of the **F1** materials. This increases to the same value as the calculated radius of gyration (40-45 Å) as the concentration increases and there is evidence of some material present in a possible perturbed conformation of second layer up to a depth of 60-65 Å. This dependence of surface excess on the bulk concentration is consistent with a build up of material at the surface resulting in a perturbed conformation of PEO chains that are relatively strongly tethered to the surface. A very similar explanation for the build up of

the surface structure can be employed to describe the **F3** materials. It is expected that there will be a concentration dependence for any adsorbing species in the dilute limit, but as the monolayer approaches the saturation point where overlapping polymer chains begin to repel, then a strongly tethering group is needed to increase the surface excess further. Therefore in this case it can be seen that the tethering strength of these **F3** materials is significantly higher than that of the **F1** and even the **F2** materials as they can be observed at a much greater depth into the bulk. To further illustrate this point it can be seen that the volume fraction of PEO at the surface increases much more quickly with respect to bulk concentration of **F3** material and the relatively low concentration of 0.066% $^w/_v$ **F3** (compared to the highest concentrations of **F1** and **F2** that were studied) shows a much higher surface excess. This high surface excess must be as a direct result of either very large amounts of chain perturbation or the formation of multiple PEO layers, both indicate a strongly surface active species, but whilst chain perturbation indicates surface tethering, multilayer adsorption also indicates a bulk aggregation.

4.6 Conclusions and Applications

Surface tensiometry and neutron reflectivity experiments have been carried out to determine the self assembly and surface organization of adsorbed solutions of PEO chains that have been functionalized with a range of fluorinated head groups at an air-water interface. Comparison of surface activity and calculated surface excesses for these materials revealed some very interesting properties for these materials.

The results from the surface tensiometry experiments reveal that while the surface activity and surface excess values for these materials are not vastly different, the surface organization is very much dependent on the type of head group that the molecule contains. More detailed study of the surface organization using neutron reflectivity experiments reveals that the **F3** material shows the highest tethering strength as the materials are held at the surface even under the pressure of a very strong perturbation from a random coil conformation. The **F1** and **F2** materials do not appear to tether sufficiently to the water surface to reach high packing densities where the PEO chains are highly perturbed and strongly stretched. This is not surprising when we consider the fact

that the surface tethering strength is primarily induced by the hydrophobicity of the fluorine contained in the head groups of the molecules; the **F3** material has a fluorine content of 5.05% by mass (the **F1** and **F2** materials have 2.47% and 3.31% fluorine content by mass respectively). This extra tethering strength allows the tethering of a much higher molecular weight of materials, where the **F1** head group has been shown to be effective in strongly tethering PEO chains up to 2000 gmol^{-1} in molecular weight[22]; these **F3** materials are shown here to be effective up to a molecular weight of 10000 gmol^{-1}.

These higher molecular weight brush-like self assembling polymer structures can be adapted to incorporate many different polymer types. Some basic polymers such as polystyrene have already been synthesized to incorporate analogous fluorinated head groups[27] and there are many possibilities for other more technically advanced polymers such as poly(thiophene-g-NIPAAm), which has been shown to respond to heat when in a polymer brush conformation[28]. The desire and uses for such polymers are numerous as they are employed in many current applications including biosensors, the stabilization of colloids and lubrication in artificial joints to name just a few. These types of polymer brush molecule are particularly useful in these applications where the situation arises that it is necessary to enhance the surface properties of a polymer without causing any unfavourable changes to the bulk properties of the material. Typical additives that consist of low molecular weight small molecules tend to cause adverse effects on the bulk polymer into which they are dispersed, such as lowering the glass transition temperature or reducing mechanical strength. Compatible polymers which will self assemble at an interface and impart the desired properties solely upon the surface are therefore highly desirable.

4.7 References

[1] A. P. Narrainen, N. Clarke, S. M. Eggleston, L. R. Hutchings and R. L. Thompson, *Soft Matter* **2006**, *2*, 981-985.

[2] Z. Funke, C. Schwinger, R. Adhikari and J. Kressler, *Macromolecular Materials and Engineering* **2001**, *286*, 744-751.

[3] G. J. Fleer, M. A. C. Stuart, J. M. H. M. Scheutjens, T. Cosgrove and B. Vincent, *Polymers at Interfaces*, Chapman & Hall, London, **1993**.

[4] R. A. L. Jones and R. W. Richards, *Polymers at Surfaces and Interfaces*, Cambridge University press, **1999**.

[5] I. Pirma, *Polymeric Surfactants*, New York, **1992**.

[6] S. J. Alexander, *J. Phys. France* **1977**, *38*, 983-986.

[7] R. W. Richards and J. Sarica, *Langmuir* **2003**, *19*, 7768-7777.

[8] A. P. Narrainen, L. R. Hutchings, I. A. Ansari, N. Clarke and R. L. Thompson, *Soft Matter* **2005**, *2*, 126-128.

[9] S. Kawaguchi, G. Imai, J. Suzuki, A. Miyahara, T. Kitano and K. Ito, *Polymer* **1997**, *38*, 2885-2891.

[10] A. W. Adamson, *Physical Chemistry of Surfaces*, John Wiley & Sons, **1982**.

[11] G. K. Batchelor, *An introduction To Fluid Dynamics*, Cambridge University Press, **2000**.

[12] A. Braslau, M. Deutsch, P. S. Pershan and A. H. Weiss, *Phys. Rev. Lett.* **1984**, *54*, 114-117.

[13] A. Couper and D. D. Eley, *J. Polym. Sci* **1948**, *3*, 345-349.

[14] H. Daust and D. St-Cyr, *Macromolecules* **1984**, *17*, 596-601.

[15] E. L. Lovell and H. J. Hibbert, *J. Am. Chem. Soc* **1940**, *62*, 2144-2148.

[16] B. H. Cao and M. W. Kim, *Faraday Discuss.* **1994**, *98*, 245-252.

[17] J. R. Lu, J. Penfold, R. W. Richards, T. J. Su and R. K. Thomas, *Polymer* **1996**, *37*, 109-114.

[18] N. Bikales, *Water-soluble Synthetic Polymers*, Plenum: New York, **1973**.

[19] K. Devanand and J. C. Selser, *Macromolecules* **1991**, *24*, 5943-5947.

[20] A. Matsuyama and F. Tanaka, *Phys. Rev. Lett.* **1990**, *65*, 341-344.

[21] P. Molyneux, *Water-soluble Synthetic Polymers; Properties and uses*, CRC Press: Boca Raton, FL, **1983**.

[22] M. T. F. Telling and K. H. Anderson, *Phys. Chem. Chem. Phys.* **2005**, 7, 11255-11261.

[23] G. F. Kirton, A. S. Brown, C. J. Hawker, P. A. Reynolds and J. W. White, *Physica B.* **1998**, *248*, 184-190.

[24] P. M. Saville, P. A. Reynolds, J. W. White, C. J. Hawker, J. M. J. Frechet, K. L. Wooley, J. Penfold and J. R. P. Webster, *J. Phys. Chem.* **1995**, *99*, 8283-8289.

[25] J. Majewski, T. L. Kuhl, M. C. Gerstenberg, J. N. Israelachvili and G. S. Smith, *J. Phys. Chem. B.* **1997**, *101*, 3122-3129.

[26] L. T. Lee, E. K. Mann, O. Guiselin, D. Langevin, B. Farnoux and J. Penfold, *Macromolecules* **1993**, *26*, 7046-7052.

[27] I. A. Ansari, A. P. Narrainen, L. R. Hutchings, N. Clarke and R. L. Thompson, *Langmuir* **2007**, *23*, 4405-4413.

[28] Robin L. McCarley, *Angew. Chem. Int. Ed.* **2005**, *44*, 4872-4876.

Chapter Five: Computer Simulations

5.1 Introduction to Simulations

This chapter describes a molecular simulation approach to modeling materials directly analogous to those synthesized and analyzed experimentally as described in the previous chapters. It is of vital importance that the simulated systems are constructed in such a way as to mirror the experimental systems as much as possible. For each constructed computer model system it is possible to monitor the movement, distribution and molecular arrangement or structure at any given time during the simulation and to follow the changes in the system as a function of time. Programs have been developed in-house to allow us to do this with relative ease. This gives us a unique perspective, where we can not only essentially freeze time on the system but also look at microscopic details such as the bond length distribution etc at any given time during the simulation, which it is not possible to do experimentally[1-7].

The first part of this chapter describes simulations of an isolated poly(ethylene oxide) chain (PEO) in water. Data obtainable from this model include the radius of gyration of the PEO at each time-step allowing us to follow the coiling and uncoiling of a polymer chain as the simulation proceeds[8]. Radial distribution functions as well as bond length, A-B-C bond angle and A-B-C-D dihedral angle distributions can also be found in this way.

The second part of this chapter introduces the idea of coarse graining. Using the data obtained from atomistic simulations of PEO and water it is possible to calculate coarse grained parameters for these molecules that allow us to simulate much larger systems.

The final part of this chapter describes in detail the methods used to construct a coarse grained simulation model employed that is as closely matched to the real experimental system as possible. Data obtained from these systems are then compared directly to experimental results.

5.1.1 Introduction to Atomistic Simulations Using Molecular Dynamics

The atomistic simulation of molecules by computer requires analysis of all of the interactions taking place between each individual atom. In order to achieve this it is necessary to select an appropriate set of parameters that represent the interatomic interactions. This set of parameters is most commonly referred to as a force field and for the simulations carried out in this project the force field employed is the *Optimized Potentials for Liquid Simulation – All Atom,* or OPLS-AA force field[9], this is discussed in more detail in section 2.2.4.1.

The simulation technique used for our simulations is known as molecular dynamics (MD). This method calculates the trajectories of all particles in the simulated system by calculating the sum of all individual forces acting upon each atom. The acceleration, velocity and position of the individual atoms are then adjusted according to Newton's laws of motion[10, 11]. More details of the molecular dynamics method can be found in section 2.2.5. The main idea behind a molecular dynamics simulation is the break down of time into a series of discreet time steps (described briefly in section 2.2.5.), otherwise the trajectories of each individual atom in the system would have to be solved analytically and this is not possible for a system with many interacting sites. Therefore it is necessary to use an integration algorithm to solve Newton's equations of motion across time-steps to calculate the trajectories of each atom. There are several integration algorithms currently is use but the most widely used ones were developed from an original algorithm by French physicist Loup Verlet in 1967 and are known as the *Verlet Leapfrog* (LF) and *Velocity Verlet* (VV) algorithms[12].

5.1.2 Verlet Algorithms

The basic Verlet algorithm calculates the positions of each atom in the next time step of a simulation from the positions of the previous and current time steps (without including velocity for these two terms). This helps to reduce any errors introduced to the integration that may arise by simply calculating from the current step. The positions and

their derivatives with respect to time are treated as two Taylor expansions of the position vector *r(t)* in opposing time directions.

$$r(t + \Delta t) = r(t) + v(t)\Delta t + \frac{1}{2}a(t)\Delta t^2 + ...$$

and

$$r(t - \Delta t) = r(t) - v(t)\Delta t + \frac{1}{2}a(t)\Delta t^2 - .....$$ Equation 5.1.2.1

Here, *r(t + Δt)* is the position at the next time step, *r(t)* is the position at the current time step, *r(t - Δt)* is the position at the previous time step and *v(t)*, *a(t)*, … are the derivatives of position with respect to time (velocity, acceleration etc) at the current time step.

Addition of these two expansions offers the advantage that the third-order terms from the Taylor expansion cancel out and we are left with an expression for the position of atoms at the next time step in terms of current position and acceleration only.

$$r(t + \Delta t) = 2r(t) - r(t - \Delta t) + a(t)\Delta t^2$$ Equation 5.1.2.2

There are several problems with this basic Verlet algorithm, the most obvious being that at time step zero there is no *r(t - Δt)* term and the inclusion of this term means that two sets of coordinates must be saved in the memory of the computer in order to calculate the position in the next step. This extra memory usage can severely limit the complexity of the system. Also the velocities for the atoms must be calculated manually and the lack of precision in adding the small *a(t) Δt²* to the much larger *2r(t) - r(t - Δt)* term often leads to the use of alternative integration algorithms such as the aforementioned *Verlet Leapfrog* (LF) and *Velocity Verlet* (VV) algorithms.

5.1.3 Verlet Leapfrog Algorithm

The Verlet leapfrog algorithm[13] calculates the trajectories of the atoms in a system using atomic velocities that are half a time step out of phase with the positions:

$$r(t + \Delta t) = r(t) + v\left(t + \frac{1}{2}\Delta t\right)\Delta t^2$$

and

$$v\left(t + \frac{1}{2}\Delta t\right) = v\left(t - \frac{1}{2}\Delta t\right) + a(t)\Delta t \qquad \text{Equation 5.1.3.1}$$

As a result of the staggering of velocity and position there are inaccuracies in calculating both potential energy and kinetic energy or instantaneous temperatures at time *t* for the same time step.

5.1.4 Velocity Verlet Algorithm

The velocity Verlet algorithm overcomes all of the previous problems and allows the calculation of both velocity and position based parameters at the same time as well as solving the first time step problem of the basic Verlet algorithm:

$$r(t + \Delta t) = r(t) + v(t)\Delta t + \frac{1}{2}a(t)\Delta t^2$$

and

$$v(t + \Delta t) = v(t) + \frac{[a(t) + a(t + \Delta t)]}{2}\Delta t \qquad \text{Equation 5.1.4.1}$$

5.2 Atomistic Molecular Dynamic Simulations

Using a classical force field (section 2.2.4) and molecular dynamics techniques (as described in the previous section) is a very powerful way of simulating small molecular systems. However, it soon becomes impractical and extremely computationally expensive as the size of the system increases. It is impossible at the present time to model enough

molecules to represent a full experimental system of, for example, 25 mL of water containing several mg of polymer, not only because of the sheer number of atoms that would need to be modeled in such a system but also the enormous number of interactions between the atoms. There are some approximations made when using molecular dynamics that help to model bulk materials without using an excessive amount of computational power and time. These approximations are known as *non-bonded cutoffs* (where atoms that are beyond a certain distance away from each other are assumed to have no interactions between one another) and *periodic boundary conditions, or PBC* (where the simulation 'box' is treated as being on an infinite lattice, surrounded on all sides by images of itself)[14-16]. These techniques are discussed in more detail in section 2.2.5.

5.2.1 Atomistic Water Simulations

Many simulation studies have been carried out on water both as a pure bulk compound and as a solvent for various types of molecule. As a result there are many different ways in which water has been modeled and it is often difficult to decide which model is best for a particular system you wish to study. Dr Philip Anderson[8] devoted some of his PhD thesis while working at Durham University to testing and comparing many of these models and drawing up conclusions about which is the best model for each simulation type (type of solvate, size of simulation system etc)[17]. From his conclusions it was decided that the best water model to use would be the 'TIP4P' water model[18] using a charge-group based cutoff scheme as this model gives the best compromise in terms of a true representation of water (accurate simulation of density etc) vs. computational cost of the system.

5.2.1.1 Transferable Intermolecular Potential Four Point (TIP4P) Water Model with Charge-group Based Cutoff
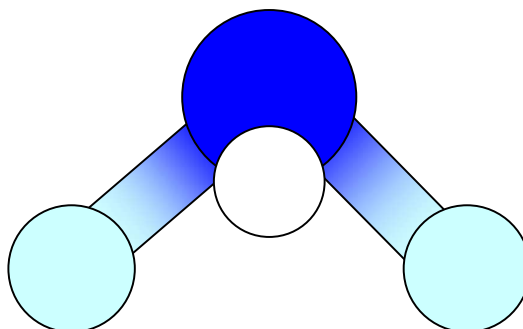
Figure 5.2.1.1.1: Structure of TIP4P water model

The TIP4P water model[18] consists of three point masses, representative of the single oxygen and two hydrogen atoms of a real water molecule, as well as an additional site, M, which has no mass and which lies on the H-O-H angle bisector. Point M carries all of the negative charge of the molecule and the oxygen atom point mass is the only part of the molecule with a Lennard-Jones interaction site (see section 2.2.4.2.).

The parameters used for the TIP4P water model are given in tables 5.2.1.1.2, the equations for bond stretching, bending and non-bonded electrostatic charges are given in section 2.2.4.2.

Bond	R_{OH}/Å	R_{OM}/Å	Angle	θ_{HOH}/$^{\circ}$
Stretching	0.9572	0.15	Bending	104.52

Non-Bonded	q_O/e⁻	q_H/e⁻	q_M/e⁻	ε_O /C^{2}N^{-1}m^{-2}	σ_O/Å
Interactions	0.0	0.52	-1.04	0.1550	3.1536

Tables 5.2.1.1.2: Parameters for TIP4P water model

The charge-group based cutoff method is employed to reduce computational power needed by neglecting any interactions between charge groups that are beyond a set

distance apart. This is illustrated in figure 5.2.1.1.3. Whereby any charge groups a greater distance apart than the two shown in the figure would be considered to have zero interaction energy between them.
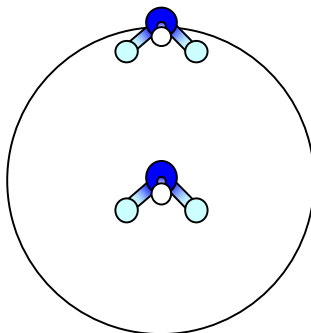
Figure 5.2.1.1.3: Illustration of a cutoff radius

Although there are various implementations of this rule the one employed by the DL_POLY molecular dynamics program that will be used for all simulations in this project is the only one of consequence. For this case, considering interactions between molecules X and Y, so long as any part of molecule Y is within the cutoff distance for any part of molecule X then all interactions between all parts of molecule X and molecule Y are included in the calculation even if the specific interactions lie outside of the cutoff radius. Otherwise there is no interaction between molecules X and Y whatsoever.

Simulation systems containing 1728 TIP4P water molecules in a simulation box with dimensions of 38.5 Å in all three dimensions have been run to equilibrium and this equilibrated water box is then ready to be used as a solvent for small poly(ethylene oxide) molecules.

5.2.2 Atomistic Poly(Ethylene Oxide) Simulations

The parameters for all of the bond length stretching, bond angle bending, dihedral torsional angles and non-bonded interactions for poly(ethylene oxide), or PEO, are all provided in the OPLS-AA force field[19] and are used without any modification. These parameters are shown listed in tables A through E in the appendix.

Two small PEO chains were constructed using the program *Macromodel*. The chains were both constructed in a linear fashion, one with 15 repeat (CH_2-O-CH_2) units (called PEO15) and one with 20 repeat units (called PEO20). Both of these chains were subjected to gas phase molecular dynamics simulations in order to allow the linear chains to collapse into a more realistic random coil arrangement.

5.2.3 Atomistic Simulations of Poly(Ethylene Oxide) in a TIP4P Water Solvent Box

Once the PEO chain is relaxed into a random walk conformation it was then inserted into the water solvent box using a program developed in-house. The program removes any water molecules that overlap within a certain distance of the centre of mass of any of the inserted PEO atoms. Appropriate PEO-water interaction parameters[20] were then added to the OPLS-AA force field (shown in tables A through E in the appendix) and then a short molecular dynamics simulation was carried out using a N_pT (constant pressure) ensemble to allow any high energy gaps or overlaps between water and PEO atoms to relax into more energetically favourable positions and to allow the density of the system to reach equilibrium (using this OPLS-AA force filed gives a density of 0.9925 g cm^{-3} for both the PEO15 and PEO20 systems). This process was carried out for the PEO15 molecule, 128 water molecules were removed to accommodate the PEO15 molecule leaving 1600 water molecules remaining and increasing the box size to 39.2 Å in all three dimensions. The same process was also carried out for the PEO20 molecule removing 171 water molecules and leaving 1557 behind and increasing the box size to 39.7 Å in all three dimensions.

All simulations were carried out using the molecular dynamics program DL_POLY as mentioned previously. The atomistic simulations of these atomistic PEO in a TIP4P water solvent were carried out for a simulation time of 1 ns (500,000 steps of 2 fs time step), with a set of coordinates and trajectories for each atom in the system being dumped into a *HISTORY* file every 1,000 simulation steps. These simulations were carried out using an N_vT (constant volume) ensemble. The *SHAKE* algorithm (developed by

Ryckaert *et al*)[21] is employed to maintain bond lengths around the equilibrium value given in the force field for each atom pair type.

5.2.3.1 Radius of Gyration Measurements

The formula for calculating the radius of gyration, R_g, for a polymer is given in section 1.2. This formula was incorporated into a program developed in-house that reads in the coordinates of each particle in the system at each time step (contained in the *HISTORY* file for each simulation) and generates a value for the radius of gyration of a polymer at that specific time interval. Using the information generated by this program it is possible to plot the change in radius of gyration against simulation time for a polymer. Figure 5.2.3.1.1 shows radius of gyration results for PEO15 and PEO20 as described in the previous section. These systems are analogous to very dilute solutions of the polymer in a water solvent and therefore the PEO chains should be free to move around. Under these conditions we would simply expect that the longer chains would have a larger radius of gyration due to their increase in mass.
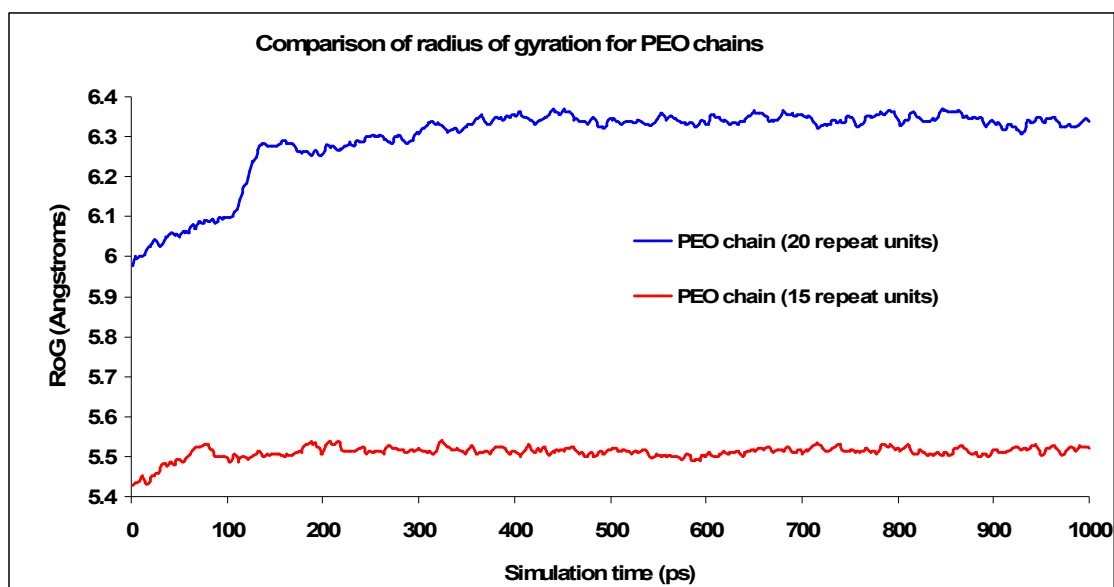
Figure 5.2.3.1.1: Radius of gyration results for 1ns atomistic simulations of PEO

The expected trend is shown clearly in figure 5.2.3.1.1 where the PEO15 system has a lower radius of gyration, reaching equilibrium at around 5.5 Å very quickly. The initial configuration of the PEO20 is slightly further away from equilibrium and takes a little time to reach the stable value of around 6.3 Å, which is higher than the PEO15 value due to the larger chain mass/length.

We would also expect that chain of equal length would have a larger radius of gyration when they include the end-cap species due to increase in mass and reduced flexibility of the molecule due to steric hindrance at one end. The end-cap to be used in this case is a simple unfunctionalized 2nd generation dendron as shown in figure 5.2.3.1.2.
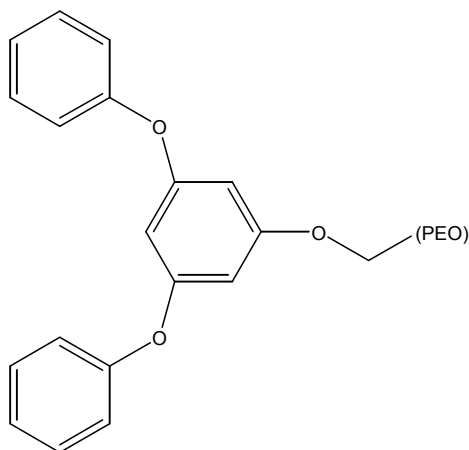
Figure 5.2.3.1.2: Head group used during atomistic radius of gyration calculations

The *HISTORY* files from the initial PEO15 and PEO20 runs took up a lot of disk space so it was decided to dump the coordinates and trajectories every 2000 time steps for the end-capped PEO15 molecule, as can be seen in figure 5.2.3.1.3 the results show a great deal of fluctuation in the radius of gyration as simulation time passes. The final configuration of the end-capped system shows the PEO chain wrapped around the end group and would result in a relatively low radius of gyration. Observing a movie of the simulation through time shows this to be the case for much of the simulation, where the chain coils and uncoils from around the bulky end-cap and results in a fluctuation of the

values for the radius of gyration. The apparent fluctuations in the radius of gyration measurements are also enhanced by the larger time step between coordinate dumps.
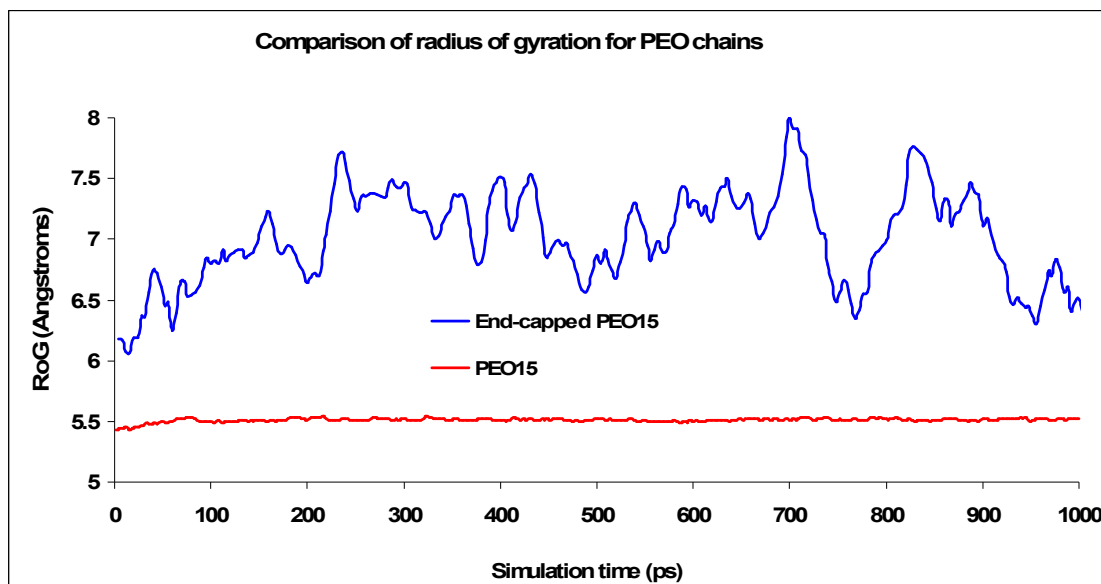
Figure 5.2.3.1.3: Radius of gyration results for an atomistic simulation of short PEO chains with and without head groups

5.2.4 Bond Length and Bond Angle Distributions
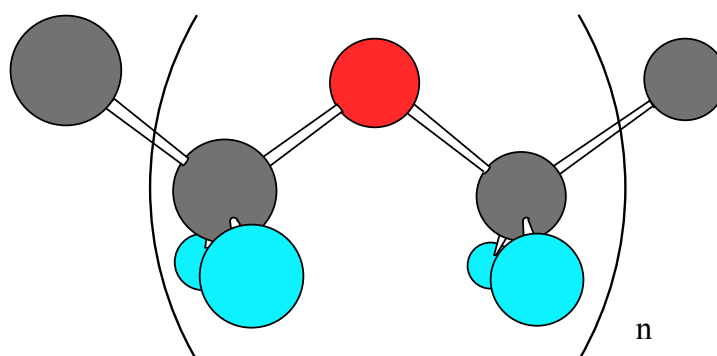
Figure 5.2.4.1: Segment of PEO chain to be coarse-grained to a single particle (in brackets)

In order to simulate larger PEO molecules that are more representative of real systems (a 10,000 g mol^{-1} PEO chain would be around 230 repeat units and a large number of these molecules with a very large water solvent box is necessary to be able to compare with experimental results) it is necessary to simplify the system in order to reduce the computational power/time required. The method employed in this case is called *coarse graining* and involves the incorporation of several individual atoms into a single coarse grained site. This coarse graining technique is explained in much greater detail in section 5.3.
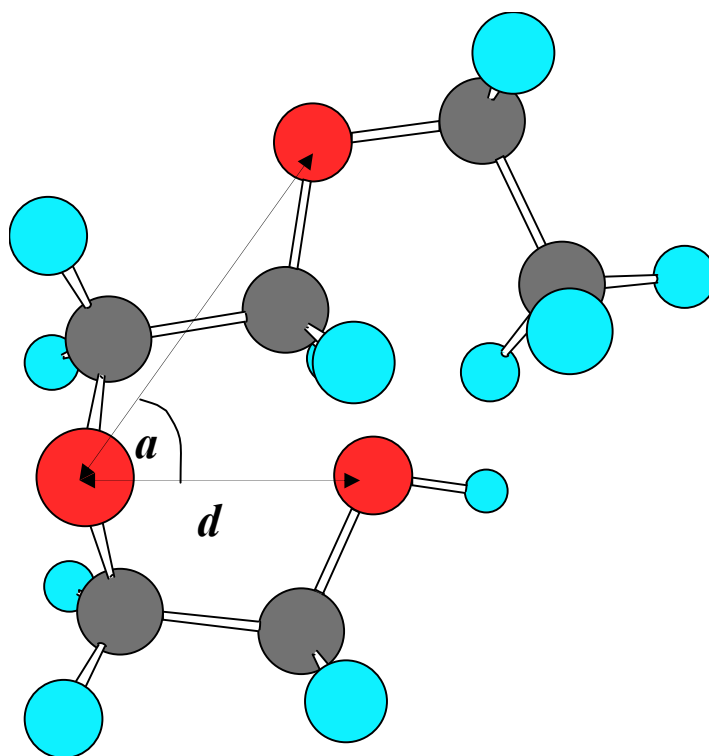
Figure 5.2.4.2: Diagram to show O-O bond distances and O-O-O bond angles

In order to coarse grain a PEO chain to a more simplistic model we first need to calculate how the sections of the molecule will behave in the coarse grained model. The central oxygen atom is taken as the point of reference for the center of the coarse-grain particle. The distances between the oxygen atoms and the O-O-O angles (*d* and *a* respectively in figure 5.2.4.2) can be calculated to give a distribution over all oxygen

atoms averaged over every time-step in the simulation (shown in figures 5.2.4.3 and 5.2.4.4).
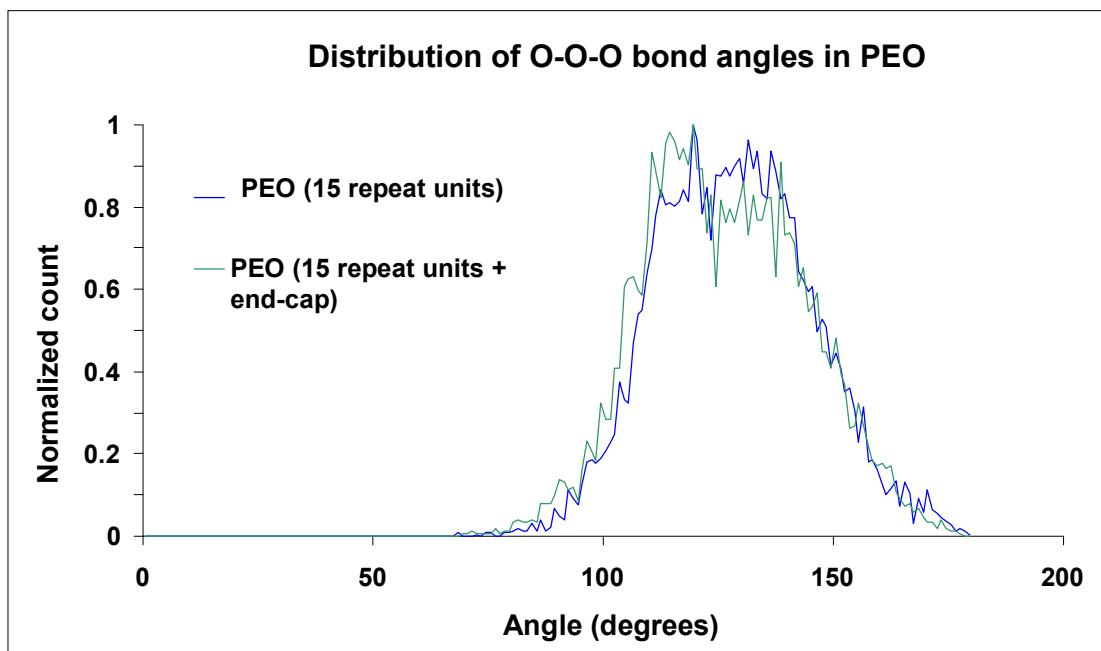
Figure 5.2.4.3: Distribution of O-O-O angles in PEO chain
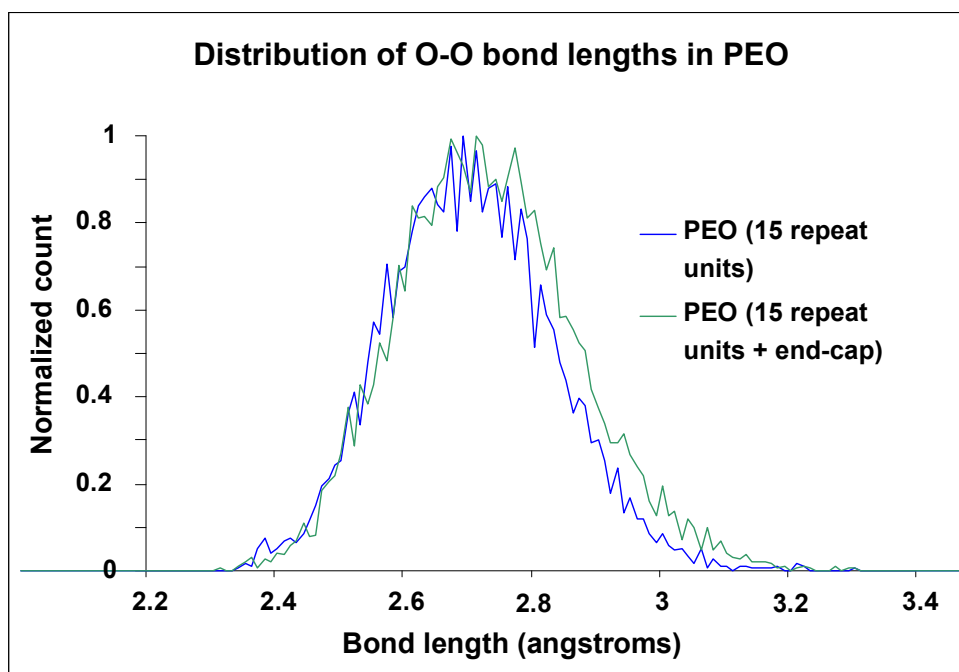
Figure 5.2.4.4: Distribution of O-O bond lengths in PEO chain

As well as calculating the radius of gyration for PEO chains it is also useful to calculate radial distribution functions. One of the programs developed can use the information contained in the output files of the simulation program to calculate the distance between specific atoms types in a bulk system. An atomistic simulation was run with 64 PEO15 chains placed into the simulation box at low density, the system is then placed under very high pressure to compress the system relatively rapidly towards the density of bulk PEO; and then allowed to equilibrate fully at atmospheric pressure. This should lead to a system configuration close to that of a real bulk PEO solid. The radial distribution calculation program (developed in-house) takes each PEO carbon atom in the *CONFIG* file (this file contains the records for all of the atom types and each atom has a number assigned in the order in which they were generated) and calculates the distance to the equivalent carbon atom in all of the other chains. Because of the specific layout of the *CONFIG* file it is possible to simply add the number of atoms in each molecule to the original atom number in order to find the equivalent atom in the second molecule. This number can then be added repeatedly until the equivalent atom in each molecule of the system is included in the calculation. A plot of distance between equivalent atoms, in this case the carbon atom located closest to the centre of the chain (repeat unit 8), versus normalized number of these atoms at the specified distance is shown in figure 5.2.5.1. Just for your information - Radial distributions from atomistic simulations of this type can later be compared with equivalent radial distributions from coarse grained simulations as a check to ensure correlation between the two techniques.

5.3 Coarse Graining

Atomistic simulations of very short poly(ethylene oxide) chains (15 and 20 repeat units) have been carried out and shown to give good consistent results for radius of gyration, radial distribution functions, bond length and bond angle distributions etc. However, in order to reach a system closer to that used in our neutron experiments etc (see chapter 4) it is necessary to model a much longer poly(ethylene oxide) chain with a much more realistic polymer molecular weight. In order to incorporate this larger

poly(ethylene oxide) molecule a much larger solvent (water) box is also required. Both of these targets can be achieved using a technique known as coarse graining[22, 23].

5.3.1 Coarse Graining Water

In the atomistic simulations carried out in section 5.2 an individual water molecule is modeled atomistically by a 4-site TIP4P water unit (described in detail in section 5.2.1.1). When creating a model for a large bulk solvent this can result in thousands of atomic sites and would take far too much computer time to simulate using molecular dynamics.
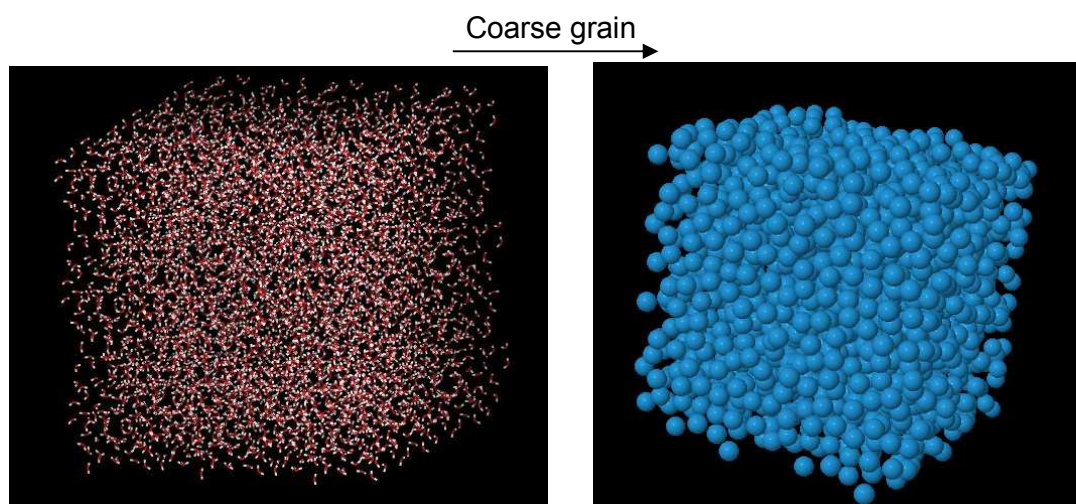
Figure 5.3.1.1: Site reduction from coarse graining of water

When coarse graining this system 3 water molecules are grouped into a single water CG site. By doing this the number of sites to be modeled in the system is reduced by a factor of 12 (illustrated in figure 5.3.1.1). This approach to coarse graining water has developed by Klein *et al*[24, 25] and employed by several groups including Marrink and Mark *et al*[26-29]. Not only is this reduction in site number advantageous to computational times but also all intramolecular forces are removed as there are no bond stretching or bond bending calculations necessary to model the single unit sites. This in turn means that a larger time step can be used because the fastest motions (vibrations etc of short

bonds) have been removed from the system. Coarse graining a system also simplifies the free energy surface of the simulation allowing the molecules to be able to move more rapidly through configurational space. The intermolecular forces between each CG water site (and eventually between CG water sites and CG poly(ethylene oxide) sites) can be calculated and modeled using a simple 6:4 Lennard-Jones[30] potential of the form:

$$E_{Van} = \sum_{a=1} \sum_{b=a+1} 4\varepsilon_{ab} \left(\frac{\sigma_{ab}^{6}}{R_{ab}^{6}} - \frac{\sigma_{ab}^{4}}{R_{ab}^{4}} \right) \qquad \text{Equation 5.3.1.1}$$

Where ε_{ab} is the energy well depth, σ_{ab} is the cross-over point (minimum A-B distance where the potential equals zero) and R_{ab} is the distance between atoms a and b at any given time. This form of the Lennard-Jones potential is much softer than that used for atomistic simulations as the coarse grained particles have much greater volume and can penetrate one another with a much smaller energy penalty than that of the much harder smaller atoms.

Some starting values of the parameters σ_{ab}, ε_{ab} and R_{ab} can be taken from previous work by Klein et al[23, 31] and these can be altered by trial and error simulations to find values that give calculated results matching experimental findings for parameters such as density, radial distribution functions etc.

All of these simplifications mean that a large water system can be modeled over a long simulation period without the need for vast amounts of computational power or time.

5.3.2 Coarse Graining Poly(Ethylene Oxide)

In order to coarse grain a poly(ethylene oxide) chain we first need to calculate how the sections of the molecule will behave in the coarse grained model[22]. The central oxygen atom is taken as the point of reference for the center of the coarse-grain site and the neighbouring CH_2 sites are incorporated into it[23, 30, and 31], reducing the number of sites by a factor of 7 (this coarse grained particle is illustrated in the dashed box of figure 5.3.2.1). Although this CG technique is similar to the one used to model the water

solvent, in this case there are still intramolecular forces present between each CG poly(ethylene oxide) site (CGPEO). In order to calculate these intramolecular CGPEO-CGPEO bond stretching and CGPEO-CGPEO-CGPEO bond bending parameters it is necessary to use information obtained from atomistic computer simulations.
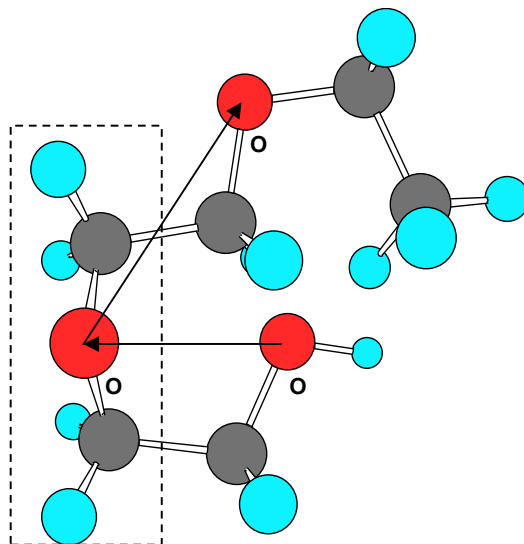
Figure 5.3.2.1: CG section of poly(ethylene oxide) chain

The O-O bond distances and the O-O-O bond angles (shown in figure 5.3.2.1) can be calculated from atomistic models to give a distribution over all oxygen atoms averaged over every time-step in the simulation (an example is shown previously in figure 5.2.4.4). A Boltzmann inversion can then be performed on these distributions to convert them into Boltzmann distributions using equations 5.3.2.1 and 5.3.2.2.

$$S_{(x)} = \exp\left(\frac{-E_{(x)}}{k_B T}\right) / q_{(x)}$$

Equation 5.3.2.1

Where $S_{(x)}$ is the bond length or angle distribution, k_B is the Boltzmann constant, T is temperature and $E_{(x)}$ is the potential to be found. Here, $q_{(x)}$ is the partition function in the coordinate space $_{(x)}$. In the Boltzmann inversion, the influence of $q_{(x)}$, is simply to act as a constant, which shifts the potential up or down. As we are only interested in relative

potentials, $q_{(x)}$, can effectively be set by ensuring that the minimum of the potential is set to zero.

Once a Boltzmann distribution has been calculated for the bond lengths and angles it is then simply a case of fitting a harmonic potential[32] (of the form shown in equation 5.3.2.2) to this distribution. An example of such a fit is shown in figure 5.3.2.3.

$$E_{Str} = \sum_{bonds} \frac{k_s}{2} (R_{ab} - R_0)^2 \qquad \text{Equation 5.3.2.2}$$

Where R_0 is the ideal bond length, R_{ab} is the actual bond length at any given time during the simulation and k_s is the bond stretching constant for a particular bond type (in this case CGPEO-CGPEO). This harmonic potential can also be applied to bond angles.
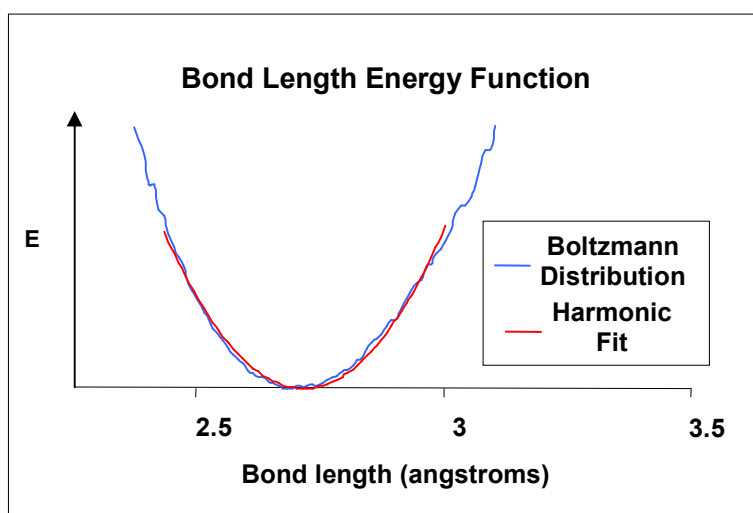
Figure 5.3.2.2: Boltzmann distribution and harmonic fit

With these bond length and angle parameters calculated from atomistic simulations it is possible to perform molecular dynamics on a coarse grained poly(ethylene oxide) chain of realistic molecular weight.
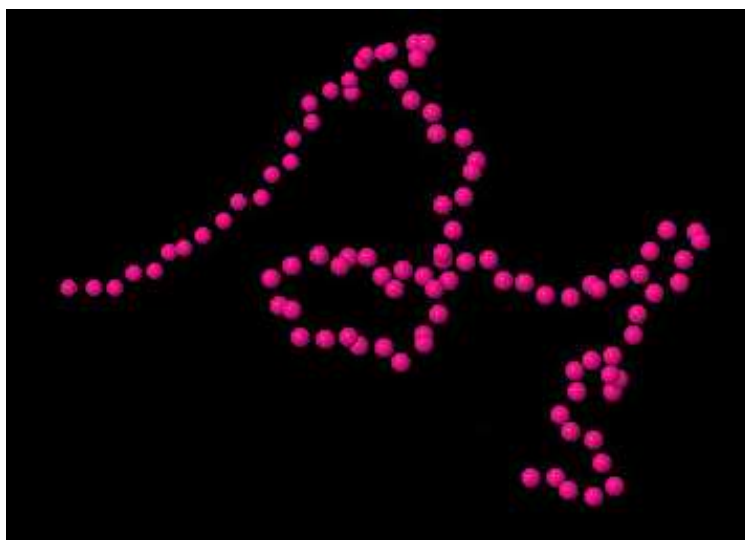
Figure 5.3.2.3: 100 repeat unit coarse grained PEO chain: here the spheres are shown at 30% of their van der Walls volume

Trial simulations were carried out on a coarse grained PEO chain of 100 repeat units of this type with some success (figure 5.3.2.3 shows one such chain in the gas phase having adopted a random walk conformation). Although this corresponds to a molecular weight of only 4,400 g mol^{-1} (much lower than the target of 10,000 g mol^{-1} to match that used in the experimental section of this project) an increase to a greater number of repeat units would run the risk of producing too many particle sites once these molecules were replicated to represent a more realistic multi-chain system. This, combined with the relatively long relaxation times found for this type of chain and the preliminary timings from trial simulations, suggested that this level of coarse-graining would still prove extremely challenging in terms of the computer time required.

As a result it was decided to abandon this coarse grain model and develop a new coarse grain particle that incorporates twice the number of atomistic sites as this first trial CG model does. Details of this new coarse grain model are given later in section 5.4.3.

5.4 Designing a Simulation Experiment

5.4.1 Head Group Simulations

Now that the techniques for atomistic and coarse grained simulations have been established and small test runs successfully carried out on simple trial molecules it is possible to start building a system that replicates the conditions implemented in the experimental section of this project.

The first stage is to construct atomistic models of the trifluorinated (3FA) and difluorinated (2FA) dendritic head groups and then to perform a short molecular dynamics calculation on the molecules under atmospheric pressure and room temperature conditions to allow them to adopt a more thermodynamically favourable structure. The illustrations in figure 5.4.1.1 are examples of the types of conformation adopted by the molecules during this short molecular dynamics simulation.
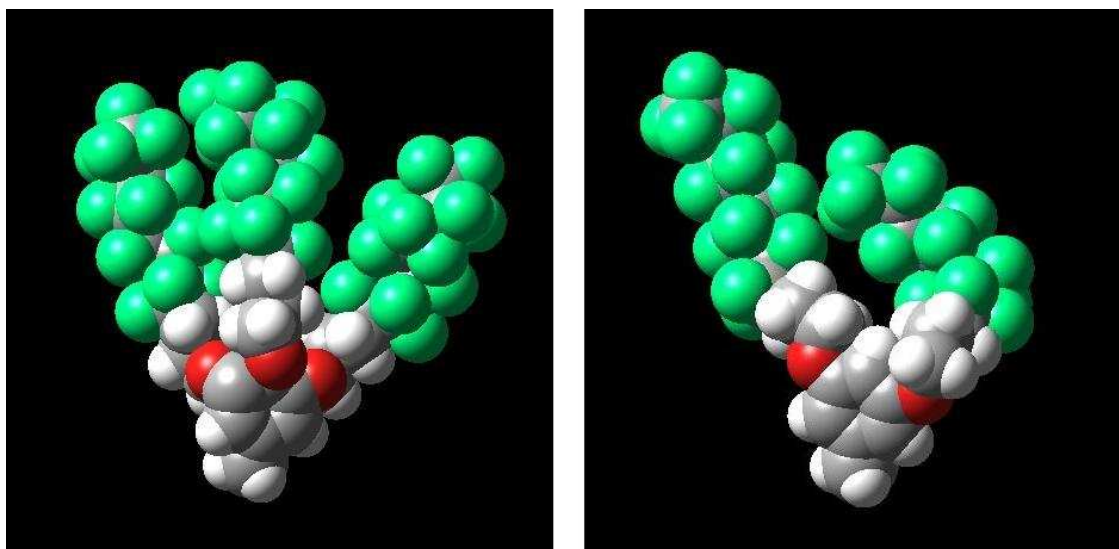
Figure 5.4.1.1: Atomistic representations of difluorinated and trifluorinated dendritic head groups

These head group simulations were carried out under the same conditions as those described earlier in section 5.2, using molecular dynamics with a time step of 1 ps. However, the standard OPLS-AA force field does not include adequate parameters for certain potentials involved in modeling perfluoroalkyl chains. Several groups have previously calculated these parameters from ab-initio, Monte Carlo and molecular dynamics calculations[33-41]. Some of these groups (in an attempt to simplify the systems to be studied even further) have calculated potentials that do not include partial charges on the perfluoroalkyl atoms[33]. I believe this to be an over-simplification and therefore the parameters employed in my simulations are those calculated by Watkins and Jorgensen[34] by ab-initio and Monte Carlo techniques and which include terms for the partial charges associated with each atom.

In order to look specifically at the interactions between the head group molecules and remove all other complications for the time being; at the end of the short molecular dynamics simulation an extra dummy atom is attached to the CH_2 group at the para position of the aromatic ring. This dummy atom is used to tether the molecules into a 2 dimensional plane and saves vast amounts of computational time by replacing the long poly(ethylene oxide) chain that would normally be at this position. Once the single molecules have been constructed and relaxed into an acceptable conformation by means of further short molecular dynamics simulations it is then a simple process to replicate the molecules onto a 2 dimensional lattice representative of the experimental air-water interface. The original single molecule is constructed in a simulation box of size 20 by 20 by 40 nm (with the z-dimension being the largest), replicating this system by 5 times along both the x and y dimensions results in a system of size 100 by 100 by 40 nm containing 25 3FA molecules. The system is subjected to further short molecular dynamics runs to allow the lattice to become relaxed, this is illustrated in figure 5.4.1.2.

Figure 5.4.1.2 shows very nicely the effects of the 2 dimensional periodic boundary conditions applied in all computer simulations carried out in this project. Where some of the atoms belonging to the molecules on the left side of the box have crossed the periodic boundary they have been introduced to the opposite side of the simulation box to interact with the molecules located there. This leads to a system where all the molecules are

essentially surrounded by other molecules (not bound by a solid non-interactive wall) allowing the maximum amount of intermolecular interactions possible.

The next step is to apply a 2 dimensional soft repulsive wall to the system to represent the effects of an air-water interface. The repulsive wall can be applied in such a way that it has specific interactions with each different atom type in the system. For this case the wall was made to act repulsively in the positive z direction on the atom in the head group and in the negative z-direction for the dummy atoms. This results in the head groups becoming anchored to the 2 dimensional plane but allowed to freely diffuse along both the x and y directions. The 2 dimensional soft repulsive wall is given by the following equation:

$$zf > Z_0f : F_z = -A(z - Z_0)$$

Equation 5.4.1.1

Where F_z is the repulsive force active on a specific atom, A is the hardness/softness of the wall (increasing A will cause F_z to increase more rapidly as the atom moves into the wall), Z_0 is the z-coordinate for the onset of the 2 dimensional wall and z is the z-coordinate of the specific atom. The system is then subjected to a short molecular dynamics simulation to allow the molecules to move to the 2 dimensional wall and try to relax the lattice positions. A system that has reached this point is illustrated in figure 5.4.1.2.

This system allows us to specifically observe the interactions between the head groups, without the complications of polymer entanglement from the poly(ethylene oxide) chains or the need for the simulation of a huge amount of water molecules. These simulations are relatively computationally inexpensive and can therefore be run over timescales of >1 ns and many different simulation conditions can be implemented, such as varying density (simply by increasing or decreasing the spacing in the initial replication step) or changing the chemical structure of the head group etc.
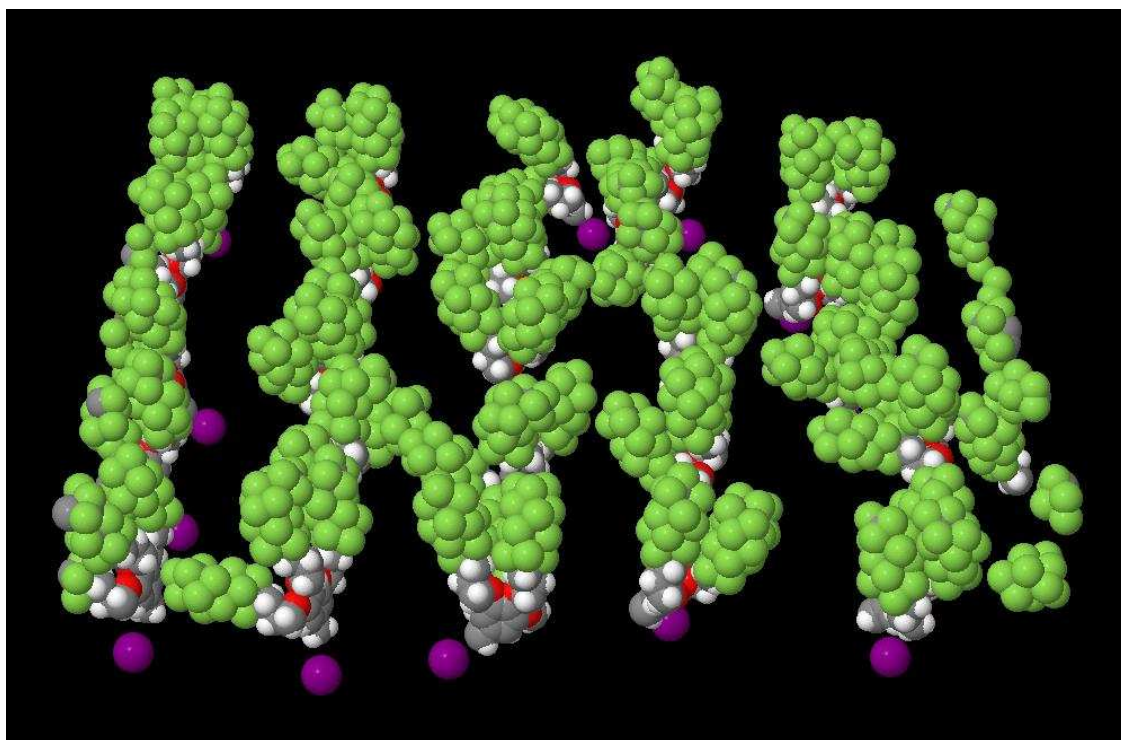
Figure 5.4.1.2: Atomistic model of trifluorinated head groups with tethering dummy atoms in a 2 dimensional plane

A 2 ns simulation (with 1 ps time steps and the coordinates dumped to a *HISTORY* file every 2000 steps) was carried out on the system illustrated in figure 5.4.1.2. In this case the atomistic head groups are densely packed into a lattice formation that has been allowed to relax a little. The final conformation of the simulation (after 2 ns) showed a close packing of the head groups in the centre of the simulation box. Observing a movie of the simulation proceeding through time reveals that the head groups appear to move independently of one another until they come into close contact with one another, at which time they begin to form clusters and eventually form one large cluster that includes all 25 molecules. For this system the close packed conformation is reached very quickly (<0.5 ns) due to the initial set up of the simulation having the molecules arranged in a fairly dense lattice. Figure 5.4.1.3 shows an illustration of the final configuration of this

simulation, the periodic boundary splitting has been left in to give an idea of the cluster size relative to the box size.
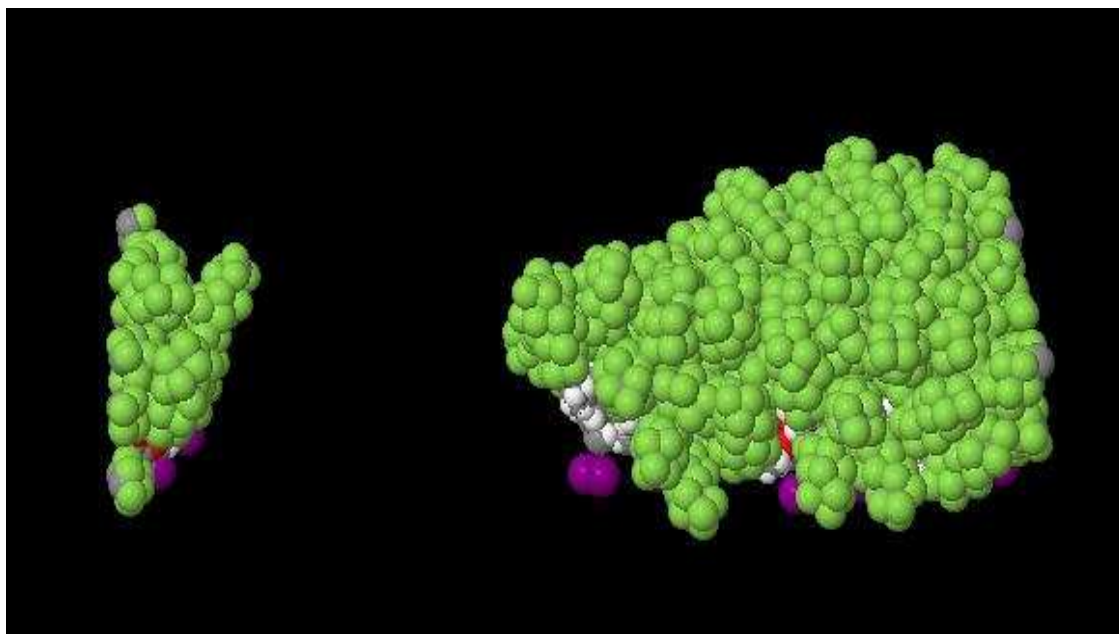
Figure 5.4.1.3: Cluster formation by atomistic trifluorinated head groups

In order to test that this clustering of the molecules was not simply as a result of the original high density of the system other, lower density, systems were simulated under the same conditions. One system was set up in the exact same way as described for the previous system but with all of the dimensions of the 2-dimensional lattice doubled (single molecule box size of 40 by 40 by 40 nm, resulting in a 25 3FA molecule system with box size of 200 by 200 by 40 nm). Another system was constructed by removing every alternate molecule from the system shown in figure 5.4.1.2 leaving only 12 molecules remaining on the lattice. These two system should be directly analogous to one another with the latter being a scaled-down version of the former.

2 ns simulations (with 1 ps time steps and the coordinates dumped to a *HISTORY* file every 2000 steps) were carried out on both of these systems. The final conformation of both simulations showed a close packing of the head groups. For the smaller system

containing only 12 molecules there was a single cluster of molecules in the centre of the box as observed in the previous simulation. By again observing a movie of the simulation proceeding through time it was possible to watch the formation of this cluster. For this lower density case the close packed conformation did not fully form until around 1.2 ns into the simulation due to the greater distance between the molecules in the initial configuration. For the larger system however, two separate clusters were observed in the final configuration with a significant space between them containing 14 molecules in one of the clusters and 11 in the other. The movie of the simulation reveals that the clusters form after a similar length of time as in the smaller system (after around 1.1 ns). This appears to show that the formation of clusters not only depends on the density of the system but also on how many molecules are present. For both systems the clusters appear to be stable once they are formed and there are no indications that the cluster will break up over time. However to be certain of this it would be necessary to run a simulation over a much longer timescale (at least 10 ns). Another observation that can be made for these movies is that once clusters of around 10 or so molecules are formed then these clusters begin to repel one another. This can be explained by the fact that the clusters are held tightly together by the head groups and the bulky PEO chains are more spread out underneath these head groups simply due to their size and steric hindrance therefore preventing the head groups of two separate clusters from interacting. If this was not the case then we would see the formation of one large cluster containing all of the molecules in the system.

A system containing 25 atomistic head group molecules with a simulation box size 4 times larger in each direction on the 2-dimensional plane than that of the original system (figure 5.4.1.2) was setup along with a system containing 64 atomistic head group molecules with a simulation box size scaled up appropriately to match the density of the 25 molecule system. For these systems 4 ns simulations (with 1 ps time steps and the coordinates dumped to a *HISTORY* file every 2000 steps) were carried out in order to allow for the longer times needed for the molecules to reach one another. Both of these simulations produced very similar results and in the final configuration of both systems there were clusters of 6-7 molecules (some with 5 or 8 in the larger 64 molecule system) with significant spacing in between. Again observing the movie reveals the time taken for

these clusters to form and after around 1.6-1.9 ns in both cases the clusters appear to form and remain intact for the rest of the simulation.

From these results it can be seen that at very high densities the atomistic head group molecules are forced to adopt a conformation where all of the molecules are tightly packed into one large cluster and the same effect is observed when there are only a very small number of molecules (in this case 12) present in the system. For systems that have a larger number of molecules it can be seen that these clusters begin to form independently of one another containing smaller numbers of molecules. When a lower density is reached the molecules appear to form a stable cluster size of around 6-7 molecules throughout the system, independent of the number of molecules present.

As a result of these observations it was decided that further simulations carried out in this project must contain at least 25 molecules and that packing density must be considered very carefully in order to give a true representation of the system.

5.4.2 Simulation of Experimental Molecules

Having now studied the specific interactions of the head groups alone under varying conditions it was then decided to move on to studying molecules that are chemically representative of those used in the experimental work. Figure 5.4.2.1 shows an illustration of a molecule with one of the head groups used experimentally attached to a very short PEO chain.

Atomistic modeling as used in the previous head group simulations is possible only on very small systems. In order to construct a molecule with a molecular weight of ~10,000 g mol^{-1} (like those used in experiment) it is necessary to include a minimum of ~1,500 atoms for each poly(ethylene oxide) chain, then the head group must also be included. Trial molecular dynamics simulations were carried out for single molecules of this type with a shorter poly(ethylene oxide) back bone than those used experimentally to test simulation times. However, the number of atoms needed to simulate a full system of these molecules is simply too great for a simulation of an acceptable length to be completed in a reasonable amount of computational time. Usually an absolute minimum

of 1 ns is needed to allow equilibrium to be reached for a short chain of around 10 repeat units, and much longer simulations are required for longer chain lengths.
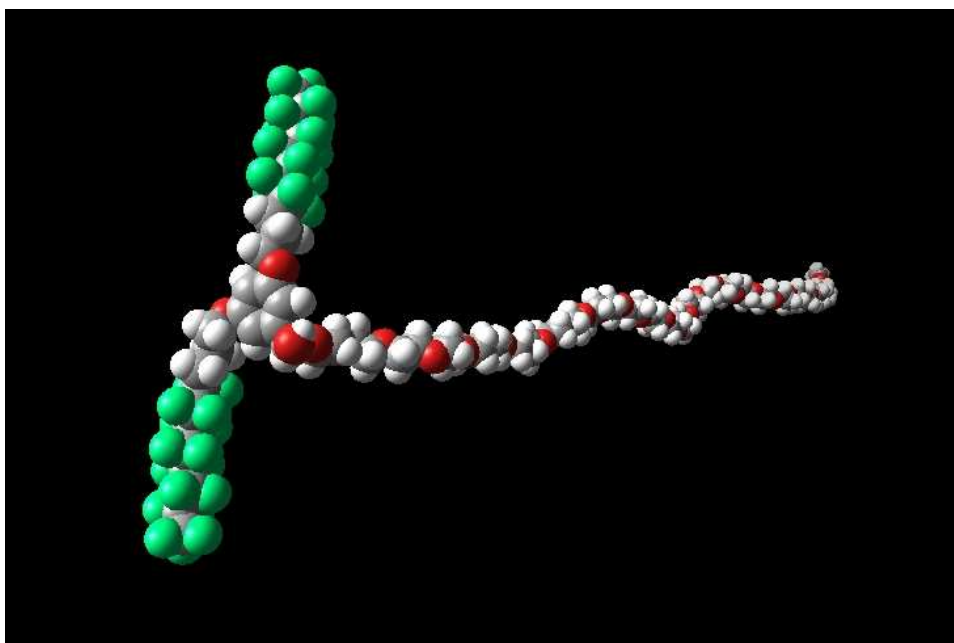
Figure 5.4.2.1: Atomistic model of short chain molecule

5.4.3 Coarse Graining to Real Systems

As shown previously it is possible to coarse grain a poly(ethylene oxide) chain to reduce the amount of computational time needed for the simulation. Earlier simulations have been carried out using each repeat (CH_2-O-CH_2) unit of poly(ethylene oxide) as a single coarse grained site. In order to construct a molecule with a molecular weight of ~10,000 (like those used in experiment) it is necessary to include a minimum of 200 of these coarse grained units. With the atomistic head group also included in this molecule it soon becomes computationally expensive even with this level of coarse graining. Previous studies[42] of PEO chains have used coarse grain units of twice this size; using each (CH_2-O-CH_2-CH_2-O-CH_2) as a coarse grained unit (from now on referred to as EO2), so it was decided to use this approach and reduce the number of coarse grained

sites needed by half again. Figure 5.4.3.1 shows (outlined by a dashed oval) one of these EO2 sections.
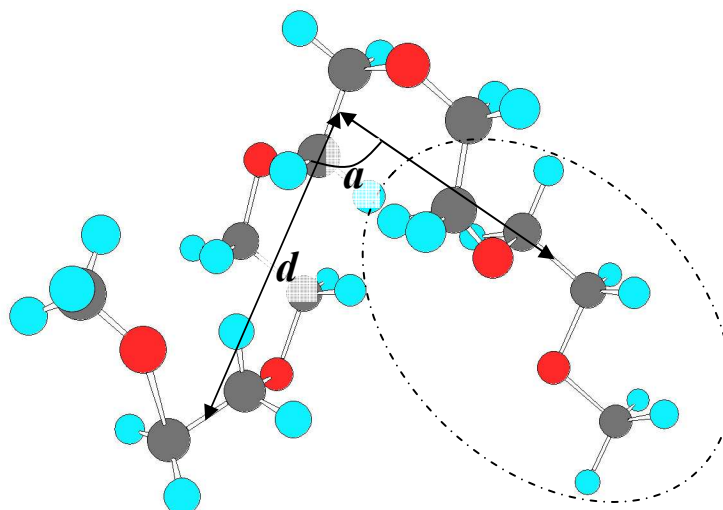
Figure 5.4.3.1: Graphical illustration of new coarse grained particles

As with the previous coarse graining methodology the parameters to be applied to the coarse grained particles can be calculated directly from atomistic simulations of PEO chains (these atomistic simulations are described in section 5.2.3). However for this system it is not possible to select a specific atom for the centre of the coarse grain particles; it is necessary to calculate the coordinates of the centre of the bond between the two central carbon atoms and then to calculate the distances (d) and angles (a) between these points, this is illustrated in figure 5.4.3.1. It is then possible to produce a distribution of EO2-EO2 bond distances, shown in figure 5.4.3.2.
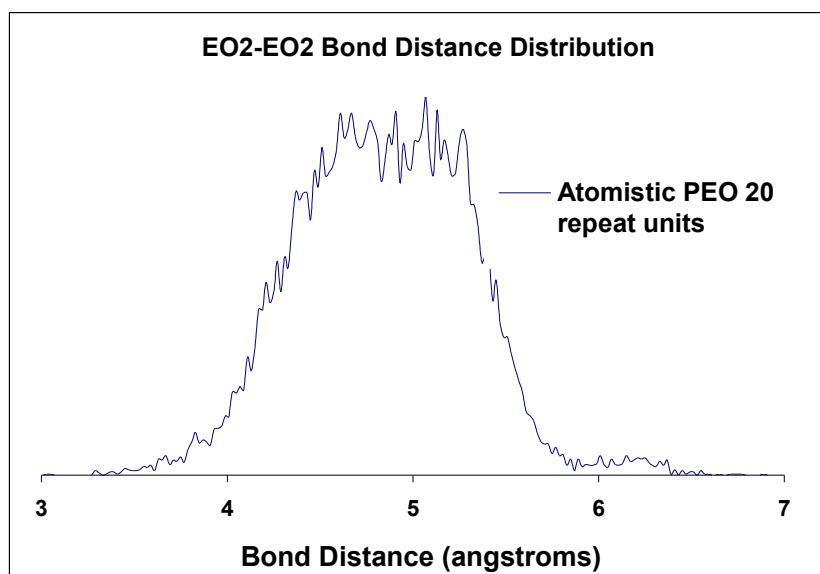
Figure 5.4.3.2: EO2-EO2 bond distance distribution
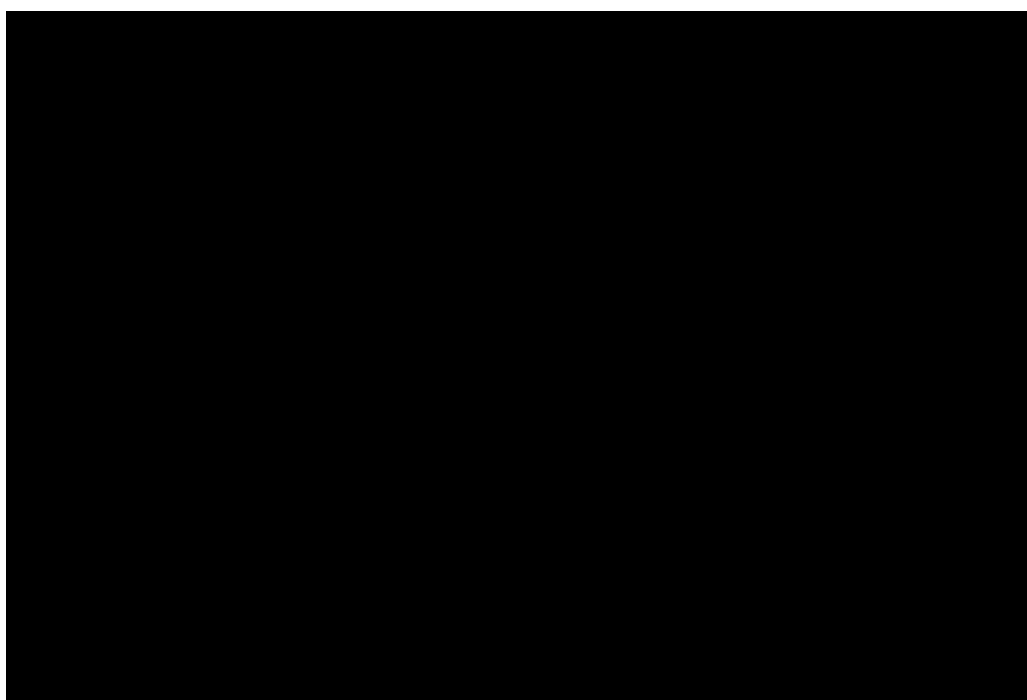
Figure 5.4.3.3: EO2-EO2 bond distance Boltzmann distribution and harmonic fit

A Boltzmann inversion can then be performed on this distribution to convert it into a potential using equation 5.3.2.1. A bond stretching potential can then be found to fit this distribution and used to calculate the coarse grain particle bond stretching parameters (see figure 5.4.3.3).

As can be seen in figure 5.4.3.3 the EO2-EO2 bond distance Boltzmann distribution can be fit to a simple harmonic spring potential as described previously in equation 5.3.2.2. A simple test system was set up to find out how close the bond distances given by the coarse grained parameters matched up to equivalent atomistic results. The test system consists of 10 repeat units of EO2 coarse grained particles (consistent with the 20 repeat units of PEO used in the atomistic model) contained within a simulation box of 40 Å in the *x, y* and *z* directions and these molecules are replicated onto a 4 by 4 by 4 cubic lattice to give 64 molecules in a simulation box of 160 Å in the *x, y* and *z* directions. These lattice spacings are small enough that the molecules will come into contact and interact with one another during a short simulation but large enough to allow freedom of movement throughout the system. The simulation is carried out at 298 K under N_vT (constant volume) conditions.

Previous studies carried out on equivalent sized EO2 coarse grained PEO particles by Chen *et al* employed an 8-6 Lennard-Jones non-bonded interaction potential between EO2 particles and this is shown in the following equation:

$$U(r_{ij}) = 3\varepsilon_{ij}\left[\left(\frac{\sigma_{ij}}{r_{ij}}\right)^8 - \left(\frac{\sigma_{ij}}{r_{ij}}\right)^6\right]$$

Equation 5.4.3.1

Here ε_{ij} is the energy well depth, σ_{ij} is the cross-over point and r_{ij} is the distance between atoms *i* and *j* at any given time. The values used by Chen *et al* for these parameters are given as $\sigma_{ij} = 5.50$ Å and $\varepsilon_{ij} = 0.167$ kJ mol^{-1}. Unfortunately the software used to carry out the molecular dynamics simulations (DL_POLY) only allows 12-6 Lennard-Jones potential to be used. There is however the option to employ a n-m potential of the form shown in the following equation:

$$U(r_{ij}) = \frac{E_0}{(n-m)}\left[m\left(\frac{r_0}{r_{ij}}\right)^n - n\left(\frac{r_0}{r_{ij}}\right)^m \right]$$ Equation 5.4.3.2

The values of n and m were set as 8 and 6 respectively and the values of σ_{ij} and ε_{ij} given in the paper by Chen *et al* were converted into values for r_0 and E_0 that would make this n-m potential match the 8-6 Lennard-Jones potential. The corresponding values for r_0 and E_0 were calculated to be 6.3509 Å and 0.01263 kcal mol^{-1} respectively.
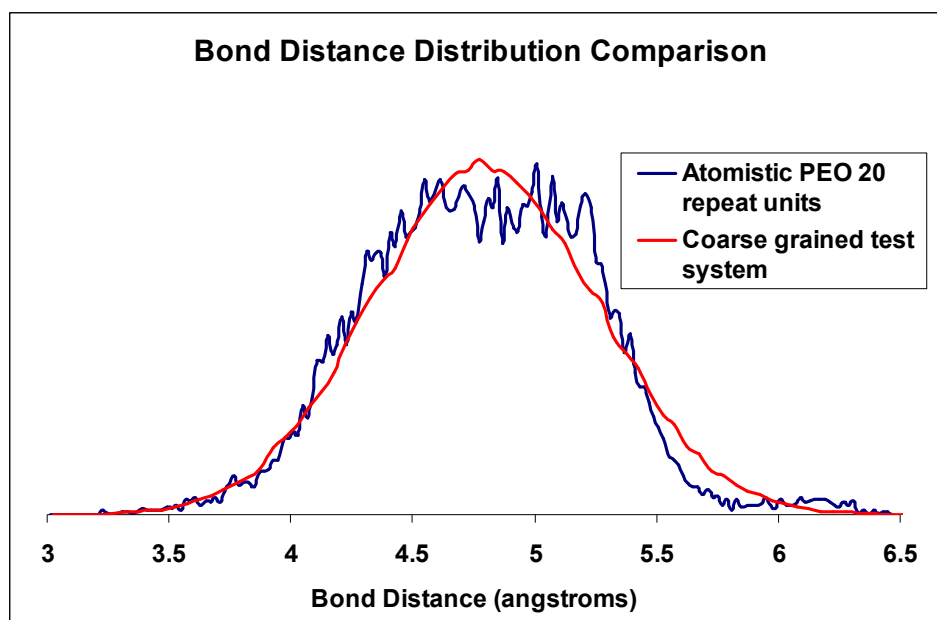
Figure 5.4.3.4: EO2-EO2 coarse grained and atomistic bond distance distributions

Figure 5.4.3.4 shows the comparison of the bond distance distributions from the atomistic simulations and from the coarse grained test system. It can be seen that the distribution of bond lengths in the coarse grained system is a very close match for that of the atomistic model. Therefore the parameters employed in this coarse grained test system will also be used in the final coarse grained system.

Using the same technique of calculating the coordinates of the centre of the bond between the two central carbon atoms in the EO2 unit it is also possible to produce a

distribution of EO2-EO2-EO2 bond angles, shown in figure 5.4.3.5. Again a Boltzmann inversion can then be performed on this distribution to convert it into a Boltzmann distribution using equation 5.3.2.1 and an angle bending potential can then be found to fit this distribution and used to calculate the coarse grain particle bending parameters (see figure 5.4.3.6).
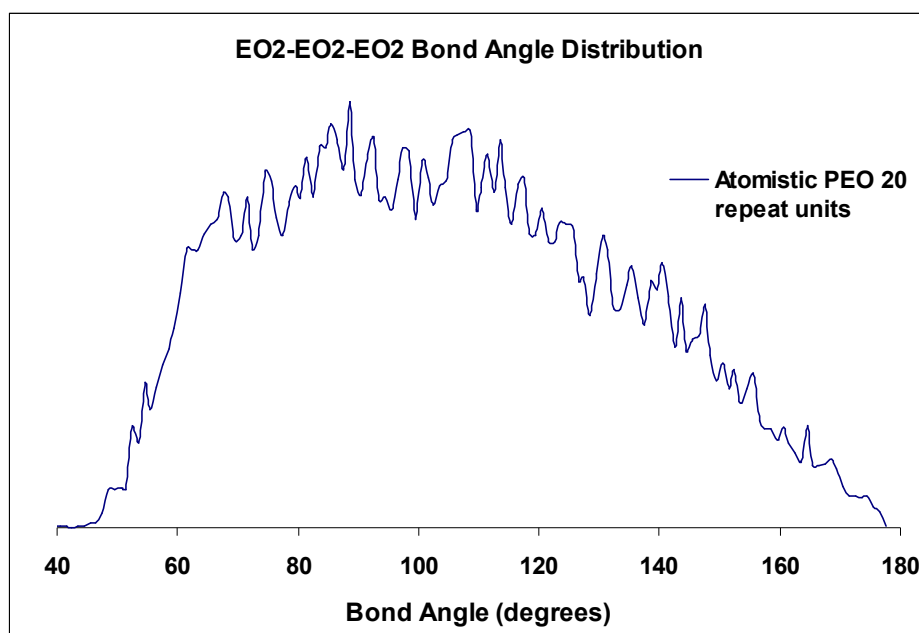
Figure 5.4.3.5: EO2-EO2-EO2 bond angle distribution

As can be seen in figure 5.4.3.6 it is necessary to use a more complex potential to fit the EO2-EO2-EO2 angle Boltzmann distribution as a simple harmonic potential will not follow the shape of the distribution correctly. In this case a Quartic polynomial potential (of the type shown in equation 5.4.3.3) can be used to capture the shape of the distribution and from this potential the coarse grained EO2-EO2-EO2 angle bending parameters can be calculated.
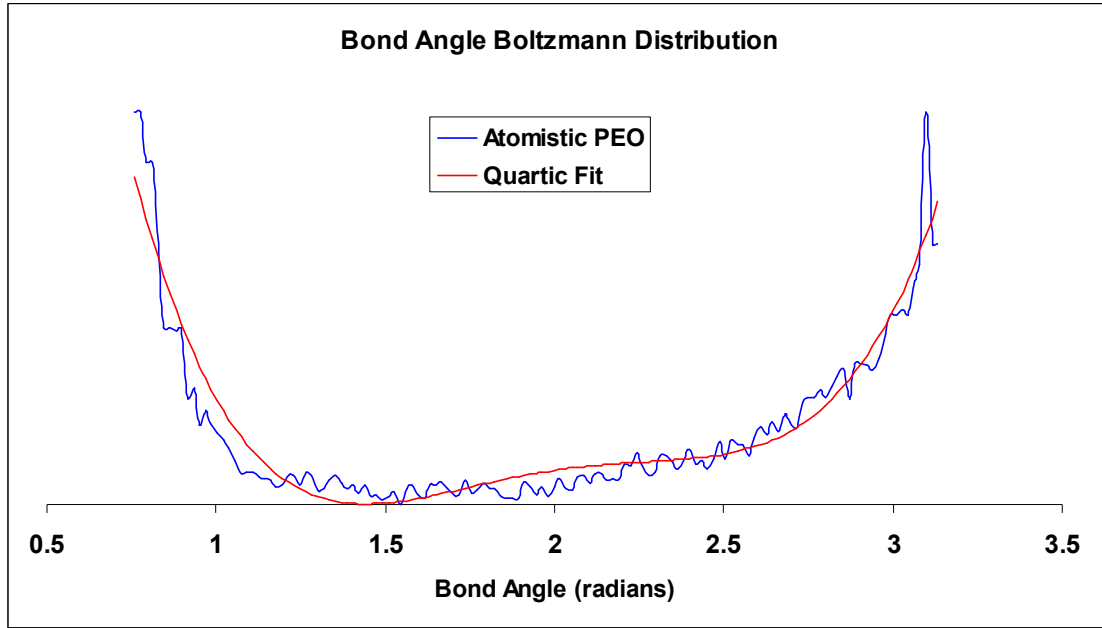
Figure 5.4.3.6: EO2-EO2-EO2 bond angle Boltzmann distribution and employed Quartic fit

$$E_{Bend} = \sum_{angles} \frac{k}{2}(\theta_{ab} - \theta_0)^2 + \frac{k'}{3}(\theta_{ab} - \theta_0)^3 + \frac{k''}{4}(\theta_{ab} - \theta_0)^4$$

Equation 5.4.3.3

Where θ_0 is the ideal bond angle, θ_{ab} is the actual bond angle at any given time during the simulation and *k, k' and k''* are the angle bending constants.

Using the same test system (as employed for the comparison of coarse grained and atomistic bond distances) it is possible to compare the coarse grained EO2-EO2-EO2 angle distribution with that of the atomistic equivalent. The results are shown overlaid in figure 5.4.3.7 and again it can be seen that the distribution of bond angles in the coarse grained system is a very close match for that of the atomistic model.
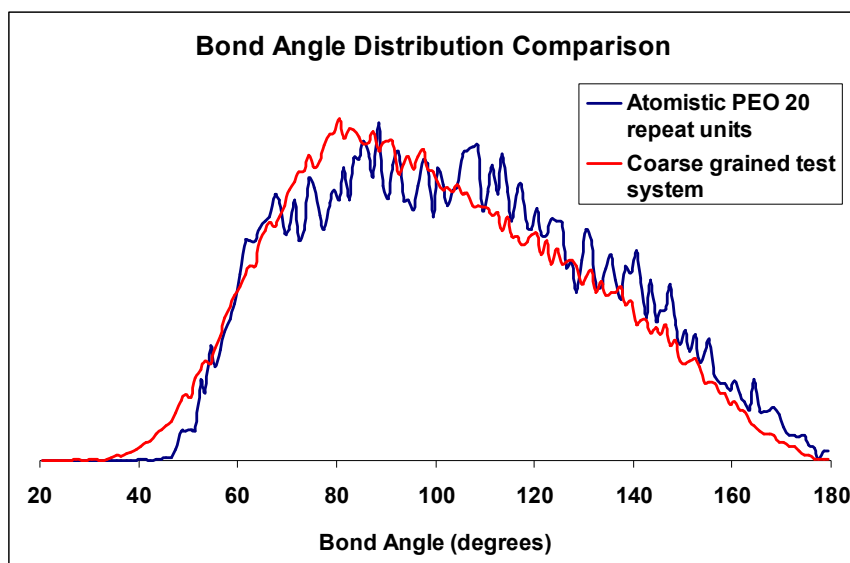
Figure 5.4.3.7: EO2-EO2-EO2 coarse grained bond angle and atomistic bond angle distributions

Figure 5.4.3.7 shows that there is good agreement between the coarse grained and atomistic systems and it is now possible to simulate much larger polymer chains over a much more realistic timescale without using an excessive amount of computational time. A simulation molecule of 100 repeat EO2 units plus the atomistic head group has a molecular weight of around 10 kg mol^{-1}, which is the same as that used in our neutron reflectometry experiments. The parameters used for the EO2 coarse grained model are shown in table 5.4.3.8.

As with the atomistic head group system; once the single molecules have been constructed they can relaxed into a more realistic conformation by performing either a short molecular dynamics simulation or even more simply by carrying out an energy minimization run. An energy minimization will result in a very ordered structure that can be used to assemble a crystalline starting structure, whereas a short molecular dynamics simulation will result in a more entropically realistic structure and can be used to assemble a liquid-like phase. Both of these starting points are constructed (as with the head group simulations) by replication of the appropriate single molecules onto a 2 dimensional lattice.

Bond Stretching Harmonic Potential	$E_{Str} = \sum\limits_{bonds} \dfrac{k_s}{2}(R_{ab} - R_0)^2$			
Parameters	k_s (kcal/Å^{-2})		R_0 (Å)	
Values	4.7046		2.6942	
Angle Bending Quartic Potential	$E_{Bend} = \sum\limits_{angles} \dfrac{k}{2}(\theta_{ab} - \theta_0)^2 + \dfrac{k'}{3}(\theta_{ab} - \theta_0)^3 + \dfrac{k''}{4}(\theta_{ab} - \theta_0)^4$			
Parameters	k (kcal/Å^{-2})	k' (kcal/Å^{-2})	k'' (kcal/Å^{-2})	θ_0 (^{0})
Values	2.4089	-5.4697	3.2310	82.7366
Non-Bonded n-m Potential	$U(r_{ij}) = \dfrac{E_0}{(n-m)}\left[m\left(\dfrac{r_0}{r_{ij}}\right)^n - n\left(\dfrac{r_0}{r_{ij}}\right)^m \right]$			
Parameters	n	m	E_0 (kcal mol^{-1})	r_0 (Å)
Values	8	6	0.01263	6.3509

Figure 5.4.3.8: Table showing coarse grained EO2 angle and distance parameters

An assembled coarse grained poly(ethylene oxide) molecule, complete with atomistic head group is shown in figure 5.4.3.9. This illustrated molecule is the final configuration of a short (50 ps) molecular dynamics simulation. These individual molecules will be referred to from now on as 'FnEOx' where n is the number of C_8F_{17} units in the atomistic head group and x is the number of EO2 coarse grained particles in the chain.

The conformation of an energy minimized F2EO100 or F3EO100 molecule is much more linear than the one illustrated in figure 5.4.3.9 and it is this initial conformation that is studied first.
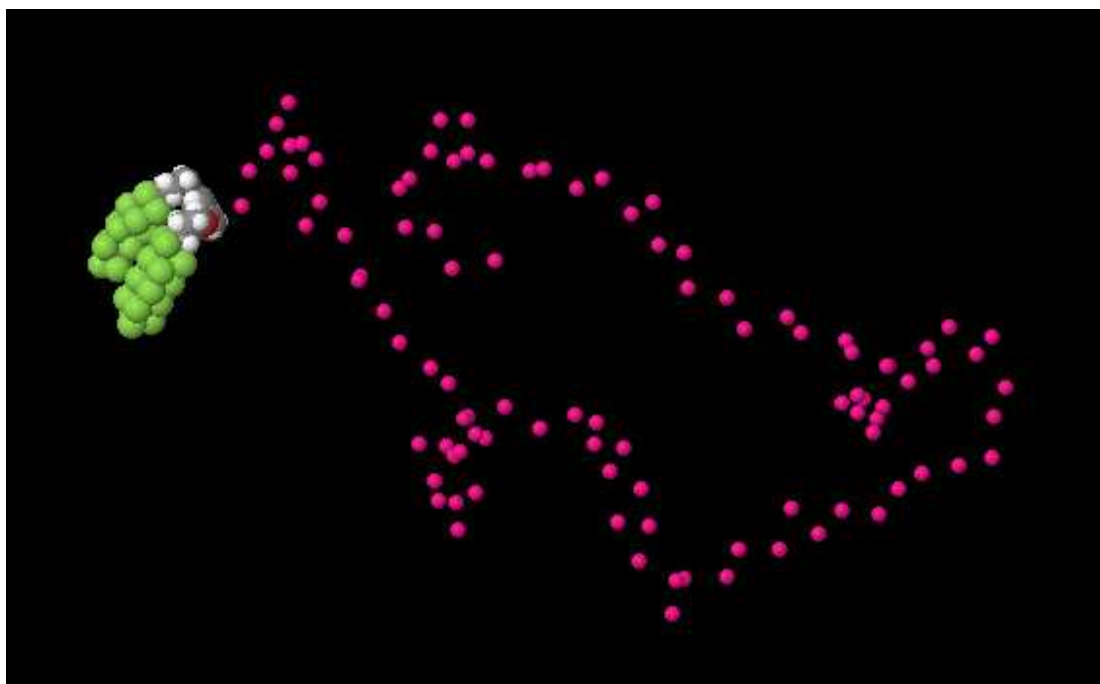
Figure 5.4.3.9: Coarse grained PEO system with atomistic headgroup (F2EO100).
Each pink group represents an EO2 unit, which for clarity is not shown to scale.

5.4.4 Simulations of Coarse Grained Systems

The single F3EO100 molecule was contained with a box size of 40 by 40 by 250 Å with the longest length being in the *z*-direction. This box was then replicated using the same methods as employed in section 5.4.1 when simulating the atomistic head groups alone. The single molecule was replicated 6 times in both the *x* and *y* directions to give a 2 dimensional lattice of 36 molecules contained in a simulation box size of 240 by 240 by 250 Å. This initial configuration is very crystalline-like in appearance with all of the EO2 chains lined up perfectly with one another due to the inherent tessellation of the method used to produce this system.
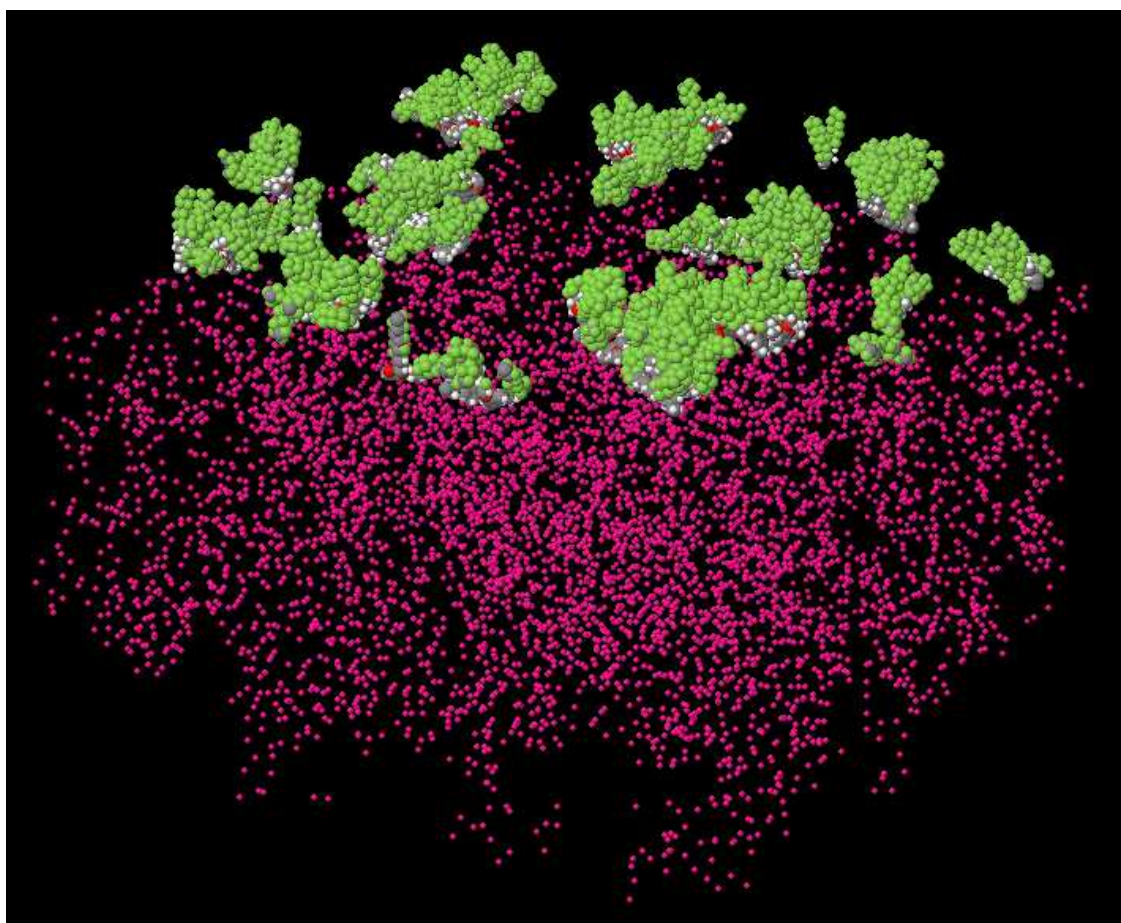
Figure 5.4.4.1: Coarse grained PEO system with atomistic head groups after a short relaxation time from the crystalline starting geometry. 36 molecules are shown.

In order to disrupt this crystalline structure a short (250 ps, with 1 fs time step) molecular dynamics simulation was carried out and the coordinates and velocities of each particle in the system were dumped into a *HISTORY* file every 7500 time steps (or 7.5 ps of simulation time)

The initial crystalline structure was soon broken up by thermal motion of the molecules and even after such a short amount of simulation time we can see that the head groups are beginning to form clusters at the air/water 2 dimensional interface (illustrated in figure 5.4.4.1). Observation of a video of the simulation through time (compiled using

a program developed in house by extraction of positional information contained in the *HISTORY* file) shows that the initial stretched out conformation of the EO2 chains rapidly changes to a more folded conformation. This is difficult to observe as an effect on each individual chain but the overall depth into the *z*-direction reached by the ends of the EO2 chains can be seen to contract even after such a short simulation period. This effect can also be seen in the illustration by the curled up ends of the chains.

After this initial short molecular dynamics simulation the final configuration (illustrated in figure 5.4.4.1) is then used as the initial conformation for a much long molecular dynamics simulation of 2 ns (2000 ps) with the same time step of 1 fs. Again the coordinates are dumped into the *HISTORY* file after every 7.5 ps of simulation time and a movie can be compiled to allow viewing of the simulation through time.

Observing the movie reveals that the head groups continue to attract one another at the surface and after a simulation time of around 1 ns (1000 ps) there are clusters of around 6 to 8 head group molecules formed. These clusters remain intact throughout the rest of the simulation and seem to slide across the surface under thermal motion as one collective and these can be seen in the final configuration of the system, which is illustrated in figure 5.4.4.2. For the simulations of the head groups alone (described in section 5.4.1) the equivalent surface packing density of these head groups leads to a situation where the cluster size is much larger (around 10-12 molecules per cluster) for a system of equivalent size (or where all of the molecules are packed together in one large cluster for smaller systems). The smaller cluster size for the system containing EO2 coarse grained chains is due to steric hindrances of these chains preventing a larger number of head group molecules being able to pack together. This observation is exactly the kind of effect that is expected and is essential in allowing the system to form a polymer brush conformation.
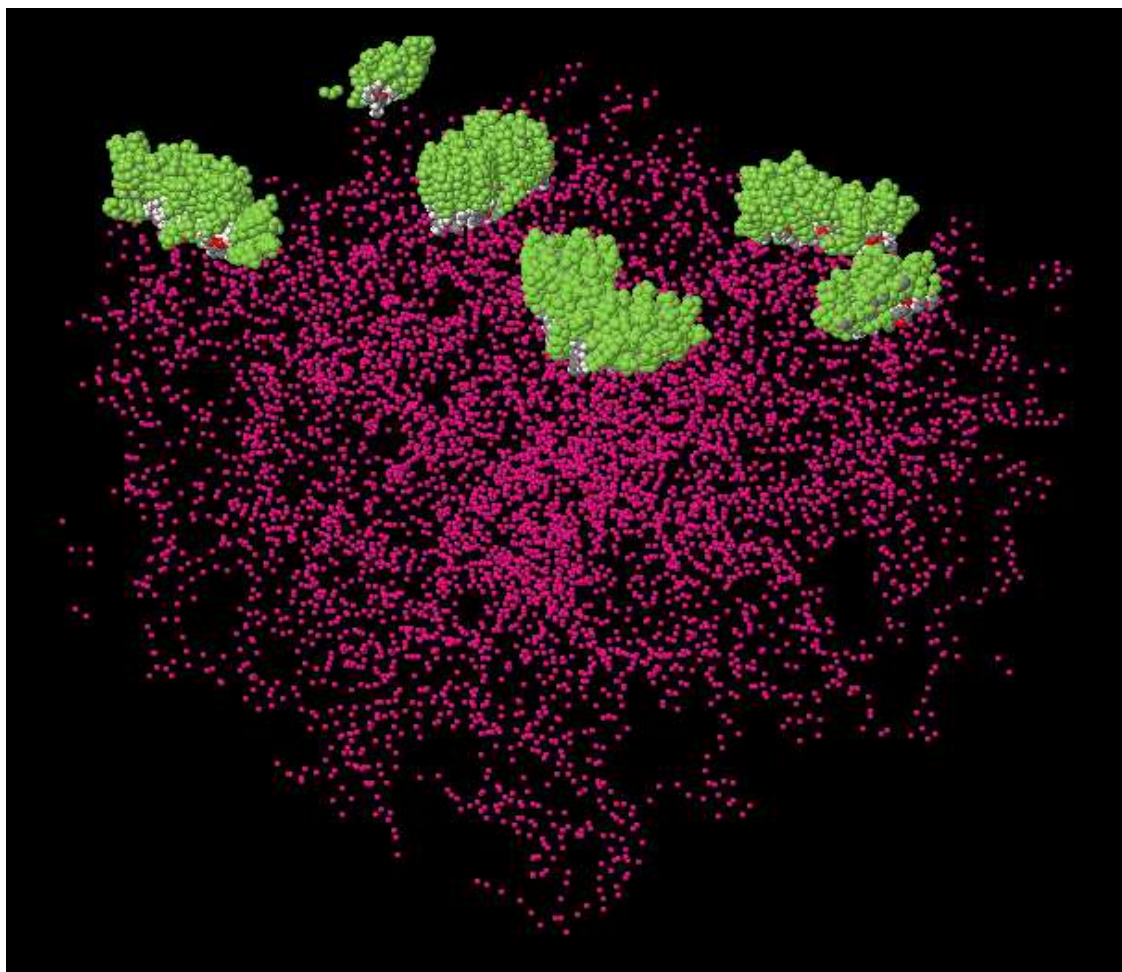
Figure 5.4.4.2: Coarse grained PEO system with atomistic headgroup after 2 ns of molecular dynamics simulation.

Observation of the movie also shows a further initial contraction of the EO2 chains followed by a slight stretching out of the chains as the head groups become closer together. Once the clusters have formed the EO2 chains appear to begin relaxing and contract slightly over time. After around 1.5 ns (1500 ps) the system appears to have reached equilibrium as the chains and head groups move around due to thermal motion without any further major conformational changes.

The next system to be studied was constructed using the single F3EO100 molecule that had undergone a very short molecular dynamics simulation as described in section 5.4.3. In this case the single F3EO100 molecule was much less linear than in the previous

system and was contained within a box size of 200 by 200 by 250 Å with the longest length being in the *z*-direction. Again this simulation box was then replicated 6 times in both the *x* and *y* directions to give a 2 dimensional lattice of 36 molecules contained in a simulation box size of 1200 by 1200 by 250 Å. Although this initial configuration is constructed in the same way as with the previous system there is enough space between the molecules to allow them to behave independently of one another for the initial part of the simulation.

The same simulation methods were employed for this system as with the previous one. A short simulation of 250 ps was carried out initially and a movie was generated from the *HISTORY* file and observed. During initial 250 ps simulation the molecules undergo random thermal motion and as the head groups come into contact with one another then formation of small clusters of 2 or 3 molecules is observed. The EO2 chains are able to move freely during this phase and keep much of their initial conformation.

As with the previous simulation the final configuration of molecules from this short run is then used as the initial conformation for a much long molecular dynamics simulation of 2 ns (2000 ps) and again the coordinates are dumped into the *HISTORY* file after every 7.5 ps of simulation time and a movie compiled to allow viewing of the simulation through time.

As the simulation progresses the head groups have an increasing chance of coming into contact with one another. This is observed clearly in the simulation movie and as with the previous study the head groups appear to have formed stable clusters after a simulation time of around 1 ns and these clusters remain intact for the rest of the simulation. In this case however the clusters contain between 3 and 6 molecules, some of the larger clusters can be seen to form as a result of a cluster of 2 or 3 coming into contact with a cluster of a similar size. As with the previous study it is possible to compare the size of these clusters to that of the atomistic head groups alone under a much lower surface packing density due to the steric hindrance of the EO2 chains.

Further observation of the movie shows that as the head groups begin to form clusters the EO2 chains start to stretch out as there is not enough room to maintain their curled up structure when they are in close contact with one another. Once the head groups have formed stable clusters the EO2 chains begin to slow down their stretching and

appear to reach equilibrium at a simulation time of around 1.2 ns and the whole system is then subject to random thermal motions and very little conformational change is observed after this time.

5.4.5 Radius of Gyration Calculations of Coarse Grained Systems

In order to quantify the observations made while viewing the movies of these simulations as they proceed through time it is necessary to calculate the radius of gyration for the EO2 chains. The technique for carrying out these calculations is described previously in section 5.2.3.1. A program developed in-house is used to extract the coordinates of each EO2 particle belonging to a specific EO2 chain from the *HISTORY* file at any given time step. Each EO2 particle is assigned a mass of 88.1063 g mol^{-1} (the molar mass of -CH_2-O-CH_2-CH_2-O-CH_2-) and the radius of gyration for the specific chain can then be calculated using the formula shown in section 1.2. The radius of gyration is calculated for every chain in the system to give an average radius of gyration for all chains at any given time step in the *HISTORY* file. This process is carried out for each time step in the *HISTORY* file and this allows us to produce a graph that shows the change in average radius of gyration for the EO2 chains as the simulation proceeds through time and this graph is shown in figure 5.4.5.1.

The initial stretched conformation of the crystalline configuration is quantified by a large starting value for the radius of gyration (around 83 Å). As was previously observed in the movie of this simulation the chains immediately begin to collapse and fold in on themselves and this is seen in the radius of gyration results as the value falls to around 65 Å after 400 ps of simulation time. Observation of the movie revealed that after this early collapse of the chains to a more folded structure they begin to stretch again as the head groups move closer together and this effect can be seen in the radius of gyration as the value increases steadily to a value of around 74-75 Å. At this stage the head groups have formed stable clusters and the EO2 chains begin to relax into a less sterically hindered conformation and reach a steady value of around 68-70 Å for the radius of gyration by a simulation time of 1.5 ns (1500ps) illustrated by the plateau region of the blue line in figure 5.4.5.1.
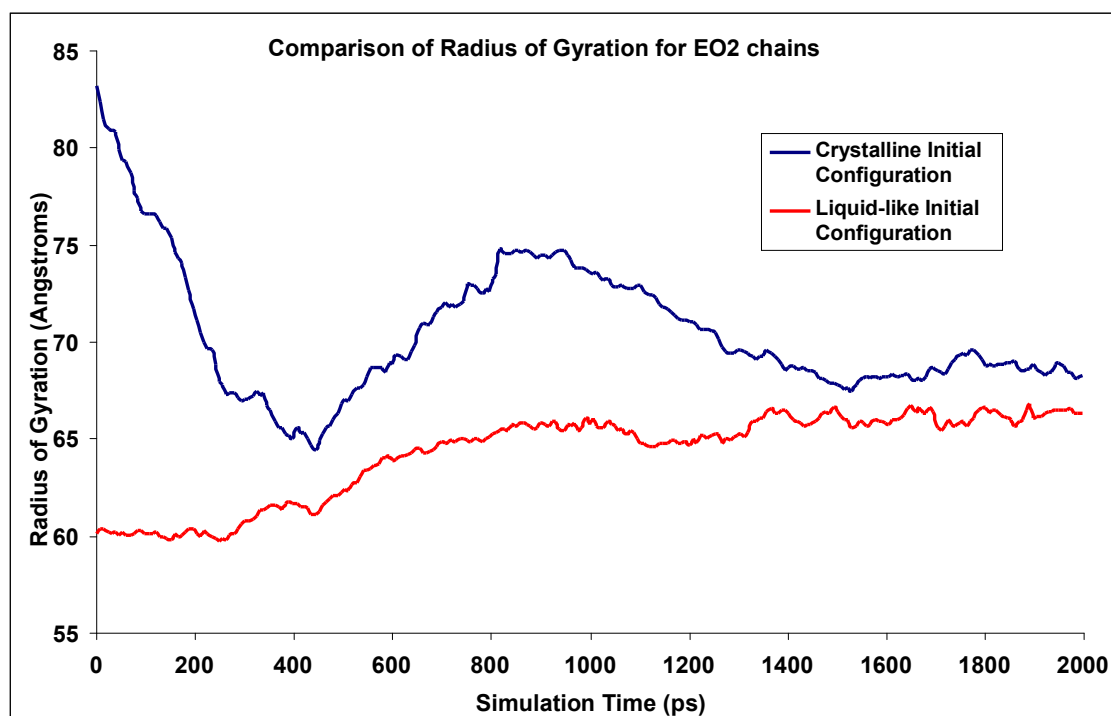
Figure 5.4.5.1: Comparison of radius of gyration measurements through time for different initial starting configurations of F3EO2 molecules.

In contrast to the crystalline system the initial configuration of the liquid-like system has a more folded or curled up conformation of the EO2 chains and this is quantified by the much lower starting value for the radius of gyration (in this case around 60-61 Å). This value for the radius of gyration alters very little over the first 250 ps and this is supportive of the observations made during the movie of the original short molecular dynamics simulation of this system where the chains are isolated from one another until thermal motion brings them into contact with one another. As the head groups begin to come into contact with one another the EO2 chains become sterically hindered by one another and this forces them to stretch out. This effect was observed in the movie of the simulation and can also be seen by the steady increase in the radius of gyration between 300 ps and 900 ps of simulation time to a value of around 65 Å. At this stage the head groups are in the final stages of forming stable clusters and the EO2 chains

appear to be undergoing very little further conformational change and this is illustrated by the plateau region of the red line in figure 5.4.5.1.

Results given in chapter four show us that the calculated radii of gyration for PEO chains of this molecular weight (around 8800 g mol^{-1}) is in the region of 37-43 Å and this value is considerably lower than the observed radii of gyration seen in the neutron reflectometry results for real systems of tethered PEO polymers at high concentration. These experiments showed that the PEO molecules of this molecular weight extended into the solvent to a depth in the region of 50-70 Å for many of the higher concentration samples and this matches up very well with the values shown here for the radius of gyration of molecules that are fixed to the interface.

5.4.6 Calculation of Density Profiles of Coarse Grained Systems

In order to directly compare the results of these computer simulations to the results obtained through neutron reflectivity it is necessary to calculate a profile of EO2 chain density versus sample depth. This is again achieved using a program developed in house that reads positional information contained within the *HISTORY* file. The program creates sections through the simulation box along the *z*-direction (the thickness of these sections is user defined) and each of the EO2 particles is binned to one of these sections depending solely on the *z*-coordinate of that particular particle. The program repeats this process for each time step contained with the *HISTORY* file and the results are averaged out. Therefore we now have information showing the average number of EO2 particles contained within a section through the *z*-dimension of the system and this information is output to a results file. The program then assigns an atomic mass of 88.1063 g mol^{-1} to each of the EO2 particles to give the average amount of mass contained within a section through the *z*-dimension of the system and this information is also output to a results file. The final part of the program requires the user to input the sizes of the *x* and *y* dimensions for the system. Using this information (and the average masses previously obtained and the user defined thickness of the sections in the *z*-direction) the program calculates the density contained within each section of the *z*-direction and this final column of information is output to the results file.

The two coarse grained systems studied in sections 5.4.4 and 5.4.5 were designed to represent the limits of the highest and lowest densities that would be necessary to simulate a system that is analogous to those studied during the experimental section of this project. The simulation of both these extremes shows us that the systems can take up to around 1500 ps (1.5 ns) before equilibrium is reached. As a result of these observations it is clearly necessary to allow the system to reach a simulation time of at least 1.5 ns before any of these density calculations are carried out as any information extracted previous to this time will contain inaccuracies from the early conformations where the system is not at equilibrium.

Density profiles calculated from the final 500 ps of the simulations of the two systems described above are shown in figure 5.4.6.1 along with a typical density profile generated from one of the neutron reflectivity experiments.
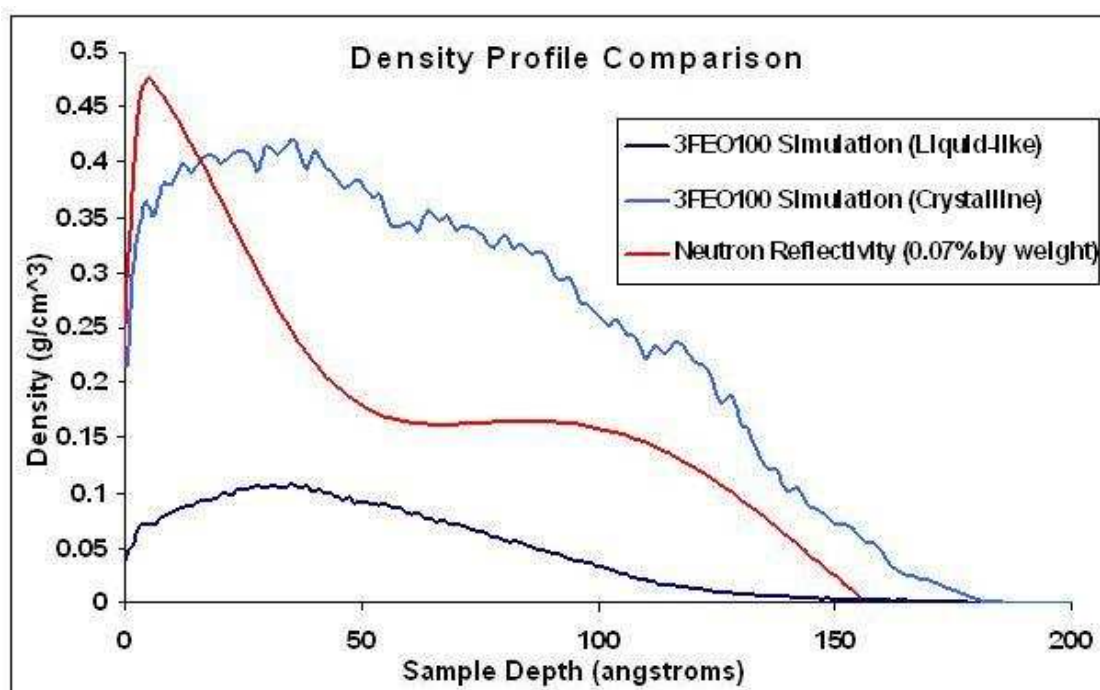
Figure 5.4.6.1: Comparison of density profiles for two extreme simulation systems and a typical experimental system.

As can be seen in figure 5.4.6.1 the 'crystalline' simulation system has a much higher overall density than that of the experimental system and the 'liquid-like' system has a much lower overall density than both of these systems. However there is one striking similarity even between these extreme simulation systems and that of the experimental system. The depth into the sample that the EO2 chains (in the simulation) and the real poly(ethylene oxide) chains (in the experiment) is comparable, in each case the chains reach a similar depth of around 125 Å before the profile tails off. In the highly packed simulation system there are some chains that reach a depth in excess of 150 Å, which is further than any chains seen in neutron reflectivity. This is probably due to unrealistic packing densities of the simulation system forcing the EO2 chain to adopt an elongated conformation of extremely high energy, or possibly due to background noise (inherent in all neutron reflectivity experiments) drowning out the signals from this very small number of chains.

A new simulation was set up in an attempt to duplicate the density profile seen in experimental results and the initial configuration of this system was that of the previously simulated liquid-like system. For this simulation the volume of the system is not fixed and is subjected to a constant pressure of 1000 bar for a simulation time of 500 ps with a time step of 1 fs. This high pressure causes the system to collapse from a box size of 1200 by 1200 by 250 Å down to a size of around 170 by 170 by 250 Å (the size of the *z*-dimension is fixed in the *CONFIG* file). Once this initial compression is complete the system is returned to a pressure of 1 bar allowing the molecules to expand and relax into a more realistic conformation. This method should allow the system to equilibrate to a realistic configuration and therefore also a realistic density. The dimensions of the system were monitored by simply running very short simulations of 100 ps and then looking at the final configuration file (named *REVCON*) and this final configuration is then used as the initial configuration for the next 100 ps simulation. The simulation box size reached a value of around 328 by 328 by 250 Å after seven of these 100 ps simulations and remained very close to this value (between 325 and 330 Å) for the following three simulations. Therefore the box size was fixed at 327.5 by 327.5 by 250 Å and a simulation of this fixed system was carried out for 1 ns (1000ps) with the same time step of 1 fs and the coordinates dumped into the *HISTORY* file every 7.5 ps.

A density profile was constructed using the information contained in the *HISTORY* file (using the program described previously) from this 1 ns simulation and this is shown in figure 5.4.6.2 along with the same experimental density profile as previously shown to give a comparison between this new simulation system and a typical experiment. The method employed to construct this simulation system (by compression of the system into a highly compact and dense configuration and then allowing this to relax) results in a system that retains a relatively high density of material. For this reason the simulated system is compared to the experimental result from the highest concentration of the $3C_8F_{17}10k51$ material that was carried out, which was at 0.07% by weight diluted in null reflecting water.

Observation of figure 5.4.6.2 reveals that the overall densities of each system are very similar and this can simply be observed by looking at the area underneath each curve on the graph and it can therefore be concluded that the density for the simulated system is correct (or at least very close to that of the observed experimental conditions).

Further observation however shows that the profile calculated from neutron experiments shows a much more densely populated surface than that of the simulated system with the EO2 chains of the simulation reaching further into the substrate. A small contributing factor to the surface excess of material in the experimental density profile is the inclusion of the effects of the head group molecules (for the simulation profile only the EO2 particles are considered). However the relatively low scattering length density and size of the head groups mean that this contribution should be almost negligible. The differences in the profiles shown in figure 5.4.6.2 can only be attributed to differences in the conformations of the molecules of the simulated system to that of the experimental equivalent and there are several reasons why this could be the case.
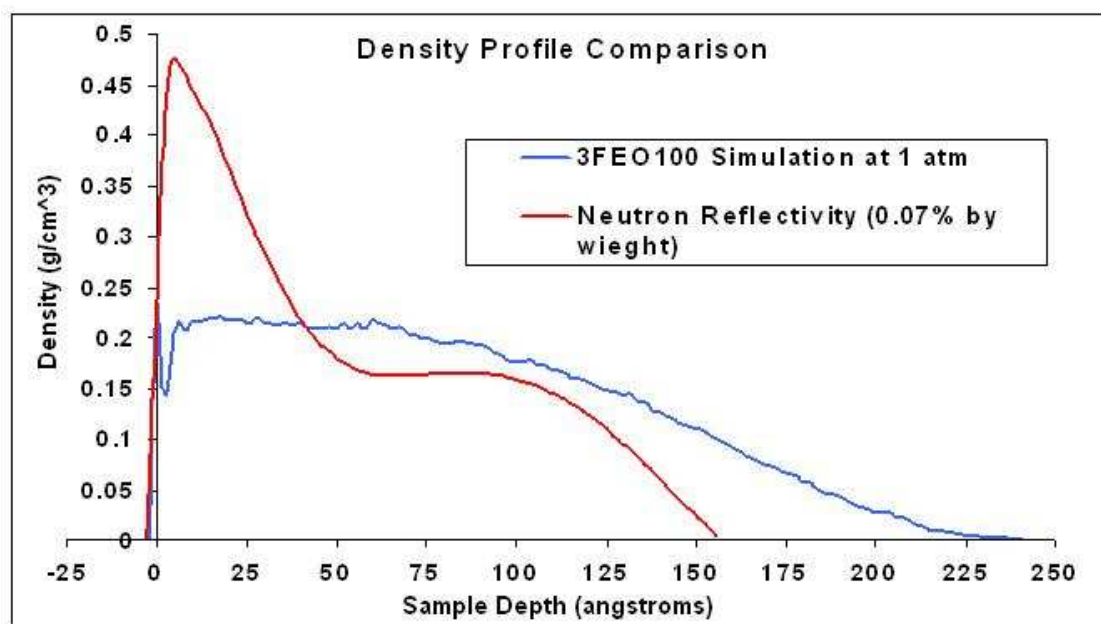
Figure 5.4.6.2: Comparison of density profiles for simulation system at atmospheric pressure and a typical experimental system.

As previously discussed the model system used in this simulation has a relatively high density of material and corresponds to a concentration that is above the critical micelle concentration. At these high surface densities the real polymeric surfactant ($3C_8F_{17}10k51$) molecules overcome the problem of overcrowding by forming micelles or additional layers below the surface to minimize the interactions of the hydrophobic head groups with water. However, the F3EO100 molecules in the simulation are tethered to the interface by a strongly repulsive 2-dimensional wall and therefore can not aggregate away from the surface to form micelles or additional layers of material. As a result, although the F3EO100 molecules have been allowed to relax into a conformation that is not excessively overcrowded, the EO2 chains are forced to adopt a stretched out conformation as they cannot move away from the surface.

The simulated models for these systems contain identical molecules of the same polymer length and chemical formula with 100% head group functionality of the PEO chains. The experimental materials however contain around 54% PEO with a head group functionalization and the rest are simple PEO molecules. These unfunctionalized PEO

molecules are linear rope-like molecules with much less steric hindrance than those functionalized with the dendritic head groups. As PEO chains have a slight affinity to adsorb to an air-water interface it is feasible that these PEO molecules could fit in and around the spaces created between the bulky head groups and chains of the functionalized molecules which are located at the surface. This would cause an increase in the density of material near the surface in the experimental system and could explain the differences in the surface density between experimental and simulation results as these molecules are not present in the simulations. Further evidence for the presence of these unfunctionalized PEO molecules present in the experimental system comes from the lack of a surface depletion layer. The head groups have a much lower scattering length density (SLD) than that of PEO and as a result you would expect to see a depletion layer at the surface corresponding to the position of the head groups. However it can be seen in figure 5.4.6.2 that this surface depletion layer is not present and this could be due to the presence of these unfunctionalized PEO chains.

The slight affinity of PEO to adsorb to an air-water interface also directly relates to another discrepancy between the experimental and simulated systems. The simulated systems include a 2-dimensional repulsive wall which tethers the head groups in place simply by repelling the head groups in the positive z-direction and the PEO chains in the negative z-direction. However, as previously stated, there is a slight affinity for PEO to adsorb towards an air-water interface and this can be seen experimentally in chapter 4 by the slight lowering of water surface tension when unfunctionalized PEO is added. This affinity for PEO to adsorb to the surface would explain the larger surface density from experimental results, where any PEO not forced into the bulk (by chain stacking or other steric hindrances) may lie at the surface and adopt a mushroom-like conformation. The simulated system does not allow for the formation of such phases as the EO2 chains are pushed away from the surface by the repulsive 2-dimensional wall leading to a more stretched conformation. Recently attempts[43] have been made to overcome this issue by employing a square energy well at the interface that would be occupied preferentially by the PEO chain segments (driven by an energy gain) and then once this well had been filled the rest of the PEO chain would extend into the substrate. The results obtained using this square well potential all display a surface excess of PEO as expected, however

this excess is overly defined due to the square nature of the energy well. This is due to the fact that once a PEO segment is entrapped within the energy well the steep walls of the well require a relatively large amount of thermal energy to allow the PEO segment to escape. A potentially more effective method of modelling the surface excess of PEO would be to replace the square energy well with a much softer one. This type of well would allow the PEO segments to move into and out of the energy well with a relatively low amount of thermal energy while maintaining an excess of PEO segments at the interface.

Another inaccuracy arising from the methods used to develop the density profiles from simulation is the fact that only the PEO chains were included in the density calculations. The contributions of the head groups to the neutron reflectivity patterns recorded experimentally are relatively small compared to that of the PEO chain. However, these are still included in the experimental neutron reflectivity pattern and not in the calculations from simulation. Despite the relatively small contribution of the head groups to the reflectivity pattern this is still another affect that (compounded with other possible affects) can result in an erroneous calculated density profile for the computer simulated systems.

Finally there is also the possibly that the differences could simply be due to an error in the calculation and implementation of the simulation parameters or in the fitting methods employed during neutron reflectivity calculations, which are never 100% certain to be accurate. Experimental results for lower concentrations of the trifluorinated material have progressively lower densities than that of the simulated system and show a surface excess similar to that of the one shown in the red line of figure 5.4.6.2.

5.4.7 Calculation of Neutron Reflectivity Profile from Simulations

Using the density profiles from computer simulations of 3FEO100 coarse grained molecules calculated in the previous section (5.4.6) it is possible to reverse engineer the

corresponding neutron reflectivity profiles in order to directly compare these with the profiles obtained directly from a neutron reflectivity experiment.

In order to produce a neutron reflectivity profile using a density profile it is first necessary to convert the values for the density of EO2 chains into a scattering length density, or SLD, value. This can be by simply multiplying the density of EO2 chains at any given depth by SLD value of deuterated poly(ethylene oxide) ($5.741*10^{-6}$ $Å^{-2}$) as this is the material used in the neutron reflectivity experiments. It is then necessary to resize the bins for the sample depth (z-direction value in the case of simulation) as the program used to calculate the reflectivity profile requires a much larger bin size that than used to generate the density profiles shown in section 5.4.6. Therefore a program was written to read in the information from the previously calculated density profiles and carry out this process of conversion from density to SLD, resizing the bins for the depth values, adding necessary values for parameters such as number and thickness of depths bins and overall sample depth etc and then reordering the information into a format that can be read directly by the neutron reflectivity fitting program. In this case the *Parrat* program (Christian Braun, HMI Berlin 1997-98) is used as there is a function contained within this program that allows a density profile of scattering length density vs depth to be converted directly to the corresponding neutron reflectivity profile.

The reflectivity profile generated from the simulation density profile of F3EO100 molecules at 1 atm (shown in figure 5.4.6.2) is compared to the neutron reflectivity profiles of the equivalent experimental molecule at various concentrations and this can be seen in figure 5.4.7.1. It can be seen that the calculated reflectivity profile from the simulated system displays a similar form to that of the experimental sample of 0.066% by weight however there are no experimental profiles that match up very closely with the calculated simulation profile. This evidence can almost certainly rule out the error in the fitting methods employed during neutron reflectivity calculations of experimental data as being the main cause of the differences in the density profile shown in figure 5.4.6.2 and therefore it must be concluded that, despite the ability of the simulation methods to correctly and accurately reproduce the density and basic structure of the experimental system, the parameters used to simulate these systems are flawed in their ability to accurately model the structural architecture of these molecules at an air-water interface.

The main issue appears to be an excess of repulsion between the molecules at high densities preventing the amount of surface density displayed in the experimental systems from being reached during simulation. Unfortunately there was not enough time available to trial and implement any other methods of simulations to try and find a way around this problem.
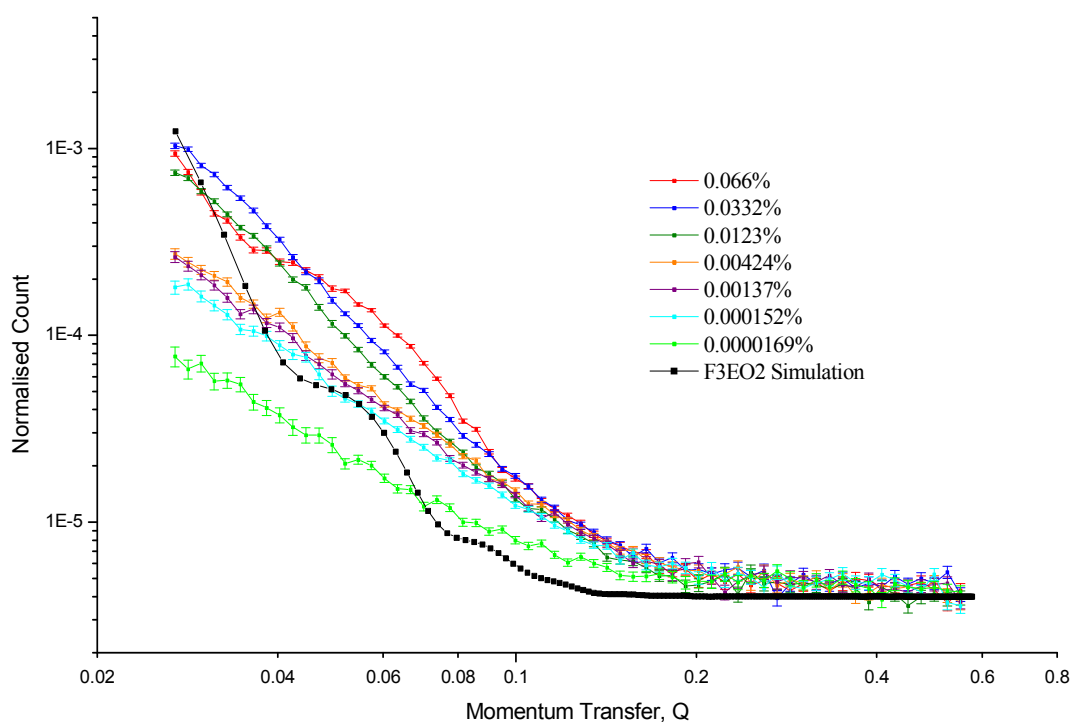
Figure 5.4.7.1: Comparison of experimental neutron reflectivity profiles and reflectivity profile calculated from computer simulations (experimental profiles are labeled by weight percentage)

5.5 Discussion, Conclusions and Further Work

In this chapter molecular simulations have been carried out on many different systems including atomistic, coarse grained and a combination of both types constructed in such a way that they were able to be built up into a system that mirrors the

experimental molecules and conditions as closely as possible. For each of these simulations the position and velocity of each atom in the system was recorded as a function of simulation time and this information was transferred to a large external storage hard drive and then used to analyze the motion, distribution and molecular architecture of the systems while allowing the on board hard drive to collect information from ongoing computer simulations. Given this unique perspective it was possible to look at microscopic details of the simulated systems and draw some conclusions and comparisons to the experimental systems also analyzed during this project (see previous chapter 4).

The first simulations were carried out on bulk atomistic water systems and the decision about which atomistic water model to be employed was based on the work of a previous PhD student at Durham University (Dr Philip Anderson[8]). Bulk systems of these atomistic water molecules were then simulated in order to provide an equilibrated solvent box into which the atomistic polymer molecules could be inserted. Short simulations were then carried out on isolated short poly(ethylene oxide) chains in order to relax the initial linear conformation into a random walk and then these were inserted into the water solvent using a program developed in-house. Results were obtained for the radius of gyration of these molecules during a molecular dynamics simulation in the water solvent. As expected the radius of gyration increased for these types of atomistic molecules as you increase the molecular weight (or chain length) and also when bulky head groups are attached to the terminal ends of the molecules. Observing movies of these simulations as they proceed through time showed the coiling and uncoiling of these short chains as well as diffusion due to thermal motion. Radial distribution functions of a bulk polymer system were also calculated as further evidence that these atomistic models are behaving exactly as would be expected and therefore I was confident in the accuracy of the simulation parameters. Information extracted from these atomistic simulations was then used to generate distributions of O-O bond lengths and O-O-O bond angles, which were then used to generate coarse grained systems.

The first coarse grained system to be constructed was that of coarse grained water, this reduced the number of particle sites necessary to simulate a water system by a factor of 4 allowing larger systems to be simulated over longer times. A-B bond length and A-

B-C bond angle distributions from atomistic simulations were then used to calculate parameters for use in coarse grained PEO systems. After trials of two different coarse grained systems for PEO it was decided to use a coarse graining method that reduced the number of particle sites by a factor of 14 and this allowed the simulation of much larger PEO molecules up to and including a molecular weight of 8,800 g mol^{-1} which is representative of those used in the experimental section of this project. Addition of coarse grained PEO molecules to a coarse grained water solvent box allowed the simulation of a much larger system than could be achieved using atomistic molecules. Comparison of the atomistic and coarse grained distributions of O-O bond lengths and O-O-O bond angles shows that there is very good agreement between the two systems and therefore the parameters governing both of the systems are correct and accurate.

Having achieved success with both the atomistic and coarse graining techniques it was then possible to construct a simulation model that employs both of these techniques to simulate a molecule that is as closely matched to the real experimental system as possible. To this end, atomistic head group molecules were constructed, tested and then incorporated onto the terminal end of the coarse grained PEO molecules and then a 2-dimensional repulsive wall was applied to the system to represent the air-water interface that is present in the neutron reflectivity experiments carried out in chapter 4. In order to save valuable computer simulation time the coarse grained water molecules are not included in this system and the effects imposed by the water molecules are incorporated into the parameters used to govern the behaviour of the coarse grained PEO molecules.

Atomistic modeling of the fluorinated head groups displayed an attraction to one another resulting in a coagulation of the molecules to form large clusters at the 2-dimensional interface. When the 100 EO2 particle coarse grained chains are attached to these atomistic head groups the head groups continue to attract one another and aggregate together but the size of these clusters is much smaller due to the steric hindrance from the presence of the large EO2 chains.

Trial simulations were carried out at high and low densities to test the robustness of this coarse grained/atomistic hybrid system and analysis of the results showed realistic values for radius of gyration and density profiles. The same system was then allowed to equilibrate at a constant pressure of 1 atm to allow direct comparison of the simulated

system to that generated from experimental results. This simulated system gave very good agreement for the overall density of the system when compared with experimental results. However there is clearly a discrepancy between the structural architectures of the two systems as the surface is more densely packed in the experimental system compared to the more stretched out conformation adopted by the simulated molecules. Comparison of the neutron reflectivity profile calculated from simulation results with those of the experimental neutron reflectivity results confirms the differences in the conformation of the molecules. There are many possible explanations for this discrepancy in the simulated structure of this system, most of which can be attributed in general to the assumptions made in the construction of such a computational model. These include the presence of an over-simplified 2-dimensional wall to represent the air-water interface, the monodispersion of PEO chains with 100% functionality (which is not present in the experimental system), the lack of a surface depletion layer and the lack of inclusion of the head groups during density profile calculations. All of these inaccuracies and assumptions have been explained and discussed in detail in the previous section and throughout the course of this chapter. However, the differences between the experimental and simulation results may be best overcome by the inclusion of a potential that can model the adsorption of PEO to an air-water interface. The effects of the assumptions mentioned previously may be insignificant when compared to the effect of the lack of this kind of potential. In order to achieve greater success when modeling PEO by computer simulation it is necessary to develop a method and a potential capable of representing this surface adsorption.

Further to previous discussions there are some issues that arise directly from coarse graining that can cause discrepancies like the ones arising in these simulations. In this specific case it is likely that the removal of atomistic water molecules from the simulation has a direct influence on the structural behaviour of the PEO molecules, as in a real experimental or atomistic simulation system the PEO molecules can form hydrogen bonding between one another via the water molecules. In a coarse grained system (and indeed when the water molecules are removed altogether) this is no longer possible and this will lead to alterations in the molecular architecture. Many of effects imposed by water are included in the coarse graining parameters for the EO2 particles and we can be

confident (for coarse grained systems similar to the atomistic system from which these parameters are extracted) that the model is efficient. However, if the conditions of the coarse grained system are altered dramatically (large changes in density for example) then this may lead to an erroneous coarse grained model where the effects of water are ill-defined. A discrepancy of this kind may account for the lack of density shown at the air-water interface in the simulated systems.

Despite the problems faced during these computer simulations of our molecular systems the simulations carried out in this section show some very promising signs for producing a computer generated molecular system that can model the behaviour of 'real' experimental molecules including the prediction of properties such as density and radius of gyration. However, there are many more trials and much more work to be done before we can confidently say that a computer simulation can accurately and reliably predict the structural behaviour of a system of this complexity.

There are several techniques that could possibly be implemented to allow these simulations to successfully predict the structure and conformation of the experimental molecules. One such technique, which I have not had chance to apply and trial due to lack of time, involves the inclusion of a second energy well in the Lennard-Jones potential of the coarse grained PEO (EO2) particles that would represent the hydrogen bonding of a water molecule sitting between two such particles. The well would allow a small energy gain for the system if the molecules were at this specific distance from one another and this may lead to a more 'realistic' structure of the simulated molecules.

In the near future there may be computers available that can carry out atomistic simulations of very large systems and this would provide a very useful tool to be able to carry out these kinds of simulation without the necessity of incorporating many of the assumptions employed in these simulations and the atomistic water molecules will allow the system to form hydrogen bonding between the PEO molecules and a much more realistic system can be modeled.

5.6 References

[1] O. Borodin, R. Douglas, G. D. Smith, F. Trouw and S. Petrucci, *J. Phys. Chem. B.* **2003**, *107*, 6813-6823.

[2] O. Borodin and G. D. Smith, *J. Phys. Chem. B.* **2003**, *107*, 6801-6812.

[3] O. Borodin, G. D. Smith and R. Douglas, *J. Phys. Chem. B.* **2003**, *107*, 6824-6837.

[4] T. Koga, H. Jinnai and T. Hashimoto, *Physica A.* **1999**, *263*, 369-377.

[5] H. Donnerberg, *Atomistic Simulation of Electro- and Magnetooptic Oxide Materials (Springer Tracts in Modern Physics)*, Springer-Verlag Berlin and Heidelberg GmbH & Co. K, **1998**, 1-5.

[6] M. J. Field, *A Practical Introduction to the Simulation of Molecular Systems*, Cambridge University Press, **2007**.

[7] P. Klaver, *Atomistic Simulation of Cu/ta Thin Film Deposition & Other Phenomena*, Delft University Press, **2004**.

[8] P. M. Anderson and M. R. Wilson, *J. Chem. Phys* **2004**, *121*, 8503-8510.

[9] W. L. Jorgensen, D. S. Maxwell and J. Tirado-Rives, *J. Am. Chem. Soc* **1996**, *118*, 11225-11236.

[10] B. J. Alder and T. E. Wainwright, *J. Chem. Phys* **1959**, *31*, 459-466.

[11] T. Schlick, *Mathematical Applications to Biomolecular Structure and Dynamics, IMA Volumes in Mathematics and Its Applications*, New York, **1996**.

[12] L. Verlet, *Phys. Rev.* **1967**, *98*, 165-201.

[13] R. P. Feynman, R. B. Leighton and M. Sands, *The Feynman Lectures on Physics, Vol. 1*, Addison-Wesley, **1963**, 1-24.

[14] T. E. Cheatham, J. H. Miller, T. Fox, P. A. Darden and P. A. Kollman, *J. Am. Chem. Soc* **1995**, *117*, 4193-4194.

[15] O. N. d. Souza and R. L. Ornstein, *Biophys J* **1997**, *72*, 2395-2397.

[16] J. J. Erpenbeck and W. W. Wood, *Statistical Mechanics, Part B: Time-dependent Processes, Modern Theoretical Chemistry*, Plenum, New York, **1977**.

[17] W. L. Jorgensen, *J. Am. Chem. Soc* **1981**, *103*, 335-340.

[18] W. L. Jorgensen, J. Chandrasekhar, J. Madura, R. W. Impey and M. L. Klein, *J. Chem. Phys* **1983**, *79*, 926-935.

[19] W. L. Jorgensen, D. S. Maxwell and J. Tirado-Rives, *J. Am. Chem. Soc.* **1996**, *118*, 11225-11236.

[20] D. Bedrov and G. D. Smith, *J. Chem. Phys.* **1998**, *109*, 8118-8123.

[21] J.-P. Ryckaert, G. Ciccotti and J. H, C Berendsen, *Journal of Computational Physics* **1977**, *23*, 327-341.

[22] V. Ortiz, S. O. Nielsen, M. L. Klein and D. E. Discher, *J. Poly. Sci. Part B: Polymer Physics* **2006**, *44*, 1907-1918.

[23] G. Srinivas, M. L. Klein, J. C. Shelly, S. O. Nielsen and D. E. Dishcer, *J. Phys. Chem.* **2004**, *108*, 8153-8160.

[24] J. Klein, *Journal of Physics: Condensed Matter* **2000**, *12*, A19-A27.

[25] M. L. Klein, P. B. Moore, S. Bandyopadhyay, R. C. Reeder, M. Y. Shelly and J. C. Shelly, *J. Phys. Chem. B.* **2001**, *105*, 9785-9792.

[26] A. H. de Vries, S. J. Marrink and A. E. Mark, *J. Am. Chem. Soc.* **2004**, *126*, 4488-4489.

[27] S. J. Marrink, E. Lindahl, O. Edholm and A. Mark, *J. Am. Chem. Soc.* **2001**, *123*, 8638-8639.

[28] S. J. Marrink and A. E. Mark, *J. Am. Chem. Soc.* **2003**, *125*, 15233-15242.

[29] S. J. Marrink and A. E. Mark, *J. Am. Chem. Soc.* **2003**, *125*, 11144-11145.

[30] J. C. Shelly, M. Y. Shelly, R. C. Reeder, S. Bandyopadhyay, P. B. Moore and M. L. Klein, *J. Phys. Chem. B.* **2001**, *105*, 9785-9792.

[31] G. Srinivas and M. L. Klein, *Molecular Physics* **2004**, *102*, 883-889.

[32] R. Faller, H. Schmitz, O. Biermann and F. Muller-Plathe, *J. Comput. Chem.* **1999**, *30*, 1009-1017.

[33] O. Borodin, G. D. Smith and D. Bedrov, *J. Phys. Chem. B.* **2002**, *106*, 9912-9922.

[34] E. K. Watkins and W. L. Jorgensen, *J. Phys. Chem. A.* **2001**, *105*, 4118-4125.

[35] S. T. Cui, J. I. Siepmann, H. D. Cochran and P. T. Cummings, *Fluid Phase Equilib.* **1998**, *146*, 51-61.

[36] B. Albinsson and J. Michl, *J. Am. Chem. Soc.* **1995**, *117*, 6378-6379.

[37] B. Albinsson and J. Michl, *J. Phys. Chem.* **1996**, *100*, 3418-3429.

[38] G. D. Smith, R. L. Jaffe and D. Y. Yoon, *Macromolecules* **1994**, *27*, 3166-3173.

[39] O. Okada, K. Oka, S. Kuwajima and K. Tanabe, *Mol. Simul.* **1999**, *21*, 325-342.

[40] M. Sprik, U. Rothlisberger and M. L. Klein, *J. Phys. Chem. B.* **1997**, *101*, 2745-2749.

[41] M. Sprik, U. Rothlisberger and M. L. Klein, *Mol. Phys.* **1999**, *97*, 355-373.

[42] C. Chen, P. Depa, V. G. Sakai, J. K. Maranas, J. W. Lynn, I. Peral and J. R. D. Copley, *J. Chem. Phys.* **2006**, *124*, 234901-234908.

[43] A. F. Miller, M. R. Wilson and M. J. Cook, *Molecular Physics* **2003**, *101*, 1131-1138.

Chapter Six: Conclusions and Outlook

6.1 Conclusions and Outlook

The adsorption to an air-water interface and subsequent surface organization of a series of solutions containing hydrophilic poly(ethylene oxide) polymers that have been functionalized with a range of hydrophobic end groups have been investigated; there were three separate phases to this project.

The first part of the project was to synthesize the series of novel end-capped poly(ethylene oxide) (PEO) based materials. This was achieved using a combination of Williamson coupling reactions to produce the dendritic head groups, anionic polymerization to make the PEO back bone and a trans-esterification method to attach the dendritic head groups that would give the polymer the desired amphiphilic properties.

The dendritic fluorinated head groups were synthesized using a Williamson Coupling reaction and using this method tri-functionalized (**F3**) and di-functionalized (**F2**) first generation dendrimers with three and two $C_8F_{17}(CH_2)_3$ groups on each head group respectively were successfully synthesized with a conversion yield in excess of 90%.

Using anionic polymerization to produce the PEO chains it was possible to control the polydispersity to within a value of 1.07 Mw/Mn and each polymer was synthesized to the correct molecular weight such as that when the head group was attached the final molecule had a molecular weight 10000 gmol^{-1} and for each PEO sample both a hydrogenous and deuterated variant were successfully produced. For the head groups that did not contain any fluorinated segments it was possible to simply use the head group as an initiator for the anionic polymerization, therefore removing the need to carry out the end capping stage.

As it was not possible to use the fluorinated head groups as initiators for anionic polymerization it was necessary to find another synthetic route by which PEO chains could be functionalized with these end caps. Trial experiments were carried out using

Williamson Coupling reactions but these were also ineffectual in synthesizing the desired materials. Successful synthesis of these materials was achieved using trans-esterification reaction, where PEO chains were successfully end-capped with the tri-functionalized and di-functionalized first generation dendrimers with a conversion rate of around 54% and 52% respectively.

While there is some room for improvement (and some suggestions are outlined in chapter four with regards to how this may be possible) in this trans esterification reaction with regards to conversion rate, it is important to note that the fluorinated materials made here are unique and this synthetic route was successful in producing the desired functionalized polymers for study by neutron reflectometry.

The second part of this project was focused on the experimental analysis of these functionalized PEO materials.

Surface tension measurements were taken at a wide range of material concentration in deionized water for each of the functionalized PEOs (as well as some carefully designed control materials) so it was possible to measure the specific effect of each type of head group functionalization. The results show a clear dependence of surface tension on material concentration and the adsorption of material is greatly enhanced by the presence of dendritic hydrophobic head groups and these effects are quantified by the measured values for surface tension and calculated surface excess. The surface tension value for the highest concentration of F3 functionalized PEO has been shown to be around 45 mN/m and a surface excess of over 16 nm was calculated from the surface tension results of this sample. Literature values give the surface tension of pure water as 71.8 mN/m and the calculated radius of gyration for a PEO molecule at this molecular weight is 3.92 ± 0.21 nm. Comparison of these values shows that the molecules are adsorbing to the air-water interface in relatively high concentrations leading to this observed lowering of the surface tension. These high concentrations leave little room for the PEO chains to adopt their natural conformation and they are forced to extend into the bulk, giving rise to the large surface excess value.

Neutron reflectivity experiments carried out on dPEO materials in D_2O solvent reveal subtle difference in R(Q) vs Q data when a large amount of functionalized material

is added to the solvent. This change in neutron reflectivity data can be attributed to a change in r.m.s surface roughness due to the adsorption of functionalized material to the air-water interface. However, it is very difficult to make more detailed conclusion about the surface organization from this data.

The next logical step in the analysis of these materials was the study of neutron reflectivity data carried out on systems with these materials dissolved in null reflecting water (NRW). Using NRW in neutron reflectometry it was possible to observe the surface organization of these materials in much more detail. Analysis of these results showed a definite and large excess of material adsorbed to the surface even for the lowest concentrations, with the amount of surface excess material clearly increasing with respect to initial bulk concentration.

Study of the concentration versus depth profiles for the two materials functionalized with fluorinated head groups reveals that, once a certain solution concentration is reached, the PEO chains extend much further into the solvent bulk than the calculated radius of gyration for the polymer chains can account for. This is evidence for polymer brush formation as the surface-tethered molecules are forced to stretch into the bulk and this observation is reinforced later by computer simulation results. At the highest concentrations the PEO chains can be seen at even greater depths into the bulk of the solvent (beyond the depths that are single polymer chain that is tethered at the surface is likely to be able to reach) and this is strong evidence for multi-layer surface structures or possibly the formation of micelles just below the surface.

While all of these observations can be seen to apply for both the **F2** and **F3** materials (as well as the **F1** materials previously studied[1]), the results for **F3** material show evidence that this head group has a significantly higher surface adsorption affinity and surface tethering than both the **F2** and **F1** counterparts. This can be seen in the fact that the highest concentration of **F3** material solution studied is more than an order of magnitude lower than that of the highest concentration studied for the other two material solutions, yet the **F3** material can be seen at much greater depths into the bulk of the solvent. This suggests that more multi-layers are being formed due to the fact that high surface adsorption influence of the three fluorinated functional groups attached to the **F3**

molecule are able to hold these molecules at the surface despite the large amount of perturbation away from a random coil conformation.

For both the **F2** and **F3** materials there is a clear change in surface organization that can be seen between the lower material solution concentrations where a simple single layer conformation is observed and the higher material solution concentrations where a more complex multi layer or micelle formation surface organizational structure is apparent. With the introduction of the new target station at ISIS[2] for carrying out neutron reflectivity experiments at higher flux and larger Q range it would be very interesting to use these instruments to take a more detailed look at this range of concentrations where the transition in surface organization takes place and to perhaps pin down an exact concentration at which this occurs. It would also be very interesting to investigate the effects of increasing the PEO molecular weight to discover the limits to the tethering strength of these fluorinated head groups in this form.

The final part of this work used computational molecular simulations of systems that were constructed in such a way as to mirror the experimental molecules and conditions as closely as possible.

Fully atomistic simulations were first carried out on small PEO molecules and head group systems so that a series of force field conditions could be built up that could be used to represent a larger coarse grained system that is representative of an experimental system. Using these parameters it was possible to run simulations in excess of 1 ns in length and several snapshot images were taken to show how the organization of these molecules rapidly reaches an equilibrated state with the fluorinated head group molecules arranged into small clusters of 4-6 molecules and the PEO chains extending into the bulk. This clustering effect is incredibly difficult to observe experimentally and these computer simulations are giving a unique insight into the detailed surface conformations adopted by these molecules.

Radius of gyration measurements of the simulated coarse grained molecules that are tethered to an interface showed very similar values to those seen for the depth into which the experimental molecules penetrate the surface in neutron reflectivity studies. Both of these studies show that the tethered polymers are stretched beyond the value of the

calculated radius of gyration and this is strong evidence for the formation of a polymer brush conformation.

When comparing the concentration versus depth profiles for computer simulation systems to those from neutron reflectivity experiments it was clearly shown that a very close packing simulated structure was needed and this is further evidence of the high adsorption affinity imparted on the experimental molecules by the fluorinated head groups.

The computer simulations carried out here give very good overview of these systems and how they behave at a very detailed and atomistic level. Some very interesting and important comparisons can also be drawn between these simulated systems and results obtained from neutron reflectivity. However, in order to use these simulated systems to predict the behaviour and to calculate neutron reflectivity profiles of similar novel molecules it is necessary to invest much more time into constructing many more systems designed to investigate the effects of surface concentration in much more detail. With the advance of computer technology this kind of study will become much more feasible and less time consuming in the near future.

The ongoing demand for polymeric materials that have unique and useful surface properties requires a good understanding and control of the interfacial properties of such materials. The synthesis and study of these end functionalized polymers has yielded a much better understanding of how these materials self assemble and arrange at an air-water interface and this understanding can help in the design of unique polymeric systems as well is improving the use of these kinds of functionalized polymer materials that are already employed in many applications (some of these applications and the advantages of these materials over smaller molecular weight additives are described in section 4.7). As the main advantage of these functionalized polymers is that they can be designed to be compatible with a host bulk homopolymer while imparting different surface properties to that which would normally be exhibited by the bulk, it is important that the molecular weight of the chain part of these functionalized molecules is large enough that it will be able anchor itself into the host polymer. If the chain segment of the functionalized polymer is too short then this will lead to sharp interfaces between the

components and poor mechanical strength between the two components[3, 4]. Therefore the inclusion of a head group that is strongly adsorbing enough to tether these higher molecular weight polymers to the interface is vital. While block copolymers would seem to be a simple way to achieve this result as they should adsorb successfully to interfaces[5], previous studies[6, 7] have shown that the formation of micelles in these systems dramatically slow down and sometimes can even prevent the diffusion of these molecules to the desired interface. It has been shown in this study that dendritic head groups are a very good potential material for overcoming this problem as (although this study was carried out in a water solvent and the restrictions of a polymer bulk material do not apply for the molecular diffusion) the equilibration times for the surface activity measurements were very fast and the tethering strength of the **F3** material in particular was shown to be high enough to allow a very large perturbation of the polymer molecule without becoming detached from the interface.

6.2 References

[1] R. W. Richards and J. Sarica, *Langmuir* **2003**, *19*, 7768-7777.

[2] M. Bull in *News from the ISIS second target station project*, *Vol.* **2007**.

[3] R. A. L. Jones, E. J. Kramer, M. H. Rafailovich, J. Sokolov and J. Schwarz, *Phys. Rev. Lett.* **1989**, *62*, 280-283.

[4] N. L. Thomas and A. H. Windle, *Polymer* **1982**, *23*, 529-542.

[5] Y. Lyatskaya, D. Gersappe, N. A. Gross and A. C. Balazs, *J. Phys. Chem.* **1996**, *100*, 1449-1458.

[6] F. T. Kiff, R. W. Richards and R. L. Thompson, *Langmuir* **2004**, *20*, 4465-4470.

[7] D. G. Bucknall, J. S. Higgins and J. Penfold, *Physica B.* **1992**, *180*, 468-470.

Appendix

Atom Name	Atomic Mass (AMU)	Description
CA	12.01	Aromatic Carbon
CT	12.01	Alkane Carbon
FC	19.00	Alkyl Fluorine
HA	1.008	Aromatic Hydrogen
HC	1.008	Alkane Hydrogen
HO	1.008	Alcohol Hydrogen
OS	16.00	Ester Oxygen
OH	16.00	Alcohol Oxygen

Table A: Standard atom names and atomic masses from OPLS_AA force field

Bond Type	K_S (kcal/Å^{-2})	R_0 (Å)
CA-CA	469.0	1.400
CA-CT	317.0	1.510
CA-HA	367.0	1.080
CA-OS	450.0	1.380
CT-CT	268.0	1.529
CT-HC	340.0	1.090
CT-OS	320.0	1.410
CT-OH	320.0	1.410
CT-FC	420.0	1.354
HO-OH	553.0	0.945

Table B: Standard bond stretching terms from OPLS_AA force field

Angle Type	K_B (kcal/Å^{-2})	θ_0 (Å)
CA-CA-CA	63.0	120.0
CA-CA-HA	35.0	120.0
CA-CA-CT	70.0	120.0
CA-CA-OS	70.0	120.0
CA-OS-CT	82.6	118.1
CA-CT-CT	63.0	114.0
CA-CT-HC	35.0	109.5
CT-CT-CT	58.4	112.7
CT-CT-OS	50.0	109.0
CT-CT-HC	37.5	110.7
CT-OS-CT	60.0	109.5
CT-CT-OH	50.0	109.5
CT-OH-HO	55.0	108.5
CT-CT-FC	80.0	109.5
OS-CT-HC	35.0	109.5

Table C: Standard bond bending terms from OPLS_AA force field

Dihedral Type	V_1 (kcal/Å^{-2})	V_2 (kcal/Å^{-2})	V_3 (kcal/Å^{-2})
CA-CA-CA-CA	0.0	9.51	0.0
CA-CA-CA-HA	0.0	9.51	0.0
HA-CA-CA-HA	0.0	9.51	0.0
CT-CT-CT-CT	1.740	-0.156	0.279
CT-CT-CT-HC	0.0	0.0	0.366
HC-CT-CT-HC	0.0	0.0	0.318
CT-CT-OS-CT	0.650	-0.250	0.670
OS-CT-CT-OS	-0.550	0.0	0.0
CA-CA-OS-CT	0.0	2.55	0.0
CA-CA-CT-HC	0.0	0.0	0.0
CA-CA-CT-CT	0.0	0.0	0.0
OS-CT-CT-FC	0.0	0.0	0.366
FC-CT-CT-FC	0.0	0.0	0.318
HO-OH-CT-CT	0.0	0.0	0.468
HO-OH-CT-HC	0.0	0.0	0.450
HC-CT-OS-CT	0.0	0.0	0.760

Table D: Standard dihedral terms from OPLS_AA force field

Atom Name	Elec. Charge (q)	σ (Å)	ε (kcal mol^{-1})
CA	-0.115	3.55	0.07
CT (CH$_2$)	-0.120	3.50	0.066
CT (CH$_3$)	-0.180	3.50	0.066
FC	-1.000	2.73	0.720
HA	0.115	2.42	0.030
HC	0.060	2.50	0.030
HO	-0.418	0.0	0.0
OS	-0.400	3.00	0.170
OH	-0.683	3.12	0.170
CT (CF$_2$)	2.000	3.50	0.066
CT (CF$_3$)	3.000	3.50	0.066
CT (C-O-H)	0.700	3.75	0.105

Table E: Standard non-bonded Lennard-Jones terms from OPLS_AA force field